THE UNIVERSITY *of* EDINBURGH

Micro and Small-scale Generation in Urban Distribution Networks

Jorge Luis Acosta

A thesis submitted for the degree of Doctor of Philosophy.
The University of Edinburgh.
January 2013

Abstract

As the world moves towards a more sustainable development, the energy coming from fossil fuels still produces the greenhouse gases that threaten the world's climate. The UK government has established targets for the penetration of renewable energy generation and low-carbon alternatives for the electricity production. One of these technologies is microgeneration. In 2006, the UK government launched the Microgeneration Strategy pushing forward micro and small-scale generation as a supplementary source of energy for the country's growing electricity demand. The proposal is focused on several technologies, including micro-wind and micro-PV, among others. These microgeneration technologies are now a reality and widespread across the distribution networks. Therefore, the analysis of the impact of these systems connected to distribution grids and the benefits of these technologies, alongside with their negative effects on the network is an important research area. Correct modelling of micro and small-scale renewable-based generation technologies implemented in urban areas, however, is not a simple task, as it requires an adequate representation of highly dispersed and uncontrolled generation systems. These systems are small in size, but high in numbers and usually experience large variations in available renewable energy inputs. This thesis presents aggregate models of urban micro and small-scale PV and wind generation systems, which are connected to low-voltage networks. The thesis analyses impact of urban PV and wind generation on the steady-state network performance (power flows and voltage profiles), taking into account variability of energy inputs. The presented analysis is of particular importance for the analysis of the future of power system supplies, which will have significantly higher penetration levels of renewable-based distributed generation technologies, resulting in a much wider range of interactions between microgeneration systems, loads and transmission/distribution networks. In order to perform this analysis, the resource assessment for urban areas has to be carried out to both quantify the potential for each technology and help in their modelling. This has been a challenge since the aggregation of microgeneration systems is far from simple, as the parameters, performance and size varies between different technologies. A solution presented in this thesis is an approach for simple yet accurate aggregation of microgeneration technologies. This approach allows to quantify and analyse their impact and effect on the power supply systems directly in terms of penetration levels and general technology characteristics.

Declaration of originality

I hereby declare that the research recorded in this thesis and the thesis itself were composed and originated entirely by myself in the Institute for Energy Systems, School of Engineering at The University of Edinburgh.

Jorge Luis Acosta

Acknowledgements

During my time in Edinburgh I have been blessed to know many people that touched my life, and that have become part of my family, I am going to try to thank each one of them.

Firstly, I thank God for his guidance, for opening the doors for me, blessing me all the way to make my life as perfect as it has been through my PhD years.

My respect, admiration and special thanks go to my supervisor Dr. Saša Djokić, for all his patience when times were difficult, for always answering my question: 'What am I doing?' for his guidance and for pushing me always to make the most of my PhD.

Also, I want to thank my parents for their endless love and support through my crazy decisions, for helping me become who I am now and for always believing in me.

I give thanks to my sister Liliana for her support, for being there, for listening to me, for her honesty, for sharing my dreams, for taking care of me and for helping me laugh at life when I stood in front of a dead end. Those moments are precious.

Starting all over again in a different place is never easy. I owe part of my sanity to the best of friends: Adam Collin, Xchel Martínez, Kate McJennett, Anup Nambiar, Dan Eager, Laura Finlay, Barry Hayes and Sarah Caraher, for always being there, for all the great times together, for looking after me and for sharing your lives with me. I will love you forever.

Having a great place to work was crucial for me and I thank all my friends in IES: Nacho, James, Paddy, Evangelos, Randy, Punim, George and Milla. Being together on the same boat made my PhD a wonderful experience, and easier to bear when things became complicated, as a PhD usually gets. I could never forget the whole IES community for being outstanding human beings, and great researchers. I take with me the best of memories.

Finally my thanks to all my friends here in the UK and in Mexico for their support and cheering for the past few years especially: Paulina Carbajal, Pedro Ponce, Artemis Parvizi, Karina Romo, Aarón Gamboa and Montserrat Vázquez.

Contents

List of figures

List of tables

Acronyms and abbreviations

AC	Alternating Current
ADMD	After Diversity Maximum Demand
BS	British Standard
CFL	Compact Fluorescent Lamp
CSA	Cross Sectional Area
DC	Direct Current
DECC	Department of Energy and Climate Change
DG	Distributed Generation
DN	Distribution Network
DNO	Distribution Network Operator
ER	Engineering Recommendation
GIL	General Incandescent Lamp
HAWT	Horizontal Axis Wind Turbine
HIT	Heterojunction with Intrinsic Thin-layer
IGBT	Insulated Gate Bipolar Transistor
LV	Low Voltage
MCS	Microgeneration Certification Scheme
MPE	Mean Percentage Error
MPP	Maximum Power Point
MPPT	Maximum Power Point Tracking
MV	Medium Voltage
NOABL	Numerical Objective Analysis Boundary Layer
NOCT	Normal Operating Cell Temperature
O&M	Operation and Maintenance
P&O	Perturb and Observe
PMSG	Permanent Magnet Synchronous Generator
PV	Photovoltaics
PWM	Pulse Width Modulation
PVGIS	Photovoltaic Geographical Information System

RMS	Root Mean Square
STC	Standard Testing Conditions
THD	Total Harmonic Distortion
uDN	Urban Distribution Network
UK	United Kingdom
VAWT	Vertical Axis Wind Turbine
WT	Wind Turbine
WWT	Warwick Wind Trials

Nomenclature

a	Diode ideality constant
a_i	Actual value of the quantity
A_{swept}	Swept area
β	Friction coefficient
C_1	LC-filter capacitance
C_p	Coefficient of Performance
ΔT	Temperature difference
E	Kinetic energy
f_a	Phase 1 in reference system
f_b	Phase 2 in reference system
f_c	Phase 3 in reference system
f_d	Direct-axis in reference system
f_i	Forecast
f_q	Quadrature-axis in reference system
Γ	Gamma function
η	Efficiency
$\eta_{inverter}$	Inverter's efficiency
η_{el}	Electrical efficiency
η_{mech}	Aerodynamic efficiency or Coefficient of performance
η_{PMSG}	PMSG's efficiency
$\eta_{PV_{panel}}$	PV panel's efficiency
i_c	LC-filter capacitor's current
i_d	d-axis current
i_q	q-axis current
i_1	LC-filter input current
i_2	LC-filter output current
I	Current
I_{mpp}	MPP current
I_o	Diode saturation current

I_{out}	PV output current
I_P	Real power constant current coefficient
I_{pv}	Photovoltaic current
I_{pv_n}	Nominal photovoltaic current
I_Q	Reactive power constant current coefficient
I_{sc}	Short-circuit current
J	Moment of inertia
k	Shape factor
k_B	Boltzmann's constant
K_I	Temperature current coefficient
K_V	Temperature voltage coefficient
L_d	d-axis inductance
L_q	q-axis inductance
L_1	LC-filter inductance
λ	Scaling factor
λ_m	Mutual inductance
m	Mass
$\dot{m}$	Mass flow
n	Number of quantities involved
n_p	Active power exponential model coefficient
n_q	Reactive power exponential model coefficient
N_s	Series cell number
ν	Wind speed
ν_{mean}	Mean wind speed
P	Actual active power
P_{aero}	Aerodynamic power of the wind per squared metre
P_{betz}	Betz power
P_{in}	Input power
$P_{impulse}$	Impulse power
P_{max}	Maximum power
$P_{max,e}$	Electrical maximum power
P_{out}	Output power
P_P	Active power, constant power coefficient

P_Q	Reactive power, constant power coefficient
P_{rated}	Rated power
P_{wind}	Power of the wind for a particular area
P_0	Nominal active power
ρ_{air}	Air density
q	Electron charge
Q_1	Actual fundamental reactive power
$Q_{1,0}$	Nominal fundamental reactive power
R	Resistance
R_p	Parallel resistance
R_s	Series resistance
R_1	LC-filter damping resistor
S_{irr}	Solar irradiance
S_n	Nominal solar irradiance
t	Time
T	Temperature
T_e	Electromagnetic torque
T_m	Mechanical torque
θ_e	Electrical angle
v_d	d-axis voltage
v_q	q-axis voltage
V	Voltage
V_{mpp}	MPP voltage
V_t	Thermal voltage
V_0	Nominal supply voltage
V_1	LC-filter input voltage
V_2	LC-filter output voltage
ω_e	Electrical speed
ω_p	Resonant pole frequency
ω_r	Rotor speed
Z_P	Active power, constant impedance coefficient
Z_Q	Reactive power, constant impedance coefficient
ζ_p	Damping factor

Chapter 1
Introduction

1.1 Microgeneration

In March 2006, the UK government launched the Microgeneration Strategy [1] with the objective of making microgeneration a realistic alternative or supplementary source to conventional energy systems. It proposed different schemes that could tackle the barriers for the development of microgeneration in the UK and published several progress reports. In June 2011, the government reported in [2] the actions for further development of microgeneration, in order to be part of the UK's energy mix. The technologies that are included as part of this Strategy are:

- Solar Photovoltaics,
- Solar thermal panels,
- Ground, and air source heat pumps,
- Wind turbines,
- Micro Hydro,
- Combined Heat and Power (CHP),
- Fuel cells,
- Heat and power generation from biomass.

The scope of the Microgeneration Strategy is delimited by the Green Energy Act 2009, where the maximum power considered is up to $50kW_e$ for electricity and $300kW_{th}$ for heat. Many schemes were implemented to incentivise the installation of these microgeneration technologies, such as the Low Carbon Buildings program, which pushed the introduction of microgeneration in new buildings [3]. This interest has brought a lot of questions on how microgeneration can be connected and what are its effects on the network, alongside with the motivation of how much the households can save on electricity bills.

1.2 Microgeneration Modelling

There is a high interest in the consequences of the connection of microgeneration to the distribution networks. The Distribution Network Operators (DNOs) have general concerns about the impact of high penetration of microgeneration. Stannard and Bumby [4] introduced the model of a single wind turbine based on a numerical model of the wind. This model was capable of reproducing the turbulence of the wind and interesting results on the power output following the wind speed pattern were presented, modelling each state of the wind turbine with particular attention on the wind dynamics to understand how the turbulence affects the power output. Following the same model and analysis, Stannard et al. presented in [5] and [6] a comparison between AC and DC aggregation of several wind turbines, showing how the power output would vary when a DC network is implemented before the inverter exported the power output to the electricity grid. The analysis of grid interaction was also presented for photovoltaic (PV) systems by Thomson et al. in [7], where the inclusion of PV systems in a distribution network at house level modelling was discussed, showing a "peak shaving" of the load demand when a 50% penetration of microgeneration is present. This type of modelling is needed to understand the performance of microgeneration connected to the grid, as a single microgeneration unit may not have any visible impact. Nevertheless, when the microgeneration penetration is high, the numbers added up might cause reversed power flows, increase/decrease of voltage levels, increase/decrease of losses in the distribution system, etc. This thesis took the essence of these references to create new microgeneration models that could consider input resources, aggregation of many individual microgeneration systems and then analyse the performance and impact of the microgeneration aggregation in the urban distribution network.

This thesis focuses on the modelling of two microgeneration technologies: PV and wind energy. These two technologies have been selected as they are the most common and dominant among the several other technologies identified by the UK government. Additionally, PV and wind technologies are the two main and most mature renewable-based microgeneration technologies worldwide. They are also selected not just due to the differences in conversion of input renewable energy into the electricity, but also due to the similarities in their grid integration. This is important, as the correct modelling of microgeneration technologies requires a "whole systems" approach, starting with the assessment of input energy resources, continuing with the analysis of mechanical, electrical and electronic system conversion efficiencies, and ending with studying the outputs and grid interactions. Accordingly, the thesis presents assessment of input energy resources for each technology, modelling of typical individual devices, calcula-

tion of the electrical power/energy outputs delivered to the grid and aggregated models able to represent large number of these devices connected to the distribution network. The modelling is aimed at assessing the performance of these two selected microgeneration technologies and their impact on the network, focusing on the future scenario with a high penetration of these systems and implementation of smart grid functionalities (e.g. demand-side management).

1.3 Aims of the Thesis

There are basically two main aims of this thesis. The first one is to assess the potential of renewable energy resources in the UK urban areas using Edinburgh city as an example. For this purpose, measured data are available with different resolutions, in order to correctly assess and understand the behaviour and possible benefits of microgeneration technologies. The second is to build accurate models of microgeneration technologies, represented in generic form, to analyse the performance of renewable-based microgeneration and their impact when they are connected to the distribution network.

1.4 Outline of the Thesis

The thesis is divided in seven Chapters, in which four general areas are discussed: assessment of renewable energy resources, modelling of selected microgeneration technologies, formulation of aggregation methodology and connection and interaction of microgeneration with the distribution network.

1.4.1 Chapter 1

This is an introductory Chapter, presenting the structure and motivations of the research reported in this thesis.

1.4.2 Chapter 2

Presents the resource assessment for two considered technologies (solar irradiance and wind speed), focusing on the UK urban areas. In the case of the wind speed, the analysis includes discussion of the measurement resolution required to properly assess wind resource in urban

area. The results present Weibull distribution as a way to correctly represent the availability of annual urban wind resources. Furthermore, the analysis presents a spatial and temporal aspects of assessing the solar irradiance and wind speed resources, in order to correlate the microgeneration output with load demand throughout the day. Similarly, the analysis of solar irradiance resources is presented using the measurements from the University of Edinburgh weather station [8], discussing how these measurements compare to the European Commission database [9], Photovoltaic Geographical Information System (PVGIS). The analysis shows the similarities and the use of these data for sites where measurement is not available. (*Paper published from this research: [10]*)

1.4.3 Chapter 3

Presents the detailed model of individual wind-based microgenerator connected to the grid, which is developed using the manufacturer specification and second-by-second wind speed measurement data. This chapter presents the analysis of the grid interconnection of a single unit with the distribution network, including the discussion of power quality issues. The presented results and analysis also consider the impact of the resolution of measured input wind speed data on the calculated power output obtained from the model. (*Paper published from this research: [11]*)

1.4.4 Chapter 4

Presents the detailed model of individual PV microgenerator connected to the grid, which is also developed using the manufacturer specification and measurement data from a site in Belgium. Again, the analysis of the grid interconnection of a single unit with the distribution network is provided, including the discussion of power quality issues.

1.4.5 Chapter 5

Presents the aggregation methodology of single-unit models from two previous chapters, in order to assess the influence of a large number of highly dispersed PV and wind microgeneration systems in the network. This chapter presents four generic wind-based microgeneration systems and four generic PV microgeneration systems, identified from the two databases built after the extensive market surveys for both technologies are performed. An economi-

cal analysis is also presented for both technologies, focusing on the payback periods required and compared with the resources available in Edinburgh city. (*Papers published from this research: [11], [12], [13]*)

1.4.6 Chapter 6

This chapter presents the analysis of the impact of microgeneration on the distribution network operation, when the aggregated units obtained in Chapter 5 are used for this purpose. The chapter presents the interaction of microgeneration connected in parallel with load models, using a detailed model of the distribution network. This chapter shows the potential that microgeneration has when connected in urban distribution networks. (*Papers published from this research: [14], [15], [16], [17], [18], [19], [20]*)

1.4.7 Chapter 7

This Chapter presents the main conclusions and indications for further work.

1.5 Main contributions

This thesis presents the results of input to output modelling of PV and wind energy systems, focused on the connection of these micro and small-scale systems in urban distribution networks.

- Resource Assessment of UK urban areas:
  - Wind resource assessment in urban areas with the identification of specific Weibull distribution for each site [10], with a particular focus on Edinburgh city
  - Solar irradiance comparison between measurements and solar calculators, such as European Commission database.
- Time-series modelling of microgeneration
  - Model of individual wind turbine [11]
  - Model of individual PV system
- Aggregation of PV/Wind models for urban area

  - Wind turbine database used for the aggregation of many systems into four generic and one aggregate generic system [10], [11], [17]
  - PV database used for the aggregation of many systems into four generic and one aggregate generic system
  - Combination of generic PV and wind systems into one aggregate model for urban distribution network connection [19].

- Connection of microgeneration models with load and distribution network models [16], [17], [18], [19].

- One Journal paper and ten international conference publications.

Chapter 2
Renewable Energy Resource Assessment

2.1 Introduction

Concerns about climate change and global warming, constantly increasing prices of fossil fuels and the recent crisis of nuclear energy have increased interest in the use of safer and cleaner energy generation technologies, such as those based on wind and solar resources. Solar photovoltaics (PV) and wind-based electricity generation systems are now mature and widely used technologies in many countries around the world. It is, therefore, important to correctly model these renewable energy resources and technologies, in order to accurately assess the impact of their widespread installation. The analysis of PV and wind-based generation systems is particularly difficult in urban areas where they are highly dispersed and small in size (due to space limitations). The built environment in these areas, causes higher levels of turbulence and shadowing (due to building obstructions).

This chapter is divided in two large parts. In the first part, the assessment of urban wind energy resources is presented with the ultimate aim to develop a complete resource assessment methodology for the analysis of interactions of wind-based micro/small generation systems with urban distribution networks. The second part presents the same analysis for solar irradiance energy resources in urban areas. The resource assessment presented in this chapter is later used to study the effects of a high penetration of these microgeneration systems in the urban Distribution Network (uDN).

2.2 Assessment of Urban Wind Energy Resources

The United Kingdom (UK) is often cited as one of the windiest countries in Europe, with estimated mean wind speed, at the height of $45m$, between $6^m/_s$ and $7^m/_s$ for England and between $7^m/_s$ and $8^m/_s$ for Scotland [21], [22], [23]. RenewableUK's Numerical Objective Analysis Boundary Layer (NOABL) wind speed database [24] provides estimated mean wind

speed values (single-value averages for the whole year) for the UK divided in $1km$ square grid at the heights of $10m$, $25m$ and $45m$ above the ground level. This database is probably one of the most used sources of information on mean wind speeds where there are no location-specific field measurements. However, this wind resource model has limitations, as it takes no account of topography on a small-scale or local surface roughness (such as tall crops, stone walls, or trees), both of which may have a considerable effect on the wind speed. It is recommended by RenewableUK (formerly named British Wind Energy Association) that the database should be used only as a guide and on-site measurement for a further assessment should be implemented. In an attempt to provide a better assessment of mean wind speeds in urban areas, reference [25] provides a set of correction factors for the NOABL database. It should be noted, however, that these corrections apply only to mean wind speed values and that the information on the correction of annual distribution of average wind speeds is not provided either in [24] or [25].
In a number of large-scale wind applications, Weibull distributions and, more commonly, Rayleigh distribution have been used to represent the annual distribution of average wind speeds. A study made by Encraft [26], called the "Warwick Wind Trials", reported that the Weibull distribution can be used even in the urban environment, but its parameters (shape and scaling factors) need to be determined depending on the specific site. These two distributions are discussed next.

2.3 Weibull and Rayleigh Distributions

According to the British Standard BS 61400-12-1, the Rayleigh distribution, which is the same as the Weibull distribution with a shape factor of 2, shall be used as the reference wind speed distribution, i.e. the annual probability density function of wind speeds in the UK can be analytically described by the Rayleigh distribution with a range of wind speeds between $4 - 11{}^{m}/_{s}$ [4], [27], [28], [29]. The Weibull distribution is represented mathematically by equation (2.1).

$$W(\nu;\lambda,k) = \left(\frac{k}{\lambda}\right)\left(\frac{\nu}{\lambda}\right)^{k-1} e^{(-\nu/\lambda)^k} \tag{2.1}$$

where, ν - wind speed; k - shape factor; and λ - scaling factor. The relationship between the mean wind speed (MWS) and the coefficients k and λ for the Weibull distribution is:

$$\lambda = \frac{MWS}{\Gamma(1 + {}^{1}/_{k})} \tag{2.2}$$

where, MWS - mean wind speed, Γ - gamma function, The Rayleigh distribution is obtained when the shape factor k = 2 is set for the Weibull distribution (with $\sigma = \lambda/\sqrt{2} =$

$MWS/\sqrt{2/\pi}$). Figure 2.1 shows the Weibull distribution for different shape factors k, where it can be seen that the Rayleigh distribution is a special case of the Weibull distribution when k = 2.

2.3.1 Aerodynamic Power and Betz Limit

In the first stage of energy conversion in a wind turbine system, the aerodynamic (air flow) wind energy is converted into kinetic (rotational) energy by the turbine. This energy can be calculated by applying the general laws of physics and thermodynamics. The maximum energy that can be extracted from the wind by a wind turbine, i.e. the power available in the wind, denoted as the aerodynamic power, can be calculated using:

$$P_{wind} = \frac{1}{2}\rho_{air} A_{swept} \nu^3 \tag{2.3}$$

where, P_{wind} - aerodynamic power of the wind for a particular area, ρ_{air} - density of air ($1.225^{kg}/_{m^3}$), A_{swept} - swept area of the turbine. The maximum energy that can be absorbed by a wind turbine is given by the Betz limit. This simplified calculation is based on the momentum theory rate change and the Bernoulli relations of the flowing through the turbine disc, for which the performance coefficient (C_p) expression is found and presented in equation (2.4):

$$C_p = \frac{P_{max}}{P_{aero}} = \frac{1}{2}\left|1 - \left(\frac{\nu_2}{\nu_1}\right)^2\right|\left|1 + \left(\frac{\nu_2}{\nu_1}\right)\right| \tag{2.4}$$

The analytical maximum comes when ν_2/ν_1 is $1/3$ and substituting it in (2.4) gives:

$$C_p = \frac{16}{27} = 0.593 \tag{2.5}$$

This theoretical maximum in the two dimensional calculation of the Betz limit [30] is given by:

$$P_{Betz} = 0.593 P_{aero} \tag{2.6}$$

The Betz limit states that a wind turbine cannot absorb more than 59.3% of the aerodynamic power of the wind.

2.4 Wind Speed in Urban Areas

Generally, due to a higher level of obstructions and turbulence, wind speeds in urban areas are lower than in open space, producing lower power outputs from wind-based generation systems.

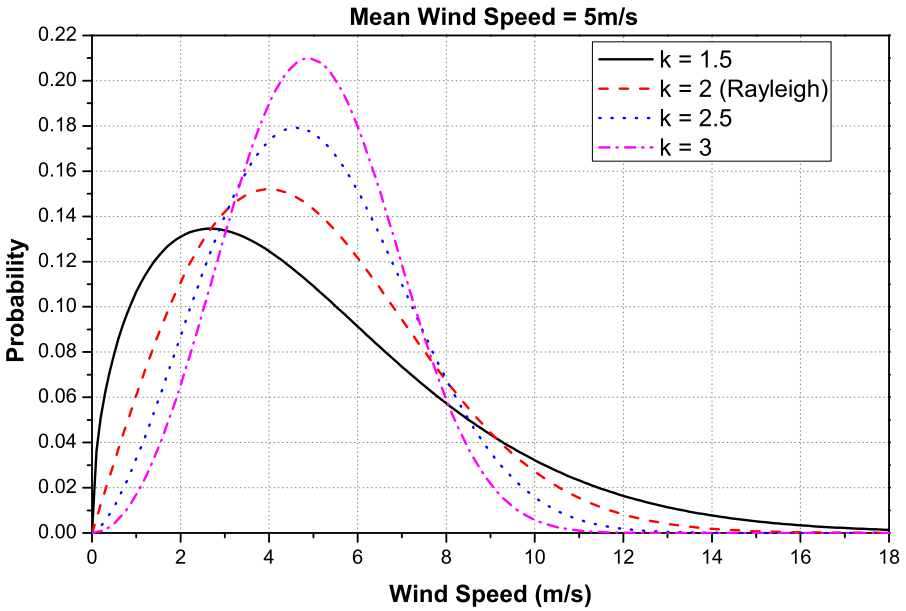

(a)

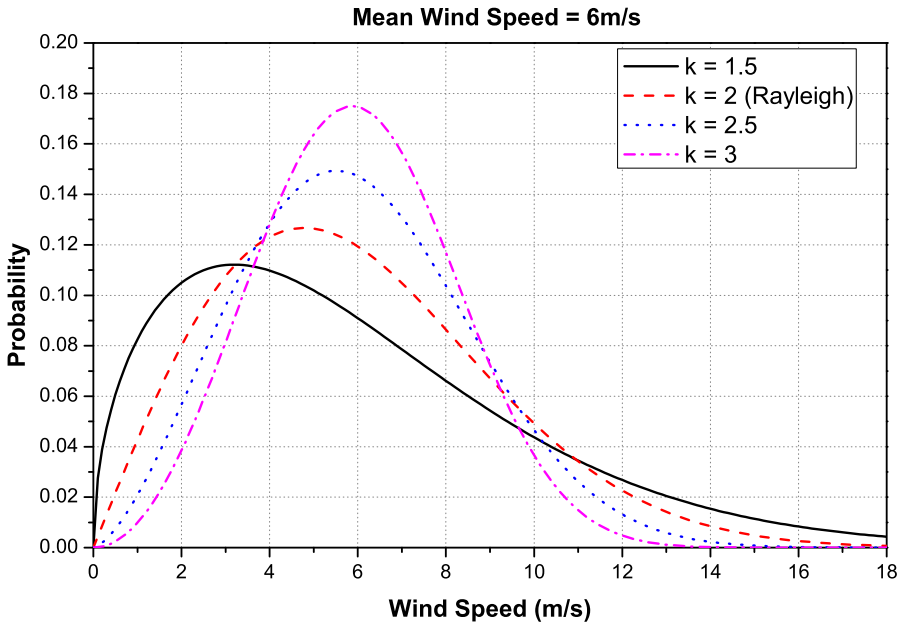

(b)

Figure 2.1: *Weibull distributions for mean wind speed (a) v_{mean}= $5^{m}/_{s}$ (b) v_{mean}= $6^{m}/_{s}$ and different values of shape factor k = 1.5, 2 (Rayleigh), 2.5 and 3.*

This section compares the Weibull wind distributions of different UK sites from [31], where measured wind speed data are provided. The presented results demonstrate the importance of accurately assessing wind resource in urban areas. There are some differences for some sites between the results using Rayleigh wind distribution and the results obtained using the Weibull fits to actual measured data. The mean wind speeds used for the Rayleigh distribution were found to be between $5^m/_s$ and $6^m/_s$ for the centre of Edinburgh city using the NOABL database and they are used as a reference.

2.4.1 Weibull Distribution Fits

The assessment of wind resources in urban areas cannot be performed in the same way as the assessment of wind resources for wind farms built in open spaces. For the latter, the Rayleigh distribution with a corresponding mean wind speed could be used for the correct analysis of the available wind resources. In urban areas however, presence of turbulence and physical obstructions influence the output of wind-based generation. In urban areas, wind turbines will experience different distributions and see larger variations in the available energy inputs, [10]. Reference [10] discussed the assessment of wind resources in urban areas and confirmed that the use of Rayleigh distribution of annual wind speed variations (advocated in [27] and [28]) sometimes cannot be used for the assessment of UK urban wind resources. Instead, a general form of Weibull distribution should be used and it is also recommended by RenewableUK. Accordingly a methodology for the assessment of urban wind resources, which involves obtaining the coefficients k and λ of the Weibull distribution fits using the maximum likelihood estimation (MLE), suggested in [29], is discussed in this section. The Matlab codes used for this analysis are reported in Appendix A. The iterative method to obtain the shape factor k and the scale factor λ is based on equations (2.7) and (2.8).

$$k = \left(\sum_{i=1}^{n} \upsilon_i^k \ln(\upsilon_i) / \sum_{i=1}^{n} \upsilon_i^k - \sum_{i=1}^{n} \ln(\upsilon_i)/n \right)^{-1} \tag{2.7}$$

$$\lambda = \left(1/n \sum_{i=1}^{n} \upsilon_i^k \right)^{1/k} \tag{2.8}$$

where, υ_i -wind speed in bin *i*, *n*-number of non-zero wind speed data points and k = 2 is a suitable initial guess.

2.4.2 UK Urban Sites

As previously mentioned, the wind data from the Met Office database [31] of six sites have been analysed. These six urban sites are selected to identify the wind speed performance in the UK urban areas: London (site UK1), Sheffield (site UK2), Manchester (site UK3), Newcastle (site UK4), Glasgow (site UK5) and Aberdeen (site UK6), (see Figure 2.2 - Figure 2.7). Additional information (including the height above the sea level, the year for which the data were available and the exact location given by latitude and longitude) for all the sites are given in Table 2.1. The wind speed data at these sites were measured at the locations in the inner city areas between the years 2000 - 2008. For the purpose of the analysis presented in this thesis, the data have been assumed to represent the UK urban wind resources in big city areas. Measurements at each site have been plotted with the corresponding Weibull distribution fits, using the previously presented method. The files with the measured data had 8,760 points, corresponding to the hourly averaged wind speeds at each site. One year's worth data from different sites have been

Site	Location	Year	Height above sea level (m)	Latitude	Longitude
UK1	London	2007	43	51.521	-0.41534
UK2	Sheffield	2002	146	53.383	-1.48728
UK3	Manchester	2008	33	53.4665	-2.25004
UK4	Newcastle	2000	52	54.9771	-1.59687
UK5	Glasgow	2000	178	55.7547	-4.17026
UK6	Aberdeen	2008	65	57.2051	-2.2037

Table 2.1: *Location reference for six analysed UK urban sites [31].*

used to plot the distribution. The years chosen for the sites are different, as it was necessary to ensure the availability of a complete year's data without corrupted data.

Figure 2.8 shows the calculated Weibull distribution for sites UK4 and UK6, these sites are compared with the Rayleigh distribution and $6^{m}/_{s}$ reference mean wind speed (found as the maximum limit for Edinburgh city in NOABL database). This comparison shows how the mean wind speed is the most important parameter to define depending on the site, since for the six UK sites analysed the shape factor is around 2, so the Rayleigh distribution could actually be used for the UK urban area.

2.4.3 Power Curves of Wind Turbines

Probability distribution of the wind speed can be used to calculate the annual energy production of a selected wind turbine. As an example, a preliminary group of four micro and small wind

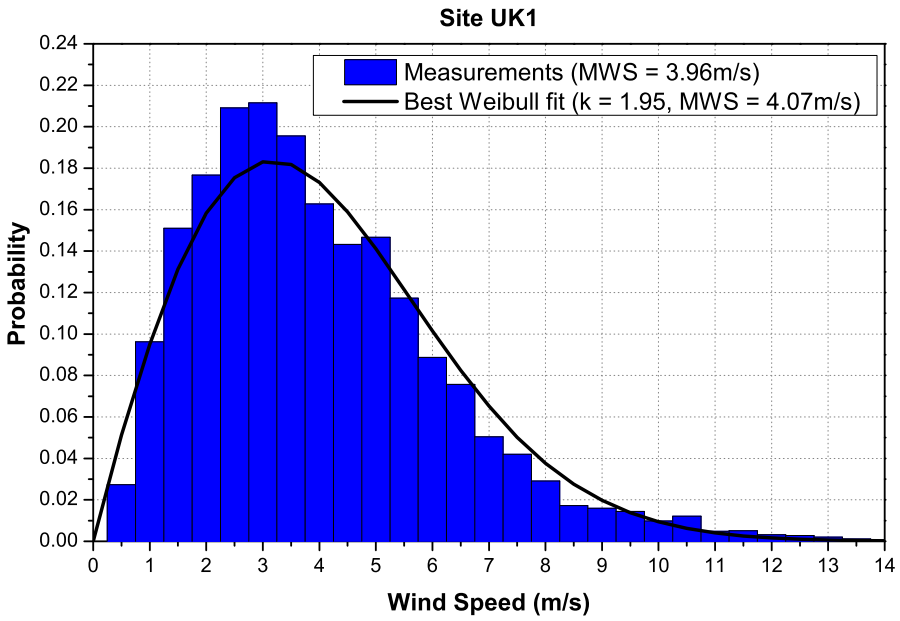

Figure 2.2: *Measured annual average wind speed distribution for site UK1 and the corresponding Weibull distribution fit.*

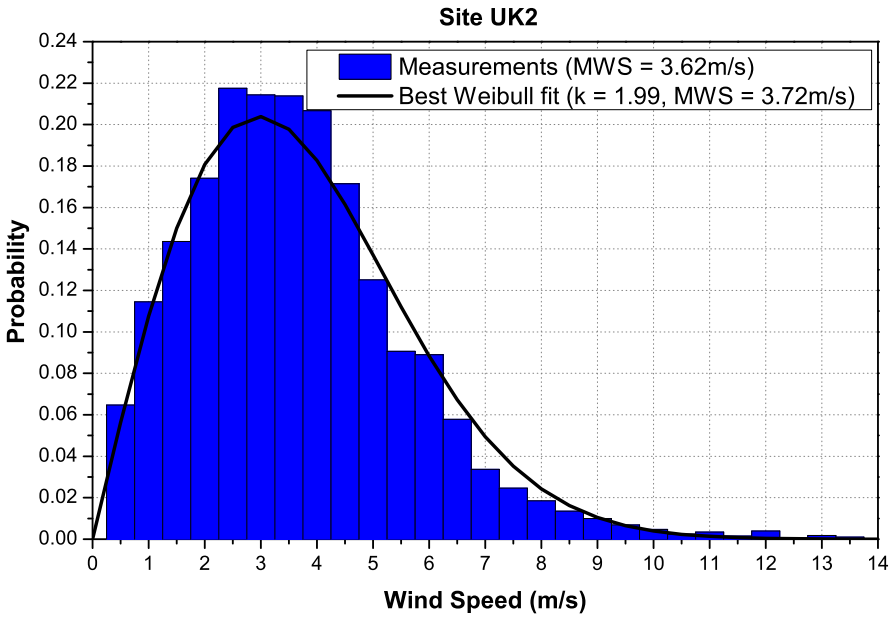

Figure 2.3: *Measured annual average wind speed distribution for site UK2 and the corresponding Weibull distribution fit.*

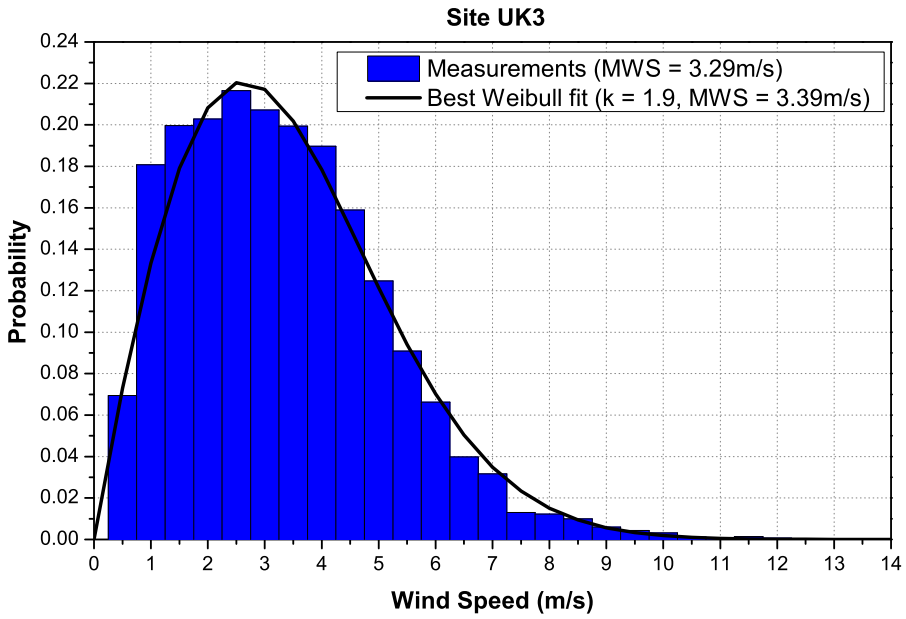

Figure 2.4: *Measured annual average wind speed distribution for site UK3 and the corresponding Weibull distribution fit.*

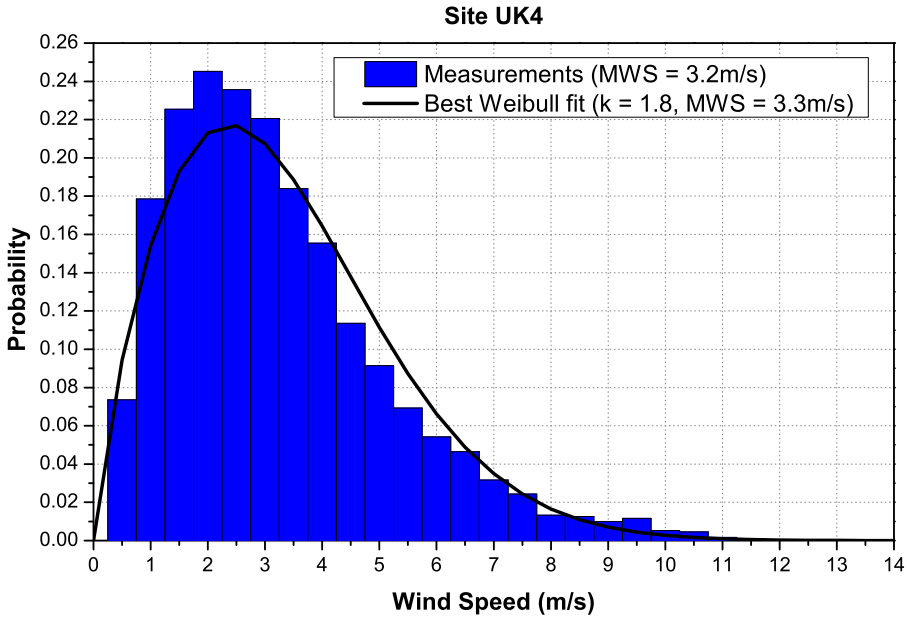

Figure 2.5: *Measured annual average wind speed distribution for site UK4 and the corresponding Weibull distribution fit.*

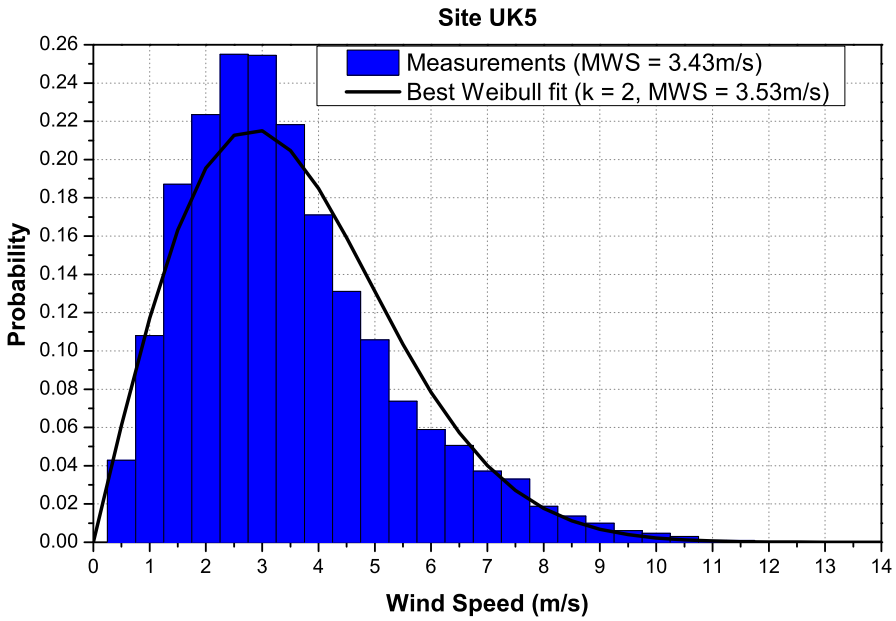

Figure 2.6: *Measured annual average wind speed distribution for site UK5 and the corresponding Weibull distribution fit.*

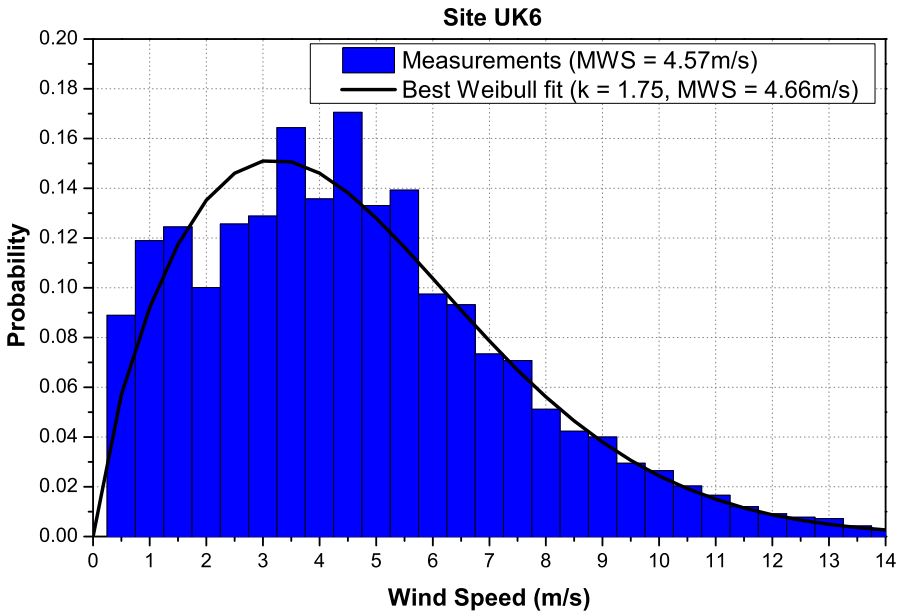

Figure 2.7: *Measured annual average wind speed distribution for site UK6 and the corresponding Weibull distribution fit.*

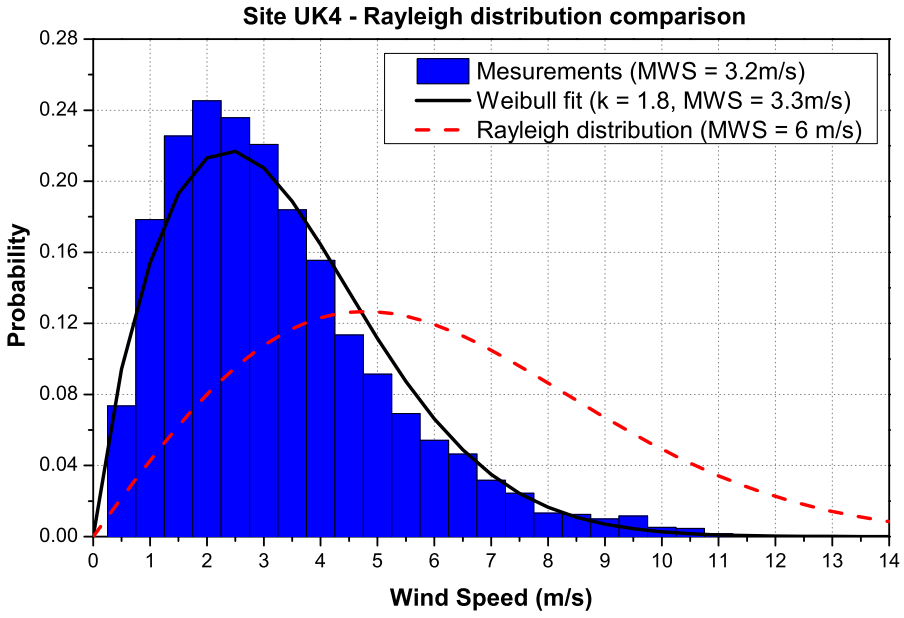

(a)

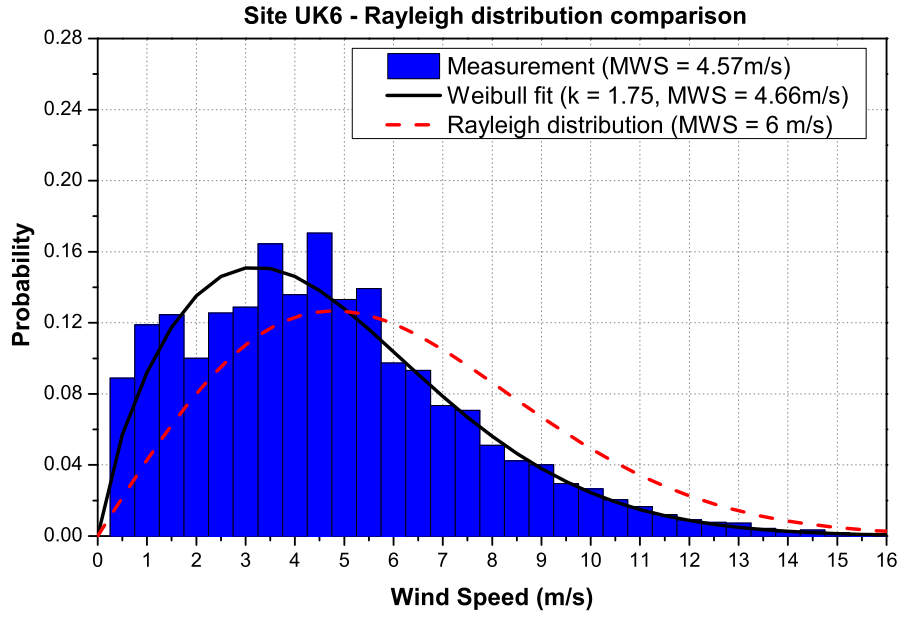

(b)

Figure 2.8: *Comparison of Weibull and Rayleigh distributions and measurements for two UK sites (a) Site UK4 with* v_{mean}*=* $3.3^{m}/_{s}$ *(b) Site UK4 with* v_{mean}*=* $4.66^{m}/_{s}$ *.*

turbines has been selected for the analysis presented in this section. The Weibull distribution has been used for calculating the annual energy output. Although the British Standard BS 61400-12-1 requires the manufacturers to provide the electrical output power curve for energy yield calculations, some manufacturers provide aerodynamic power curves to show the design capabilities of their products. However, unless stated otherwise all turbines power curves are electrical power output curves. In this section, the selection of wind turbines includes both building-mounted and free standing (i.e. pole-mounted) turbines typically found in domestic and commercial sector wind applications and one turbine providing the aerodynamic power curve:

a) WT1 (Figure 2.9), a pole/building mounted vertical axis wind turbine (VAWT), with $6kW$ rated aerodynamic power at $12.5^{m}/_{s}$, $7.4kW$ peak aerodynamic power at $14^{m}/_{s}$ and a swept area of $13.6m^2$ [32]. This turbine manufacturer gives both power curves (electrical output as required by [28] and the wind tunnel testing aerodynamic power curve),

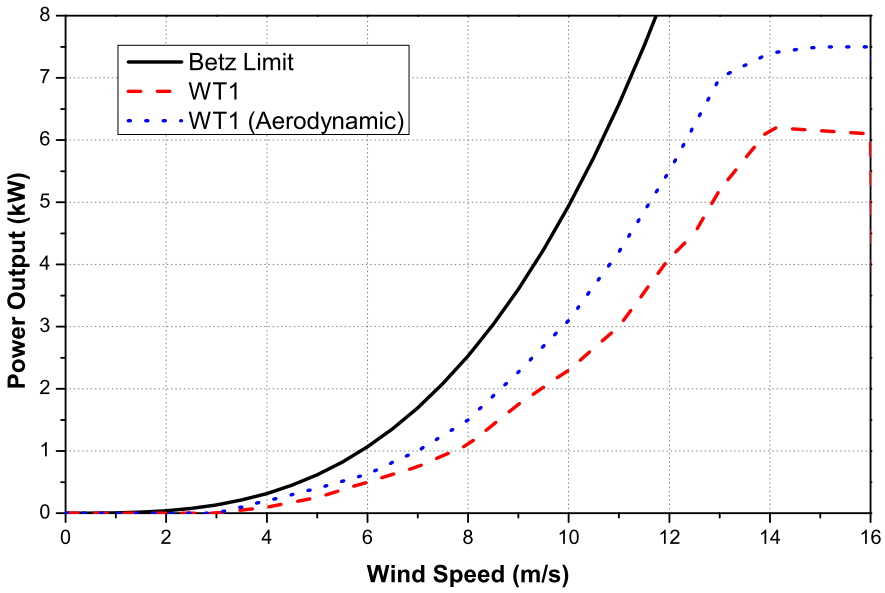

Figure 2.9: *Manufacturer specified power curves of wind turbine WT1.*

b) WT2 (Figure 2.10), a pole-mounted horizontal axis wind turbine (HAWT), with $10kW$ rated power at $11.5^{m}/_{s}$ and a swept area of $40m^2$ [33],

c) WT3 (Figure 2.11), a building-mounted micro HAWT turbine with $600W$ rated power at $9.5^{m}/_{s}$ and a swept area of $2.27m^2$ [26],

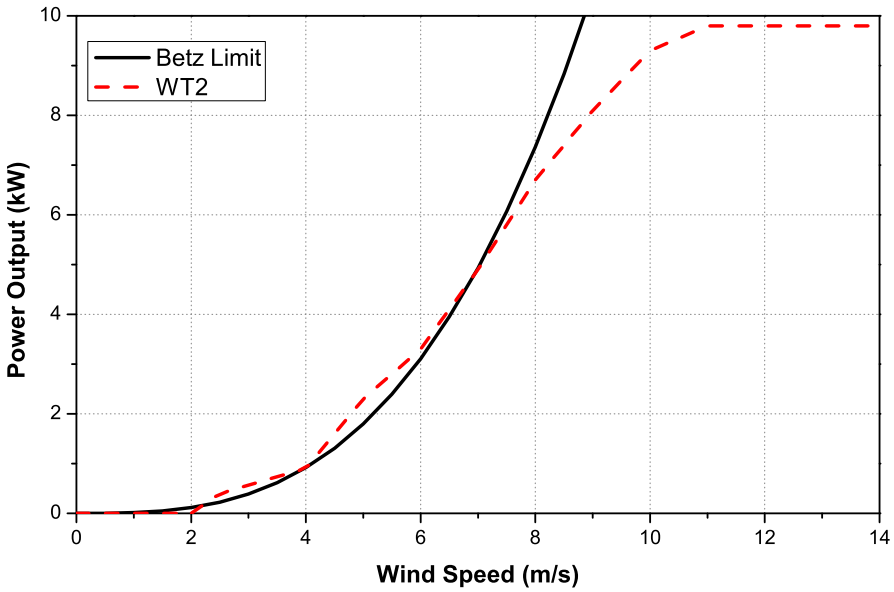

Figure 2.10: *Manufacturer specified power curve of wind turbine WT2.*

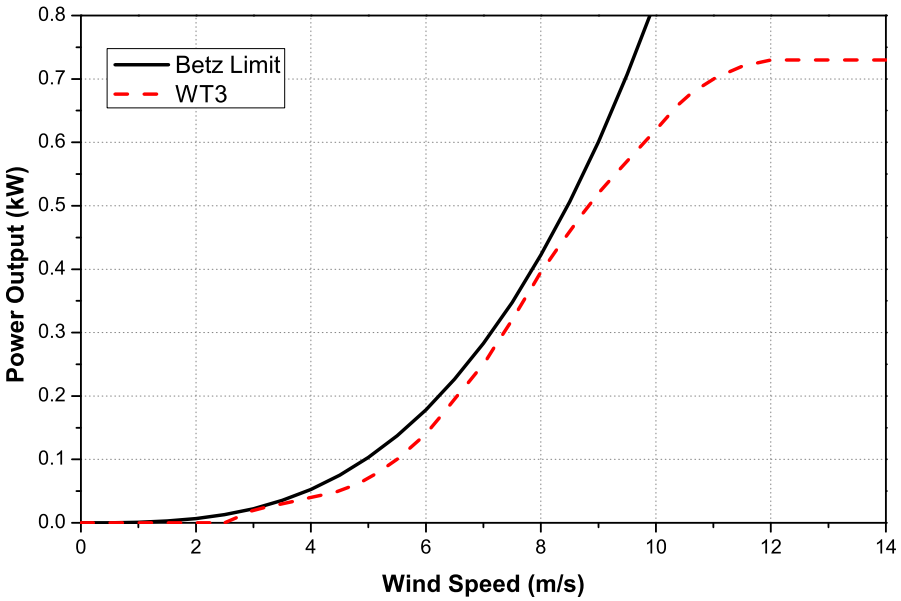

Figure 2.11: *Manufacturer specified power curve of wind turbine WT3.*

d) WT4 (Figure 2.12), a building-mounted micro HAWT, with a peak power of $1.1kW$ at $14^{m}/_{s}$ and a swept area of $2.4m^2$ [34].

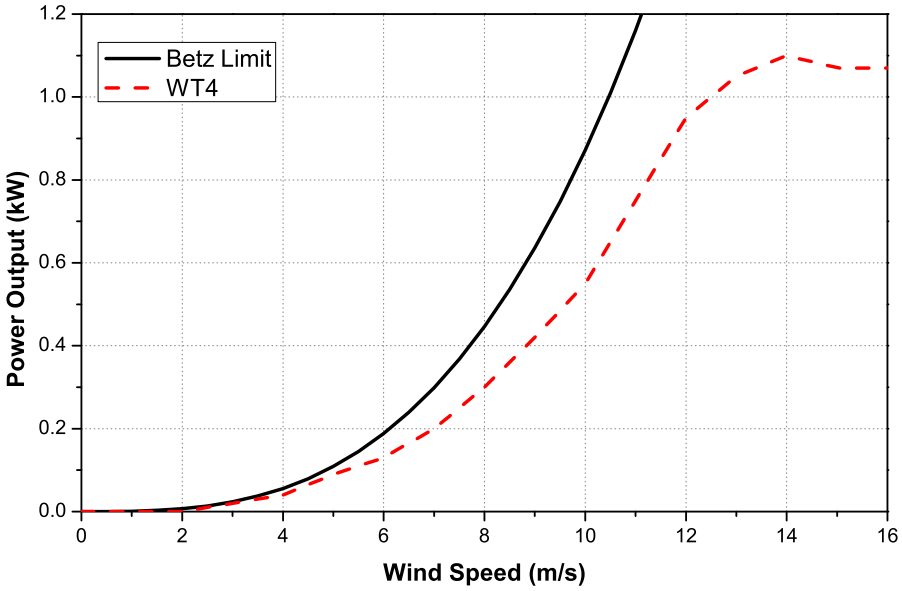

Figure 2.12: *Manufacturer specified power curve of wind turbine WT4.*

The manufacturers of wind turbines provide information on expected annual energy output, which is typically done using the information on rated power outputs for (mean) wind speeds significantly higher than those identified in the measurements at the selected urban sites. In order to provide a more realistic assessment of wind turbine outputs, the UK Government through the Department of Energy and Climate Change (DECC) established the Microgeneration Certification Scheme (MCS) [35]. This scheme certifies all the manufacturers of microgeneration systems powered by renewable energy, confirming through tests the data published by the manufacturers for the power/energy output. This certification process for all the manufacturers is ongoing. Even with the certified turbines, the published data is stated to be very site-specific. Instead of using the mean wind speeds, a more accurate information on power outputs of selected wind turbines can be obtained (i.e. roughly estimated) from the power curves of the turbines for different wind speeds (e.g. from wind speed probability distributions) provided in the manufacturer's technical specification. The provided information on a turbine's power output (averaged over certain time intervals, i.e. $10min$ according to the small wind turbine standard BS61400-12-1 [28]) during normal operation, as prescribed in the wind turbine operations manual. (Figure 2.9 [32], Figure 2.10 [33], Figure 2.11 [26], Figure 2.12 [34]). Actual

power curves of wind turbines show (sometimes substantially) lower power outputs.
The turbine WT1 [32] was selected as it is one of the few small VAWTs available in the UK market and because it is specifically designed for urban wind applications. The turbine WT2 [33] is a bigger pole-mounted HAWT, which can be used in suburban wind applications. The other two micro turbines (WT3 and WT4, [26] and [34]) were chosen in order to allow direct comparison of the results presented in this section with those obtained in [26], which is one of the first studies to indicate the significant overestimation of the UK urban wind resource. Although the overestimation of power outputs is normally caused by an inaccurate wind energy resource assessment, it can be seen that the WT2 has performance above the Betz limit, which will be analysed further in this chapter.

2.4.3.1 Calculation of Annual Energy Outputs

Using the measurements, the Weibull and as previously mentioned the reference Rayleigh distributions, the annual energy outputs of WT1-WT4 have been calculated using their power curves and are shown in Table 2.2. Figure 2.13 (c) shows the calculated energy output for WT3 and the Rayleigh distribution, where the probability distributions are given as fractions for each wind speed so the area below the curve is 1 (100% probability). The annual energy output in MWh is obtained when the distribution is multiplied by 8,760 hours. The energy output in Figure 2.13 assumes 100% availability and neglects the short term variations of wind throughout the day, any turbulence effects and the reorientation of the wind turbine.

2.4.3.2 Overperforming WT2

Figure 2.14 illustrates how the annual energy output of WT2 is calculated: for the assumed mean wind speed of $3.22^{m}/_{s}$ and Rayleigh distribution of annual average wind speeds, aerodynamic power P_{wind} and the corresponding power P_{Betz} (P_{wind} scaled by the Betz factor 0.593) have also been plotted against the calculated WT2 power outputs.
It is evident that the electrical power output of wind turbine WT2 is mostly above the theoretical maximum limits for input mechanical power for the considered wind speeds. Similar concerns about the power curves of wind turbines, i.e. overestimations of turbine output powers, have also been reported and discussed in the Warwick Wind Trials [26]. It can be assumed that the manufacturer of this particular turbine is not providing specification in accordance of [28] testing requirements.

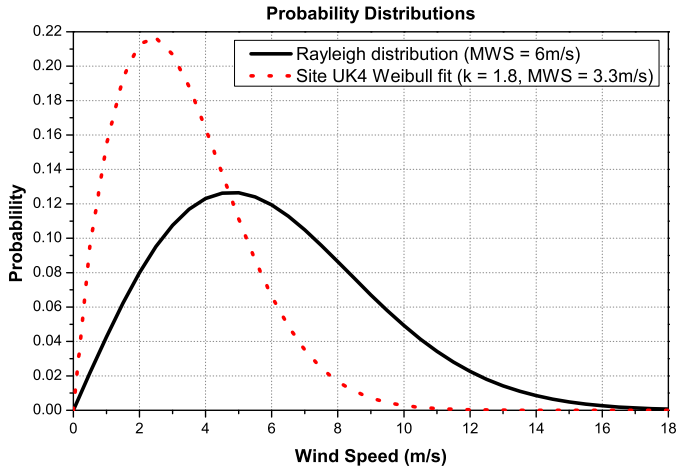

(a)

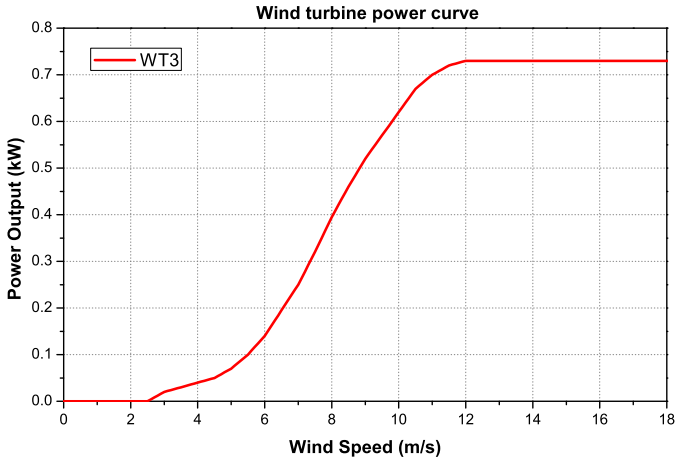

(b)

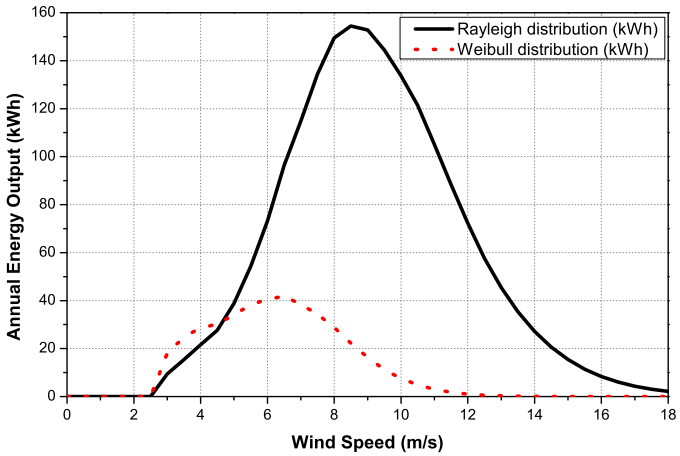

(c)

Figure 2.13: *Calculation of the annual energy output using (a) Rayleigh distribution, (b) WT3 manufacturer power curve and (c) annual energy output for different wind speeds.*

	MWS	k	WT1 Output (MWh)	WT2 Output (MWh)	WT3 Output (MWh)	WT4 Output (MWh)
UK1 (measured)	3.96	-	2.2	14.67	0.69	0.68
UK1 Weibull	4.07	1.95	2.26	15.94	0.75	0.7
UK2 (measured)	3.62	-	1.35	10.86	0.47	0.47
UK2 Weibull	3.72	1.99	1.45	11.48	0.52	0.5
UK3 (measured)	3.29	-	1.06	9.75	0.4	0.4
UK3 Weibull	3.39	1.9	1.14	10.36	0.43	0.42
UK4 (measured)	3.2	-	1.13	9.44	0.41	0.4
UK4 Weibull	3.3	1.8	1.15	10.05	0.43	0.42
UK5 (measured)	3.43	-	1.16	10.09	0.43	0.42
UK5 Weibull	3.53	2	1.23	10.83	0.45	0.45
UK6 (measured)	4.57	-	3.36	17.94	0.94	0.92
UK6 Weibull	4.66	1.75	3.44	18.68	0.99	0.95
Rayleigh ($5^{m}/_{s}$)	5	2	4.41	25.54	1.3	1.21
Rayleigh ($6^{m}/_{s}$)	6	2	7.746	33.74	1.96	1.93

Table 2.2: *Energy outputs obtained with different distributions for the four tested turbines.*

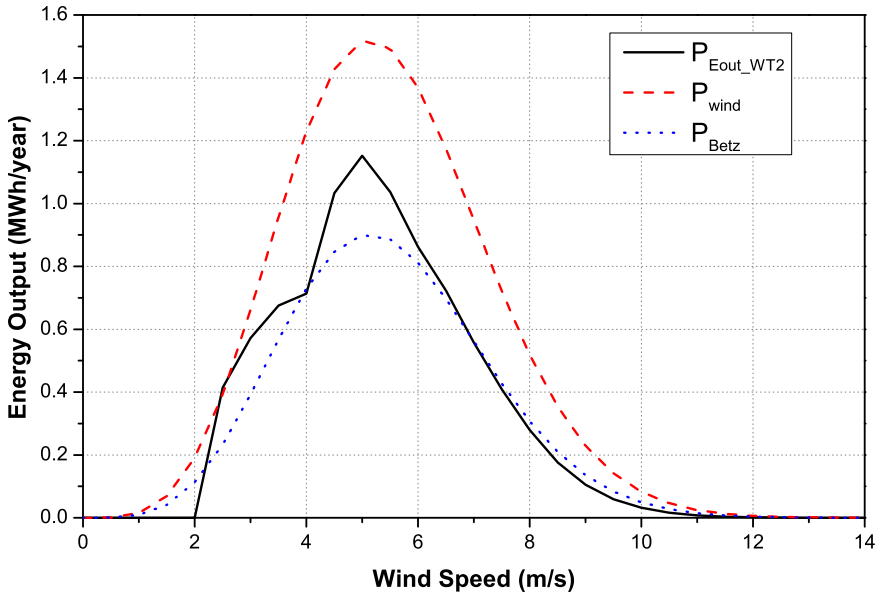

Figure 2.14: *Comparison of the power output of WT2 (P_{Eout_WT2}) with the aerodynamic wind power (P_{wind}) and the maximum/Betz limit power (P_{Betz}) for mean wind speed $3.22^{m}/_{s}$ using the Rayleigh distribution of the annual average wind speed.*

The results presented in Table 2.2 compare the energy outputs calculated for six UK urban sites using the measured wind speed data, the Weibull fit for each site and Rayleigh distributions (with used values of $5^{m}/_{s}$ and $6^{m}/_{s}$) for the four considered wind turbines. It is important to clarify the difference between the Weibull fit mean wind speed and the measured mean wind speed. When the fitting is calculated, the mean wind speed might slightly differ from the measured one in order to properly represent the annual histogram. The results in Table 2.2 show that substantial overestimation of expected annual energy outputs of the selected wind turbines are obtained if the reference mean wind speeds found in NOABL database (these being $5^{m}/_{s}$ and $6^{m}/_{s}$) are used. These two calculations are made for comparison between the measured data and the use of the mean wind speeds found in the database with the recommended Rayleigh distribution without assessing the urban wind resource.

The presented results further show that the annual distribution of average wind speeds at the considered UK urban sites can be accurately described using Weibull distributions, for which factors k and λ have been correctly identified from the measured wind speed data. It should be noted that no attempt has been made in this thesis to assess the effects of turbulence, obstructions, excessive short-term variations in wind speed and the absence of prevailing wind direction(s), as these are highly site-specific factors and should be estimated on a case-by-case basis.

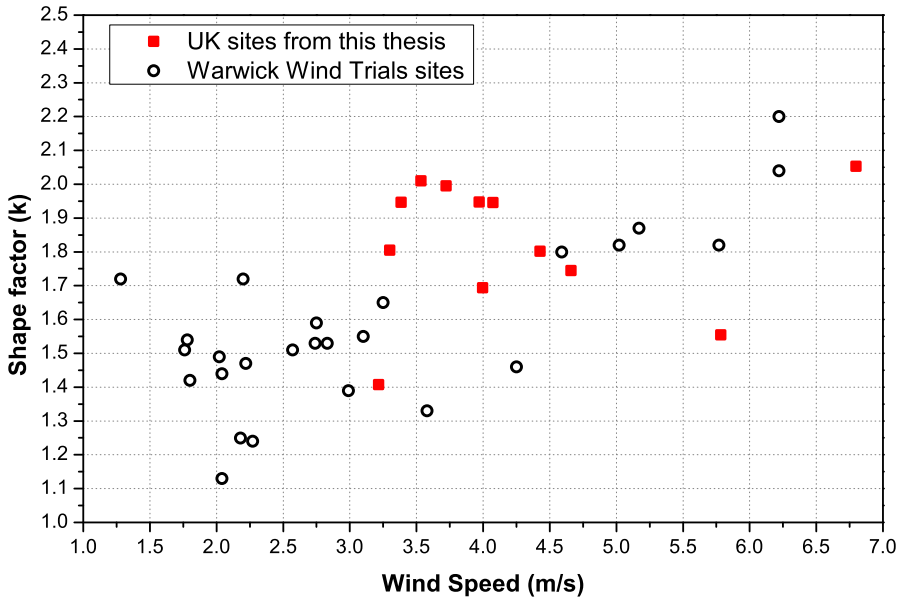

Figure 2.15: *Mean wind speed and shape factor k in the Weibull distribution fits identified in [10], at UK urban sites considered in this thesis and in [26].*

The results shown in Figure 2.15 further confirm that the mean wind speeds are very different depending on the site. However, the shape factor for the UK sites analysed in this thesis were found to be close to a Rayleigh distribution, but if all available data for shape factor k (from this thesis and [26]) are plotted in the same graph the shape factor can vary between 1.1 and 2.2 based on 38 sites. From this figure, similar results as for the mean wind speed are found, the shape factor should be carefully determined to avoid overestimation or underestimation of the energy outputs.

2.5 Edinburgh as the Urban Area for the Analysis

For this thesis, Edinburgh city has been selected as a large urban area for the analysis, assessment and aggregation of PV and wind microgeneration technologies, since the University of Edinburgh has a weather station where solar irradiance and wind speed data are recorded with a resolution of 1-minute. Additional data, provided by the Met Office [31], were also available for other locations within the Edinburgh city area and have been used for the analysis and aggregation strategies as shown in Figure 2.16.

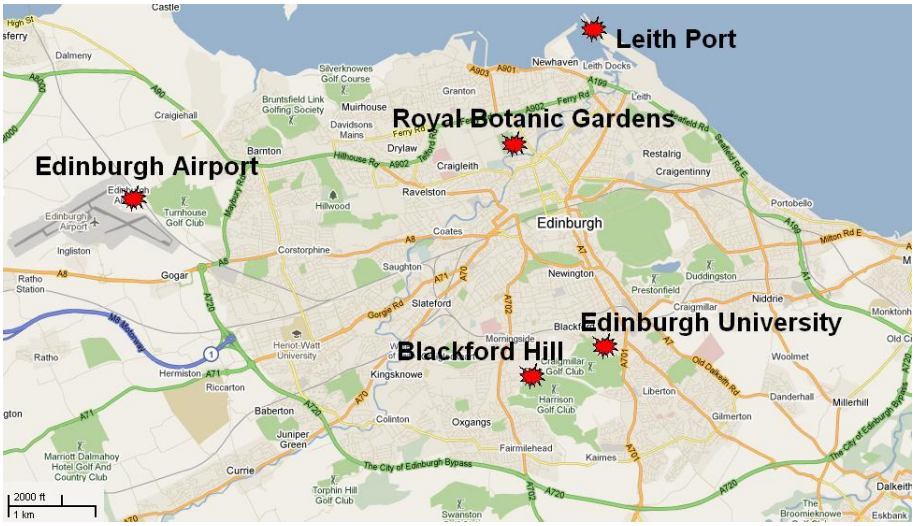

Figure 2.16: *Sites analysed in Edinburgh city.*

2.5.1 The University of Edinburgh Weather Station

Minute-by-minute measurements, recorded during the period between January 2007 and December 2010, were available for one location in Edinburgh (The University of Edinburgh, site

ED1, [8]. The recordings of the weather station include: atmospheric pressure ($mBar$), rainfall (mm), wind speed ($^m/_s$), wind direction ($degrees$), surface temperature (°C), relative humidity ($\%$) and solar irradiance ($^{kW}/_{m^2}$). These measurements are given as 1-minute averaged values and 1-hour averaged values. The 1-minute resolution data are given in four annual data sets, each consisting of $60 \times 8,760 = 525,600$ measurements for three consecutive years and $527,040$ measured values for 2008, since it was a leap year. It is important to note that due to some problems with the logger of the weather station, some values were lost or simply not recorded. Therefore, in order to get full data sets values, available data from previous year were used to substitute the data for the missing periods. The data used in this thesis are solar irradiance and wind speed. As the available wind speed data for all other UK urban sites (obtained from [26]) are related to hourly measurements of average wind speeds, the results for mean wind speeds and annual wind speed distributions obtained using minute-by-minute data and hour-by-hour data for site ED1 are first compared. The bar charts in Figure 2.17 illustrate the very similar annual distributions of average wind speeds measured at 1-minute (Figure 2.17a) and 1-hour (Figure 2.17b) time intervals. Mean wind speed values (i.e. average wind speeds for the whole year) in these two cases are also very close. Additionally, the solid lines in Figure 2.17.a and Figure 2.17.b show Weibull distribution fits for the measured data, i.e. the two Weibull distribution curves that match the measured data most closely. Figure 2.17 shows the small difference between the shape factor (less than 8%) and the mean wind speed (less than 2%) for two resolutions of wind speed data. This difference is due to the way the equipment makes the measurement, the logger measures the average wind speed between one minute span and makes an additional calculation for every hour, these measurement are independent to each other, i.e. the hourly values are not calculated from the minute measurement data. Figure 2.18 additionally illustrates this difference, when a time series of the measured data (i.e. temporary variations) are taken into account. It can be seen that the averaging of the wind speed data results in a loss of maximum/minimum wind speeds measured in a given interval, which has been analysed further and discussed in Chapter 3.

2.5.2 Edinburgh City Data

The analysis described in the preceding section attempted to roughly assess urban wind resources for the UK in general. This section provides a more detailed analysis of the wind energy in urban areas, using Edinburgh city as a particular study case. Using the same Met Office database [31] and the same analytical procedure, the Weibull distribution fits were found for

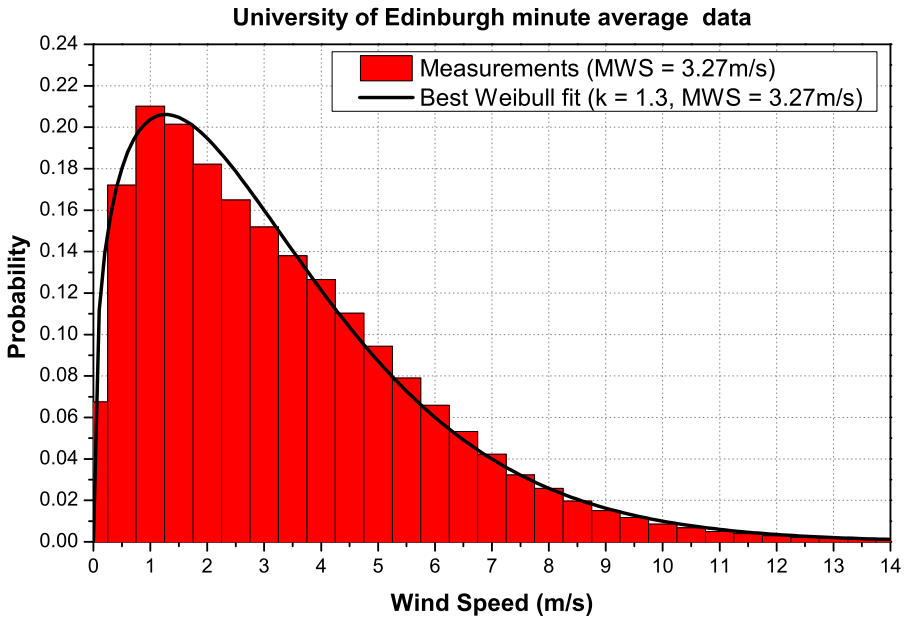

(a)

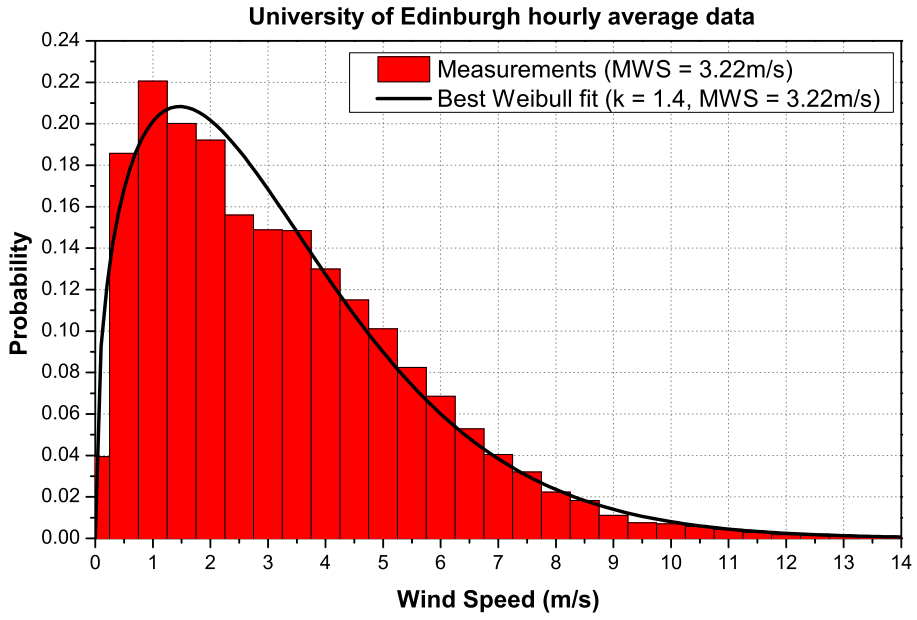

(b)

Figure 2.17: *Comparison of the mean wind speeds and the annual distributions of average wind speeds measured at The University of Edinburgh (site ED1, [8]) based on period of averaging: (a) minute by minute and (b) hour by hour.*

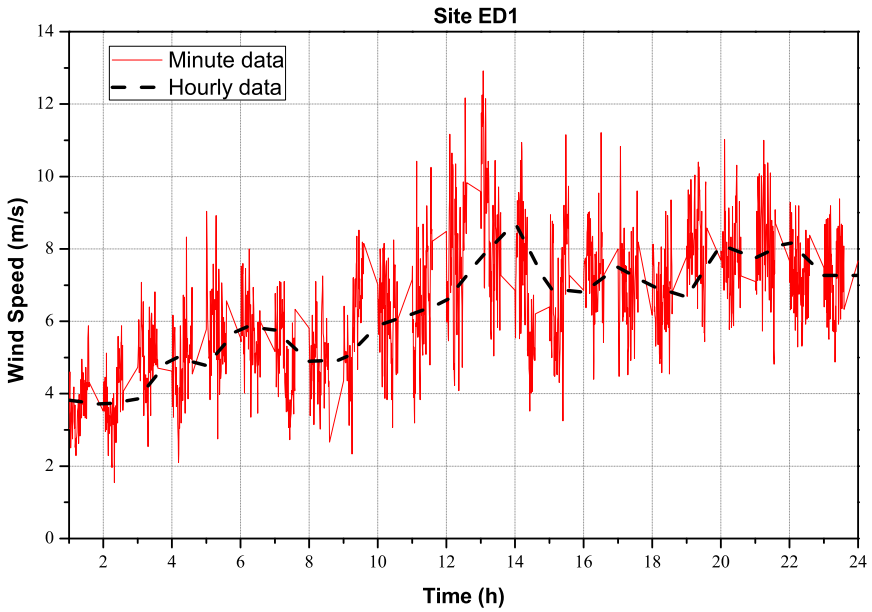

Figure 2.18: *Comparison between the minute-by-minute and the hourly wind speed measurement data for a typical day in Edinburgh [8].*

three additional sites in Edinburgh city area (apart from The University of Edinburgh weather station), Figure 2.19 - Figure 2.23 between January 2007 and December 2010 for sites ED1 to ED4, for site ED5 only one year (2009) was available. This site was considered nevertheless to see the variations in wind speeds across Edinburgh city. At these sites, a relatively wide range of wind speeds is measured: Edinburgh Royal Botanic Gardens (site ED2) is an urban site with less obstructions compared to ED1, Edinburgh airport (ED3), an open site without obstructions, but with lower wind speeds, Edinburgh Blackford hill (ED4), which is a suburban open site without obstructions and Leith port (site ED5) is exposed to strong winds coming from the North Sea. Table 2.3 and Figure 2.16 show the details and location for the Edinburgh city sites considered for this section.

Site	Location	Year	Height above sea level (m)	Latitude	Longitude
ED1	University of Edinburgh	2007-2010	69	55.9229	-3.1731
ED2	Royal Botanic Gardens	2007-2010	26	55.9667	-3.21063
ED3	Edinburgh airport	2007-2010	35	55.9508	-3.34692
ED4	Blackford hill	2007-2010	134	55.9228	-3.1875
ED5	Leith port	2009	6	55.9903	-3.17994

Table 2.3: *Location reference for five analysed Ediburgh city sites [8], [31].*

These results already presented in [10] show that for some sites in UK urban area the wind

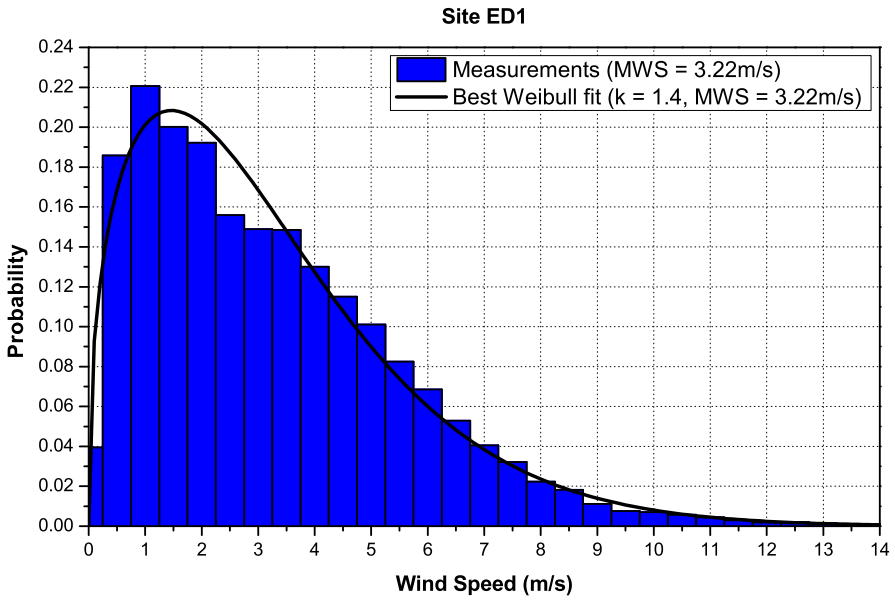

Figure 2.19: *Measured annual distribution of average wind speed at site ED1 in Edinburgh city area: hourly averages, [8] and the corresponding Weibull distribution fit.*

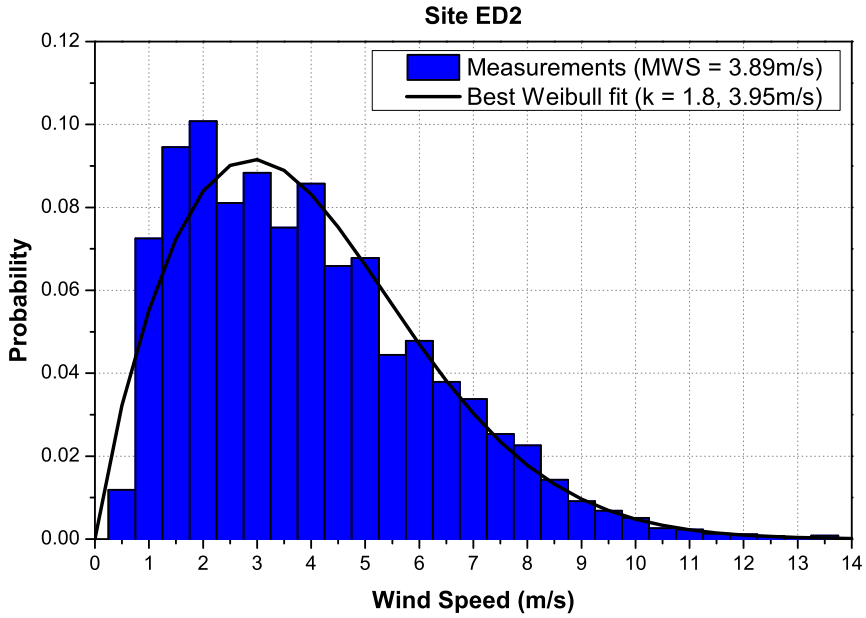

Figure 2.20: *Measured annual distribution of average wind speed at site ED2 in Edinburgh city area: hourly averages, [31] and the corresponding Weibull distribution fit.*

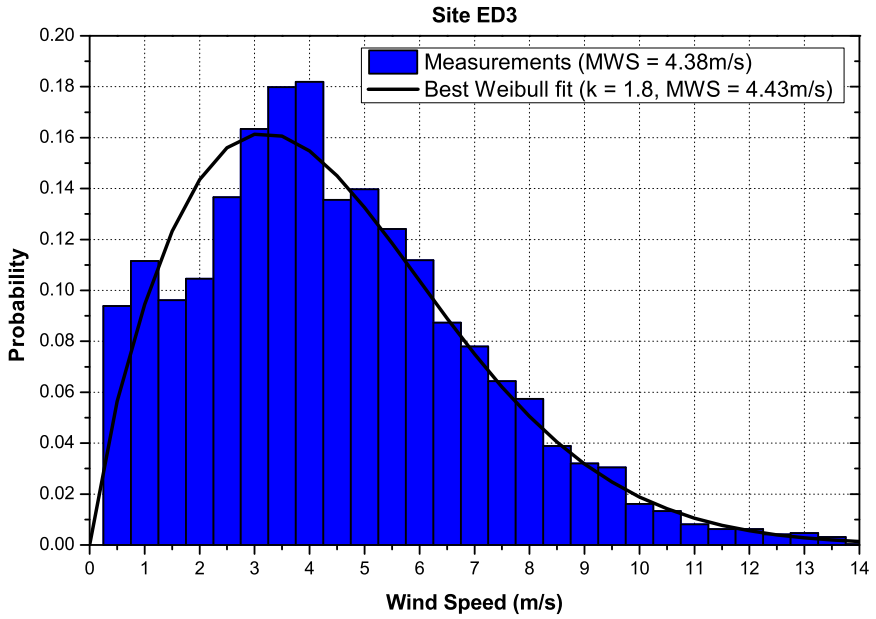

Figure 2.21: *Measured annual distribution of average wind speed at site ED3 in Edinburgh city area: hourly averages, [31] and the corresponding Weibull distribution fit.*

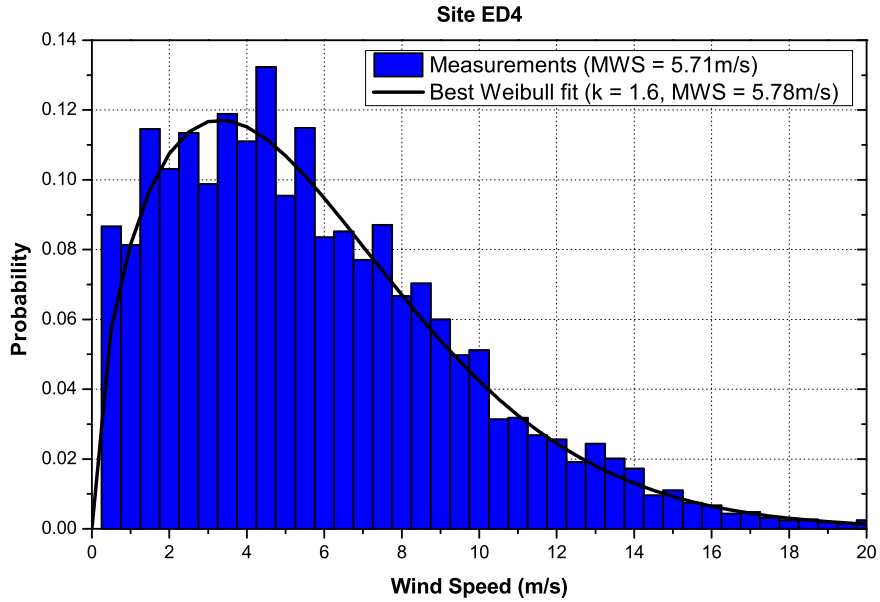

Figure 2.22: *Measured annual distribution of average wind speed at site ED4 in Edinburgh city area: hourly averages, [31] and the corresponding Weibull distribution fit.*

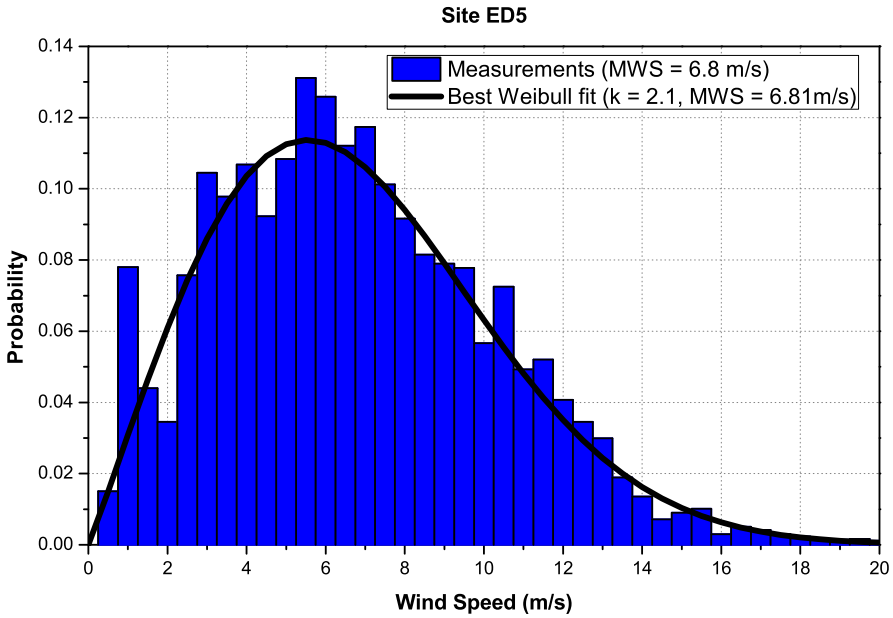

Figure 2.23: *Measured annual distribution of average wind speed at site ED5 in Edinburgh city area: hourly averages, [31] and the corresponding Weibull distribution fit.*

speed can be represented by Weibull distribution fits with shape factors lower than 2. The mean wind speeds throughout a year for each site also show that the wind speeds found in NOABL database for Edinburgh city between $5^m/_s$ and $6^m/_s$ cannot be used for every site in Edinburgh. The windiest site in Edinburgh city was Blackford hill (ED4), with an average wind speed of $5.78^m/_s$ which is good enough for urban areas and in compliance of the NOABL database. However, more urban sites with more building obstructions (e.g. ED1 with $3.22^m/_s$) have lower mean wind speeds, which for some wind turbines may be below the cut-in wind speed. As RenewableUK suggests, a proper assessment with measurements should be done for every site.

2.5.3 Turbulence Impact on Small-scale Wind Turbines

The previous section presents the probabilistic distributions commonly obtained for wind energy applications. The methodology followed in this thesis intends to aggregate or unify the wind speed profiles to be used as an input for a time-series simulation on wind power production. Before presenting this analysis it should be discussed why the methodology in this thesis does not consider the effect of turbulence into account. Turbulence effects on wind turbines, especially those installed in urban area, depend on the intensity of the turbulence, the wind

speed and the wind turbine characteristics. It is not easy to quantify or introduce the turbulence across different sites at different heights and different seasons. The interaction of a small wind turbine with turbulence is very complex and will depend primarily on the wind turbine characteristics [36].

Lubitz [36] presented a trial on different levels of turbulence for small wind turbines. Turbulence depending on the Reynolds number (research that will not be extensively presented in this thesis) can be classified as low turbulence (turbulence intensity less than 0.14) and high turbulence (turbulence intensity higher than 0.18) according to the ASCE 7-98 standard [37]. It was found that low turbulence reduced the power output by around 2%, for wind speeds between $4\ ^{m}/_{s}$ and $7\ ^{m}/_{s}$. Interestingly high turbulent wind for wind speeds between $4\ ^{m}/_{s}$ and $7\ ^{m}/_{s}$ produce an increase in the power output of a range up to 4%. This means that high turbulent wind produces more power at low wind speeds and aids the turbine to reduce the cut-in wind speed. These results are consistent with the ones found in [38] and [39].

Aditionally, Smith [40] using performance measurements from the National Renewable Energy Laboratory (NREL), analysed the data from seven wind turbines for different levels of turbulence. These data were used to obtain annual energy production, as it is done in section 2.4.3.1 in this chapter, and found that the turbines showed a 9% to 32% decrease in energy output depending on the level of turbulence. Only one turbine exhibited an increase in the energy output at higher levels of turbulence. Therefore, this thesis assumes that averaging effects of both increased and decreased power outputs of a number of small wind turbines placed over a larger area due to turbulence, allow to exclude turbulence from the analysis. However, if the effects of the turbulence on a large number of wind turbines become available, this could be easily included in the presented analysis.

2.5.3.1 Wind Gusts

Wind gusts are also an important issue when it comes to small wind turbines installed in urban area. The wind gust is a rapid change in the wind speed and/or wind direction, which as an aspect of turbulence, can affect the performance of the wind turbine. Many authors have found that when the wind gust lasts for less than a second, it does not impact the power output of the turbine [36]. Furthermore, the effects of a rapid change in wind speed depends entirely on the inertia of the wind turbine and its controls, which sometimes has difficulty to respond to a short time scale turbulence event [41]. It is also reported in [42] that there is a limited understanding on the extent on which small wind turbines respond to the rapid change in wind speed and the

extraction of energy of the wind gust.

Turbulence is an issue that has to be carefully considered before being generalised. The results found in literature conclude that depending on the turbine characteristics the effects of turbulence vary. Therefore, turbulence will not be taken into consideration in the presented analysis, since it is very difficult to generalise and simplify the effects of turbulence to be adopted by the methodology presented in this thesis. The turbulence has impact on the wind turbine alignment, airfoil performance and power production and it is not the purpose of this work to detail the turbulence, but to generate a generalised methodology for power flow analysis and quantification of micro and small-scale generation in distribution networks. However, the results found may be additionally processed to consider a lower or higher energy/power production depending on the sites and the turbines.

2.6 Time-series Wind Speed Analysis for Edinburgh City

Wind energy resources exhibit significant short, medium and long-term variations (i.e. hourly, daily, weekly and inter-annual variations). It is, therefore, necessary to perform temporal assessment of wind energy resources by taking into account both daily (time of the day) and seasonal (day of the year) variations. The Weibull distribution provides the wind speed performance throughout a year for a given site and this is used for the energy yield calculation, as presented before using the wind turbine power curve. However, this approach is not useful for the purpose of assessing time-varying electricity production. It is therefore, necessary to represent the wind speed as wind profiles, assigning to these profiles temporality and spatiality associated with the time of the day, the season of the year and the location of the considered sites. Apart from the Met Office data found in urban area, there is a lack of wind speed measurements available to make a detailed assessment of the wind behaviour in urban areas. This section shows a quick assessment of the wind energy resources and build wind profiles for Edinburgh city.

Using the data from the five sites (ED1-ED5) for the same year of measurement, Figure 2.24 to Figure 2.27 present 28 days of hourly wind speed measurements for each site depending on the season of the year. Each season consists of three months, so a day in the middle of the season (i.e. the middle day in Spring is the 14th of April) is used. Then, the wind speed measurements are plotted together with the range of ± 14 days (14 days before and 14 days after a day representing a given season), in order to assess the expected range of variations in the daily wind

speeds at all sites within each season.

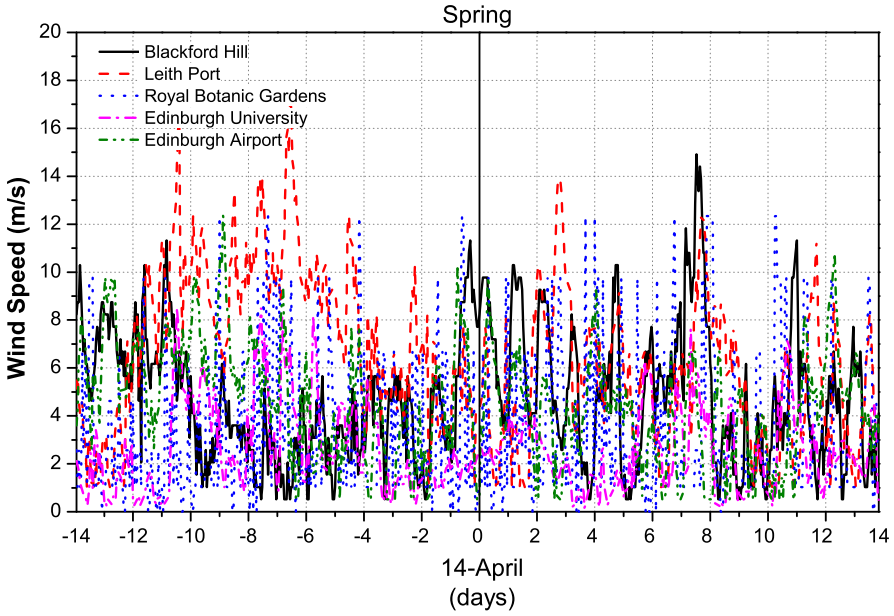

Figure 2.24: *Wind speed measured at all Edinburgh sites ±14 days around the 14^{t}h of April, representing Spring.*

The five sites around Edinburgh city with very different wind exposure show the maximum and minimum hourly averaged wind speeds during the 28 days period. This analysis intends to identify the variability in available wind energy resources, in an attempt to aggregate the city's wind resources into a single-day wind profile. For this purpose, it is assumed that these five sites represent the wind energy resources in Edinburgh city as a whole.

2.6.1 Temporal Assessment: Range of Wind Speed Variations

The ±14 days of wind speeds are used to build three ranges of wind speeds for each season and each site, these ranges being: average, minimum and maximum. Each range is calculated considering the maximum and minimum values at each hour from the considered 29 days window, while the average range is obtained as the arithmetic mean for each site, as equation (2.9) describes.

$$MWS_k = \frac{1}{n}\sum_{i=0}^{n}(h_k)_i \tag{2.9}$$

where, k is the hour of the day (k = 1 to 24 hours) when the mean is calculated i.e. same hour of the day for the 29 days; n is the number of days used, in this case 29 days; h_k is the hour k of the day i for the given site.

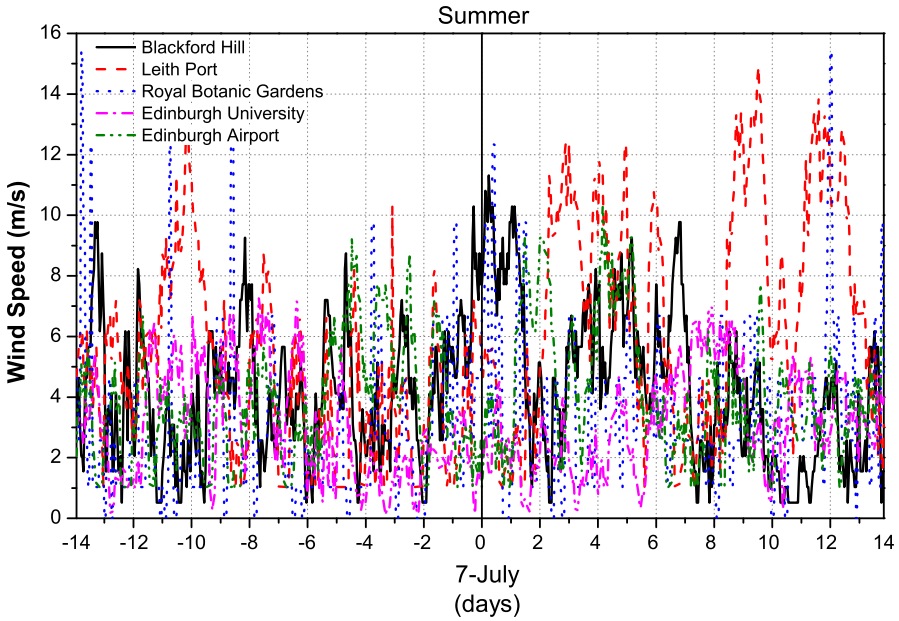

Figure 2.25: *Wind speed measured at all Edinburgh sites ±14 days around the 7^{t}h of July, representing Summer.*

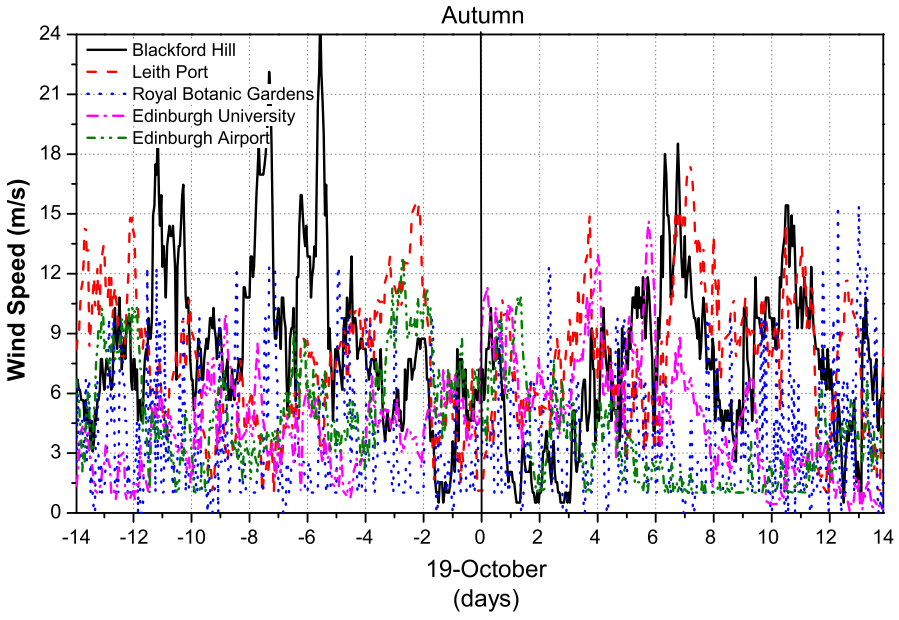

Figure 2.26: *Wind speed measured at all Edinburgh sites ±14 days around the 19^{t}h of October, representing Autumn.*

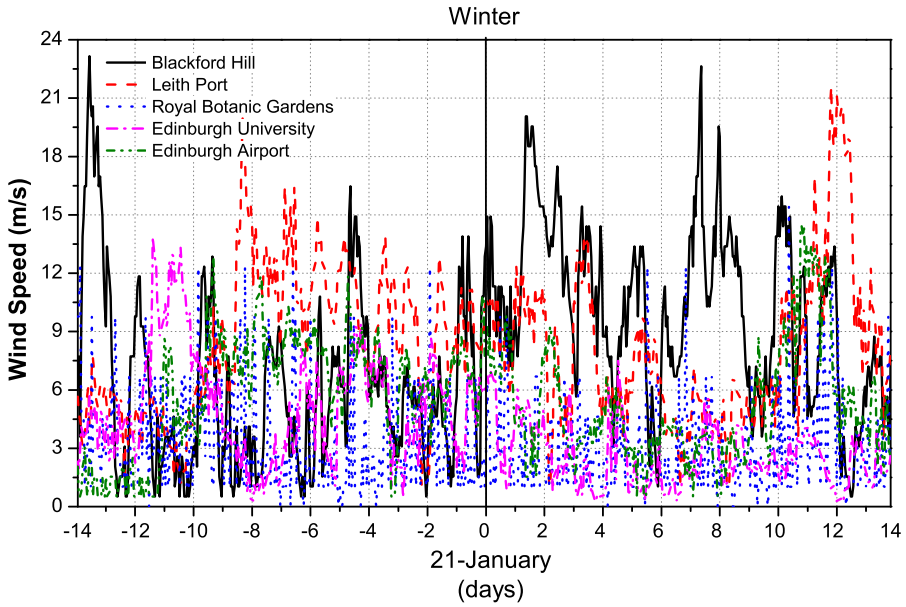

Figure 2.27: *Wind speed measured at all Edinburgh sites ± 14 days around the 21^th of January, representing Winter.*

Using these calculated maximum, average and minimum profiles per site, Figure 2.28 to Figure 2.31 show the envelope of wind speeds expected in each season for all sites, showing three ranges: the maximum, the average and the minimum wind speeds that can occur over the whole urban area of Edinburgh.

The purpose of analysing these sites in urban area is to obtain an aggregated wind profile for Edinburgh city with a small amount of data per season. Therefore, from the presented ranges, a single-curve representation is calculated by the arithmetic mean of the values within the envelopes. These new plots are presented in Figure 2.32 to Figure 2.35, giving the ranges of maximum, minimum and average wind speeds for the whole city of Edinburgh for each season.

The single-curve plots show the difference in wind speed between seasons for the whole city of Edinburgh. The average value for Edinburgh city is around $4\ ^m/_s$ for Spring and Summer and around $6\ ^m/_s$ for Autumn and Winter, this approach provides a single value of mean wind speed that can represent the city of Edinburgh per season with maximum and minimum mean values expected for the city as a whole. The analysis has some advantages such as: a small period of measurement is required to carry out the procedure and also provides general information on how the wind speed performs in the city more accurately than the wind speeds suggested by the NOABL wind database , also providing a time-domain wind speed profile that includes

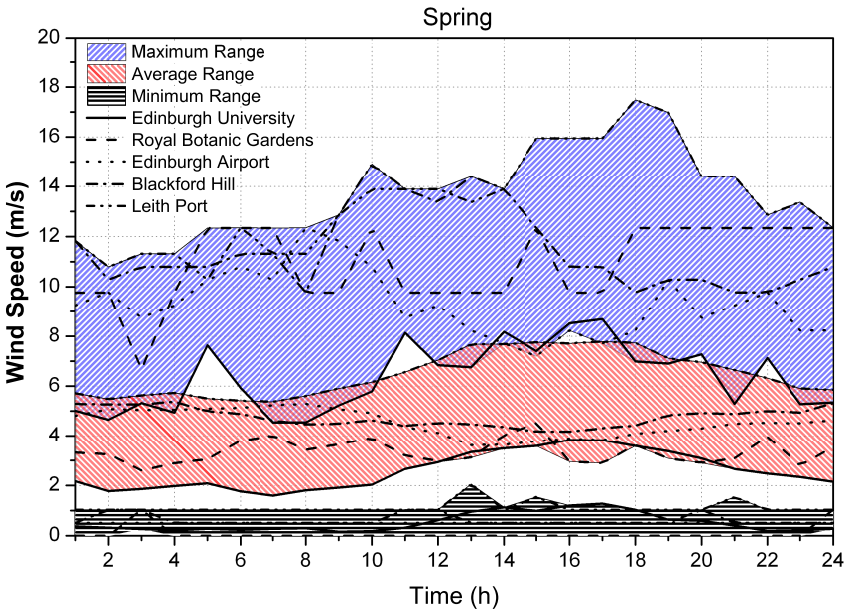

Figure 2.28: *Range of maximum, average and minimum daily wind speeds for all sites in Spring.*

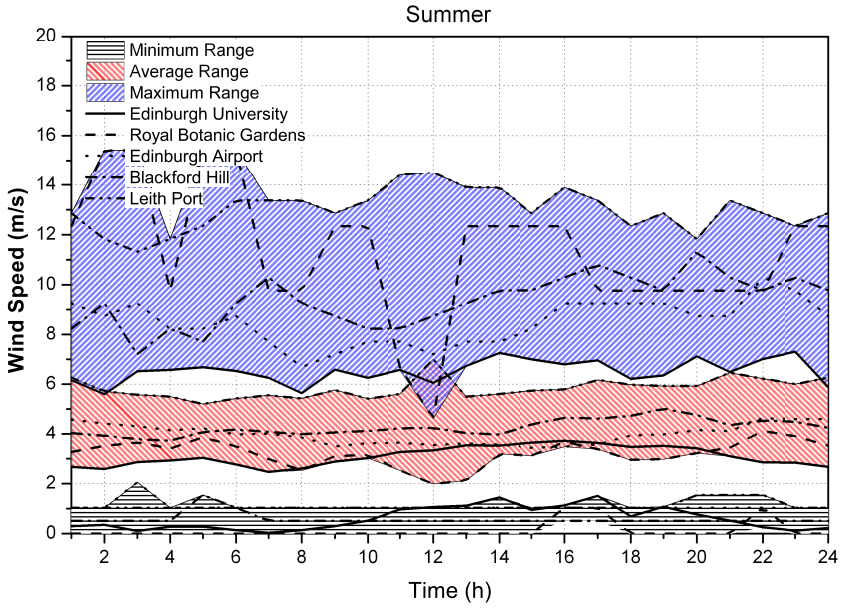

Figure 2.29: *Range of maximum, average and minimum daily wind speeds for all sites in Summer.*

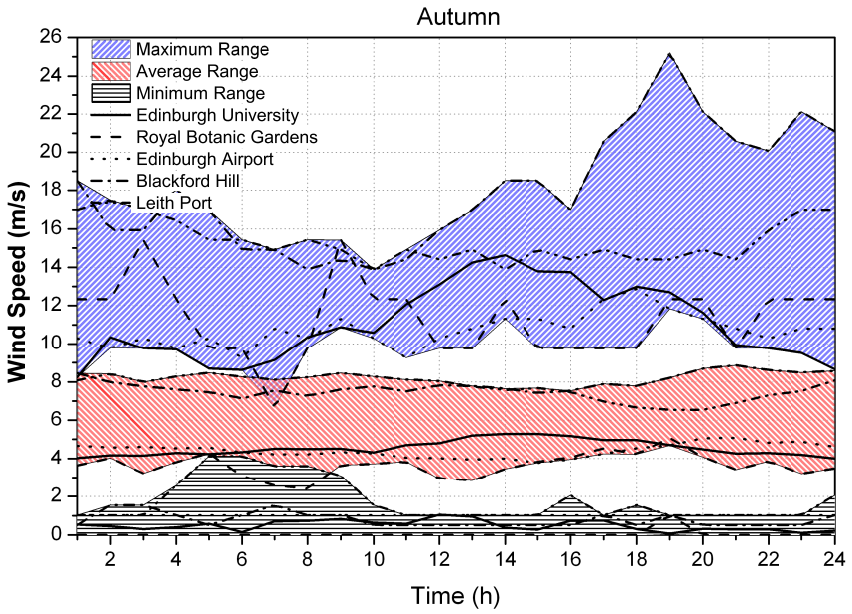

Figure 2.30: *Range of maximum, average and minimum daily wind speeds for all sites in Autumn.*

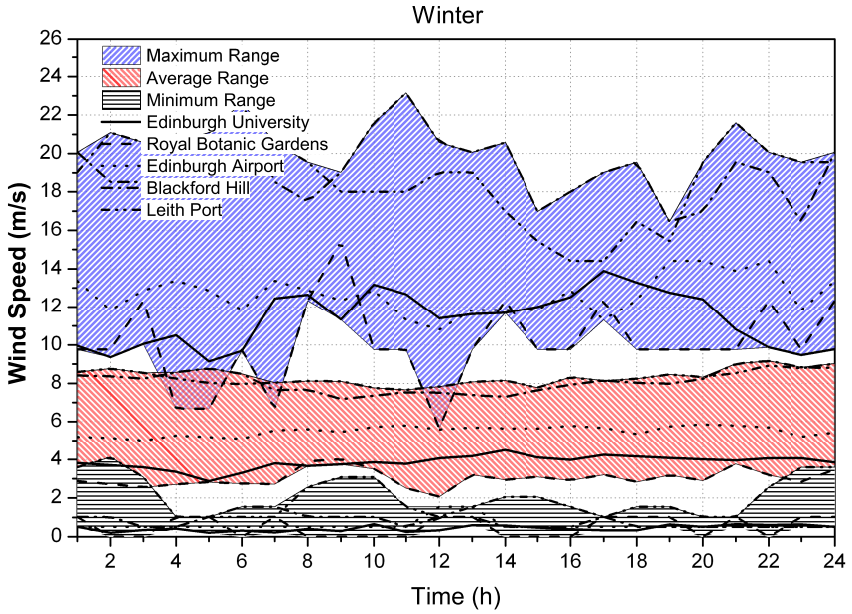

Figure 2.31: *Range of maximum, average and minimum daily wind speeds for all sites in Winter.*

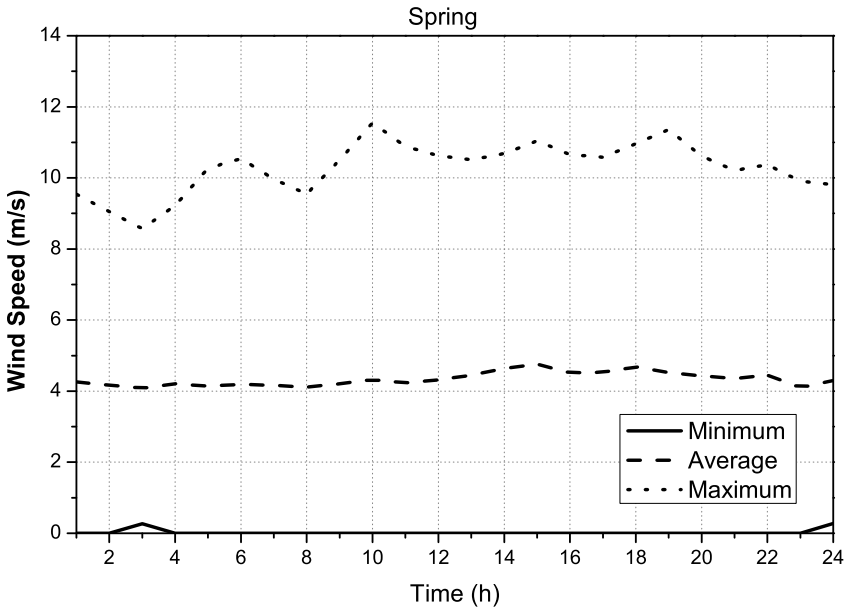

Figure 2.32: *Average values for maximum, average and minimum daily wind speeds for all sites in Spring for the whole city of Edinburgh.*

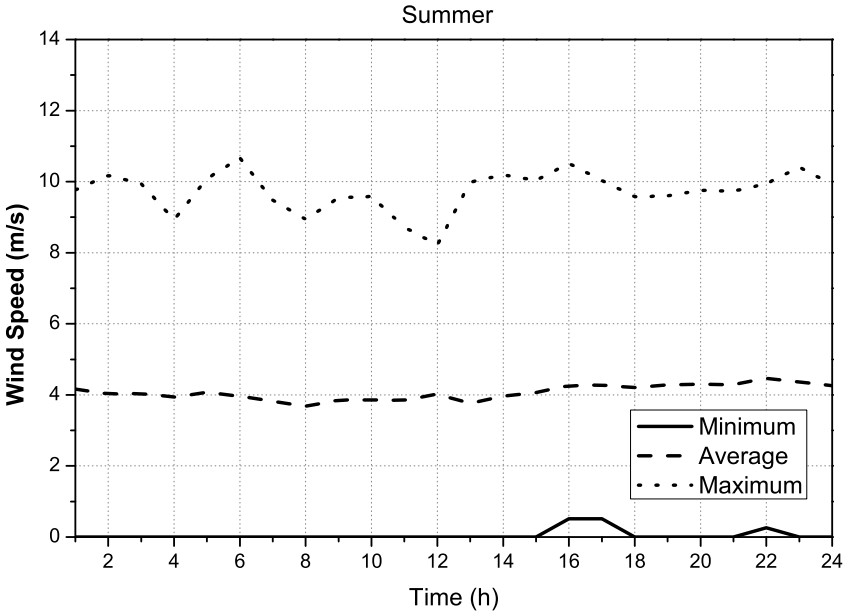

Figure 2.33: *Average values for maximum, average and minimum daily wind speeds for all sites in Summer for the whole city of Edinburgh.*

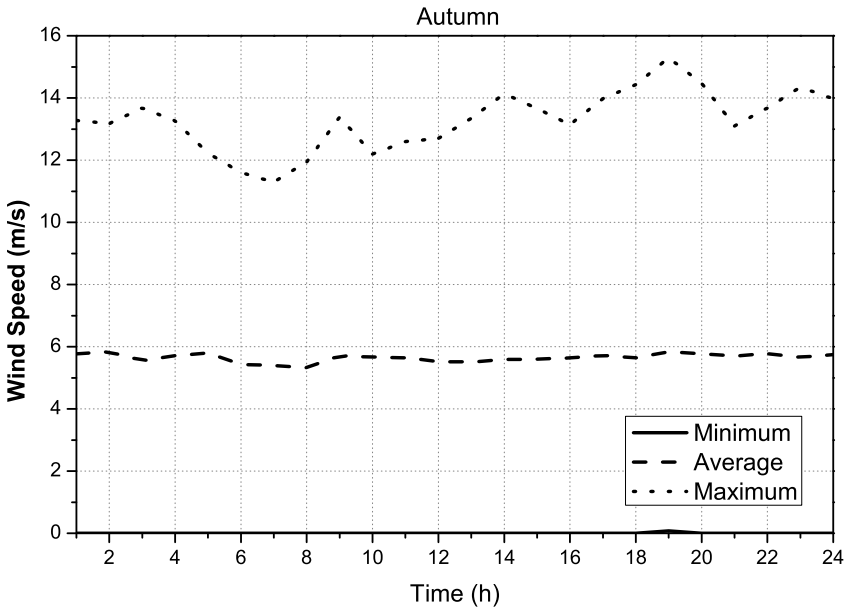

Figure 2.34: *Average values for maximum, average and minimum daily wind speeds for all sites in Autumn for the whole city of Edinburgh.*

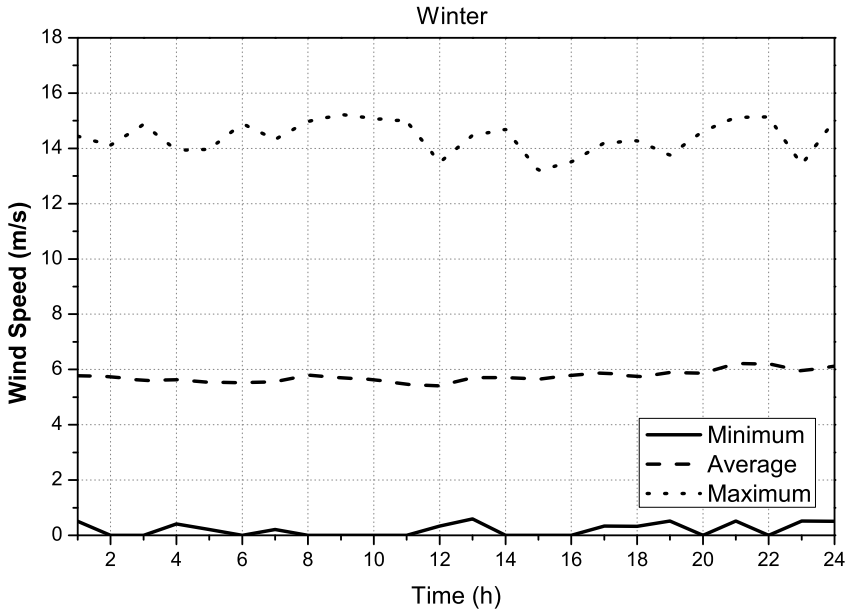

Figure 2.35: *Average values for maximum, average and minimum daily wind speeds for all sites in Winter for the whole city of Edinburgh.*

the stochastic behaviour of the wind in a short-term (1 hour) time frame. However, the diurnal variation of the wind per season is somewhat lost, as it is to be expected due to the reduced considered time, the Spring and Summer present an apparent variation throughout the day than the variation found in Autumn and Winter, showing a trend.
The presented approach is used since the measurements of urban wind speeds are not widely available and one of the sites considered for Edinburgh city is not available for more than one year. It should be noted that ± 14 day averaging window could be used to calculate a range of expected wind speed variations for any specific day in the year, providing a range of expected maximum, minimum and average wind speeds for each hour of the considered day.

2.6.2 Temporal Assessment: Diurnal Variations

Daily wind profiles have been identified for the considered Edinburgh sites and classified by season in the previous section, representing the wind profile for Edinburgh city as a whole. These profiles show almost full absence of diurnal variations due to a small window of data considered (i.e. only 28 days) and the averaging of the sites around Edinburgh city. One of the purposes of this analysis is to relate variations in wind speed with variations in load demand through calculated wind electricity generation. This section demonstrates that the same analysis could be used to confirm the presence of diurnal variation if longer data set are applied.
To generate the wind profiles for diurnal variations, the analysis includes the four years of data found for Edinburgh city. The site ED5 is not used in this section, because only one year of data is available. The remaining four sites are then used to provide an average wind profile. Using the same approach as in the previous section, but increasing the time window to three months to consider the complete season over the four years of data, an average is made to obtain a profile per season for each site. This average is calculated with equation 2.9 using the three months of the season for the four years of available hourly data.
The daily wind speed distributions (wind speed profiles for four seasons) are plotted in Figure 2.36 to Figure 2.39. These profiles lost the stochastic maximum/minimum details from hour to hour, found in the previous section, but clearly show the different diurnal variation values throughout the seasons and average hourly wind speed values for each site.
Figure 2.37 shows that Summer has the lowest wind speed in a year, whereas Autumn (Figure 2.38) and Winter (Figure 2.39) show more constant wind speeds over a day. However, during Spring (Figure 2.36), the diurnal variation peak in the afternoon can be observed, with low wind speeds during the night and morning hours. The afternoon and evening hours are

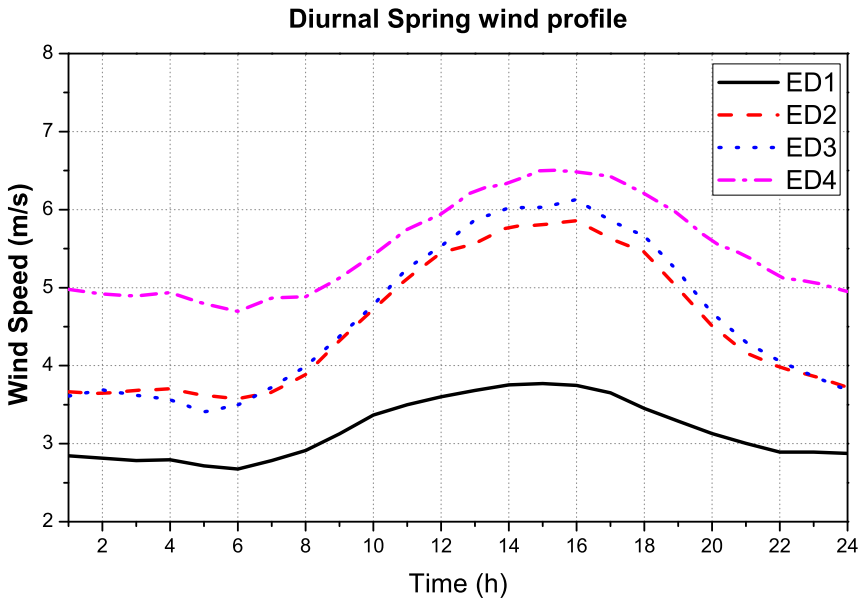

Figure 2.36: *Wind profile of Spring for the 4 selected Edinburgh city sites.*

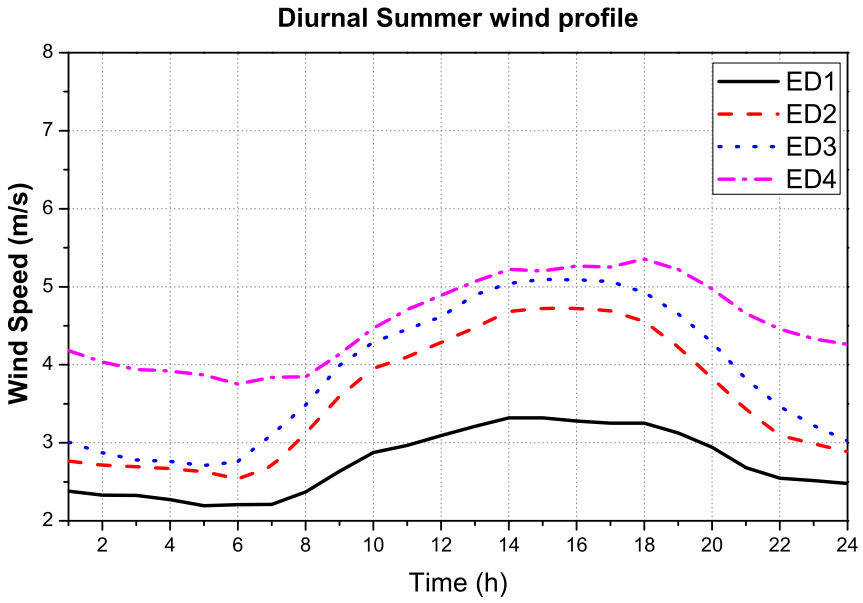

Figure 2.37: *Wind profile of Summer for the 4 selected Edinburgh city sites.*

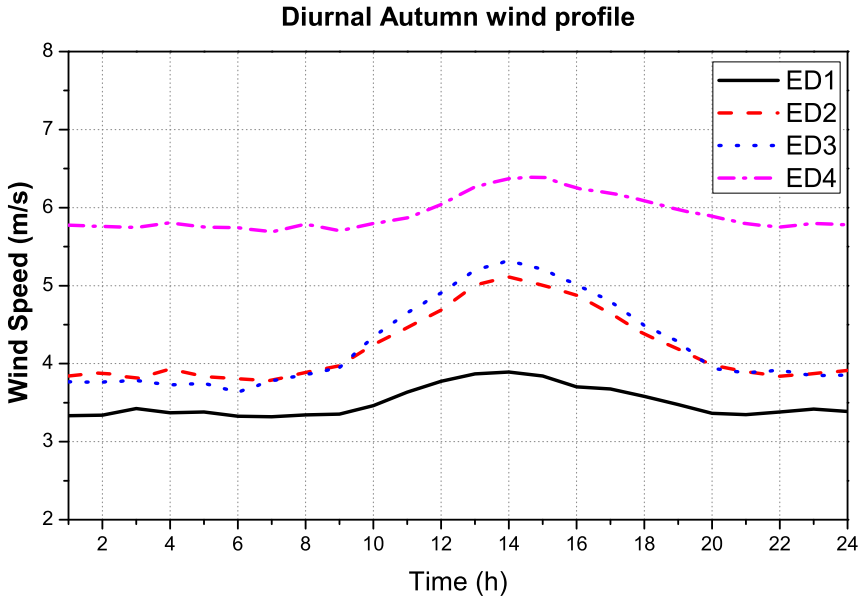

Figure 2.38: *Wind profile of Autumn for the 4 selected Edinburgh city sites.*

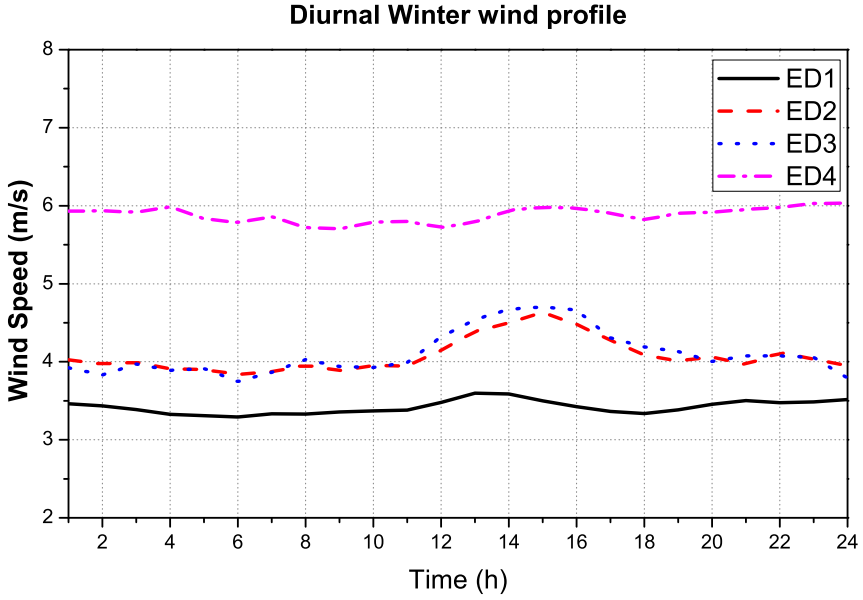

Figure 2.39: *Wind profile of Winter for the 4 selected Edinburgh city sites.*

windy, resulting in increased energy outputs.

The presented approach takes advantage of the available wind data to provide a more detailed wind profile per site. Considering the difference in wind speed and the geographical location of every considered site, they can be now classified in sub-sectors, representing the "highly-urban", "urban", "suburban" and "rural" areas around Edinburgh city. This is done in order to assess variations in the wind energy resource at different geographic locations (spatial variations) and to allow location-specific analysis of the distribution networks to which the wind-based microgeneration systems are connected. The four considered sites are represented in the following way: highly-urban (ED1), urban (ED2), suburban (ED3) and rural (ED4) locations. Section 2.5.2 provides more details about the sites and why this classification is assigned.

2.6.3 Method Comparison

The previous sections have presented two different approaches to the data for Edinburgh city. Both methods have different purposes, as the 29 days (range of wind speed variation) intends to aggregate Edinburgh city as a whole with maximum, average and minimum profiles to assess the wind speed that can be expected in the city. The other approach (diurnal variation) takes advantage of the availability of 4 years of measurement that helps creating an average profile for every season and for each site with the expected diurnal variation.

The applicability depends on the differences and limitations of both methods to understand how they could actually be used. Just to make a comparison (not that this is the manner to use the profiles in this thesis) an arithmetic mean of the temporal assessment profiles is obtained to only use a single curve per season. Figure 2.40 shows the comparison of these two approaches, plotted together per season and showing how different are to each other.

It can be seen from Figure 2.40 that the diurnal variation is more evident for Spring and Summer in the case of the temporal assessment. The range assessment profiles however, present a very small variation that is almost lost due to the small period of time used for building the profile. The average daily values are shown in Table 2.4 and for Spring and Summer the values are very close to each other. The biggest difference comes when Autumn and Winter seasons

Mean Wind Speed ($^m/_s$)				
	Spring	Summer	Autumn	Winter
Diurnal profiles	4.21	3.69	4.46	4.37
No-Diurnal profiles	4.34	4.07	5.64	5.75

Table 2.4: *Mean wind speed calculated for each profile per season.*

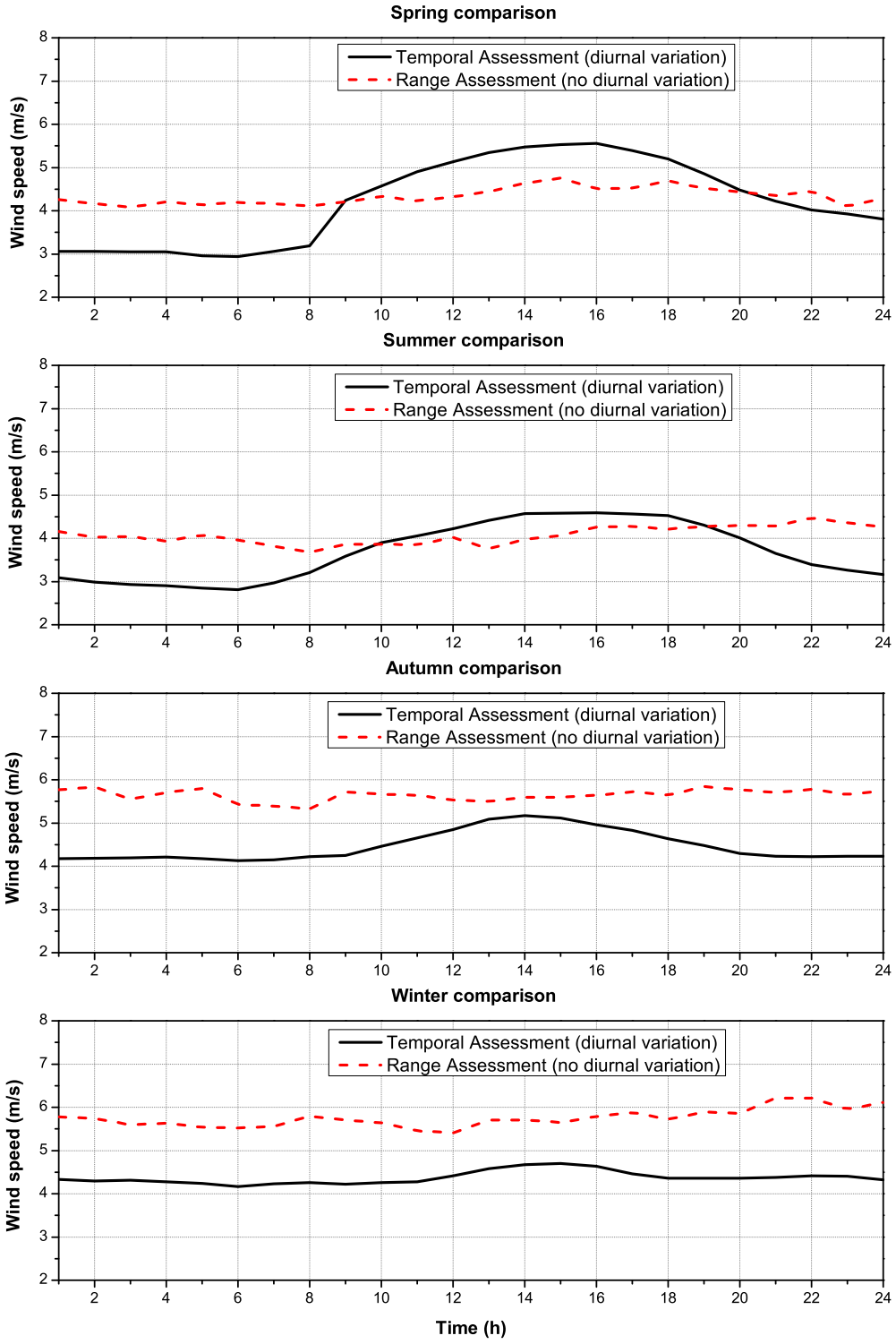

Figure 2.40: *Comparison of the temporal assessment and range assessment wind speed profile approaches for Edinburgh city sites.*

are compared. For both profiles the range assessment gives values higher than the temporal assessment and it can be appreciated in Figure 2.40, but also the values found in Table 2.4 show a higher wind speed obtained from the range assessment profiles. The diurnal variation is also present but as it can be observed from Figure 2.38 and Figure 2.39 the diurnal variation for these two seasons is not as evident as Spring and Summer.

These two approaches are going to be used to correlate in time the load profile with wind generation. Both methodologies present limitations that should be understood before applying them for the mentioned purpose. The range assessment is intended for situations when a limited amount of data is available for different sites, this approach allows using the small amount of data per season for a quick assessment of the wind speed in a city like Edinburgh. The diurnal variation although generally lost, it can be slightly appreciated. The main advantage comes when the maximum and minimum calculations are provided. The data coming from 5 different sites gives this method an advantage when spatial aggregation is applied since considers the wind speed for all of the sites providing a maximum average useful for obtaining maximum steady-state power production. On the other hand the main limitation is the availability of many sites (even if it is for small period of time), the lost of the diurnal variation and the assumption that wind turbines are uniformly distributed across the sites, but this could be changed using a weighted average if the number of turbines per site is known.

The temporal assessment uses the 4 years of data available for Edinburgh city. This method provides detailed information on the diurnal variation and the shape of the wind during this period of time per season. The analysis in this case conveniently also features the 4 sub-sectors (as Chapter 6 classified the network) in which the city has been divided. The load profile is produced based on statistics of many years of data as it will be described in Chapter 6 which allows this methodology to be easily correlated with those profiles. However, this analysis is limited in the maximum possible wind speed that can be expected in Edinburgh, there is no aggregation in the wind resource and the profile depends on large amounts of measured data to be built.

Knowing the limitations and the differences between them, these approaches will be later used as an input to the wind generation model to feed the electricity grid, correlating the site with the appropriate distribution network sub-sector and load profile.

2.7 Solar Irradiance

Solar energy is the most abundant energy resource on Earth. The solar energy that hits the Earth's surface in one hour is about the same as the amount consumed by all human activities in a year [43]. The analysis similar to the previously presented assessment of wind energy resources has been carried out for the assessment of solar irradiance resources. However, in the case of solar irradiance, the availability of measured data is limited, since solar irradiance is not typically measured by the Met Office. Therefore, online "solar calculators" are used for this purpose. Using the data from the University of Edinburgh weather station [8] and the online calculator from the European Commission [9], the analysis of the solar resource focusing on Edinburgh city has been performed and is presented in this section. A comparative study of the online calculator data and the actual measurements is also presented.

2.7.1 Measurements and Online Calculators

As previously mentioned, the measurements at the University of Edinburgh weather station cover a range of parameters one of them being the solar irradiance. It was measured as 1-minute and 1-hour averaged data for the period between 2007 and 2010. Figure 2.41 shows the raw solar irradiance data for all the four years, comparing 1-minute measurements and hourly measurements. It can be appreciated how the averaging process reduces the maximum solar irradiance measured, similar reduction was identified for wind in Figure 2.18. An increase in solar irradiance in the middle of the year (Summer) and low values at the end of the year (Winter) can be seen in Figure 2.41.

When the data from all the years are averaged into a single day (i.e. when annual average values of the measured solar irradiance at specific hours of the day are calculated over a year) and compared, only a small difference between the different years is seen. Figure 2.42 shows the comparison of the four analysed years. As expected, the four solar irradiance curves are very similar. A maximum difference of around 15% is seen for the sunniest year of 2009. This comparison suggests that the solar irradiance does not change largely from one year to another. As previously done for wind energy resource, the variability of the solar irradiance can be presented in the form of seasonal variations, allowing to identify the difference in the irradiance between the seasons with the same approach as the diurnal variation analysis for wind profiles. Figure 2.43 shows how the solar irradiance can be calculated using the data from Figure 2.41. The highest solar irradiance in the year is during the Summer months, whereas the lowest so-

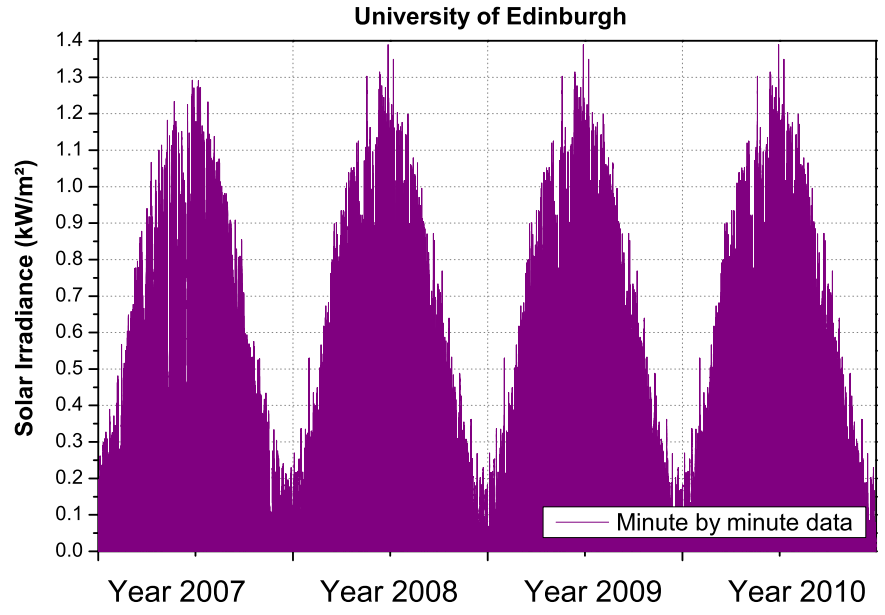

(a)

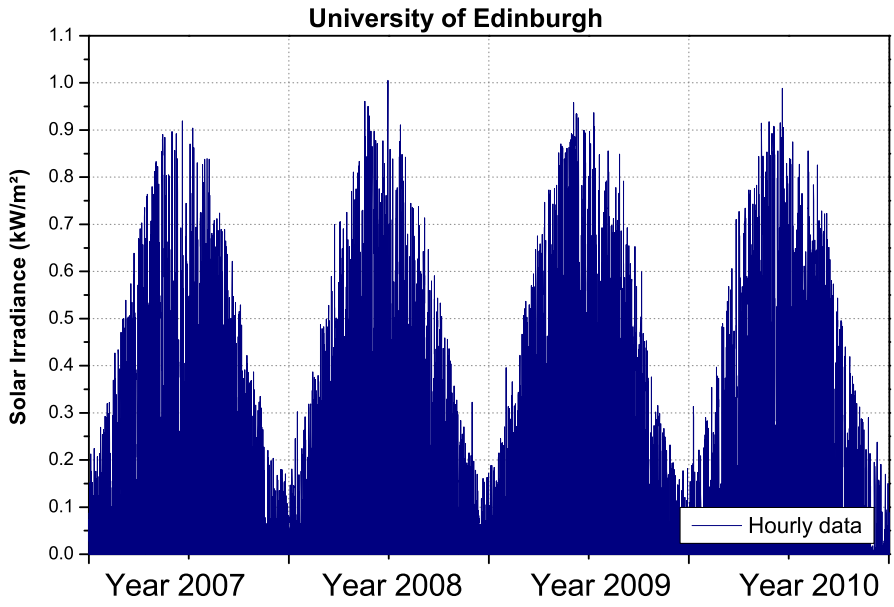

(b)

Figure 2.41: *Four years of hourly solar irradiance measured at the University of Edinburgh weather station: a) 1-min measurements, b) hourly measurements.*

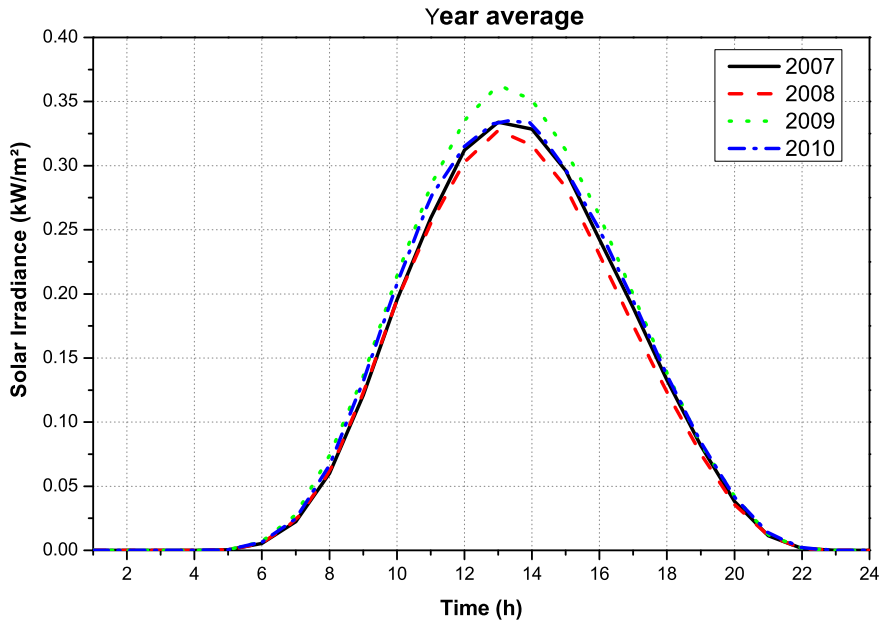

Figure 2.42: *Daily variations of the solar irradiance on average days per year.*

lar irradiance is available during the Winter months. Also, the hours of daylight significantly change between the Summer and the Winter months, which is a general characteristic of the input solar irradiance and the output of solar PV systems for locations far from the equator (e.g Edinburgh, UK).

In this presented study, the European Commission Photovoltaic Geographical Information System (PVGIS) research [9] has also been used. This database was consolidated using the climatological data homogenised for Europe, available in the European Solar Radiation Atlas [9], providing a 24 hour variation of the solar irradiance for any specific site in Europe at any specific day.

The database uses this data to estimate the three components of the solar irradiance: direct solar irradiance (clear-sky), diffused and reflective components of the clear-sky and real-sky. These components are calculated using the model developed by the European Commission, giving the solar irradiance in $^{kW}/_{m^2}$ for horizontal or inclined surfaces. This model also allows an assessment of the shadowing effect, caused by the local terrain features, which can be input through an elevation model.

Using the University of Edinburgh weather station data (the actual measurements), it was observed that the temporal variations of the solar irradiance does not change much from one year to another. Additionally for this work it has been assumed that the solar irradiance resource can be taken as constant for the whole Edinburgh city (no spatial variations). In order to jus-

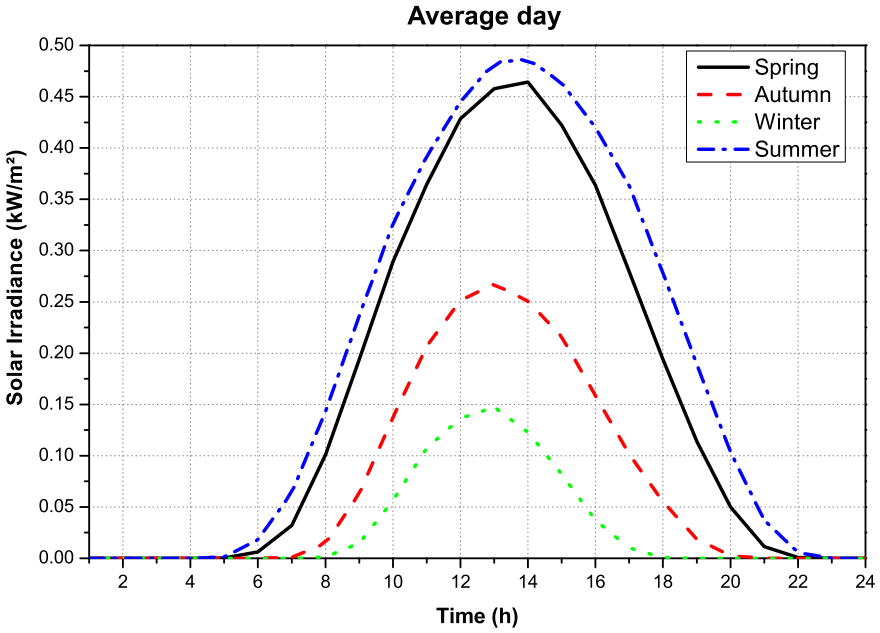

Figure 2.43: *Daily variations of the solar irradiance for each season.*

tify this assumption, the European Commission calculator (PVGIS) has been applied for five selected locations in Edinburgh and Mean Percentage Error (MPE) is calculated using the equation (2.10):

$$MPE = \frac{1}{n}\sum_{i=i}^{n}\frac{|f_i - a_i|}{a_i} \tag{2.10}$$

where, a_i is the PVGIS value at the location i, f_i is the forecast value and n is the number of quantities involved in the analysis. Figure 2.44 shows the five uniformly spread locations analysed using the PVGIS for which the MPE has been calculated using the equation (2.10), setting a_i as the irradiance reference site (The University of Edinburgh) and f_i as the irradiance data for the other at the i^{th} interval site. The results shown in Table 2.5 prove that the difference between the irradiance estimates for the five different sites in Edinburgh city is very small (less than 1%). Therefore, it can be concluded that only one set of data can be used for the entire Edinburgh city and this justifies the assumption made earlier in this section. The University of Edinburgh weather station data have been used for further analysis, regardless of the actual location of the site within the city.

Site	2	3	4	5
MPE	0.69%	0.85%	0.83%	0.86%

Table 2.5: *Mean Percentage Error (MPE) between the solar irradiance of the reference site and the other four sites in Edinburgh city.*

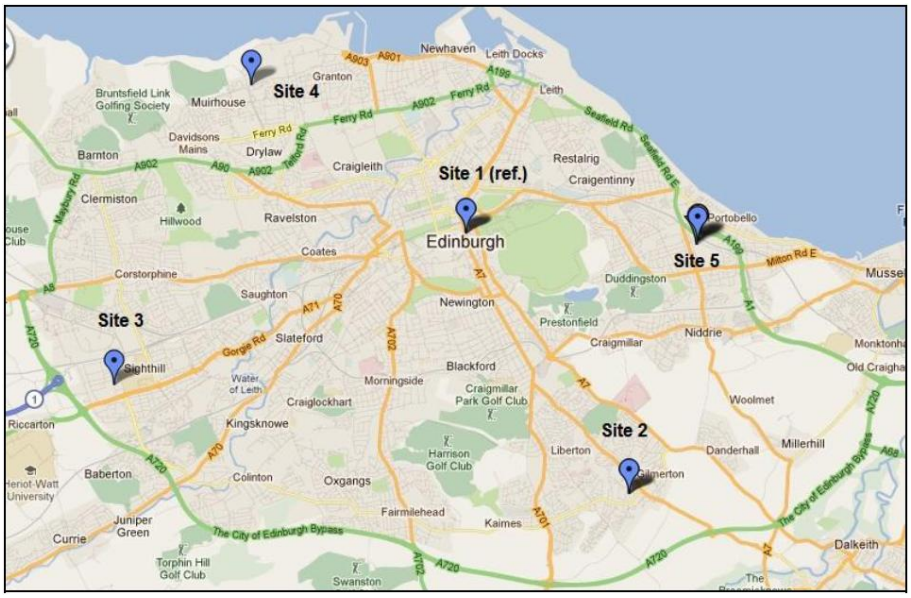

Figure 2.44: *Five different locations used to assess the data provided by the European Commission online calculator (PVGIS).*

Using the data from the four years of recordings at the University of Edinburgh weather station, a single average day has been generated as the average of all the years on a day-by-day basis. This is directly compared with the PVGIS data from the European Commission in Figure 2.45 to Figure 2.48. These figures show the comparison between the real-sky and the measurement-based average day results for a particular month. It is known that for a certain site, depending on its location with respect to the equator, floor reflection, cloud-level and many other variables that can influence solar irradiance, the real-sky component ca be lower than the recorded solar irradiance.

The PVGIS is one of the most useful sources of solar irradiance for Europe [43]. In the case of wind speed, measurement was available for several sites that allowed to give an overall performance of the wind speed in Edinburgh city. For solar irradiance was intended the same type of validation using another source of data, PVGIS was compared with the actual measurement at the University of Edinburgh and was found not to be adequate for Edinburgh city. After this review of the PVGIS the only data considered for the analysis is the measurement from the University of Edinburgh.

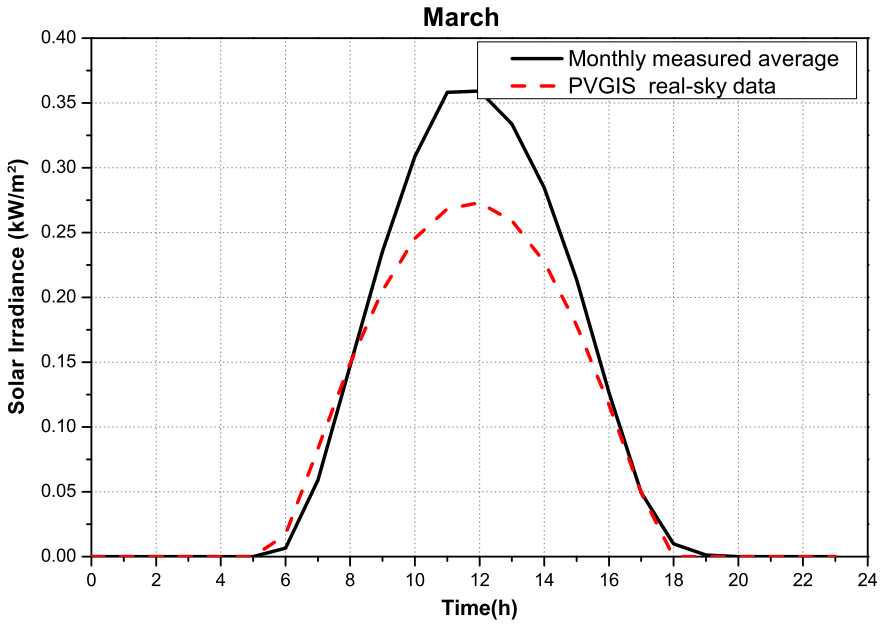

Figure 2.45: *Measurement-based solar irradiance over an average day in March compared with the PVGIS-based real-sky.*

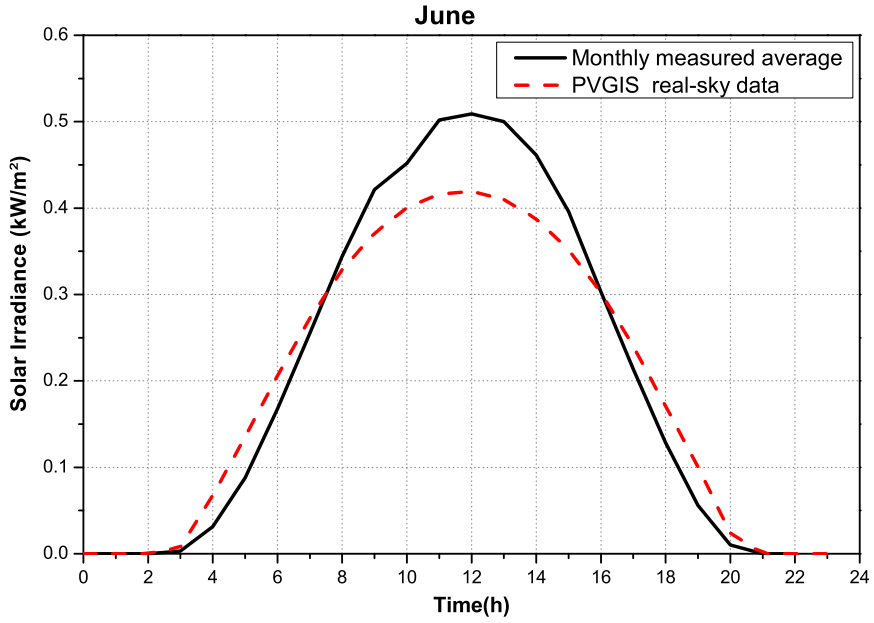

Figure 2.46: *Measurement-based solar irradiance over an average day in June compared with the PVGIS-based real-sky.*

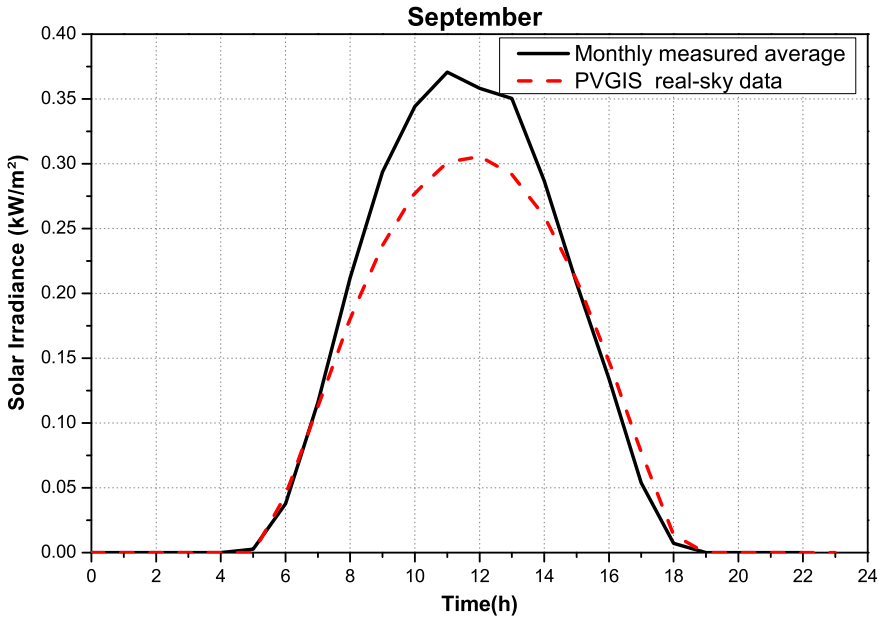

Figure 2.47: *Measurement-based solar irradiance over an average day in September compared with the PVGIS-based real-sky.*

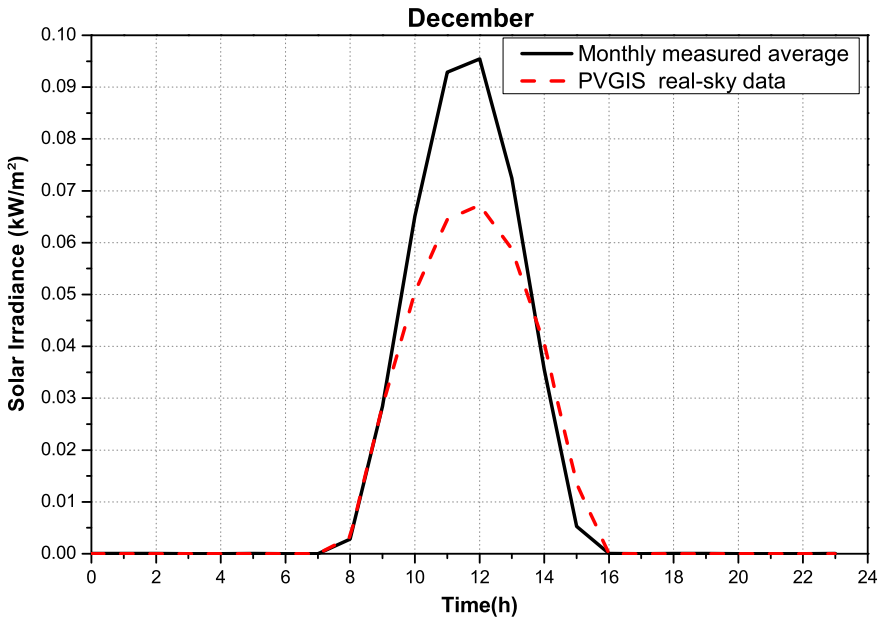

Figure 2.48: *Measurement-based solar irradiance over an average day in December compared with the PVGIS-based real-sky.*

2.7.2 Shadowing Effects

Obtaining the variation of solar irradiance throughout the year is important because in later chapters of this thesis a combination of the solar PV and the wind turbine outputs will be combined together to assess corresponding microgeneration electricity generation on hourly/daily basis. The clearness index values provide only a single value that is not enough to create a solar profile to be directly correlated with the load profile and the wind profile. Additionally, these average curves obtained for Edinburgh are based on measurement, which in the process include the shadowing effects considered from the solar irradiance point of view as an input to generation models presented later in this thesis.

It has been found that even though extensive research has been carried out on the shadowing effects on energy yield and performance of PV panels, it is far from clear to quantify and model the impact [44]. Furthermore, the models needed to predict the impact of shadowing on specific panels have to be quite detailed [45]. The scope of this thesis is to provide an assessment of the aggregated effect of the microgeneration systems in urban area without going into the detailed effects of the variations in resource, for this purpose the analysis excludes local shadowing for a particular PV panel as it is simply assumed that the PV systems installed in urban area are well exposed with no local obstructions (which is the case in practical applications).

2.8 Time-series Solar Irradiance Analysis for Edinburgh City

The previous analysis was focused on comparing the PVGIS data and the measured data from the University of Edinburgh weather station. That analysis was important to check wether another source of solar irradiance data when solar irradiance measurements are not available is applicable. The conclusion is that PVGIS data do not to match the measurements and therefore it are not considered for the time-series analysis.

The idea behind assessing the renewable resource in this thesis is to obtain a range of 24-hour variations for each season in the solar irradiance similar to what was found for wind speed in section 2.6.1. In the case of PV, the variations in the solar irradiance are required to assess the potential output of solar PV systems installed in Edinburgh. It was found from the analysis that for lower resolution measurements, some information about the variations of both the wind resource (Figure 2.18) and the solar irradiance are lost due to the the process of averaging the data (Figure 2.41). In order to determine the maximum and minimum solar irradiance for the four seasons, similar approach as the one used in the assessment of the wind resource has been

applied. The main difference lies in the availability of sites for solar irradiance measurement, as previously discussed the difference between measurement point around Edinburgh city was less than 1%. Therefore the maximum, average and minimum solar irradiance are obtained only from the University of Edinburgh weather station data. The maximum and minimum values are found using the whole season and for the same hour of the day the maximum and minimum of the three months is reported (as it was used for wind speed profiles). For the average the three month period is used and the average of all days is obtained for a single curve representation, the results are discussed in this section. The maximum, average and minimum expected solar irradiance values in the four seasons have been identified and are plotted together in Figure 2.49 to Figure 2.52.

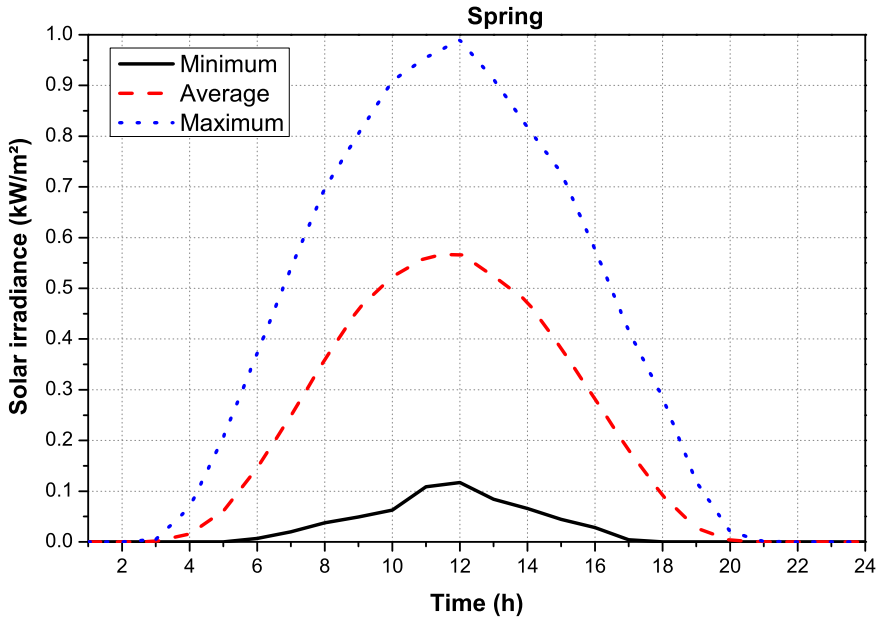

Figure 2.49: *Maximum, average and minimum solar irradiance in Spring.*

This methodology produces a single average year from the four years available as it was done for the wind speed profiles. Additionally the maximum and minimum solar irradiance values are included to be considered as power outputs of PV systems, which will show its importance when it shows the maximum value of power output that can be obtained from connecting the PV systems to the power grid.

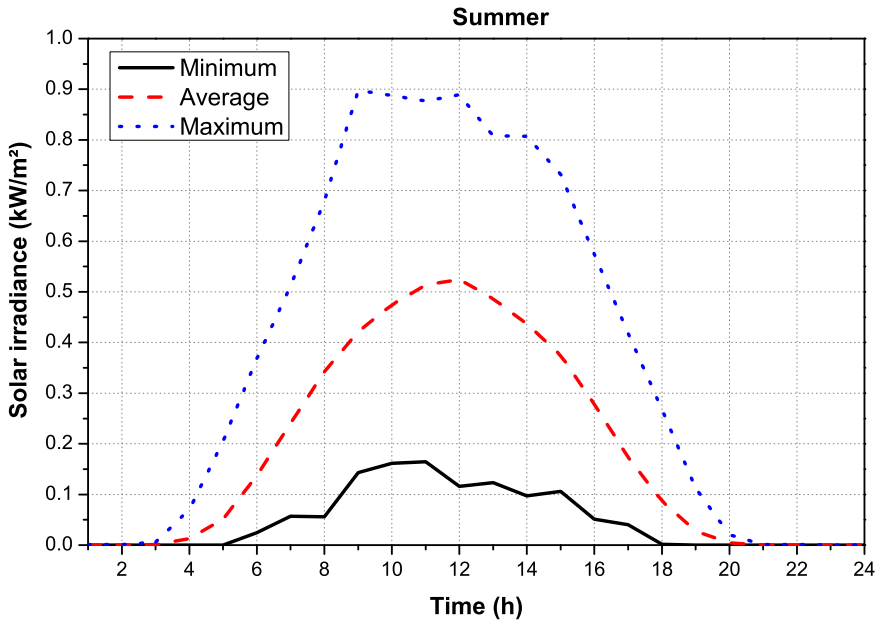

Figure 2.50: *Maximum, average and minimum solar irradiance in Summer.*

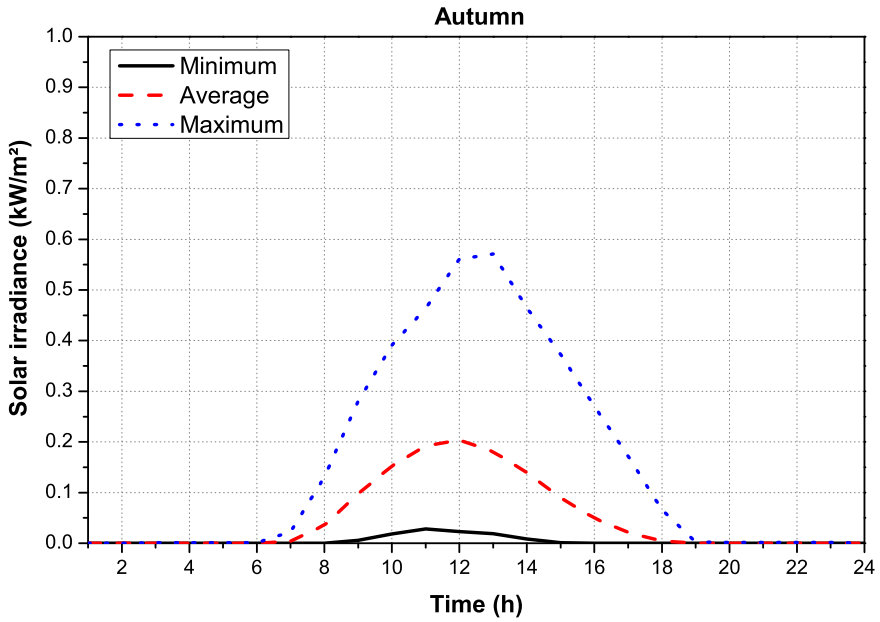

Figure 2.51: *Maximum, average and minimum solar irradiance in Autumn.*

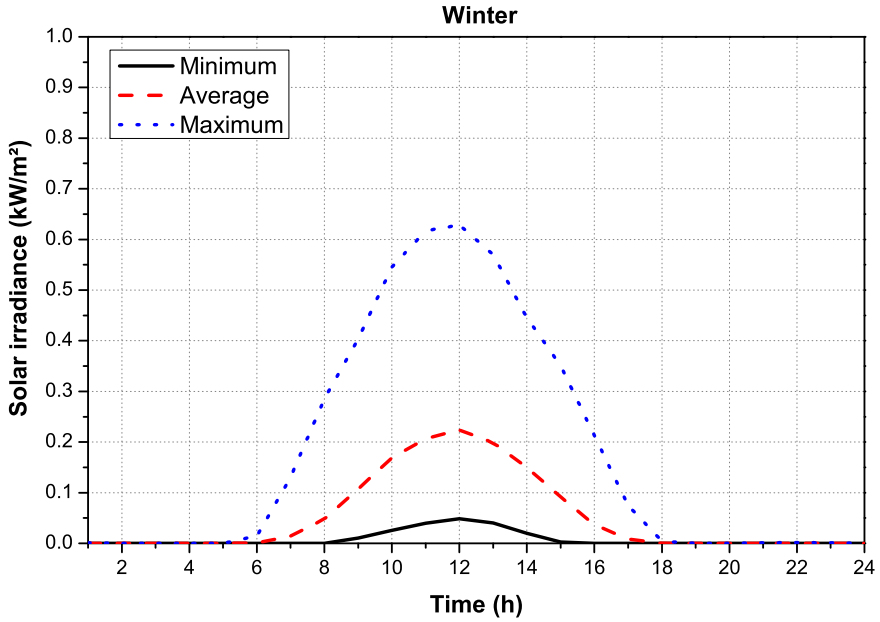

Figure 2.52: *Maximum, average and minimum solar irradiance in Winter.*

2.9 Conclusions

This chapter presented an analysis of the wind and solar resource in the UK urban areas, particularly around Edinburgh city. It was shown that the reference values of mean wind speed to quantify the wind resource cannot be applied for the analysis of urban areas and site-specific data needs to be used to assess the potential of urban wind. An assessment of the averaged daily and spatial variations of the two renewable resources was also presented. In the case of solar irradiance, it was found that online calculators could not be used for the assessment of average solar irradiance in Edinburgh city.

The maximum and minimum solar irradiance available at a particular site, in our case Edinburgh city, can be assessed only if actual measurements are available. This was done in the presented analysis by using data from the University of Edinburgh weather station. These maximum and minimum profiles are reported in order to assess the maximum/minimum microgeneration output scenarios, because these values are already hourly average values found in the data set for the specific analysed site and season. This is important, because they can be found for at least one hour in these sites, therefore they will be considered in the future analysis as the possible maximum and minimum power output of microgeneration systems.

The main aim of the presented analysis is to assess the output of aggregate PV and wind-based microgeneration systems in urban areas with the average values that can normally produce and

the maximum power output that can be obtained from these systems. The profiles (24-hour variations of solar and wind energy resources) for different seasons in the urban area around the Edinburgh city, developed in this chapter, will be further used to feed generic models of wind and solar PV to analyse the effects of connecting microgeneration systems to distribution networks. For this purpose, the next chapters discuss the building of particular systems and generic models of micro and small-scale PV and wind generation systems.

Chapter 3
Modelling of Micro and Small-scale Wind Generation Systems

3.1 Introduction

Chapter 2 discussed the assessment of wind resources in urban areas and concluded that measurements are needed for an accurate assessment of UK urban wind resources. Chapter 2 also discussed how the resolution of the measurements does not significantly affect the outcome of the Weibull distribution, when minute by minute data and hourly averaged data were used. The analysis in this chapter further discusses the calculation of energy outputs when a Weibull distribution and simple wind turbine power curve representation are used, in comparison with the quasi-dynamic wind turbine model developed and more detailed wind data. The proposed analysis requires high-resolution wind data to make a comparison between hourly averaged values and second by second measured values. This chapter is divided into four main parts. The first one presents the high-resolution wind data used for the analysis, the second presents the turbines selected for the modelling, the third presents a quasi-dynamic model of the wind generation system with all its components considered separately (component-based model: wind turbine, generator, inverter, filter) and finally the last part shows the validation of the model by measurements and by comparing Weibull distribution and time-series model outputs.

3.2 High-Resolution Wind Data

Several UK field trials reported very low energy outputs of micro and small-scale wind turbines (WTs) installed in urban areas (e.g. [26] and [46]). In order to analyse some of the possible reasons for the underperformance of urban wind turbines, this section introduces high-resolution input wind speed data (i.e. second-by-second measurements) at one UK site [47], for a period of seven continuous days. This site is based in the north of Scotland and the data were obtained for a wind farm development. It is assumed that high-resolution data correctly represent wind dynamics and can be used in combination with a simple power curve wind model

instead of a component-based wind model (e.g. [5]). Figure 3.1 illustrates actual 1-second wind measurements and calculated 1-hour average values on the same graph, showing that the high wind speeds present in the 1-second wind data are lost in 1-hour data. It is further illustrated

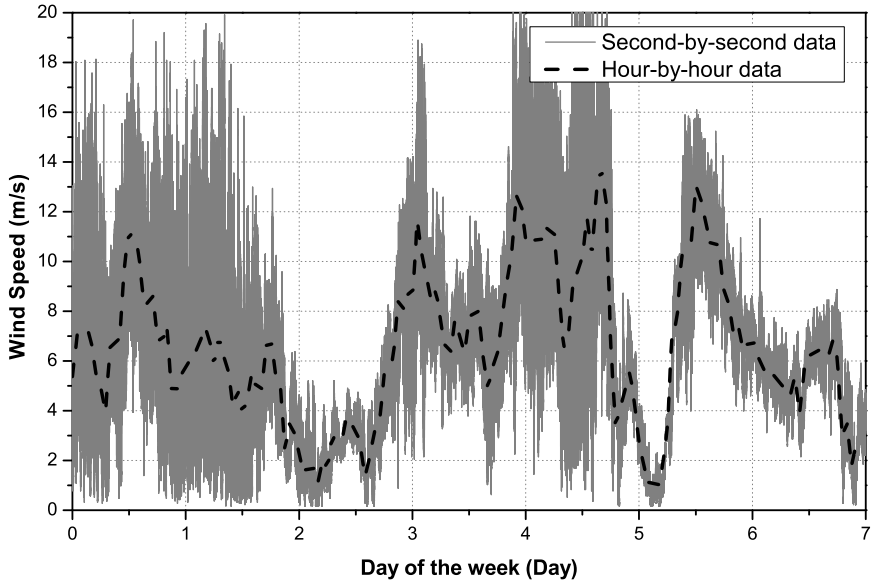

Figure 3.1: *High-resolution (second-by-second) wind speed measurements for one arbitrary week at one UK location and the corresponding hourly averages [47].*

in Table 3.1 where it is immediately clear that when lower resolution data are calculated from second-by-second measurement, the information on average wind speeds is preserved, but the information on the actual maximum/minimum wind speeds is lost. This is particularly important since it is assumed that below and above certain values of wind speeds the wind turbines will stop producing energy output due to the "cut-in" and "cut-out" speed limits. With these data selected for the analysis, the same procedure as in Chapter 2 is applied and the appropriate Weibull distribution is fitted to the data. For this assessment, Figure 3.2 shows the distribution for a period of seven days with a mean wind speed (MWS) of $6.54^{m}/_{s}$. The selected site is a windy location that might not represent urban areas, but for the purpose of this analysis the high-resolution data is used to analyse the response of the wind turbine model and the difference between the energy outputs obtained by the use of the Weibull distribution and different resolutions applied to the actual component-based wind model.

Input Wind Speeds (m/s)									
Data Set		Day 1	Day 2	Day 3	Day 4	Day 5	Day 6	Day 7	Whole week
$1s$	Min	0.27	0.17	0.17	0.62	0.17	0.17	0.22	0.25
	Ave	7.18	5.35	3.64	8.25	9.03	7.24	5.11	6.54
	Max	19.7	19.9	14.2	23.1	22.8	16.1	11.7	18.2
$10s$	Min	0.47	0.29	0.17	0.71	0.17	0.17	0.24	0.32
	Ave	7.18	5.35	3.64	8.25	9.03	7.24	5.11	6.54
	Max	17.2	18.1	13.1	18.4	20.3	15.1	10.1	16.04
$1min$	Min	1.14	0.91	0.22	1.28	0.27	0.17	0.35	0.62
	Ave	7.18	5.35	3.64	8.25	9.03	7.24	5.11	6.54
	Max	14.3	15.9	11.1	16.3	16.1	14.3	8.6	13.8
$10min$	Min	2.63	1.38	0.52	3.66	0.87	0.43	0.88	1.48
	Ave	7.17	5.39	3.58	8.24	9.1	7.18	5.15	6.54
	Max	12.2	10.5	10	13.8	15	13.4	7.7	11.8
$1hour$	Min	3.93	2.41	1.1	4.87	3.38	0.91	1.76	2.62
	Ave	7.24	5.48	3.36	8.67	9.7	7.07	5.43	6.71
	Max	11.2	7.4	8.4	12.6	13.8	13	6.9	10.48

Table 3.1: *Input wind speed characteristics of different data sets (different resolutions) for seven individual days of the selected week.*

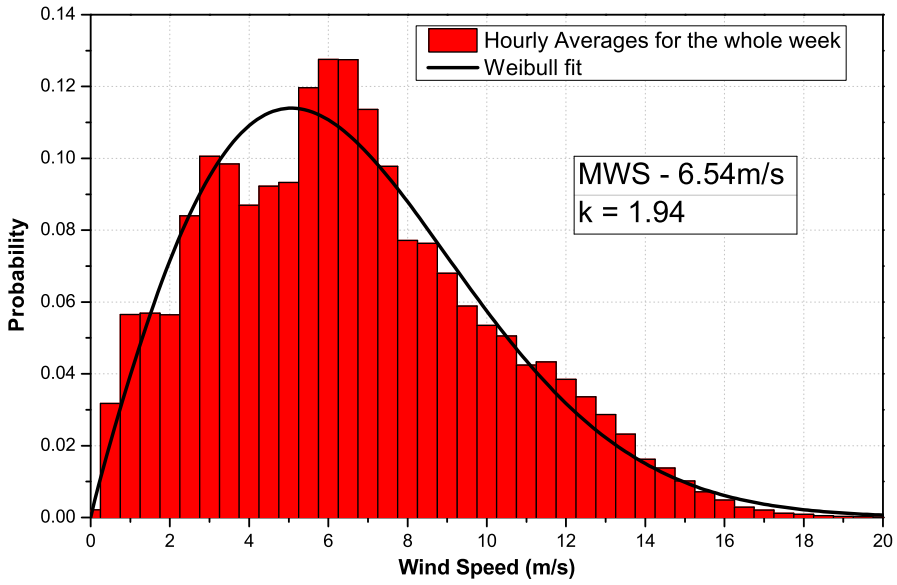

Figure 3.2: *Weibull distribution fit for hourly averaged wind speed over seven days.*

3.3 Modelled Wind Turbines

The power curve of a wind turbine could be expressed using the aerodynamic power of the wind (2.3) and including the performance coefficient C_p (2.4). Therefore, the equation for the power output of a turbine would be:

$$P_{WT_{mech}} = \frac{1}{2} C_p \rho_{air} A_{swept} \nu_{wind}^3 \tag{3.1}$$

The C_p is normally a function that defines the efficiency of the turbine depending on the wind speed. The power coefficient varies for different wind speeds and for different wind turbines. It is typically obtained through the power curve as British Standard BS61400-12-1 specifies [28]. In this section three particular wind turbines are modelled in detail. These wind turbines are selected in order to represent common wind turbine technologies, covering the range of micro and small-scale wind applications in urban areas from $500W$ to $2.5kW$. As mentioned before in Chapter 2, some manufacturers provide aerodynamic power curves to show the design capabilities of their products, which allows to model the wind energy system component by component. Also, the aerodynamic measurements to validate the model were available for these three turbines.

The turbine power curves are plotted up to $12^m/_s$ wind speed as it was found in Chapter 2 that the probability of higher wind speeds than this are very low in urban areas (Figure 2.19 to Figure 2.22). The turbines considered in this chapter are as follows:

(a) WT1 (Figure 3.3) is a Horizontal Axis Wind Turbine (HAWT) with rated aerodynamic power of $500W$ at $13^m/_s$, swept area of $4.83m^2$ and employs a dynamic brake for speed control [48],

(b) WT2 (Figure 3.4) is also a HAWT with rated aerodynamic power of $1.4kW$ at $13^m/_s$, swept area of $3.4m^2$ and dynamic brake for speed control [49],

(c) WT3 (Figure 3.5) is a Vertical Axis Wind Turbine (VAWT) with rated aerodynamic power of $2.5kW$ at $12^m/_s$, swept area of $16m^2$ and has a mechanical braking system that is applied after $14^m/_s$ to stop the turbine, [50].

3.4 Permanent Magnet Synchronous Generator

The vast majority of micro and small-scale wind turbine applications utilise a permanent magnet synchronous generator (PMSG) with an inverter interface for the grid connection. Figure 3.6

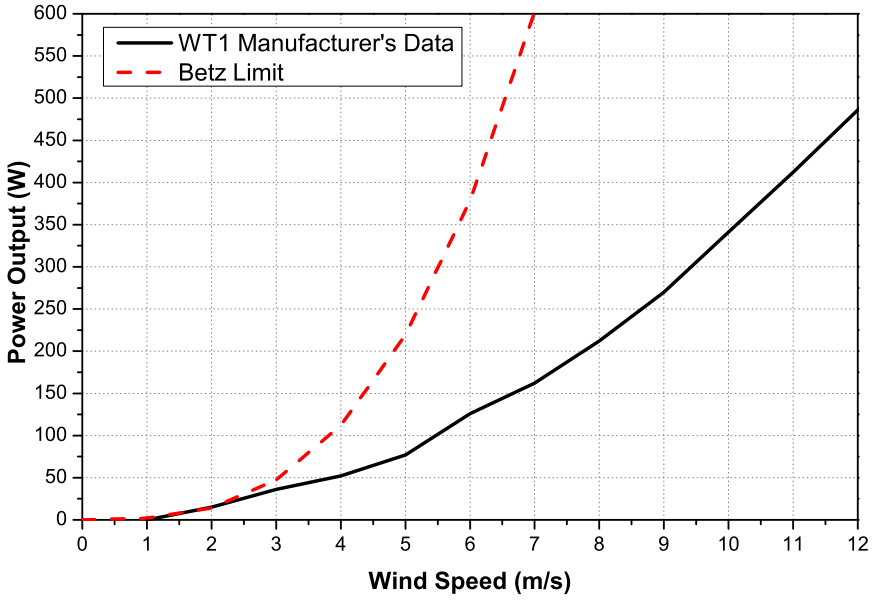

Figure 3.3: *Considered aerodynamic wind turbine WT1 and Betz limit.*

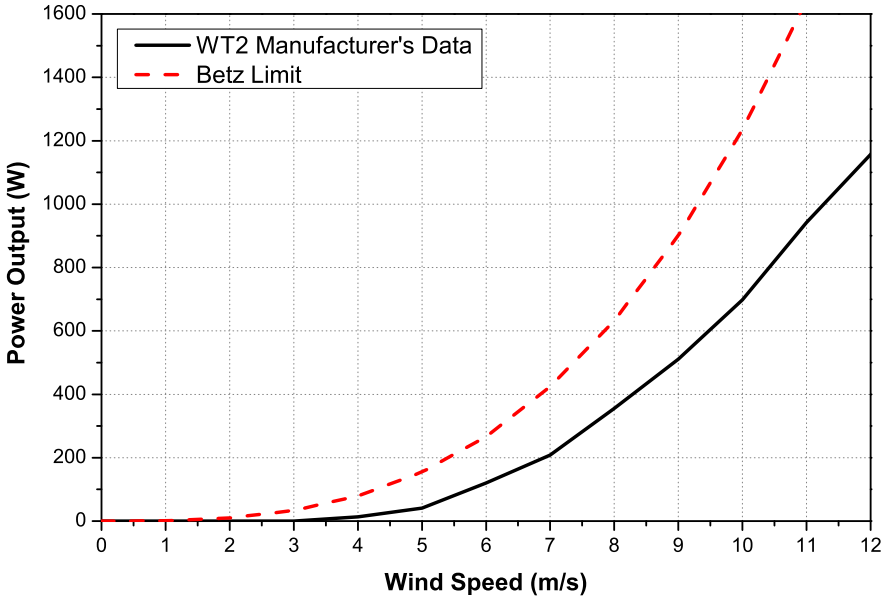

Figure 3.4: *Considered aerodynamic wind turbine WT2 and Betz limit.*

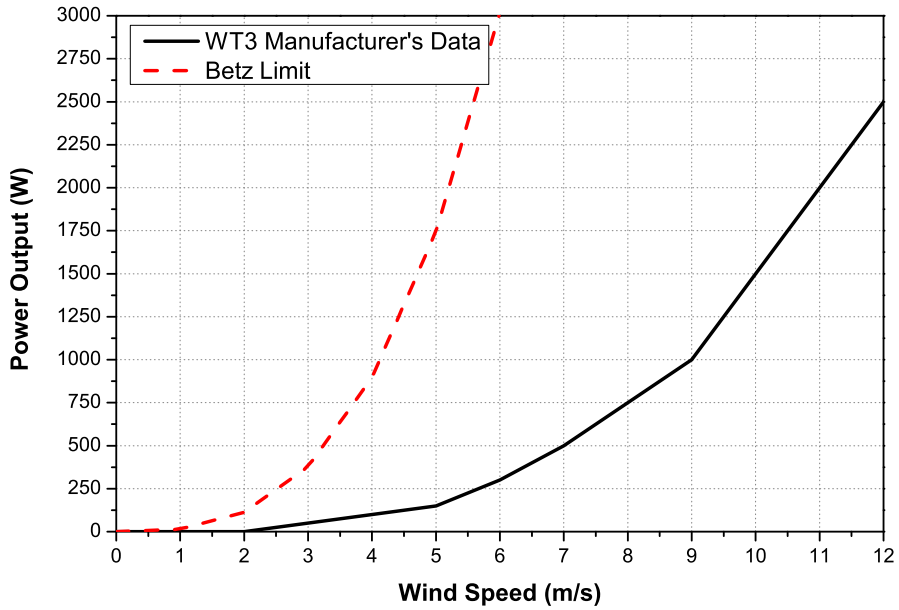

Figure 3.5: *Considered aerodynamic wind turbine WT3 and Betz limit.*

shows the main parts involved in the process of converting wind energy into usable electrical power delivered to the grid. The blades of the wind turbine rotate delivering mechanical power to the shaft of the PMSG. Due to the variability of the wind resulting in a variation of shaft speed, the frequency and magnitude of the electrical power output is variable. Therefore, this power is rectified and then inverted to a fixed grid frequency. Depending on the size of the system, the required output filter varies from a single inductance (L-filter) to a second or third order low-pass filter.

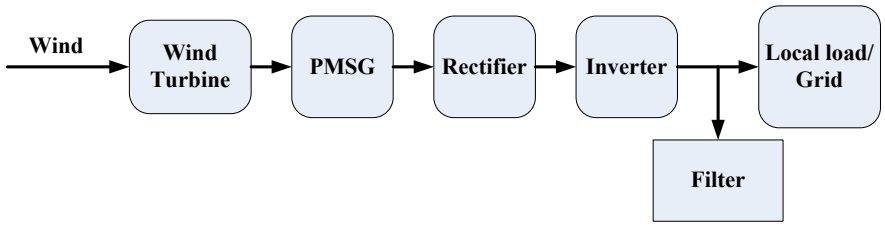

Figure 3.6: *Main components of a PMSG-based micro/small wind turbine system.*

Table 3.2 shows the parameters of the generators for considered wind turbines and the calculation of their mechanical to electrical power conversion. The generators are air-cored and iron-cored which according to [51] are the typical generators in wind turbine applications. The parameters can be divided into mechanical characteristics such as the rated speed, the number of poles, the inertia of the rotor and the electrical characteristic needed for the model (e.g. the

	WT1 [48]	WT2 [49]	WT3 [50]
Type	Air-cored Axial flux	Iron-cored Axial flux	Air-cored Axial flux
Nominal power (W)	500	1000	2500
Speed (rpm)	750	450	250
Pole Number	8	8	16
Resistance (Ω/ph)	23.6	0.7	11.5
Inductance (mH/ph)	289	35.34	101
EMF constant (Wb)	1	0.39	0.65
Inertia ($kg.m^2$)	3.6	11	18

Table 3.2: *Characteristics and parameters of considered PMSG of selected wind turbines.*

inductance, resistance and the electromotive force constant).

In order to develop a correct component-based model of the wind energy system, it is, therefore necessary to model the conversion of energy of the PMSG to see the performance of the wind turbine component by component. The sensible approach in this case is modelling the three-phase PMSG machine using Park's transformation. The rotor of the PMSG is a permanent magnet, therefore the reference frame used for the modelling is synchronous. Figure 3.7 shows the d/q reference frame model. According to Park's transformation, the three phases

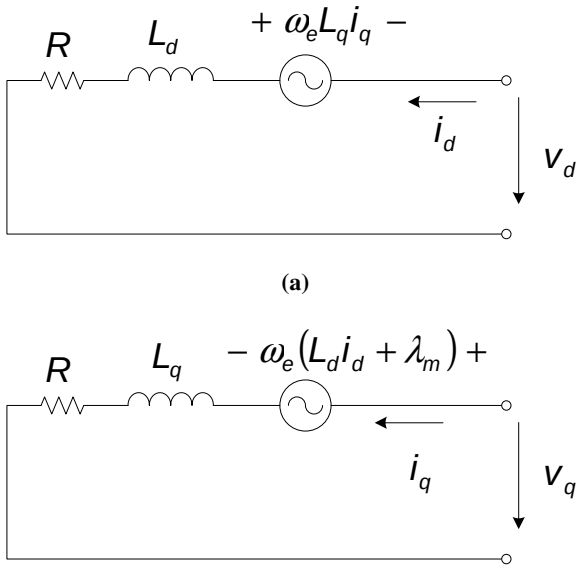

Figure 3.7: *Equivalent circuits in a synchronous d/q reference frame (a) d-axis circuit, (b) q-axis circuit.*

of the PMSG can be transformed to direct-axis and quadrature-axis. The transformation of the PMSG in a synchronous reference frame is defined by the following equations:

$$\begin{bmatrix} f_a \\ f_b \\ f_c \end{bmatrix} = \sqrt{\frac{2}{3}} \begin{bmatrix} 1 & 0 \\ -1/2 & \sqrt{3}/2 \\ -1/2 & -\sqrt{3}/2 \end{bmatrix} \begin{bmatrix} \cos\theta_e & -\sin\theta_e \\ \sin\theta_e & \cos\theta_e \end{bmatrix} \begin{bmatrix} f_d \\ f_q \end{bmatrix} \tag{3.2}$$

$$\begin{bmatrix} f_d \\ f_q \end{bmatrix} = \sqrt{\frac{2}{3}} \begin{bmatrix} \cos\theta_e & \sin\theta_e \\ -\sin\theta_e & \cos\theta_e \end{bmatrix} \begin{bmatrix} 1 & -1/2 & -1/2 \\ 0 & \sqrt{3}/2 & -\sqrt{3}/2 \end{bmatrix} \begin{bmatrix} f_a \\ f_b \\ f_c \end{bmatrix} \tag{3.3}$$

$$v_d = Ri_d + L_d \frac{di_d(t)}{dt} - L_q \omega_e i_q \tag{3.4}$$

$$v_q = Ri_q + L_q \frac{di_q(t)}{dt} + L_d \omega_e i_d + \lambda_m \omega_e \tag{3.5}$$

where, in equation (3.2) to (3.5): i_d, v_d, L_d - d-axis current, voltage and inductance, i_q, v_q, L_q - q-axis current, voltage and inductance, R - coil resistance, λ_m - magnetic flux of the permanent magnet, p - number of pole pairs, ω_r - mechanical (rotor) speed, θ_e - electrical angle, ω_e - electrical (synchronous) speed and T_e - electromagnetic torque, β - friction coefficient.

When the machine is implemented as a motor, terminal voltage is fixed, determined by the power supply, while speed is a function of the system's frequency and the number of pole pairs, also the mechanical loading at the shaft of the machine determines the motor's current. In the case of a generator the output will depend on the electrical loading connected at the terminals, the input torque and speed at the shaft of the machine, thus determining the output voltage and frequency. Equilibrium between the electromagnetic and mechanical torques is determined by Newton's Second Law, with the following equations describing shaft rotational speed depending on the acceleration and the inertia of the rotor:

$$T_e = \frac{3}{2} p \Big[\lambda_m i_q + \big(L_d - L_q\big) i_q i_d \Big] \tag{3.6}$$

$$\omega_e = p\omega_r \tag{3.7}$$

$$T_m - T_e = J \frac{d\omega_r(t)}{dt} + \beta \omega_r(t) \tag{3.8}$$

3.5 Inverter Model

Typically, a (grid-connected) micro/small PMSG-based wind turbine will utilise a full-size single-phase inverter (e.g. [52]). This inverter will influence the wind turbine power output and

has to be considered during the analysis and modelling of the wind turbine performance. Accordingly, a full component-based model of a wind turbine includes a three-phase full-bridge diode rectifier and a single-phase IGBT inverter. The inverter and rectifier are connected together by a boost chopper circuit, used for decoupling the rectifier and the inverter and to control the inverter's input voltage, i.e. keep it constant at all times. Figure 3.8 shows a block diagram of a current-control loop for maximising the rectifier output DC power before the inverter. By adjusting the modulation index of a PWM stage, the boost chopper circuit controls

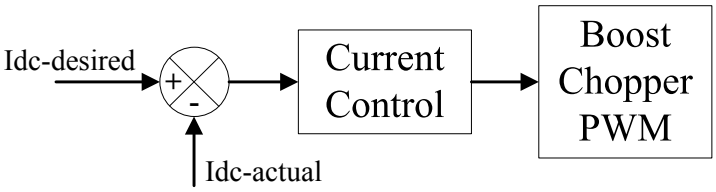

Figure 3.8: *Boost Chopper Control.*

the inverter's input DC voltage and therefore the DC current, in order to track the maximum power operating point. The flowchart in Figure 3.9 illustrates the Perturb and Observe (P&O) algorithm, which is sometimes used in wind turbine applications for maximum power point tracking [53], [54]. The algorithm adjusts the reference DC voltage value depending on the sign of the slope of the $^{\delta P}/_{\delta V}$ characteristic. The inverter control considers its input DC volt-

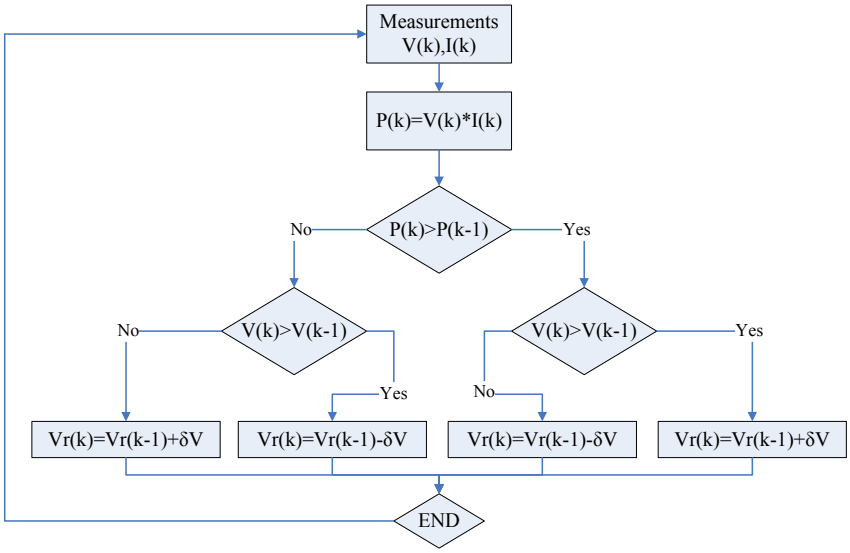

Figure 3.9: *Boost Chopper control (P&O) algorithm: V, voltage, I, current, P, power, δV, increase or decrease of voltage reference value.*

age (output coming from the chopper control), output ac current and grid voltage to operate correctly. Figure 3.10 shows the inverter block diagram control. The inverter interface will influence the overall performance of a wind turbine in two ways. First, an inverter will introduce losses (typical inverter efficiencies are between 90% [55] and 93% [56]). Secondly, an inverter will allow the export of generated wind turbine power to the grid only if the input inverter voltage is within a required range (typically between $220V$ - $600V$ DC).

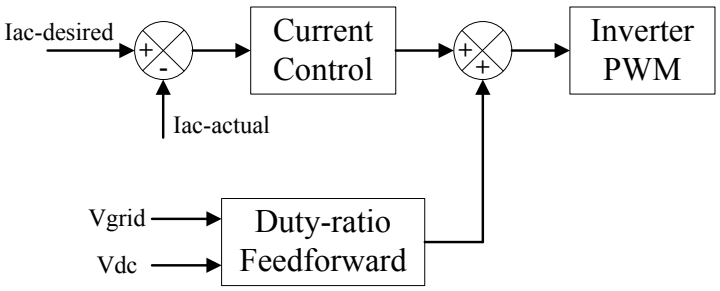

Figure 3.10: *Inverter Control.*

3.6 Low-Pass Output Filter

The model of the particular wind turbines considers every stage of the actual device and the filter for grid connection is an important part of the system. Operation and control of microgeneration systems have been regulated since September 2003, when the Engineering Recommendation G83/1 [57] came into force. This engineering recommendation is based on the previous Engineering Recommendation G59/1 [58], which is still valid for the embedded generation plant in distribution networks. Typically, small systems are not expected to contribute to voltage control, regulation or network support. The main requirement for these systems is disconnection when the mains is lost, which is particularly important for the protection of the power electronics used in microgeneration systems. The other requirement, according to Engineering Recommendation G83/1 [57], is the harmonic emission to the grid, which points towards the British standard 61000-3-2, where the harmonic content should comply with the limits for "Class A" equipment in [59]. It should be noted that harmonic emission of micro and small-scale DG systems (including discussed wind turbine applications) is currently attracting a lot of interest, with the specific regulation still pending in Europe (e.g. [60]). For this particular reason, filtering design for inverter-based microgenerators is an important issue, which is

further discussed in this section [61], [62].

3.6.1 First Order Filter

A first order filter consists of a simple inductance coil connected between the microgenerator and the point of connection of the low-voltage network. This is commonly used due to its simple design but the value of the inductance must be high to achieve the required attenuation of the harmonics (e.g. [63]). This results in low attenuation the filter is unable to filter the high switching frequencies of the inverter and the DC current component is not corrected. Due to a high inductance value, the voltage drop causes a prolonged time response. This type of filter is useful for systems such as induction generator micro-CHP, where the harmonics emitted by the generator are easily filtered by the inductance and the level of harmonics depends mainly on the voltage of the grid. For the interest of this thesis, the first order filter will not be considered in the analysis since the application for microgeneration is limited and does not help the inverter-based generator to comply with the harmonic regulation.

3.6.2 Second Order Filter

The LC filter is suited for inverter-based configurations and has become very popular for its simple design [64], [65], [66]. To reduce the voltage drop the capacitance has to be high and the inductance will then be reduced, nevertheless, it has to be considered that a very high capacitance may cause a high inrush current. The reactive power of the fundamental frequency fed into the capacitor from the grid side can also lead to a resonance of the system. The resonant frequency can vary depending on the system impedance and the characteristics of the microgenerator. This problem can be generally solved by adding a damping resistance, as shown in Figure 3.11.

The transfer function of the LC filter without the damping resistor is given by equation (3.9). The transfer function including the damping resistor is shown in equation (3.10).

$$G(s) = \frac{1}{LCs^2 + 1} \tag{3.9}$$

$$G(s) = \frac{1}{LCs^2 + Rs + 1} \tag{3.10}$$

The difference in the filter response when a damping resistor is included is shown in Figure 3.12, illustrating damping at certain frequencies avoiding the critically damped response

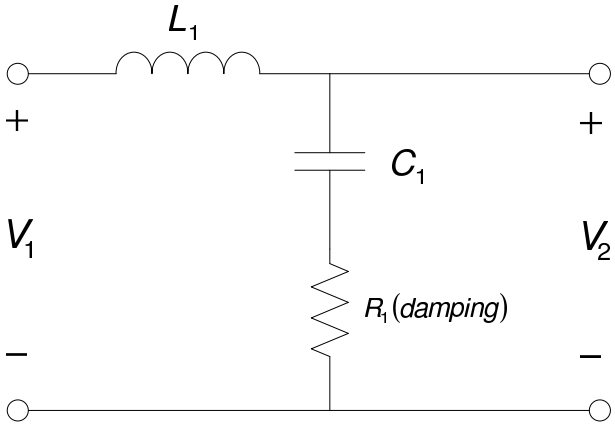

Figure 3.11: *Second order (LC) filter topology.*

and the resonance of the system.

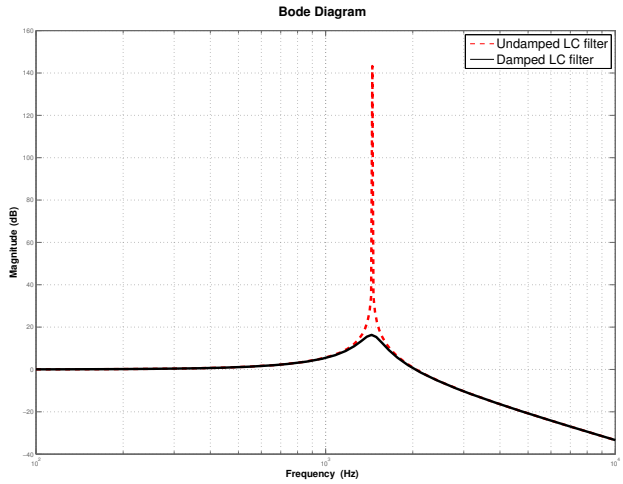

Figure 3.12: *Comparison between Bode diagrams of undamped and damped second order (LC) filters.*

3.6.3 Third Order Filter

The LCL-filter is becoming increasingly popular due to its capability to filter the harmonics of inverter-based generation. However, the complexity of its design makes it somewhat inconvenient and expensive for microgeneration [67]. Figure 3.13 shows the schematics of the LCL-filter. The system is analysed and the design of the system relies on the space-state solution since the system has two inputs and two outputs. The controlled variable inputs are considered to be the voltage of the inverter (v_1) and the voltage of the grid (v_2). The outputs of

the filter are the current from the inverter (i_1) and the current exported to the grid (i_2), with the voltage of the capacitor's branch (v_3) being an output dependant on both currents. The LCL-

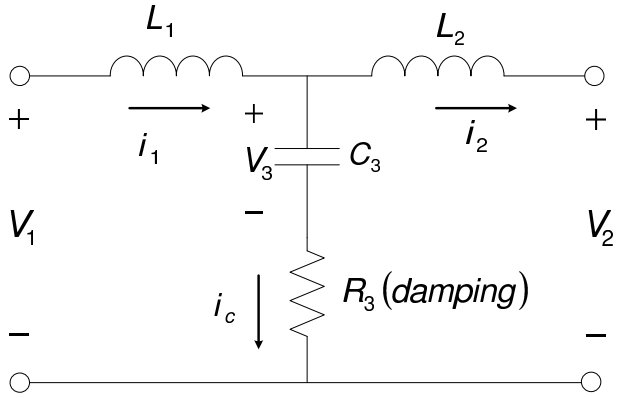

Figure 3.13: *Third order (LCL) filter topology.*

filter model from Figure 3.13 has three state variables, the output current from the inverter (i_1), the exported current to the grid (i_2) and the capacitor voltage (v_3) of the branch between both sides of the system represented by the vector x:

$$x = \begin{bmatrix} i_1 & i_2 & v_3 \end{bmatrix}^T \tag{3.11}$$

In this system the capacitor voltage v_3 is an internal value defined by the currents on both sides of the system. This parameter is important for the voltage output, in order to solve the system the output vector will be equal to the state vector:

$$y = x \tag{3.12}$$

Therefore the input vector is:

$$u = \begin{bmatrix} v_1 & v_2 \end{bmatrix}^T \tag{3.13}$$

where, v_1 is the voltage of the inverter and v_2 is the voltage of the grid. After writing the differential equations corresponding to the proposed system shown in Figure 3.13 and transforming into the frequency domain and solving for the state variables the model can be expressed as

$Y(s) = G(s)U(s)$, where $G(s)$ is:

$$G(s) = \frac{\begin{bmatrix} \frac{1}{L_1}\left(s^2 + \frac{R_3}{L_2}s + \frac{1}{L_2L_3}\right) & \frac{-R_3}{L_1L_2}\left(s + \frac{1}{R_3L_3}\right) \\ \frac{R_3}{L_1L_2}\left(s + \frac{1}{R_3C_3}\right) & \frac{-1}{L_2}\left(s^2 + \frac{R_3}{L_1}s + \frac{1}{L_1C_3}\right) \\ \frac{1}{L_1C_3}s & \frac{1}{L_2C_3}s \end{bmatrix}}{s\left(s^2 + \frac{R_3}{L'}s + \frac{1}{L'C_3}\right)} \tag{3.14}$$

with, $L' = \frac{L_1L_2}{L_1+L_2}$. Therefore, equations (3.15) and (3.16) are the transfer function used for the output of this filter.

$$Y_{11}(s) = \frac{I_1(s)}{V_1(s)} = \frac{1}{L_1}\frac{s^2 + \frac{R_s}{L_2}s + \frac{1}{L_2C_3}}{s(s^2 + 2\zeta_p\omega_p s + \omega_p^2)} \tag{3.15}$$

$$Y_{21}(s) = \frac{I_2(s)}{V_1(s)} = \frac{R_3}{L_1L_2}\frac{s + \frac{1}{R_3C_3}}{s(s^2 + 2\zeta_p\omega_p s + \omega_p^2)} \tag{3.16}$$

Where, ω_p is the resonant pole frequency, the ζ_p is the damping factor defined as:

$$\omega_p = \frac{1}{\sqrt{L'C_3}} \tag{3.17}$$

$$\zeta_p = \frac{R_3}{2}\sqrt{\frac{C_3}{L'}} \tag{3.18}$$

The third order filter, despite being a very good passive filtering solution for microgeneration, is reported to be too expensive and complex to design [61], [62]. It is therefore only recommended for higher power generation systems. This thesis will focus on the second order low-pass passive filter in the models presented with values from [65].

3.7 Validation of Developed Wind Turbine Model by Measurement

The wind turbine model is assembled by each modelled part reported in the previous sections, the aerodynamic power curve reported by the manufacturer, the PMSG, the inverter with P&O control and the filter. Using the model, this section presents a comparison of experimental results, simulated results and manufacturer specifications for WT1-WT3, [5], [48], [49], [50]. The presented results correspond to steady-state operating conditions. The Matlab/Simulink wind generation model is shown in Appendix B.

Figures 3.14 - 3.16 compare the aerodynamic (i.e. before PMSG and inverter, reported by the

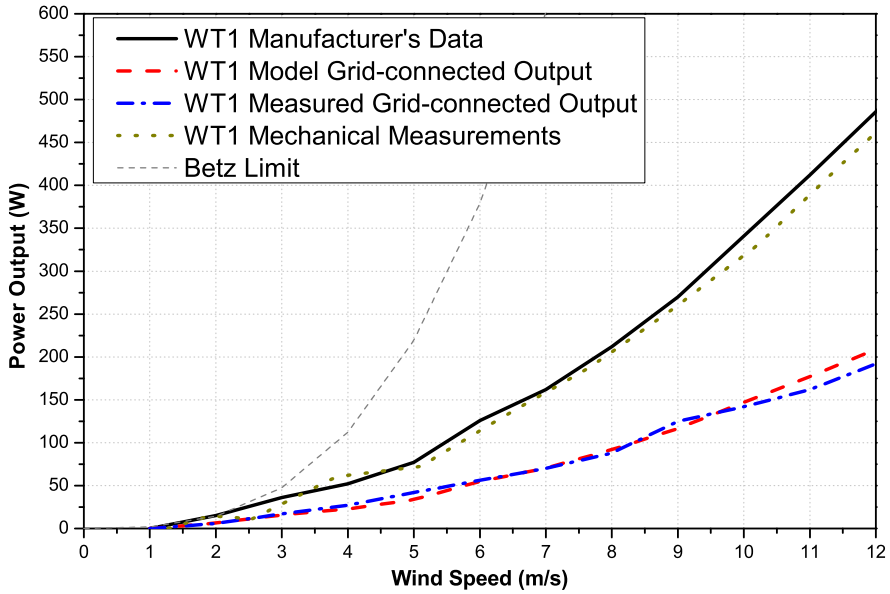

Figure 3.14: *Comparison of experimental (mechanical and electrical outputs), simulated (electrical output) and manufacturer (mechanical output) WT1 data.*

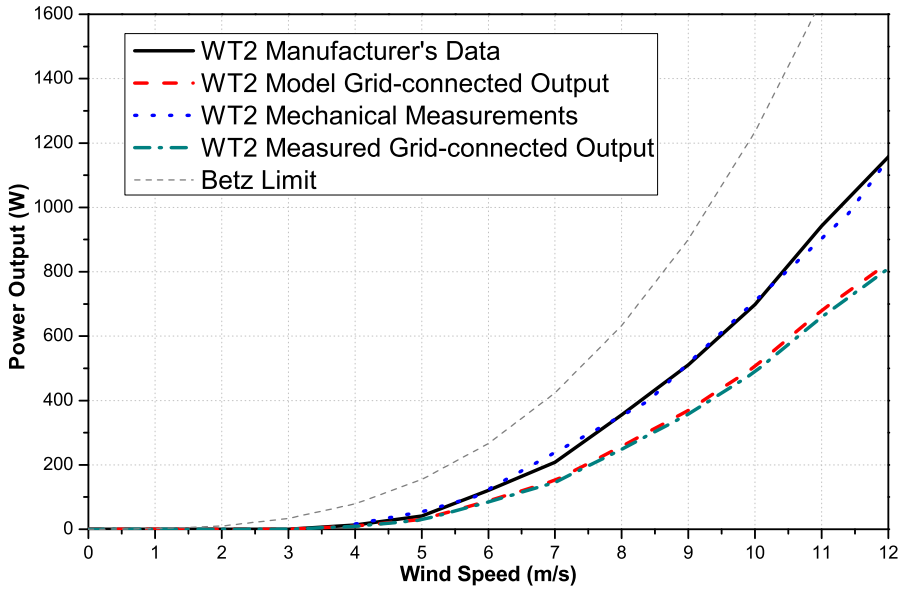

Figure 3.15: *Comparison of experimental (mechanical and electrical outputs), simulated (electrical output) and manufacturer (mechanical output) WT2 data.*

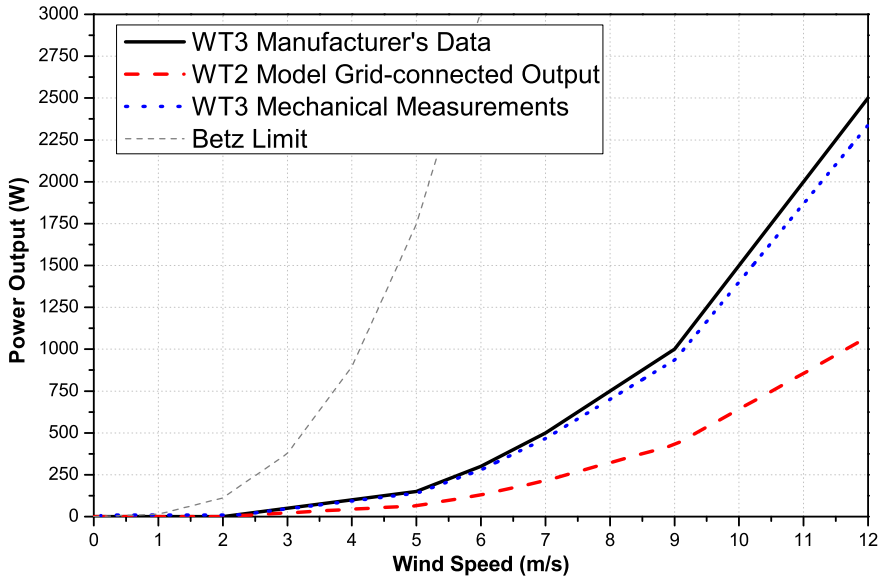

Figure 3.16: *Comparison of experimental (mechanical and electrical outputs), simulated (electrical output) and manufacturer (mechanical output) WT3 data.*

manufacturers) and electrical power curves, with the experimental data and simulations for grid-connected wind turbines. The electrical wind turbine outputs are obtained using the described d/q model of the generator, inverter and output filter. It can be appreciated that the results of the simulation provide a good match (maximum 3% error) with the experimental results.

3.7.1 Low-Voltage Network Model

The network modelled for grid connection represents a typical residential low-voltage (LV) network, supplying a number of house-type dwellings (one to few-storey buildings). This network is assumed to have medium to high load density supplied via cables, where MV and LV feeders are short ($L1$ up to few kilometres, $L2$ up to few hundreds of metres and $L3$ up to few tens of metres, as illustrated in Figure 3.17). In order to analyse connection of a modelled wind turbine to the grid, typical parameters and components of urban UK primary/secondary distribution network in Figure 3.17 have been identified from the data provided by distribution network operators and manufacturers (as shown in Table 3.3, [68]). The first component considered is an $11kV/0.4kV$ secondary distribution transformer. In UK urban areas, these transformers are typically ground/pad mounted, allowing for the voltage regulation with a summer/winter tap setting range of $\pm 5\%$, in 2.5% steps [69]. The second part of the modelled network is related

Transformer				
Voltage (kV)	Type	Rating (kVA)	R (pu)	X (pu)
11/0.4	Ground/pad mounted	500	0.0102	0.046
		315	0.0108	0.046
		200	0.015	0.045
Feeder				
Cable/Voltage	Length (m)	Cross-section	R (Ω/km)	X (Ω/km)
L_1, $11kV$	2500	185 mm^2	0.1485	0.0796
L_2, $0.4kV$	200	185 mm^2	0.1485	0.0796
L_3, $0.4kV$	30	35 mm^2	0.9217	0.0800

Table 3.3: *Transformer and feeder parameters for the modelled network.*

to MV and LV cables representing supply from $11kV$ to each individual customer (i.e. to the actual point of wind turbine connection).

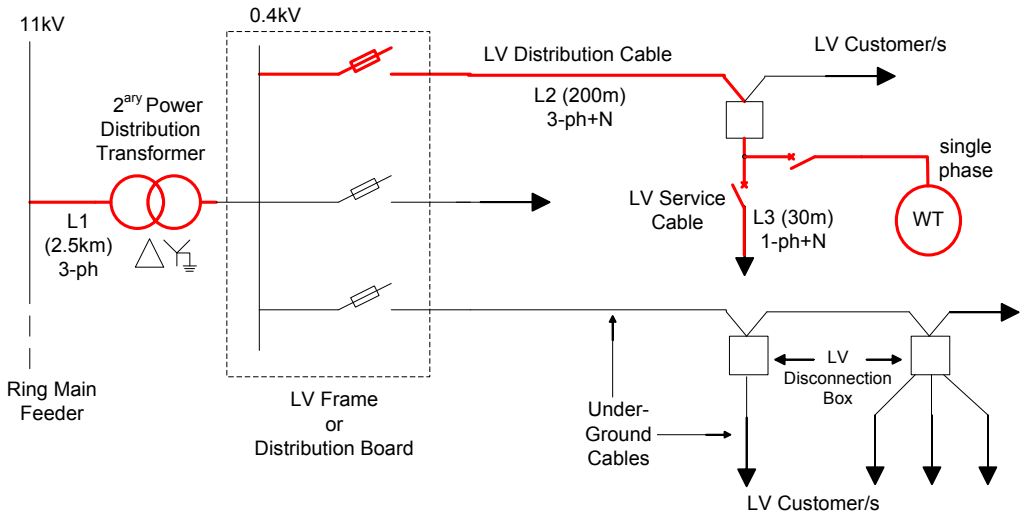

Figure 3.17: *Typical UK urban low-voltage network configuration [68].*

3.7.2 Simulation Results for Grid Connected Wind Turbine

The quasi-dynamic model provides details of the power delivered to the grid. The model represents in detail every component of the system and therefore the simulation is short due to computer limitation. Nevertheless, the 5-second window provides some basic information on the power quality and overall performance of the model. The purpose of this analysis is to give a general overview on how the wind turbine model operates and to show how the steady state measurements of the efficiency and power output are in accordance with the ones found in the

validation process (Section 3.7). The rms values of the output voltage and current for modelled WT1 are illustrated in Figure 3.18 and Figure 3.19 respectively. The inverter maintains the output voltage at the constant value ($230V_{rms}$) and the complete wind turbine systems now performs as a current source, providing the output power shown in Figure 3.20.

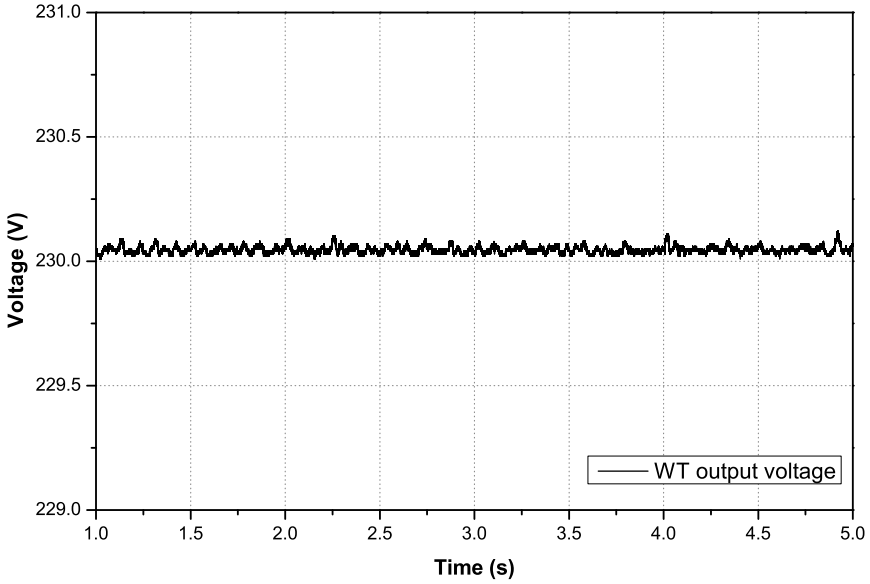

Figure 3.18: *Wind turbine output rms voltage.*

It can be inferred from Figure 3.20 that the output power of the wind turbine follows the variation of the input wind speed shown in Figure 3.23. Figure 3.21 and Figure 3.22 show voltage and current total harmonic distortion (THD) values, which exhibit relatively small variations, with maximum values around 3% and 5% respectively.

The THD values of the output voltage are in accordance with the specified limits in IEEE Standard 519 [70] and Engineering Recommendation G83/1 [57]. According to Engineering Recommendation G83/1 [57], current THD values and harmonic content should comply with the limits for "Class A" equipment in British Standard 61000-3-2 [59], as discussed in Section 3.6. Figure 3.24 illustrates that modelled WT1 has a DC component of the output current above the $20mA$ limit, which is recommended for small-scale generators in Engineering Recommendation G83/1 [57]. This result explains why the Office of Gas and Electricity Markets has proposed an increase in the limit of DC current injection [71] to overcome this as one of the barriers for the implementation of inverter-based microgeneration in UK urban areas. The results of this proposal were to stay within the $20mA$ limit for generators up to $2kW$ of rated power and 0.25% of the AC current for generators above $2kW$. This DC current component

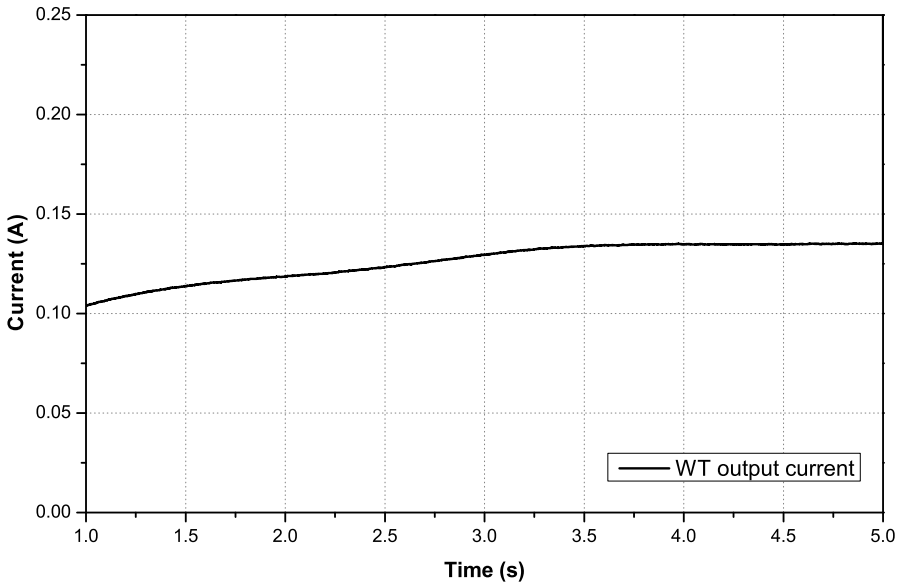

Figure 3.19: *Wind turbine output rms current.*

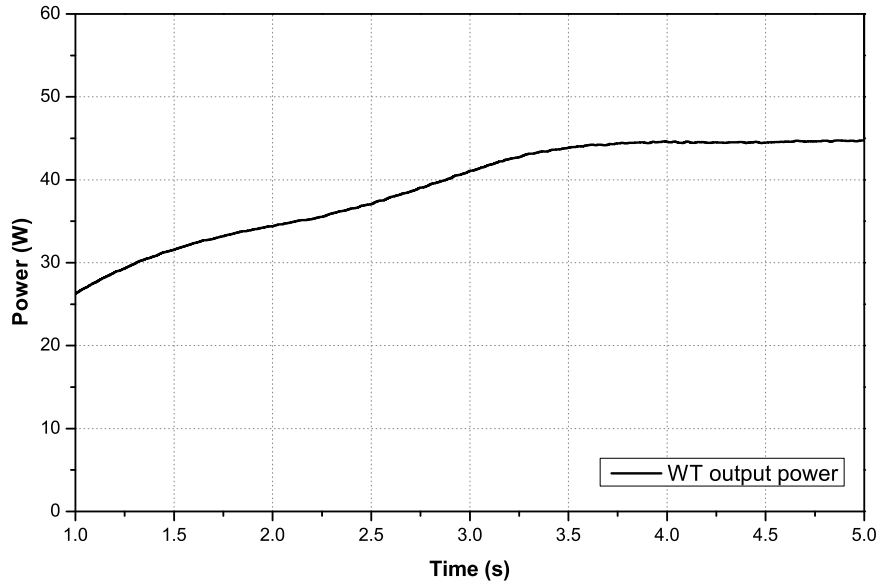

Figure 3.20: *Wind turbine output Power.*

issue is discussed by Infield et al. in [72], where is also concluded that the DC current might be a problem, especially when these installations lack transformers to cope with this problem. This suggests that the topologies are important and, in order to achieve a very small DC current component to flow into the network, more cost effective inverter topologies have to be carefully selected to ensure that DC current component is within the prescribed limits.

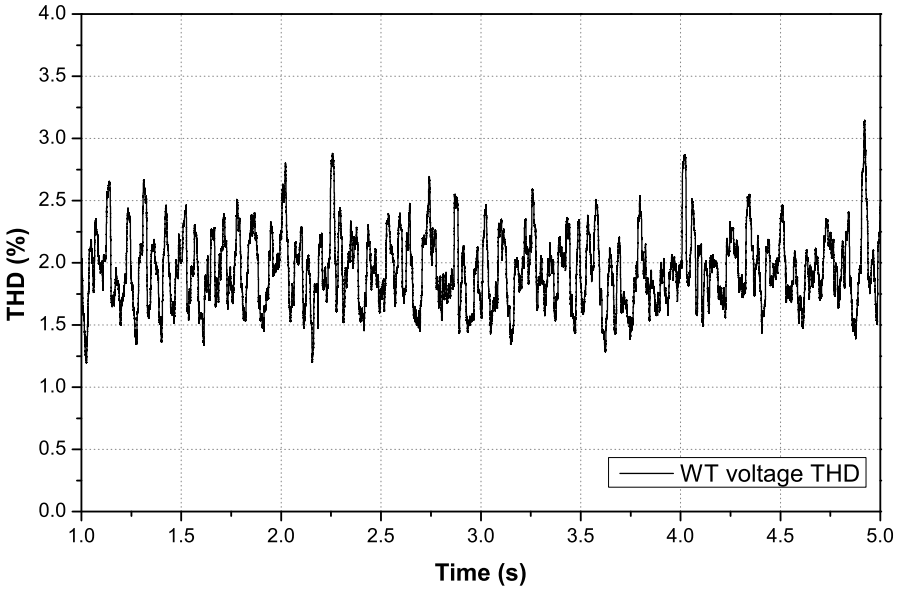

Figure 3.21: *Wind turbine voltage THD.*

The overall performance of the wind-based generation system is determined by the mechanical conversion efficiency of the turbine/blades, mechanical to electrical conversion efficiency of the generator and electrical AC-DC-AC efficiency of the inverter. For the presented wind turbine model and considered operating conditions in Figure 3.25, generator and inverter efficiency (i.e. electrical wind turbine efficiency, η_{el}) oscillates between 50% and 75%. These efficiencies comply with the efficiencies obtained from Figure 3.14.

$$\eta_{el} = \frac{P_{WT_{el}}}{P_{WT_{aero}}} = \frac{P_{WT_{el}}}{P_{aero} \cdot \eta_{aero}} \tag{3.19}$$

where, $P_{WT_{el}}$ is the output electrical power exported to the grid and $P_{WT_{mech}}$ is the mechanical input power at the shaft of the generator as extracted by the blades from the aerodynamic wind power.

Modelled PMSG of WT1 has an efficiency of 83% at the rated power (which is within the range of typical efficiencies of PMSG-type wind turbine specified in [51]). The efficiency of the modelled inverter is 91% at the rated power output [52] ($\eta_{el} = 0.83 \cdot 0.91 = 0.755$). A

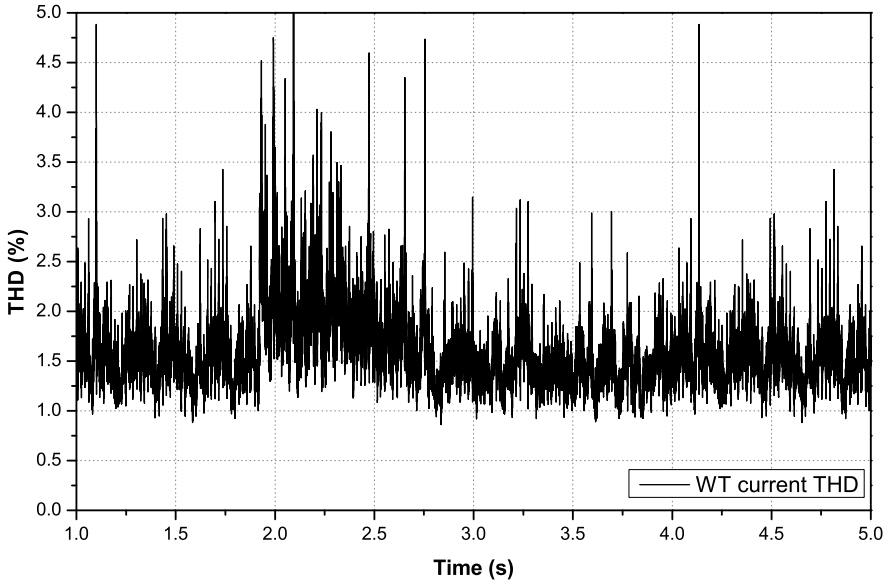

Figure 3.22: *Wind turbine current THD.*

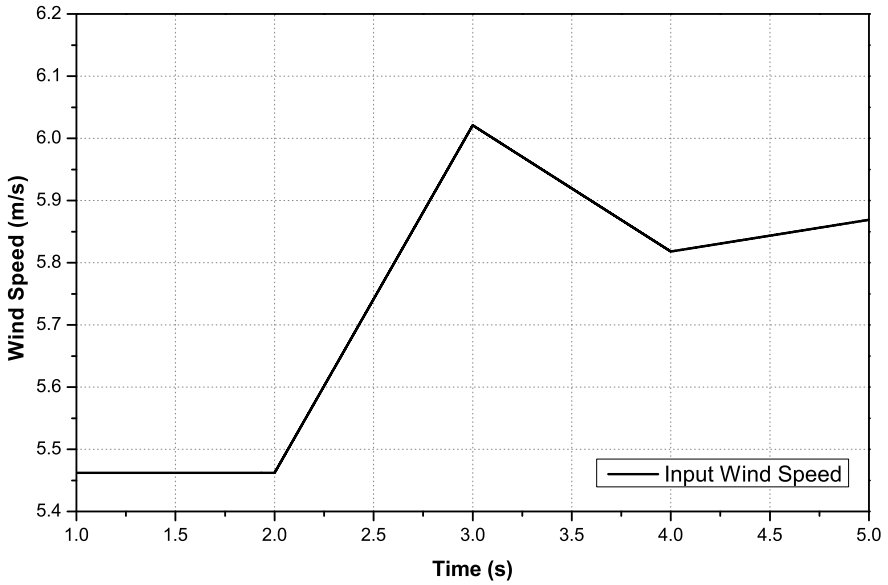

Figure 3.23: *Wind turbine input wind speed.*

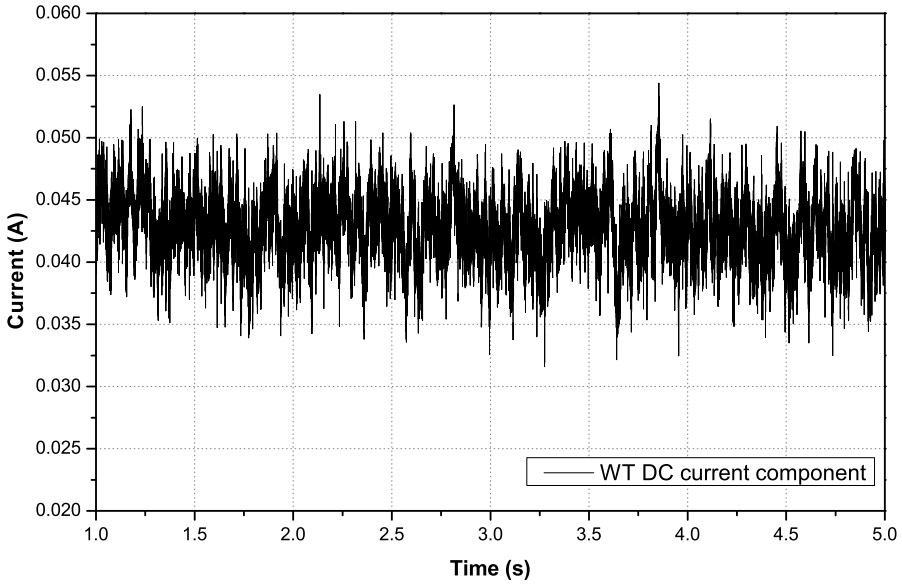

Figure 3.24: *DC component of wind turbine output current.*

wind turbine with a 100% efficient generator and inverter will still have its overall maximum efficiency limited by the mechanical conversion efficiency, as determined by its performance coefficient ($\eta_{aero} = C_p$), given by (2.4). For example, the aerodynamic conversion efficiencies, given by the manufacturer and validated through measurement, for WT1 and WT2 at a considered input wind speed (around 6 $^m/_s$, Figure 3.23) are about 22% and 27%, respectively (Figures 3.14 and 3.15):

$$\eta_{aero} = \frac{P_{WT_{aero\ at\ 6\ ^m/_s}}}{P_{aero\ at\ 6\ ^m/_s}} \tag{3.20}$$

where, $P_{WT_{aero\ at\ 6^m/_s}}$ is the aerodynamic output power of a wind turbine at a considered wind speed, $P_{aero\ at\ 6^m/_s}$ is the total available aerodynamic wind power at the considered wind speed. When the efficiencies of the inverter and generator are considered the total/overall efficiencies of WT1 and WT2 ($\eta_{tot} = \eta_{el} \cdot \eta_{aero}$) at the same considered input wind speed (i.e. $6^m/_s$ input wind speed) are about 16% and 20% obtained from the power curves shown in Figures 3.14 and 3.15, respectively, which have been validated by measurement and simulation, these values have not been calculated from the 5-second window shown previously. These low values of wind turbine overall efficiencies are in accordance with the substantial underperformance of micro and small-scale wind energy systems reported in Warwick Wind Trials [26], Energy Saving Trust [46] and Renewable UK [73]. As for these three considered wind turbine manufacturers published their power curves based on the wind turbine aerodynamic outputs,

showing only wind turbine aerodynamic efficiencies, the use of this information without taking into account electrical efficiency of the overall wind turbine system results in an overestimation of the calculated/estimated electrical power outputs. The aerodynamic power curves were obtained as AC-DC-AC conversion system (PMSG, rectifier, inverter and filter) was not included in the specifications by these manufacturers and which is not in accordance with the British Standard 61400-12-1 [28].

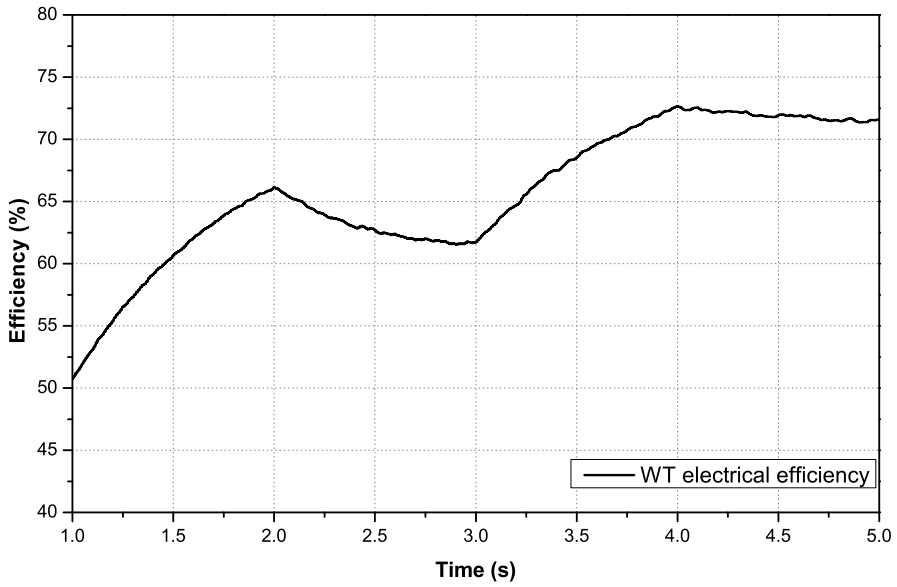

Figure 3.25: *Efficiency of wind turbine generator and inverter.*

3.7.3 Comparison of Results for Time-series Model and Weibull Energy Output

After the validation in the previous section, the developed wind turbine model is used for the calculation and comparison of energy outputs of three real wind turbines (WT1-WT3) for actual high-resolution input wind speeds (measured 1-second data) and for calculated lower resolution wind speeds (averaged 10-second, 1-minute, 10-minute and 1-hour data) when the data used are time-series, as well as for the input wind speeds modelled using the corresponding Weibull distribution (Figure 3.2) and manufacturer's aerodynamic power curve data and the electric output power curve (Figures 3.14 - 3.16). Table 3.4 presents the results for the calculated annual energy outputs, where one week of available data is multiplied/repeated for 52 weeks, in order to represent a whole calendar year. Table 3.4 shows that every averaging of high-resolution input wind speed data results in a relatively small, but still evident overestimation of the calculated

Wind Turbine	Energy ($MWh/year$)						
	$1s$	$10s$	$1min$	$10min$	$1hour$	Weibull Electrical power curve	Weibull Aerodynamic power curve
WT1	0.848	0.853	0.856	0.857	0.859	0.868	1.460
WT2	1.763	1.771	1.780	1.782	1.813	1.864	2.500
WT3	3.821	3.823	3.852	3.881	3.893	3.966	5.490

Table 3.4: *Calculated annual energy output.*

energy outputs, which is as higher as the averaging periods are longer. In accordance to the high-resolution wind data, when the energy was calculated using the Weibull distribution (with shape factor 1.94 and mean wind speed $6.54^{m}/_{s}$, Figure 3.2) with the electrical power curve the results are very similar, proving the model works and the Weibull distribution calculation is valid for energy yield analysis. The biggest overestimation as expected ($\geq 50\%$), occurs in the case when the Weibull distribution is used with the aerodynamic power curve.

3.8 Conclusions

In order to address some difficulties and uncertainties related to the analysis of micro and small-scale wind-based generation systems in urban areas, this chapter discussed and compared two general approaches: steady-state performance assessment and time-series steady-state performance assessment. The steady-state performance assessment is based on the use of low-resolution input wind speed data (i.e. measured, estimated, or Rayleigh/Weibull distribution represented hourly annual average wind speeds) and use of only some basic information on considered wind turbines (i.e. wind turbine manufacturer's power curve). For the time-series steady-state performance assessment, a component-based model of a wind turbine was used in conjunction with a higher-resolution input wind speed data in order to obtain more realistic results of the analysis. As this is not sufficiently documented in the existing literature, the chapter presents necessary information for the development of a detailed component-based model of a PMSG-based wind turbine in a d/q reference frame, connected to an inverter, which is fully validated using the experimental results for three actual wind turbines. The presented results of a time-series steady-state performance assessment suggest that the annual energy output of wind turbines will be calculated with a relatively small error for all considered resolutions of input wind speed data. This is important as the European Wind Energy Association recommends that input wind speeds should be recorded with a ten minute averaging period [74].

For the steady-state performance assessment, as well as for the initial selection of optimal wind turbines in target applications, this chapter selected three wind turbines for which all the analysis was presented. However, the only issue regarding this model that remains to be corrected is the DC current component for the injected current to the grid, where the value is above the $20mA$ limit required by the Engineering Recommendation G83/1. Nevertheless, this model is fully capable to realistically model outputs for the second-by-second measurements. Finally, the results of the assessment of performance of a grid connected wind turbine demonstrated the importance of modelling the whole wind-based generation system, where electrical efficiencies of the generator and inverter should be considered together with the aerodynamic conversion efficiency of the wind turbine. The 5-second window given in the last section provides information on the steady-state performance of the model when it is connected to the grid. These results even though important, are not detailed enough to provide a full dynamic response, indicating a need for a further work in modelling the system.
This model will be simplified in the forthcoming chapters and used with Chapter 2 results to aggregate the wind generation systems into the distribution network.

Chapter 4
Modelling of Micro and Small-scale Photovoltaic Generation Systems

4.1 Introduction

Chapter 2 presented the analysis of solar irradiance resources for Edinburgh city using the European Commission database (PVGIS) and the data obtained from the University of Edinburgh weather station. This analysis resulted in time-series profiles for Edinburgh city as a whole, where these days were built to be used in steady-state analysis of the power system performance of renewable-based microgeneration systems connected to the distribution network. However, before this analysis can be carried out, as presented for wind resource in Chapter 3, a detailed model of the PV system has to be developed. This model is validated with measurements from the Lemcko Energy & Power Quality Lab [75] also presented in this chapter. This chapter is divided in four main sections. Firstly, an introduction to the PV systems is presented. The second section presents the data used for validation of the PV models. In the third section, special attention was given to the main types of photovoltaic (PV) technologies that should be considered. Finally, the modelling of the PV system and its validation for the grid connection conditions is presented in the last section.

4.2 Photovoltaic Technology

The photoelectric effect was discovered by Alexandre Edmond Becquerel in 1839, when he observed that sunlight reaching a solid or a liquid between two electrodes produced an emf between them [76]. Since Becquerel's observation, many improvements and studies have been undertaken to develop systems capable of maximising the potential of the photovoltaic effect, making the PV panels one of the most mature and economically feasible technologies in the market of renewables. Many attempts to make a low-cost and efficient PV systems have been based on the use of semiconductor materials for making small photovoltaic cells. The PV cell

is the fundamental element of the PV system. This cell is made by two layers of semi conducting material, which has the property of absorbing light and producing electricity. Nowadays, silicon has been used as the preferred semiconducting material for PV systems. Although it has relatively low performance in terms of absorbing light compared to other semiconductors, it is one the most abundant materials in the Earth's crust, which makes it suitable for low-cost PV panels. The solar PV cells are large p-n junctions which operate like a diode that creates an electric field when exposed to sunlight. This causes the electrons to move and generate an electric current. It is therefore the "Diode" or "Shockley" equation (4.1) that describes the behaviour of the solar panels. Figure 4.1 shows the schematics of the typical model of the PV cell. The diagram is divided in two parts: the first part on the left shows the ideal PV cell which contains the current source with the diode that will generate an exponential response of the cell, the output of which will vary depending on the solar irradiance; the part on the right is the practical device side that considers the losses of the system. From Figure 4.1, focusing

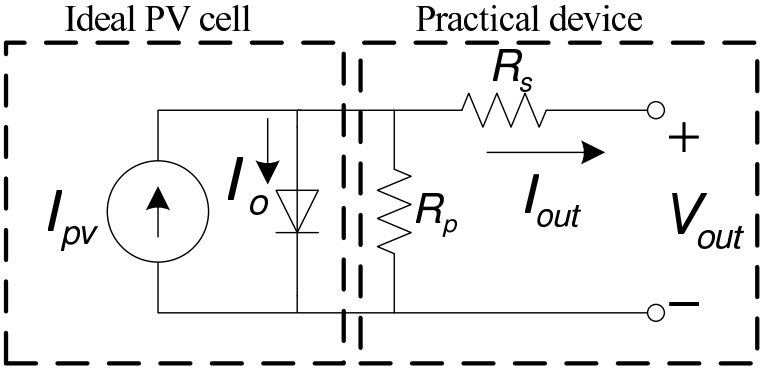

Figure 4.1: *Theoretical model of a PV cell.*

on the ideal PV cell part of the diagram, the basic model of the PV cell is presented by (4.1). This model shows the general approach for PV modelling, with its essential parameters (i.e. the photoelectric effect current) without considering the losses of the real system [77].

$$I_{out} = I_{pv} - I_o\left[e^{(\frac{qV}{ak_BT})} - 1\right] \tag{4.1}$$

where, I_{out} is the output photovoltaic current directly proportional to the input solar irradiance, I_o is the diode reverse saturation current, q is the electron charge $(1.6 \times 10^{-19}C)$, k_B is the Boltzmann constant $(1.38 \times 10^{-23}J/^{\circ}\mathrm{K})$, T is the temperature of the p-n junction $(^{\circ}\mathrm{K})$, V is the cell voltage, a is the diode ideality constant. Using this equation it is possible to predict the typical shape of the output of the PV cell, Figure 4.2 shows the VI (voltage-current) characteristic of a PV cell at a constant solar irradiance. The response is exponential and as can be

appreciated from the diode equation, there are four variables in the system: the V_{oc} is the open circuit voltage, V_{mpp} is the maximum power point voltage, I_{sc} is the short circuit current and the I_{mpp} is maximum power point current. Although, all these variables depend on the input solar irradiance, the output current of the cell is the most sensible to its change.

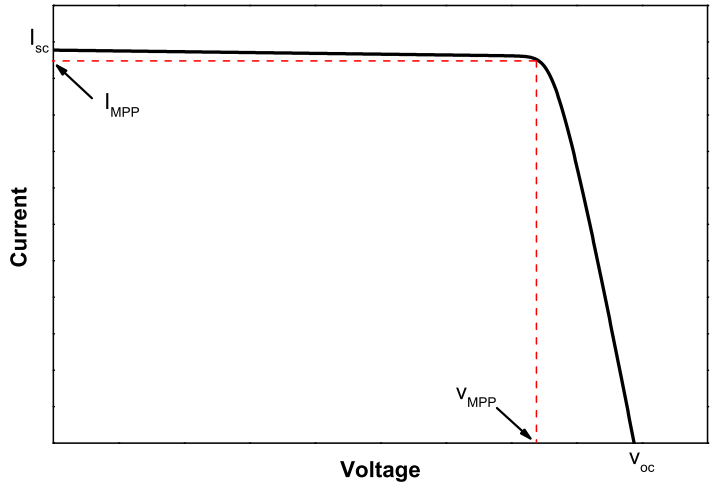

Figure 4.2: *Voltage and current typical characteristic of a PV cell.*

Figure 4.3 shows the power output of the cell at a certain solar irradiance. This output presents the V_{oc}, V_{mpp} and the P_{mpp}, the latter being the power achieved when the system operates at the maximum power point. The maximum power points of the system depend on the solar

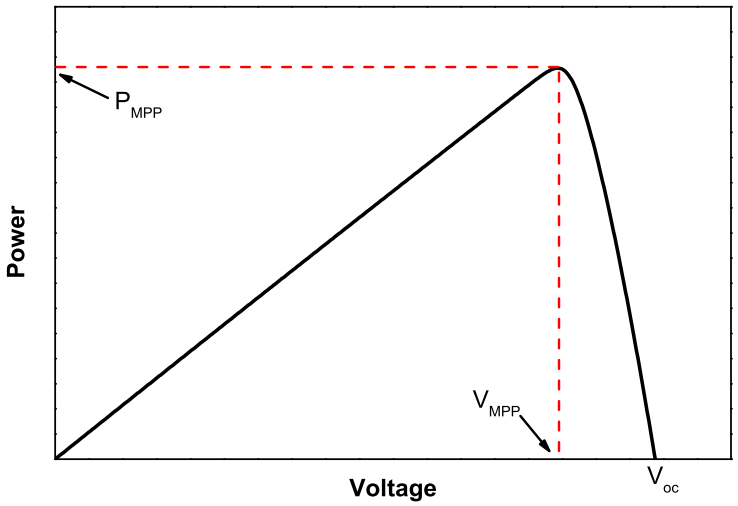

Figure 4.3: *Power and voltage characteristic for a PV cell.*

irradiance and the particular characteristics of the PV cell. These characteristics are typically

reported by the manufacturers of PV devices and can also be obtained through lab experiments and measurement, these characteristics are detailed in Table 4.1. This table defines the characteristics detailed later on in this chapter in Table 4.3. Generally, these characteristics vary depending on the fabrication method of the PV cell.

Solar PV characteristics	
Characteristic	Description
V_{oc}	Open-circuit voltage
I_{sc}	Short-circuit current
V_{mpp}	Voltage at the maximum power point
I_{mpp}	Current at the maximum power point
K_V	Voltage temperature constant
K_I	Current temperature constant
N_s	Cells connected in series
$NOCT$	Normal operating cell temperature
$Area$	Area of the panel in m^2

Table 4.1: *PV characteristics reported by manufacturers, as required by the British Standard BS60904-3 [78].*

The PV technologies analysed in this thesis are classified into three main categories: first generation (Crystalline technologies), second generation (Thin-film technologies) and the alternative cell manufacturing technologies, the latter being part of the recent thin-film generation technologies.

4.2.1 First Generation Technologies

This generation of PV systems is based on crystalline silicon, which is the most common technology for PV systems currently found in the market with over 80% of the market participation. These PV cells are composed by slices of crystalline silicon called wafers that come from a single block (ingot) of silicon. There are three types of crystalline cells, which differ in their fabrication method. The crystalline cell types are:

- Monocrystalline,
- Polycrystalline or Multi-crystalline,
- Ribbon and sheet-defined film growth.

For this technology it is typically found that between 60 to 72 crystalline cells are connected to build a panel which depending on the manufacturer rates between $120W_p$ and $300W_p$, with efficiency between 12% and 19%.

4.2.2 Second Generation Technologies

This group of PV cells is based on the Thin-film fabrication, consisting of thin layers of photosensitive materials on top of plastic, glass or stainless steel. While this causes the cost of the panels to decrease, it also reduces the efficiency. However, this technology allows to make flexible panels which brings the advantage in various consumer applications. The typical four types of thin-film technology are:

- Amorphous Silicon (a-Si),
- Multi-junction thin silicon film (a-Si/μc-Si),
- Cadmium telluride (CdTe),
- Copper-Indium-Gallium-Selenide/Sulphide (CIGS) and Copper-Indium-Selenide/Sulphide (CIS).

Table 4.2 shows the efficiencies reported from the installations of thin-film technologies in comparison with the lab reported efficiencies of these technologies. Even though the efficiencies are roughly 30% lower with respect to the first generation (crystalline) technologies. The advantage of this fabrication technique is the lower manufacturing costs implied and the use of raw materials, making these technologies attractive to the market.

Thin-film technology	Commercial module efficiency	Lab tested efficiency
a-Si	7.1%	10.4%
a-Si/μc-Si	10%	13.2%
CdTe	11.2%	16.5%
CIGS/CIS	12.1%	20.3%

Table 4.2: *Commercial and lab reported Thin-film PV technology efficiencies [43].*

4.2.2.1 Alternative Cell Manufacturing Technologies

One of the main challenges for PV technologies is to increase the cell capability, so that it can absorb a larger spectrum of sunlight and therefore increase its efficiency whilst lowering costs of manufacturing. New technologies have emerged with these characteristics, but they are still not available on a large scale for the PV market. These technologies fall into the advanced second generation technologies based on various manufacturing techniques. For example, within the Solar division of Sanyo the electric company, a panel has been developed (a panel with a manufacturing technique called "Heterojunction with Intrinsic Thin-layer HIT") which has brought the efficiency of the cell up to 20%. This new technology consists of a thin single-crystal wafer combined with amorphous silicon (a-Si) layers, maximising the overall efficiency of the cell.

4.2.3 PV Testing Procedure

As previously mentioned, the characteristics of the PV panels are supplied in the manufacturers specifications. These characteristics are determined by a standardised testing procedure for each PV cell in order to be replicated. In general, the PV cell in field applications is exposed to non-uniform conditions such as temperature and solar irradiance. Therefore, a standard approach is required to establish a set point for manufacturers in order to correctly obtain and specify the characteristics of the PV cell. This issue is regulated is the British standard BS60904-3:2008 [78], which defines the Standard Testing Condition (STC) as:

- Vertical irradiance S of $1000^{W}/_{m^2}$,
- Air temperature T of $25\,^{\circ}\mathrm{C}$,
- Light spectrum through an air mass of 1.5.

The vertical irradiance is defined as the radiant power from the Sun's disk and from the circumsolar region of the sky within a subtended angle of 5° incident upon unit area ($^{W}/_{m^2}$). The air mass is defined as the length of path through the Earth's atmosphere traversed by the direct solar beam, expressed as a multiple of the path traversed to a point at sea level with the Sun directly over head. The value of air mass is 1 at sea level with cloudless sky when the Sun is directly overhead and the air pressure $P = 1.012bar$ ($760mmHG$) [78]. The characteristics obtained under the Standard Testing Conditions are the nominal values of the PV cell and they

are provided by the manufacturers in their specification sheets. In these specification sheets, the manufacturer also has to provide the temperature that the PV cell is going to reach under operating conditions. This temperature is reported as Normal Operating Cell Temperature (NOCT) and according to standard the normal operating conditions for this temperature are:

- Irradiance S of $800 W/m^2$,
- Air temperature of $20\,^{\circ}\mathrm{C}$,
- Wind speed of $1 m/s$.

This temperature will depend on the material of the PV cell and the technology used for the fabrication, but typically the NOCT values are between $33\,^{\circ}\mathrm{C}$ and $58\,^{\circ}\mathrm{C}$, with a value of $48\,^{\circ}\mathrm{C}$ being the average value for a PV cell [76].

4.3 Measured Data from Belguim

Measurements are crucial for the validation of the developed models. In the case of the wind model, the data were available from previous lab tests of the considered wind turbines. In the case of the PV panels, measured data were available from the Lemcko Energy & Power Quality Lab [75]. These data were used for the purpose of validation of the model because raw data for the UK were not found. Nevertheless, the raw data was required for this part of the validation and therefore this set of data is extremely useful for that purpose. These data consist of one year of five minute average measurements for four different technologies: monocrystalline, polycrystalline, low-efficiency thin-film and HIT thin-film technology. The set of measured data include power output delivered to the grid of these four technologies in three different scenarios, open, closed and tracker output. "Open" represents a typical PV installation with the panels exposed to the air allowing natural convection (air cooling the back surface of the panels). The "closed" installation has the back part of the PV panel covered to avoid natural convection and therefore the cooling of the system. Finally, the polycrystalline and thin-film panels were installed together on a pole-mounted structure equipped with a sun-tracking device. This device positions the entire structure to the ideal angle for maximum solar irradiance. Figure 4.4 shows the comparison between the "tracker" measurements of solar irradiance with the normal fixed solar irradiance measured when no tracking device is used. The difference between them is considerable and a tracking device will increase outputs of PV systems. The

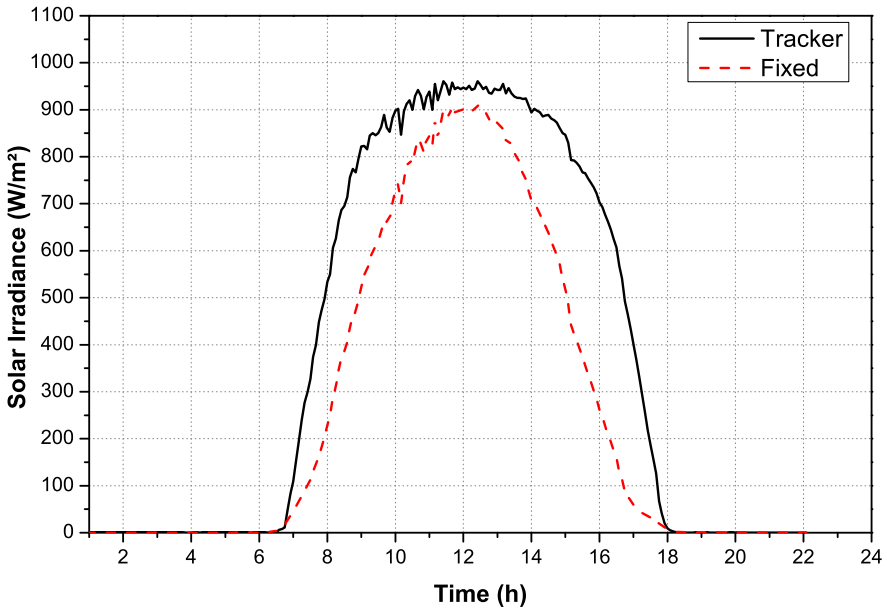

Figure 4.4: *Solar irradiance measurements, "Tracker" compared to "Normal".*

other available measurement was the temperature of each panel.

The purpose of this thesis is to identify the properties of a typical PV system as it would be installed in an urban area location (e.g. rooftop of a building). Therefore, the data used for the validation are the open and fixed to optimal angle systems. The power output of a PV panel for a given input solar irradiance is recorded as the AC output. The manufacturers specification for each technology is reported in Table 4.3. These are the characteristics needed for the modelling of the PV system. Six monocrystalline panels have been connected together to make an instal-

	Monocrystalline	**Polycrystalline**	**Thin-film**	**Thin-film (HIT)**
Manufacturer	Suntech [79]	Yingli Solar [80]	Sharp [81]	Sanyo [82]
Power Output	180W	180W	121W	230W
V_{mpp}	36V	23V	45V	34.3V
I_{mpp}	5A	7.83A	2.69A	6.71A
V_{oc}	44.8V	29.5V	59.2V	42.3V
I_{sc}	5.29A	8.3A	3.35A	7.22A
K_V	-0.34%/°C	-0.37%/°C	-0.3%/°C	-0.106^V/°C
K_I	0.017%/°C	0.06%/°C	0.07%/°C	2.17^{mA}/°C
N_s	6	6	180	6
NOCT	45 °C	46 °C	44 °C	25 °C
Area per panel	$1.27m^2$	$1.29m^2$	$1.42m^2$	$1.38m^2$

Table 4.3: *Manufacturer specifications of considered PV panels.*

lation of $1.28kW$, seven polycrystalline panels with a peak power of $1.26kW$, ten thin-film

panels connected for a maximum power of $1.21kW$ and five HIT Thin-film panels with a peak power of $1.15kW$. These configurations are available for the three scenarios: closed, open and tracked installations.

4.4 The PV Model

Equation (4.1) showed the ideal model of the PV cell. In order to properly model the four main technologies considered in this thesis some variables have to be added to make the model more detailed and applicable to the different technologies. This modification includes the second part of the schematic diagram shown in Figure 4.1, where the practical device side of the PV cell has to be taken into account to model the real PV system [77].

$$I_{out} = I_{pv} - I_o\left[e^{\frac{V_{out}+R_sI_{out}}{aV_t}} - 1\right] - \frac{V_{out}+R_sI_{out}}{R_p} \tag{4.2}$$

where, I_{out} is the total current produced by the PV cell (A), I_{pv} is the photovoltaic current directly proportional to the available solar irradiance (A), I_o is the diode saturation current (A), V_{out} is the cell voltage (V), a is the diode ideality constant, V_t is the thermal voltage (V) (defined by (4.3)), R_s is the series equivalent resistance of the PV cell (Ω), R_p is the parallel equivalent resistance (Ω). Thermal voltage is given as:

$$V_t = \frac{N_s k_B T}{q} \tag{4.3}$$

where, q is the electron charge ($1.6\times10^{-19}C$), k_B is the Boltzmann constant ($1.38\times10^{-23}J/^{\circ}\mathrm{K}$), T is the temperature of the p-n junction in $^{\circ}$K, N_s is the number of cells connected in series within the PV array. The model can be used to reproduce the VI curves of any PV system if the parameters are known. The output current of the PV cell depends on solar irradiance. From specification sheets, I_{sc} can be obtained, assuming the series resistance is very low and the parallel resistance is very high, it can be then assumed that $I_{pv,n} \approx I_{sc}$. Therefore the photovoltaic current can be described as:

$$I_{pv} = (I_{pv,n} + K_I\Delta_T)\frac{S}{S_n} \tag{4.4}$$

where the $I_{pv,n}$ is the current measured according to the standard testing condition (i.e. $25\,^{\circ}C$ and $1000^{W}/_{m^2}$), K_I is the temperature current coefficient, Δ_T is the difference between the nominal temperature and the actual temperature in $^{\circ}K$, S is the actual solar irradiance in $^{W}/_{m^2}$, S_n is the nominal solar irradiance of $1000^{W}/_{m^2}$. The diode saturation current is a function of

the variables of the system,

$$I_o = \frac{I_{sc} + K_I \Delta_T}{e^{(\frac{V_{oc}+K_V \Delta_T}{aV_t})} - 1} \tag{4.5}$$

where, V_{oc} is the open circuit voltage (V), I_o is the diode saturation current (A), K_I is the temperature current coefficient (in $\%/^\circ C$ or $^{mA}/^\circ C$ depending on the manufacturer), Δ_T is the difference between the nominal temperature and the actual temperature in $^\circ K$, K_V is the temperature voltage constant (in $\%/^\circ C$ or $^V/^\circ C$ depending on the manufacturer) and V_t is the thermal voltage (V) given by (4.3). The value of the diode ideality constant a may be arbitrarily chosen. Many papers discuss ways to estimate the correct value of this constant [83]. Usually, $1 \leq a \leq 1.5$ and the choice depends on the rest of the parameters of the model. Some values for a are found in [84] based on empirical analyses. Because a expresses the degree of ideality of the diode and it is totally empirical, any initial value of a can be chosen in order to adjust the model. The two remaining parameters R_s and R_p can be calculated using an iterative method reported in [77]. This method uses the manufacturer's specification to obtain the correct pair of resistances that can reproduce specified values. Equation (4.6) shows the relationship between R_s and R_p.

$$R_p = \frac{V_{mpp}(V_{mpp} + I_{mpp}R_s)}{\left[V_{mpp}I_{pv} - V_{mpp}I_o e^{[\frac{(V_{mpp}+I_{mpp}R_s)q}{N_s a k_B T}]} + V_{mpp}I_o - P_{max,e}\right]} \tag{4.6}$$

The values of the resistances can affect the value of the rated photovoltaic current:

$$I_{pv,n} = \frac{R_p + R_s}{R_p} I_{sc} \tag{4.7}$$

In the first iteration, the value of $R_s = 0$, which is then increased in each iteration. The starting value for R_p is defined by:

$$R_{p,min} = \frac{V_{mpp}}{I_{sc,n} - I_{mpp}} - \frac{V_{oc} - V_{mpp}}{I_{mpp}} \tag{4.8}$$

The iterative algorithm is illustrated in Figure 4.5, using the equations described previously until the target values are achieved. After running this algorithm and obtaining the values of the resistances they are fed into the model. In order to reduce computational time and simplify the modelling, the model is built under some assumptions. The first assumption is that the maximum power point voltage is constant and achieved regardless of the actual solar irradiance. This can only be possible if assumed maximum power point tracking (MPPT) algorithm works almost ideally, i.e. with an error less than 5%. The second assumption is that the resistances calculated under the Standard Testing Conditions (STC) will remain constant once they have

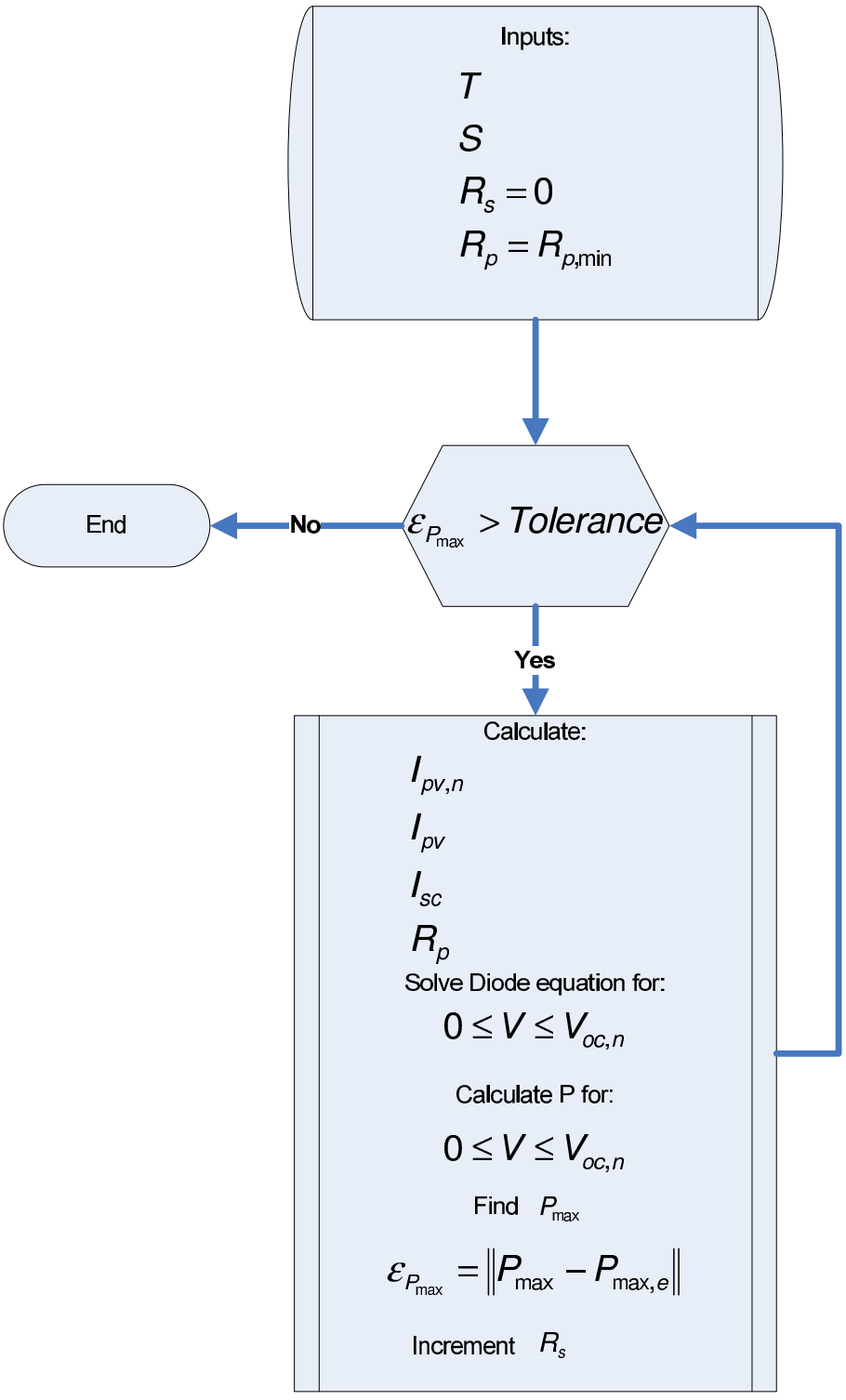

Figure 4.5: *Algorithm used for calculating R_p and R_s [77].*

been calculated by the algorithm. This means their values are not affected by the temperature changes in the PV cell throughout the day. The final assumption is that the power factor is always equal to 1.

4.4.1 The Inverter Model

The inverter model that has been presented in Chapter 3 is also used in this chapter. The model has been tuned to operate with the PV panels instead of the PMSG-rectified output and no further modification of the model is required in this chapter.

4.5 Validation of PV Models by Measurement

Even though the set of measurement data is very useful for this chapter, there is a problem with the first half of the day solar irradiance measurements. As previously mentioned, shadowing effect is an issue difficult to quantify and important to address. The measured solar irradiance vector of this set of data has a shadow in the first half of the day that is not present (because of the Sun positioning) in the second half of the day. This effect causes a lower registered solar irradiance value than the actual. A similar problem is reported in [85]. When these values are used to obtain the power output from the models, they give as a consequence a lower power output. This reflects a problem with matching the first half of the day data for the modelled technologies. It is not perceptive in the form of power output, but the efficiency plots show the difference between the first and the second halves of the day, which is given later in this chapter.

Using the values presented in Table 4.3 and the equations described in Section 4.4, the model is built and validated using the measurements from Lemcko Energy & Power Quality Lab. For the validation, two days were selected from the recorded year: one clear day (i.e. clear sky with no obstructions) and one cloudy day (i.e. high variations of solar irradiance throughout the day). Using these days, the model is adjusted (i.e. parameters calculated) to represent the four considered technologies.

The results for the monocrystalline technology are given in Figure 4.6 and Figure 4.7, showing that for both cases the validation has some discrepancies for the day selected due to the solar irradiance recording as previously mentioned. Also, other contributions to the small mismatch between the model and the measurements is caused by the assumption of the constant

resistances of the system, the actual temperature being outside the Standard Testing Conditions (STC) and the small imported/exported reactive power from the grid at certain points of the day causing the difference in power outputs.

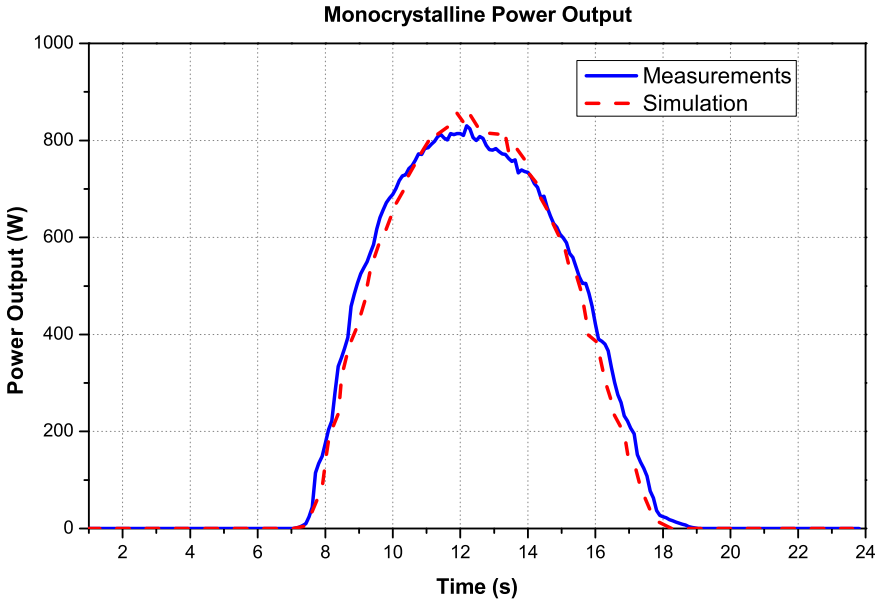

Figure 4.6: *Validation by measurement of the modelled PV monocrystalline technology: clear day.*

Figure 4.8 and Figure 4.9 show the validation for the polycrystalline technology, showing a good matching of the model's results with measurements for both days. This technology has been found to be less sensitive to changes of the model's parameters, compared to the monocrystalline technology. Figure 4.10 and Figure 4.11 show that the other modelled thin-film technology also can match the measurements with no substantial differences.
For the case of the HIT Thin-film technology shown in Figure 4.12 and Figure 4.13, the model is able to match the measured outputs more accurately than the first generation crystalline technologies analysed previously, as this technology is not sensitive to changes in the model's parameters for different operating conditions.

4.5.1 Tracker Measurements

As the developed model can be adapted to the specific solar irradiance, the measured tracker solar irradiance is used as the input and fed into the model for the two technologies installed with this tracking device. Figure 4.14 shows the validation for polycrystalline technology, which,

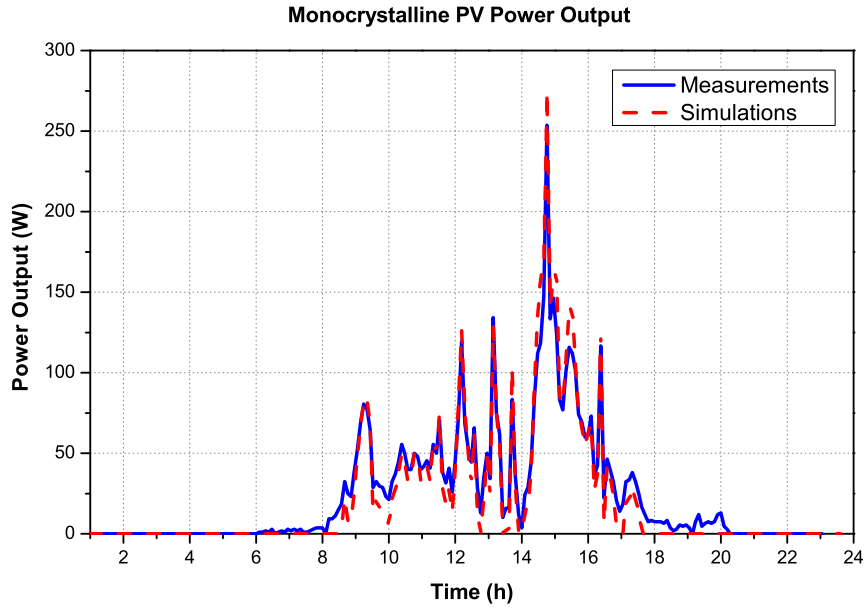

Figure 4.7: *Validation by measurement of the modelled PV monocrystalline technology: cloudy day.*

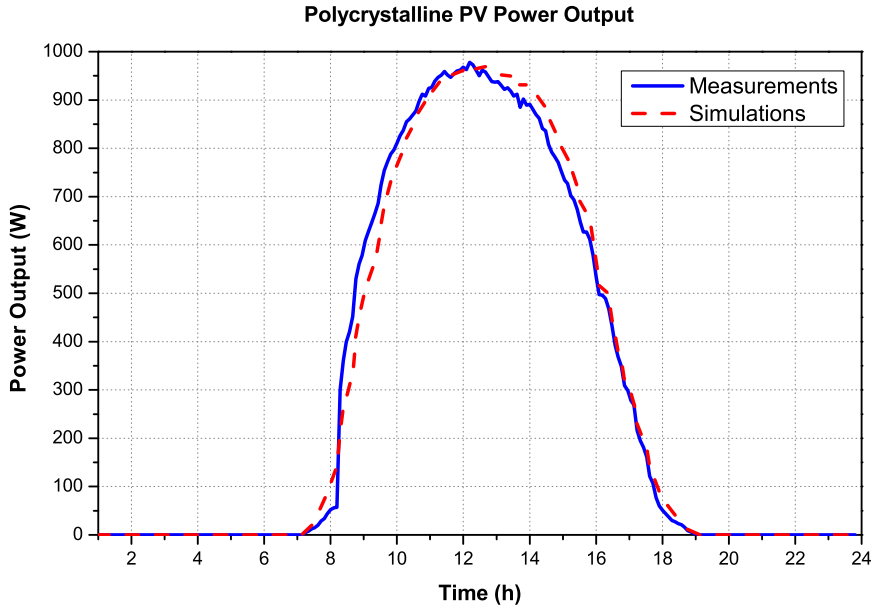

Figure 4.8: *Validation by measurement of the modelled PV polycrystalline technology: clear day.*

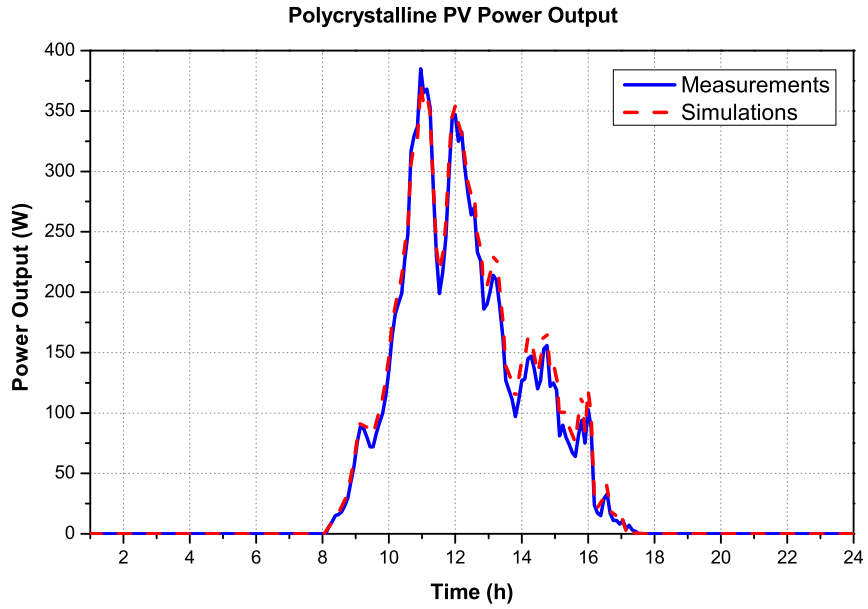

Figure 4.9: *Validation by measurement of the modelled PV polycrystalline technology: cloudy day.*

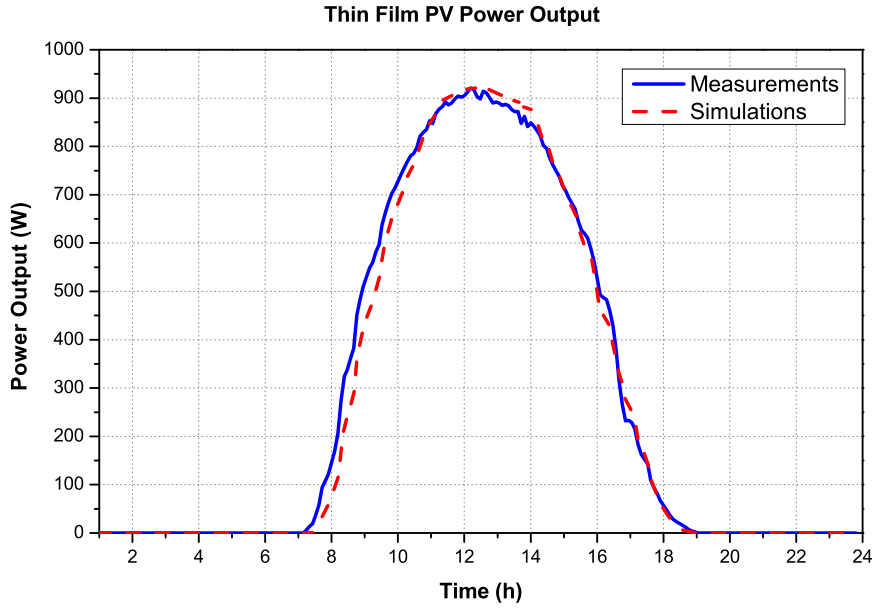

Figure 4.10: *Validation by measurement of the modelled PV thin-film technology: clear day.*

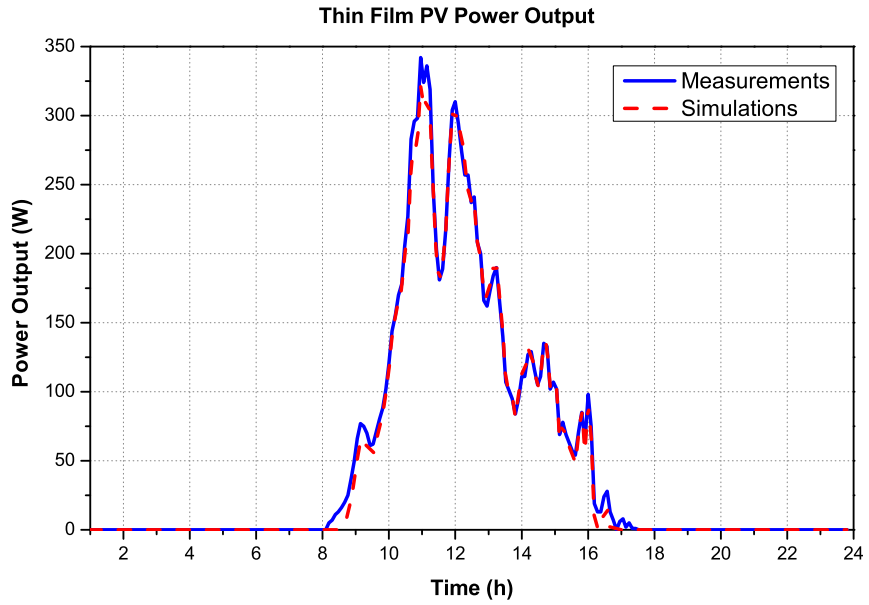

Figure 4.11: *Validation by measurement of the modelled PV thin-film technology: cloudy day.*

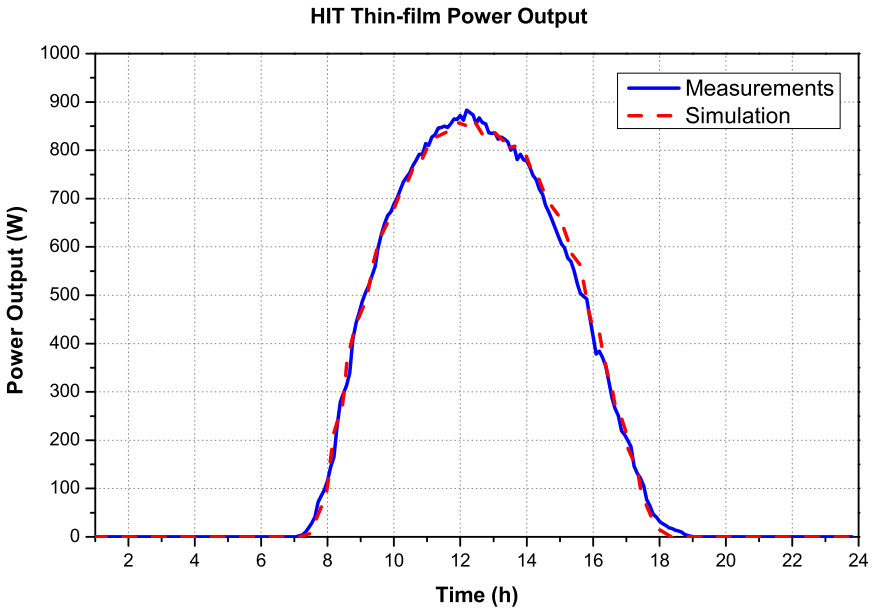

Figure 4.12: *Validation by measurement of the modelled PV HIT thin-film technology: clear day.*

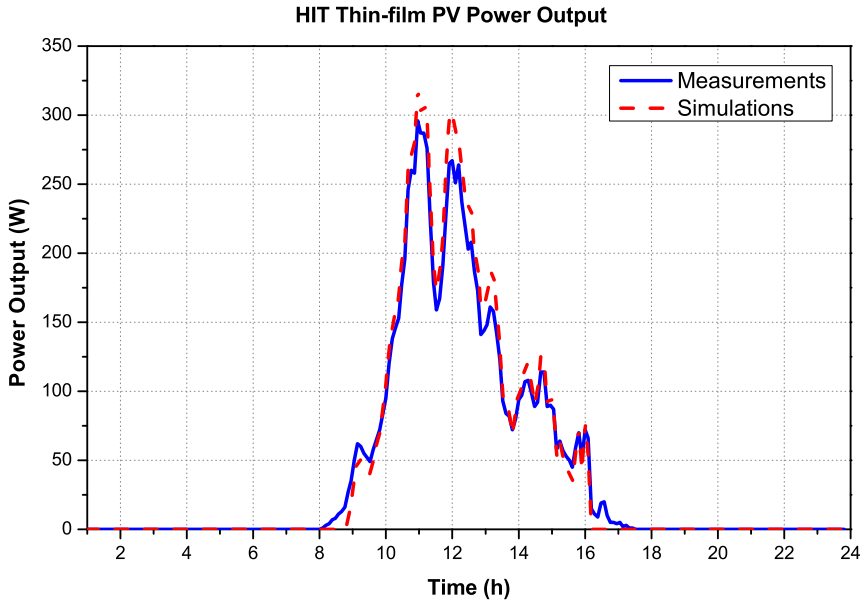

Figure 4.13: *Validation by measurement of the modelled PV HIT thin-film technology: cloudy day.*

as previously mentioned is highly sensitive to temperature changes. This technology was only available for two technologies and the shadowing is not present throughout the data set. Therefore, for the first half of the day the model matches more closely the measurement. Similarly, Figure 4.15 shows the validation of the developed PV model with the tracker measurements for the thin-film technology. Again this model is able to even more closely match the measured power outputs.

4.5.2 Efficiency Measurements

As with any other energy system, the efficiency of the PV panel is the one of the most important characteristics for the analysis. The efficiency will influence the area needed for installing the PV system with a desired rated power or, in other words, the desired peak power achieved by a selected system on a certain exposed area. It is therefore important to determine the efficiency of the considered and modelled PV systems. This efficiency can be simply computed as:

$$\eta_{pv} = \left[\frac{V_{mpp} I_{mpp}/A}{S_{SCT}}\right] \times 100 \tag{4.9}$$

where, the V_{mpp} is the voltage at the maximum power point, I_{mpp} is the current at the maximum power point, A is the area of the panel in m^2 and S_{SCT} is the solar irradiance at Standard Testing Conditions ($1000^{W}/_{m^2}$). Using this equation, Table 4.4 shows the efficiency of the panels

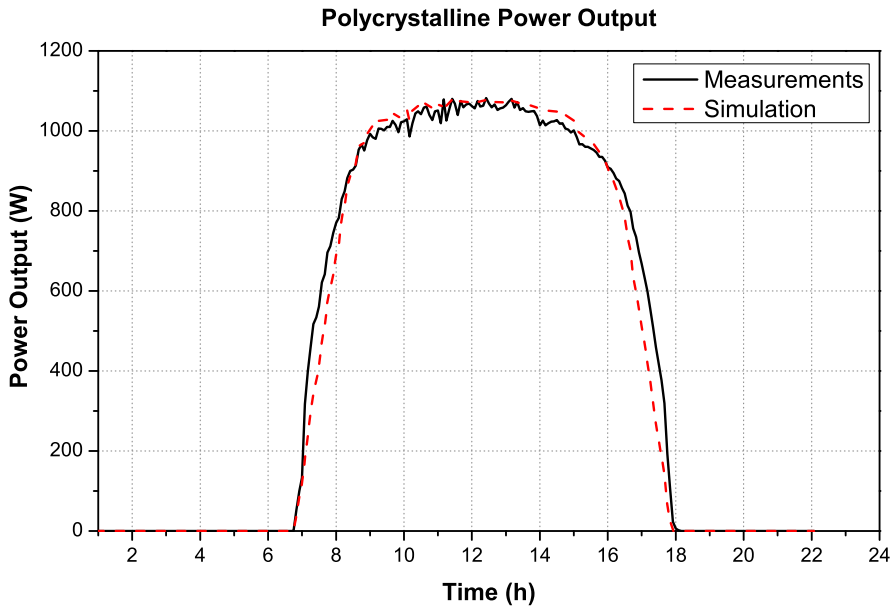

Figure 4.14: *Validation by measurement for the polycrystalline technology, using the tracked solar irradiance on a clear day.*

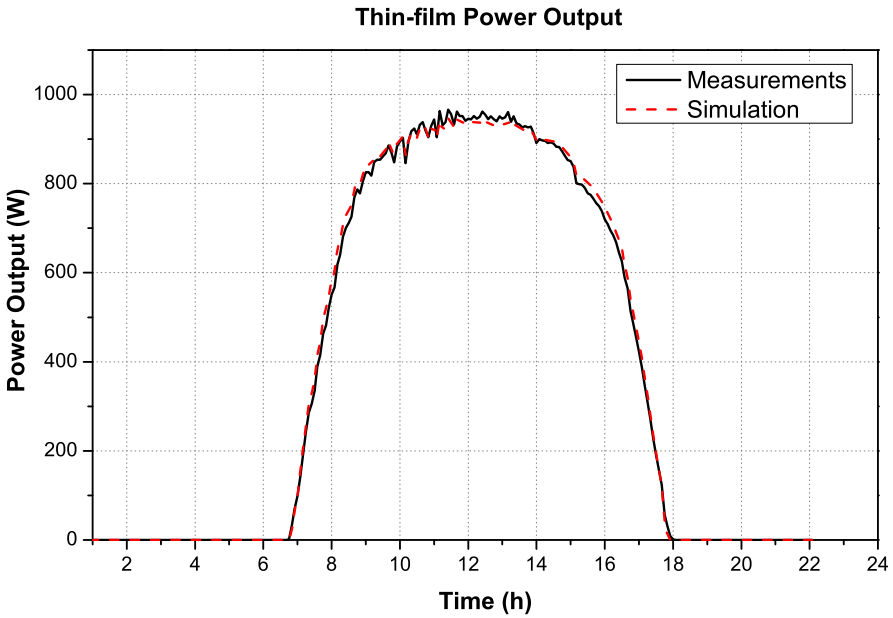

Figure 4.15: *Validation by measurement for the thin-film technology, using the tracked solar irradiance in a clear day.*

considered in this chapter. Apart from the calculation, the efficiency of the panel is typically reported in the manufacturer specification sheets.

Manufacturer	Technology	Manufacturers Reported Efficiency
Suntech	Monocrystalline	14.17%
Yingli Solar	Polycrystalline	13.95%
Sharp	Thin-film	8.5%
Sanyo	HIT Thin-film	16.67%

Table 4.4: *Calculated efficiencies of the considered PV installations, [79], [80], [81], [82].*

It is important for the model to reproduce the same efficiency of the actual PV panels, since it describes the maximum power which the panel can absorb from the available solar irradiance. Using the measurements from Lemcko Energy & Power Quality Lab [75], the simulated and the measured efficiencies are compared as an additional way to validate the developed PV models of the four considered technologies. The power measured is the final stage electrical power exported to the grid. Figure C.1 to Figure C.5 in Appendix C show an attempt to use the data for the full year and identify the efficiency of the PV panels, the analysis was focused on the polycrystalline technology. This is important to understand the behaviour of the system and understand the limitations of the modelling and the data used to validate the models. In order to analyse particular cases, Figure 4.16 to Figure 4.19 show the efficiency measurements divided into two parts of the day. As it can be appreciated from the results, during the first half of the day the efficiency is higher for all cases in all of the days. As explained before, this is caused by a shadowing effect that affects the solar irradiance input in equation (4.9) giving a higher than possible efficiency. In other words, the irradiance measured was lower than the actual solar energy that reaching the panels.

In further analysis, this shadowing effect over the solar irradiance measurement is overcome by ignoring the first half of the day for the validation and using the second half of the day to validate the models.

Temperature is part of the model, the effect of temperature over the panels is shown in Figure 4.20, where the temperature causes 1% difference in efficiency for every $5°C$ change at high solar irradiance. This is roughly in accordance to [86] and [87], where the ratio is up to a 1% for every $10°C$. The power output measurements obtained from the Belgian lab are logged for the point of connection between the terminals of the inverter and the grid, containing the full response of the system (i.e. the PV panel, the inverter with controls and the grid).

The simplest/traditional panels are the ones based on the crystalline silicon wafers (monocrys-

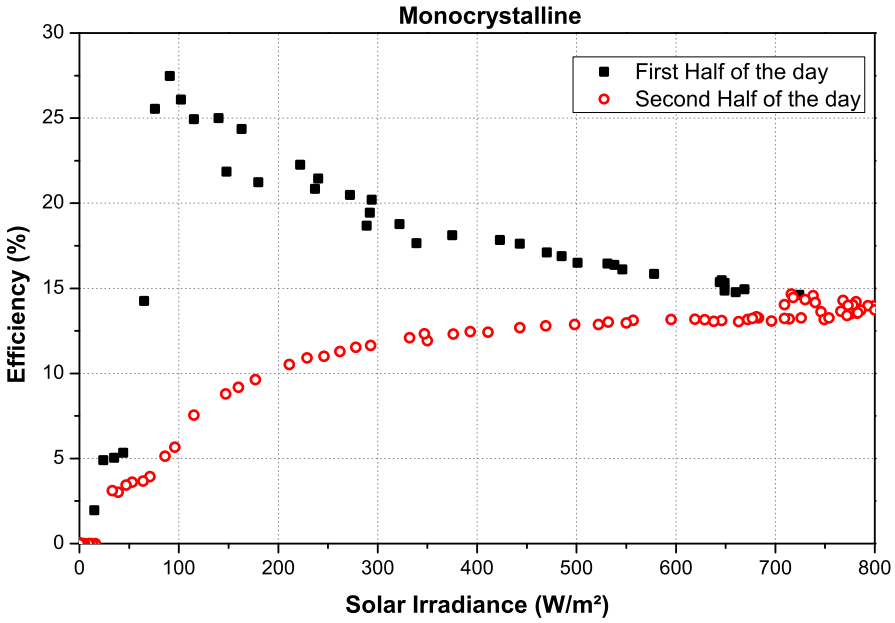

Figure 4.16: *Measured efficiency for two parts of the day for monocrystalline technology.*

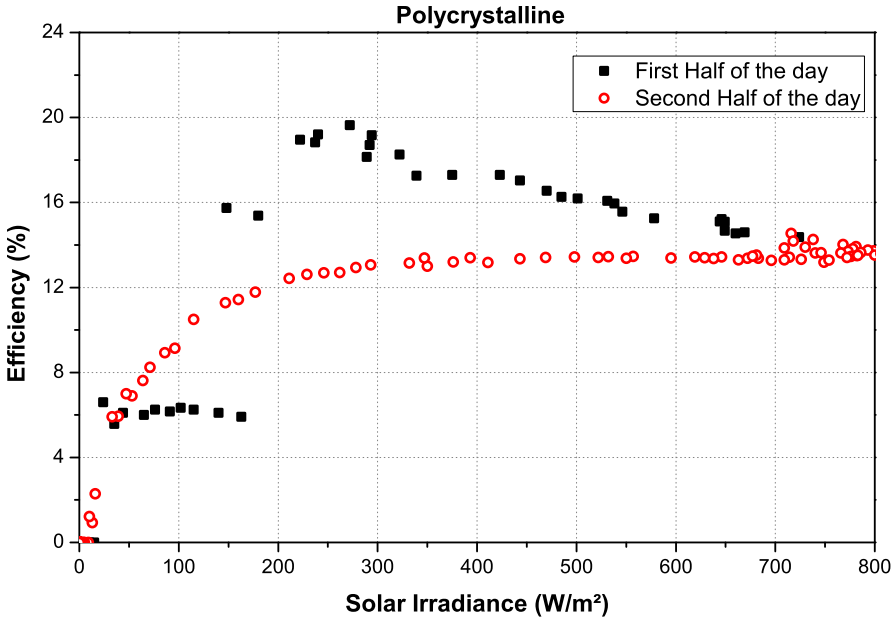

Figure 4.17: *Measured efficiency for two parts of the day for polycrystalline technology.*

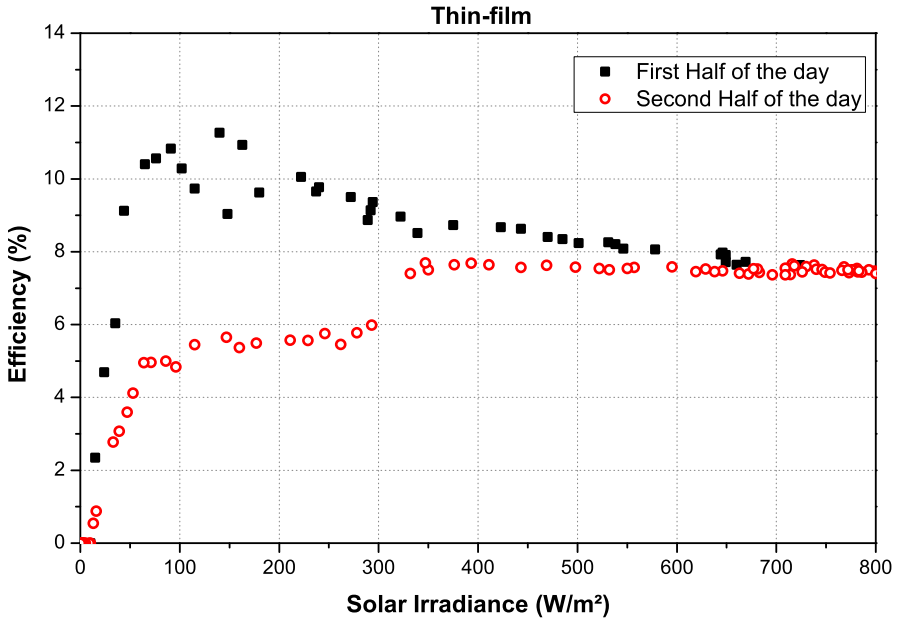

Figure 4.18: *Measured efficiency for two parts of the day for thin-film technology.*

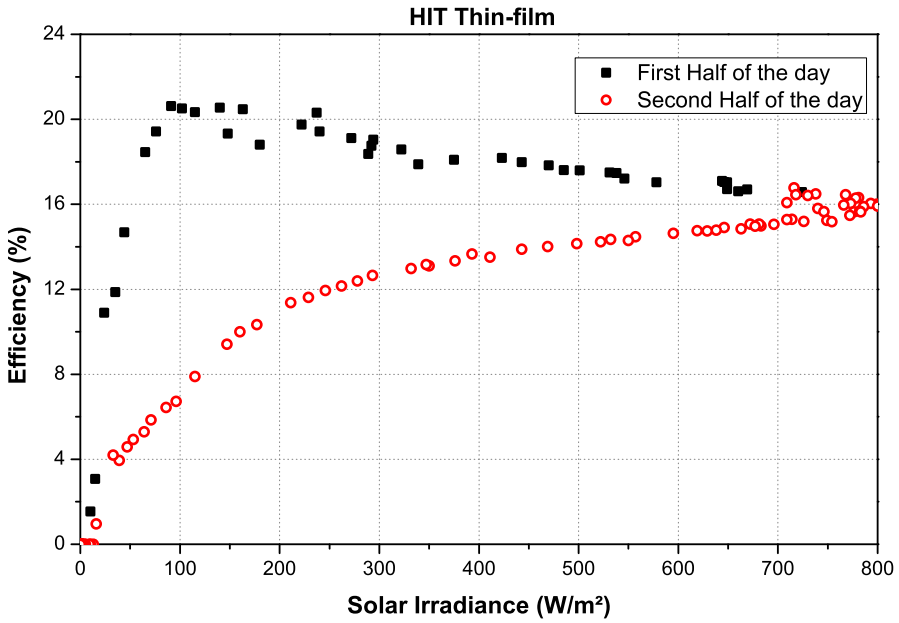

Figure 4.19: *Measured efficiency for two parts of the day for HIT thin-film technology.*

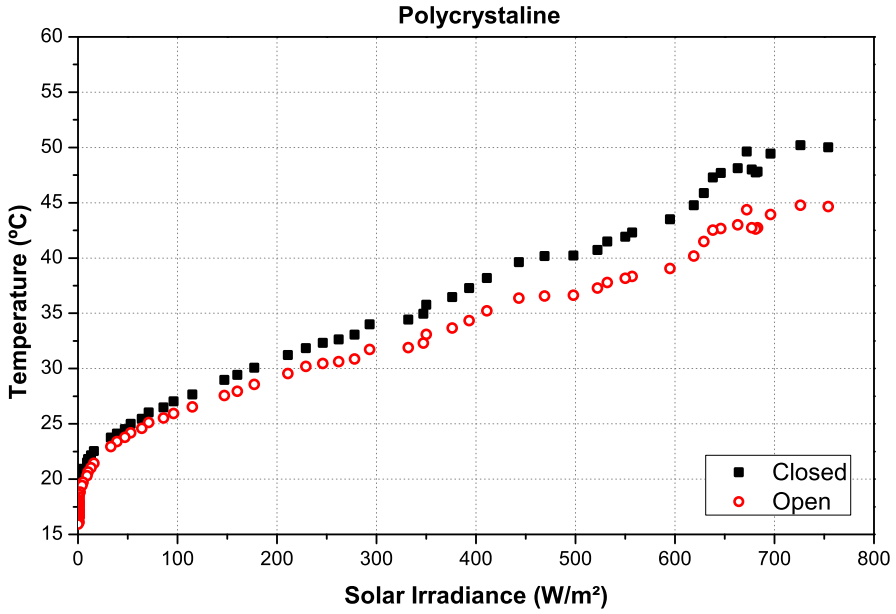

(a)

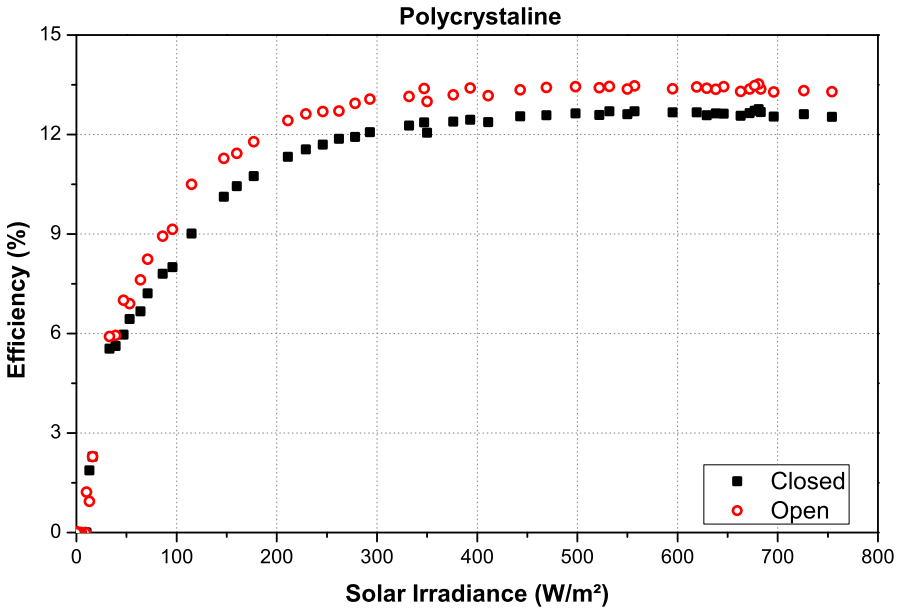

(b)

Figure 4.20: *Polycrystalline technology response to temperature: a) Temperature affecting same technology panels, b) Efficiency change due to this temperature difference.*

talline and polycrystalline). Figure 4.21 and Figure 4.22 show how the model fits closely with a very small error compared to the measurement. This fully validates the developed PV models, proving their ability to reproduce the actual PV systems. From the compared power outputs, it could be seen that the model does not match the thin-film's efficiency. Figure 4.23 and Figure 4.24 show the difference between the modelled and the measured efficiencies. HIT thin-film efficiency shows a jump in the efficiency around $300 W/m^2$. The model is based on the equation (4.2) considering a semi-conductor material of the cell, while thin-film technologies are based on crystalline silicon with other particles that affect the nature of the PV cell and the developed model is not detailed enough to reproduce these singularities in the panel's output.

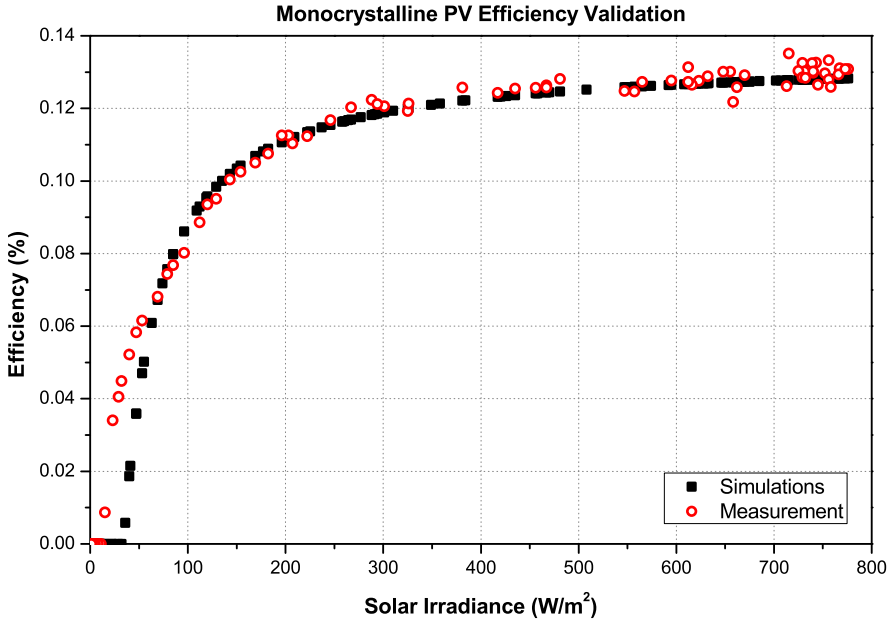

Figure 4.21: *Model efficiency plotted against measured efficiency for monocrystalline panel.*

In the case of the thin-film panels, a trend is evident, but the efficiency was found to be lower than the modelled one. These differences, especially in the case of the thin-film technologies, are due to the resistances of the model and the complexity of these systems. Nevertheless, the model is accurate enough for the purposes of this thesis, as the aim is to develop simple models of microgeneration systems for the integration of these systems to the network. Additionally, the efficiencies comply with the outputs found in [85], [87], which gives confidence on the measured efficiencies and the model outputs.

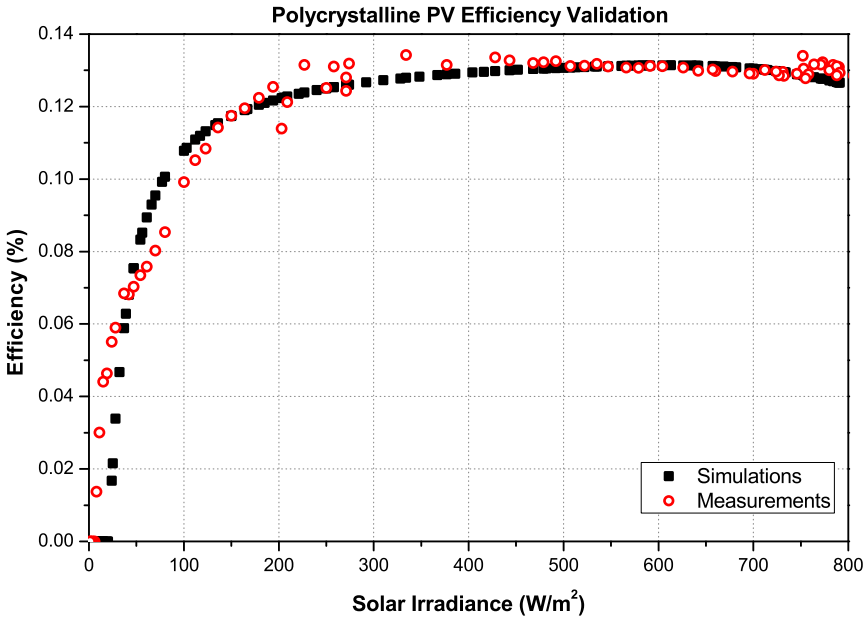

Figure 4.22: *Model efficiency plotted against measured efficiency for polycrystalline panel.*

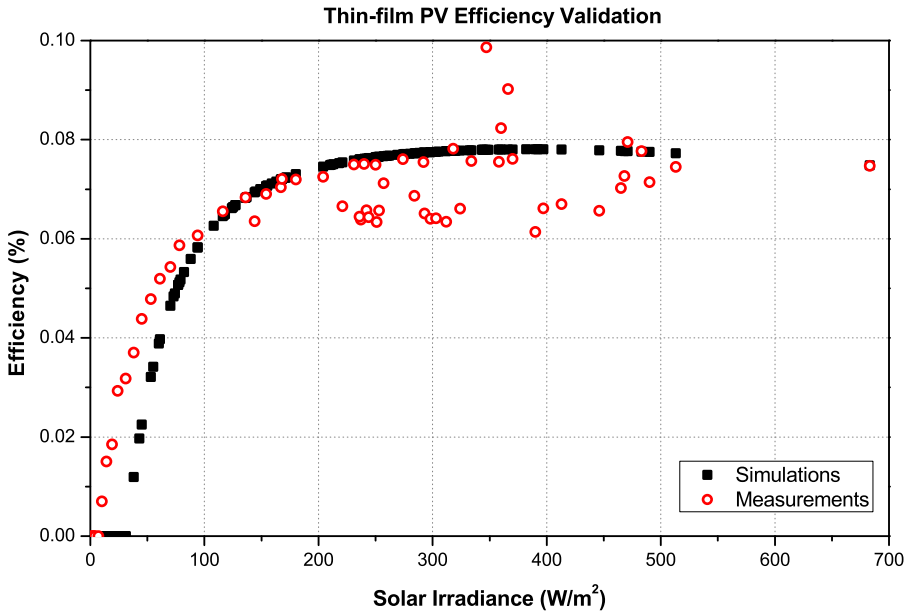

Figure 4.23: *Model efficiency plotted against measured efficiency for thin-film panel.*

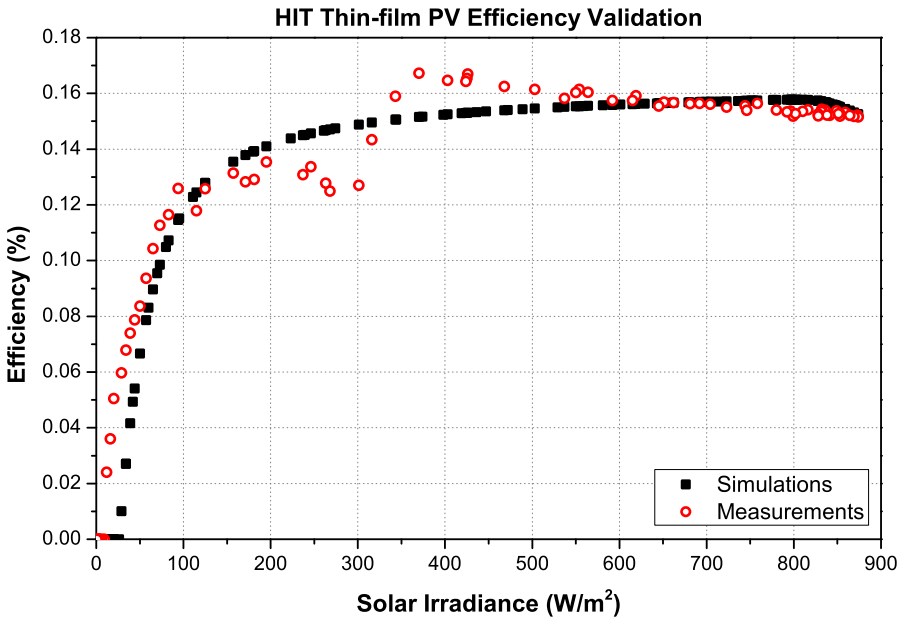

Figure 4.24: *Model efficiency plotted against measured efficiency for HIT Thin-film panel.*

4.6 Grid Connection

The modelled PV system is connected to the grid in order to further analyse the performance of the model. Unlike the wind generation system, it was not possible to find high-resolution solar data since these data are not widely available. Furthermore, the variations of solar irradiance tends to be much smaller than the variations of wind speed over the same period of time. Therefore, a sample test vector is used as an input to the model. This second by second input solar irradiance vector starts up with $600 W/m^2$, then, changes to the normal operation conditions (NOC) irradiance of $800 W/m^2$, then to the 50% of the Standard Testing Conditions (STC $500 W/m^2$). Using this testing vector, it is possible to observe the response of the PV model and analyse it in the same way as for the wind generation system.

4.6.1 Low-voltage Network Model

The low-voltage network model is the same as that described in Section 3.7.1 and illustrated in Figure 3.17. The simulation results are based on the monocrystalline PV model output. This technology was chosen due to the higher participation of these panels in the global market and therefore, greater importance for the analysis. The Matlab/Simulink PV generation model is shown in Appendix B.

Figure 4.25 to Figure 4.31 show the response of the PV model when it is connected to the grid. The results are based on a 5 second period due to computer limitations, but this sections intends to show the quasi-dynamic output of the model, showing the efficiency obtained by the model and compared to the one already validated in Section 4.5.

It can be seen that there is a difference between the wind turbine model regarding the current THD output (Figure 4.29), which is due to the differences in the modelled technology. The PV model is a current source model (similar to the wind turbine) exhibiting an interesting change in the current THD: the higher the power output, the lower the THD and vice versa. This demonstrates that the model follows the optimal operating point of the system when it reaches rated power. There are small oscillations in the power output, in contrast with the smooth power output obtained by the wind turbine model. This is attributed to a lack of "mechanical filter", i.e. the inertia of the wind turbine generator's rotor (whereas in the PV system this variable is not involved). The inertia allows that any noise created by the wind speed or some electrical variable is filtered in the DC side of the system and not visible in the output, achieving a smoother power output. It can be appreciated from Figure 4.25 how a change in the power

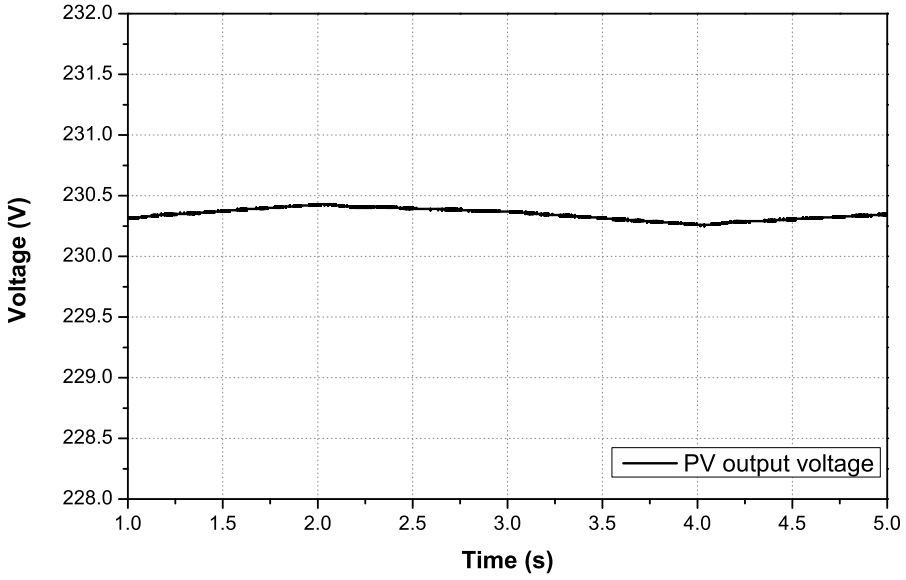

Figure 4.25: *PV output rms voltage.*

output of the system produces a slight variation of the RMS voltage of the grid (less than 0.01%). This change can also be appreciated in the current THD (Figure 4.29): the closer the system gets to the rated power output, the current distortion decreases. Otherwise, it increases the current distortion.

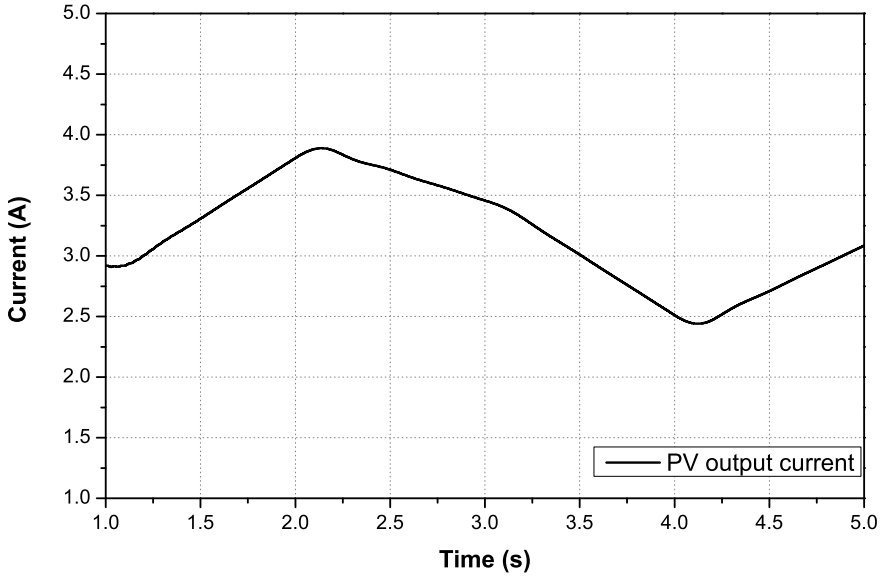

Figure 4.26: *PV output rms current*

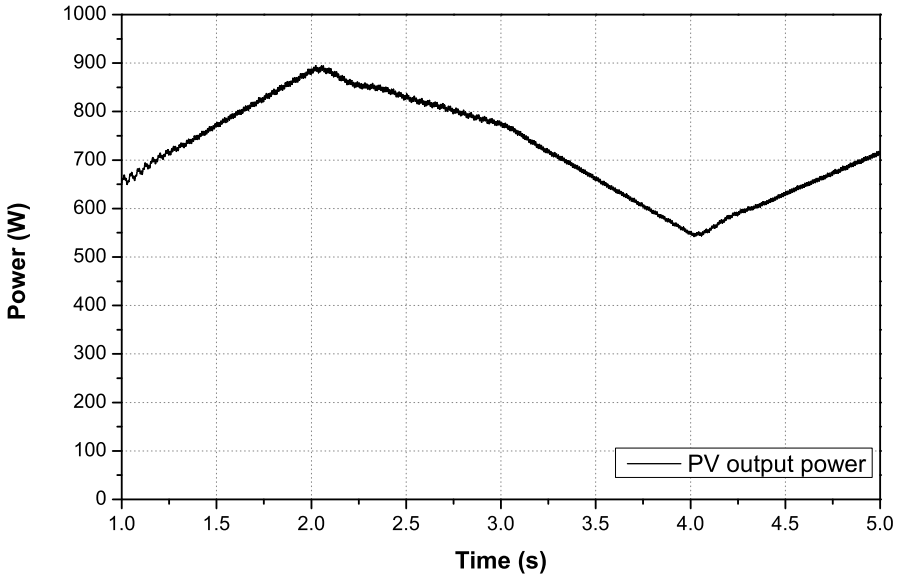

Figure 4.27: *PV output power.*

The voltage distortion (found to be around 2%) is lower than the 5% limit imposed by the Engineering Recommendation G83/1 [57], which allows this model to be connected to the grid. However, the DC current component of the inverter shown in Figure 4.31, is again higher than the stipulated value in the standard. The limit is $20mA$ for systems below $5kW$ and the model injects the similar $40mA$ DC current as the wind turbine, since they are modelled with the same power electronics (inverter) and similar control scheme.

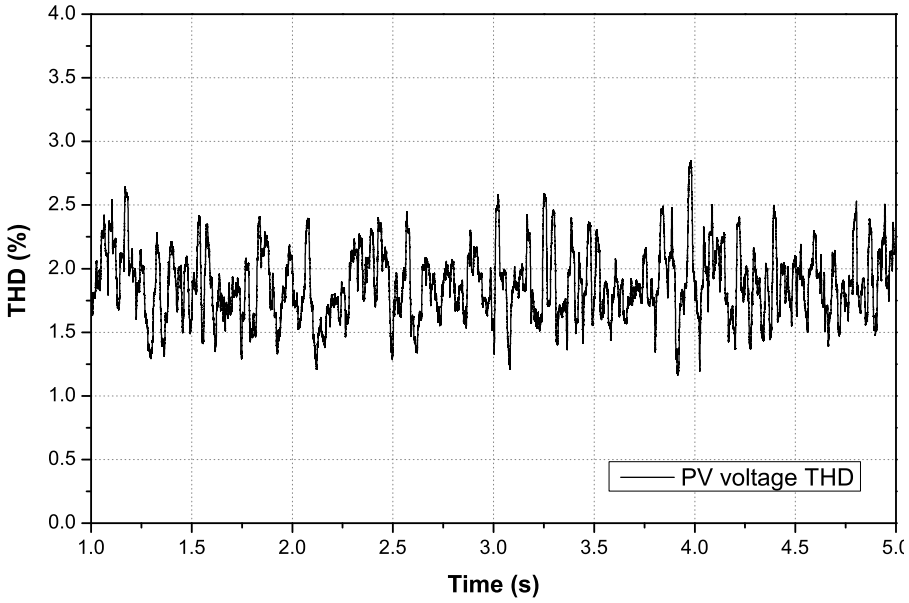

Figure 4.28: *PV voltage THD.*

Similar to the wind turbine model, the voltage THD is found to be no more than 3%, in accordance to [57]. As previously mentioned, the current THD is higher than expected, but still in compliance of British Standard 61000-3-2 [59] where it is stipulated that the voltage and current THD should comply with "Class A" equipment requirements. Nevertheless, this standard is designed primarily for electrical loads, while the technologies analysed here are small generators with the capability of injecting higher and variable harmonic currents into the grid. The test vector of input solar irradiance is shown in Figure 4.30. This vector is used to substitute solar irradiance measurement since there was no 1-second measurement available. Nevertheless, for the purpose of validating the model and comparing the power output, data from the Belgian lab was used. It was found to be the same for the given solar irradiance in the Belgian data set. Figure 4.32 shows the efficiency of the complete system from input to exported output. Table 4.4 shows that the efficiency of the modelled monocrystalline PV panel is 14.17%. This

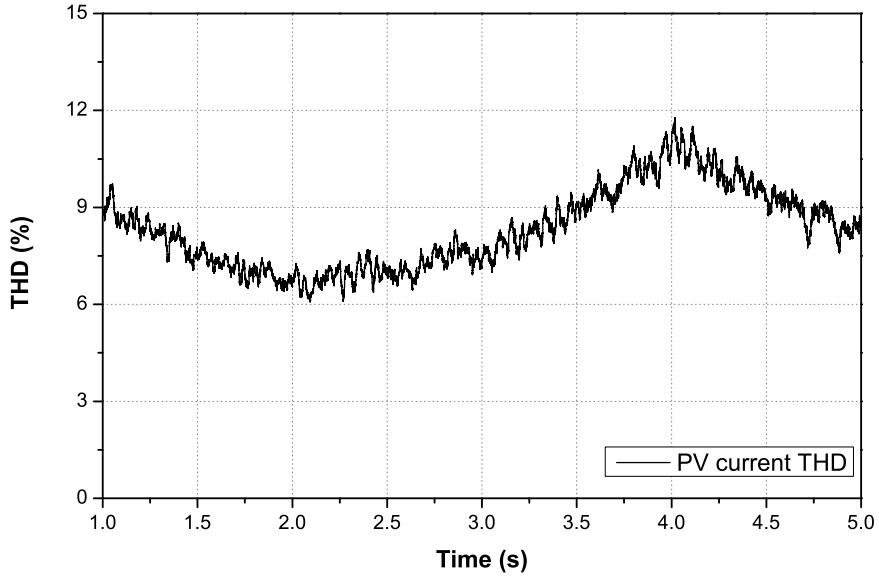

Figure 4.29: *PV current THD.*

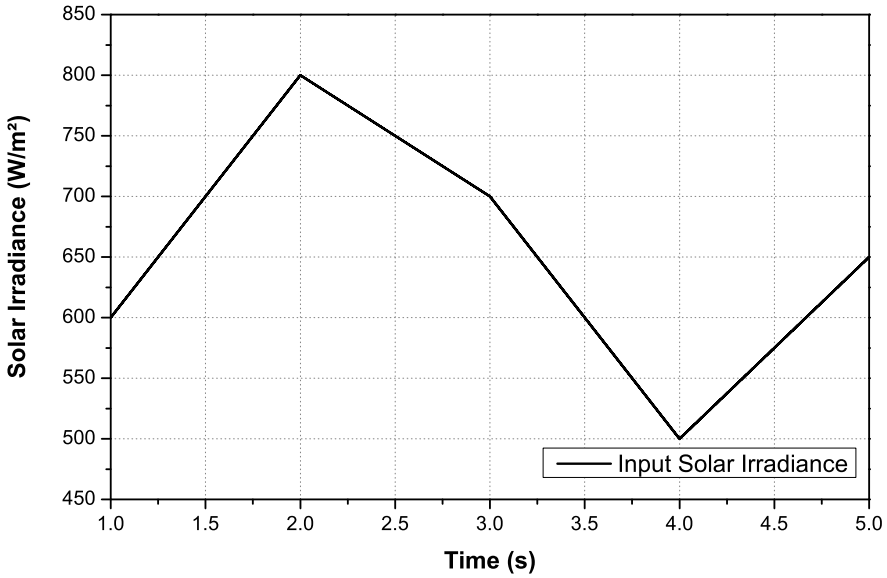

Figure 4.30: *PV input solar irradiance.*

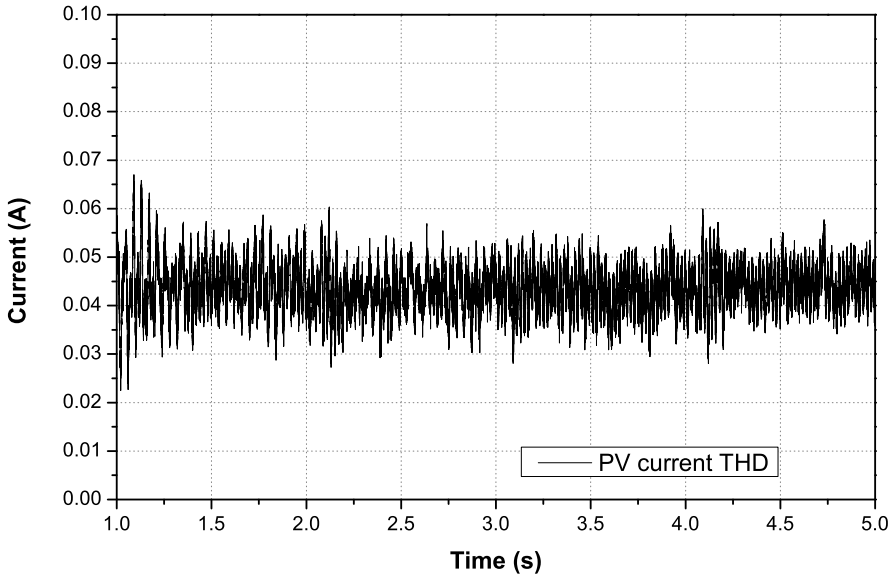

Figure 4.31: *DC component of PV output current.*

efficiency only considers the losses in the panel, while the losses from the complete conversion system also have to be taken into account.

$$P_{in} = S_{irr} \cdot A_{panel} \tag{4.10}$$

$$P_{out} = P_{in} \cdot \eta_{PV_{panel}} \cdot \eta_{inverter} \tag{4.11}$$

$$\eta_{PV_{total}} = \frac{P_{in}}{P_{out}} \times 100 \tag{4.12}$$

where, S_{irr} is the input solar irradiance ($^{W}/_{m^2}$), A_{panel} is the exposed area of the PV system (m^2), $\eta_{PV_{panel}}$ is the rated efficiency of the panel found in Table 4.4, $\eta_{inverter}$ is the rated efficiency of the used inverter, P_{in} and P_{out} are the input and output power, respectively, the input power is the solar power and the output power is the electrical power exported to the grid. The efficiency of the reported inverter is 91%, the same as one modelled for the wind turbine in the previous chapter and the total efficiency is:

$$\eta_{PV_{total}} = (\eta_{PV_{panel}} \cdot \eta_{inverter} = 0.1417 \cdot 0.91) \times 100 = 12.9\% \tag{4.13}$$

Therefore the model efficiency found in Figure 4.32 (where the efficiency is around 12.5%) complies with the calculated the efficiency by (4.13).

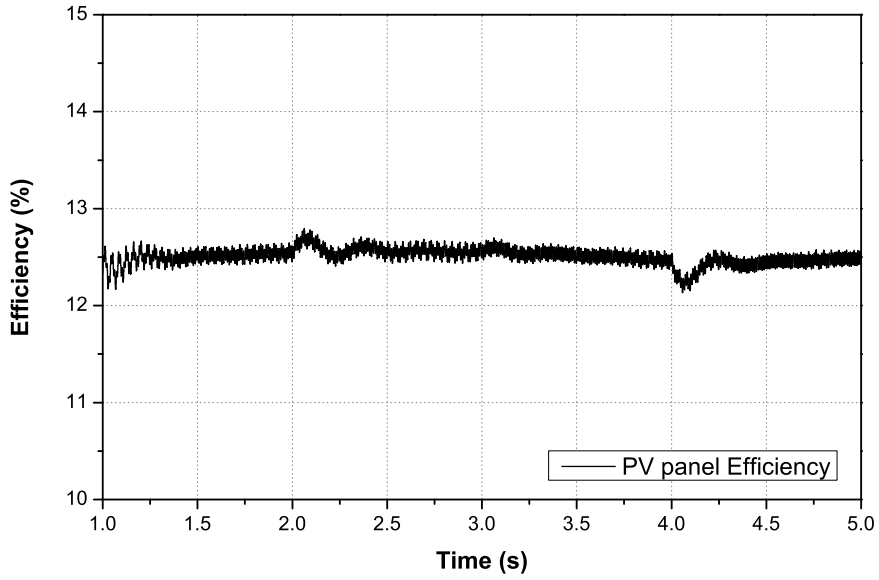

Figure 4.32: *Efficiency of PV panel and inverter.*

4.7 Conclusions

The PV microgeneration is a mature technology steadily increasing its share in the market. The possible technical barriers for a wider use of the PV panels are the lack of cost effective efficiency ranges (discussed further in this thesis), relatively large size of the systems and lack of suitable locations higher lower availability of solar irradiance. However, there are solutions such as the "tracker" systems, which can increase the power output that can be drawn from the PV energy systems, making them work with rated efficiency and absorbing more power from the solar irradiance spectrum. The variety of current PV technologies results in different efficiency, size and cost, which will be all analysed later in this thesis. These technologies can be modelled to a high level of accuracy as this chapter demonstrated. However, the interaction of the inverter and its control with the grid established presents challenges from the modelling perspective. These are, e.g. the impact of temperature variations and the reactive power demand (imported from the network to keep the PV system energised for the production of the output power), which cannot be quantified without more specific data for each part of the system. However, the model can reproduce the "tracked" device and the characteristic exponential response of the PV systems with a high accuracy. Wind energy and PV systems share the same power converter to be coupled with the grid and the models also share the filter design and inverter control. The developed PV model complies with the standard requirements from

the Engineering Recommendation G83/1 [57], except regarding the modelling of the DC current component, which exceeds the $20mA$ limit stipulated by the regulation. Nevertheless, the model is able to reproduce the measured power output and efficiency values with appropriate accuracy.

Chapter 5
Aggregation of Micro and Small-scale Generation Systems

5.1 Introduction

Due to space limitations and lower levels of primary energy resources, renewable-based distributed generation (DG) technologies are usually implemented as micro and small-scale systems in urban areas. Although highly dispersed and small in sizes, the total number of micro and small-scale DG units in a large urban area can be high. Their aggregate effects and benefits could be, in essence, comparable to those of medium-size DG technologies. A few thousands micro wind turbines or micro PV panels with rated powers in the range of few kWs could make an impact in the network. Having effects on the reduction of loading and congestion, deferment of investments in transmission and distribution networks, improvement of system voltage profiles and reduction of losses and CO_2 emissions, on-site renewable micro and small-scale DG systems will provide the end-users with an attractive option for reducing their energy bills. This is particularly true when appropriate incentives and subsidies can be incorporated into their installation grants and when they can negotiate suitable tariffs for generated and exported electricity, especially after the introduction of Feed-in Tariffs in the UK [88].

According to the British Wind Energy Association [89], the installed capacity of micro and small-scale wind turbines in the UK by 2020 could be as high as $1.3GW$, if suitable incentives and plans are devised and put in place. Similarly, the American Wind Energy Association forecasts that $1.7GW$ of microwind could be installed in the US by 2013 [90]. According to the International Energy Agency roadmap [43], PV systems will have an average annual market growth rate of 17% in the next decade, reaching a global cumulative installed PV power capacity of 200GW by 2020. Even more ambitiously, the European Union has set a target of 400GW of installed PV by 2020, increasing to 700GW by 2030. This clearly suggests the importance of modelling PV systems and technologies.

This chapter is divided in three parts. In the first part, after an analysis of the micro and small-scale DG market, with all the manufacturers of solar panels and wind turbines up to $50kW$,

a corresponding database is built and plotted. Using the PV/wind manufacturers database, a statistical aggregation methodology for micro and small-scale generation in urban areas is presented, introducing "generic models", which can represent a majority of micro and small-scale generation systems currently available on the market. The second part shows the generic representation of the electronic interface for the photovoltaic energy market. The inverter for PV systems can be represented by the corresponding exponential models. The last part shows the analytical representation of the generic models including electronic conversion efficiencies and the actual electrical power output delivered by the generic models. Using the market participation of generic models in the total aggregate, a final aggregated model of PV and wind microgeneration is presented and analysed.

5.2 Micro and Small-Scale Wind Energy Market

During the last 30 years, large-scale wind turbines have increased their size considerably. Nowadays, turbines up to 7MW [91] can be found in the offshore market for wind generation applications. However, in the case of micro and small-scale wind energy systems, there are many limitations for their applications in urban areas: space, low levels of wind resources, costs and planning permits, to mention but a few. This is why urban wind turbines have to be smaller in size and therefore smaller in rated power. In order to analyse microwind generation, a worldwide database has been built from a survey of 60 different manufacturers with the number of actual turbines being more than 190 wind turbines (shown in Figure 5.1).
Statistics available from the British Wind Energy Association [89] suggest that 84% of the micro and small-scale wind turbines currently installed in UK urban areas have rated power less than 1.5kW. Around 97% of all micro and small-scale wind turbines installed in the UK are Horizontal Axis Wind Turbines (HAWT), these numbers help to simplify the analysis in this chapter.

5.2.1 The Generic Wind Turbine Models

The database, as previously mentioned, is a worldwide database with 60 manufacturers of wind turbines. The wind turbines identified in this market survey and used to build the database vary in size, rated power and efficiency. These differences are difficult to quantify if their power curves are plotted together and compared. The methodology for this analysis has been

presented in [11], where it is found that the characteristics (i.e. power curves) of the majority of microwind turbines identified in the database and currently available in the market could be correctly represented using only four "generic wind turbine models". The database contains turbines with rated power from $500W$ up to $50kW$. In order to compare and group them and identify the generic characteristics, all turbine power curves are normalised using their swept areas. This ensures that instead of having the power curves output in W the output can be depicted in $^{W}/_{m^2}$. Figure 5.1 shows the four "generic wind turbines" identified and plotted together with all wind turbine power curves identified from the market survey. It is important to clarify that all the manufacturers included in the database are assumed to be in compliance of the British Standard BS61400-12-1 [28]. The standard requires the manufacturers to report the electrical output power curve in their specification sheets. Each generic wind turbine model

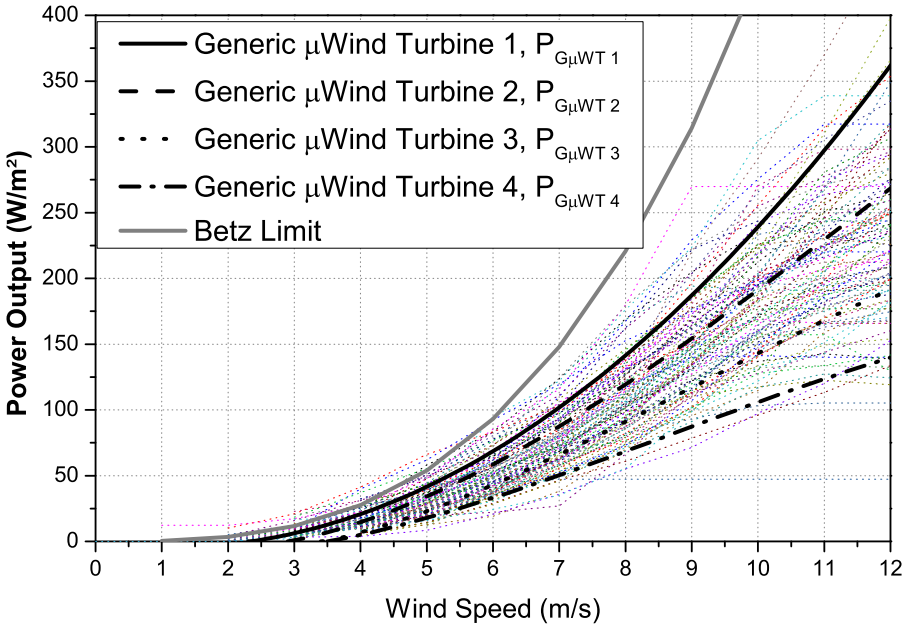

Figure 5.1: *Comparison of four generic and a number of actual wind turbine power curves, all normalised using the corresponding swept areas.*

has been obtained as the average power curve of the turbines clustered around it, expressed using a polynomial formulation to obtain a suitable mathematical expression that can substitute all wind turbines in the identified cluster of turbines. The main purpose of these generic wind turbine models is to substitute the number of individual turbines and use a generic wind turbine model for network impact assessment, annual power calculation, efficiencies, etc. The generic wind turbine models have been identified by their C_p. Generic wind turbine 1 has the highest C_p whereas generic wind turbine 4 has the lowest. The generics are plotted up to 12 $^{m}/_{s}$ because,

as mentioned in Chapter 3, the probability of wind speeds higher than 12 $^{m}/_{s}$ in urban areas is very low. These four generic power curves are shown as follows, generic wind turbine 1 is analytically represented by:

$$P_{G_{\mu WT1}} = -7.29\nu + 3.12\nu^2 \left[\frac{W}{m^2}\right], \qquad for\ \nu \geq 2.4^{m}/_{s} \tag{5.1}$$

This equation is plotted together with all the turbines represented by generic wind turbine 1 in Figure 5.2. Generic wind turbine 2 is analytically represented by (5.2) and plotted together

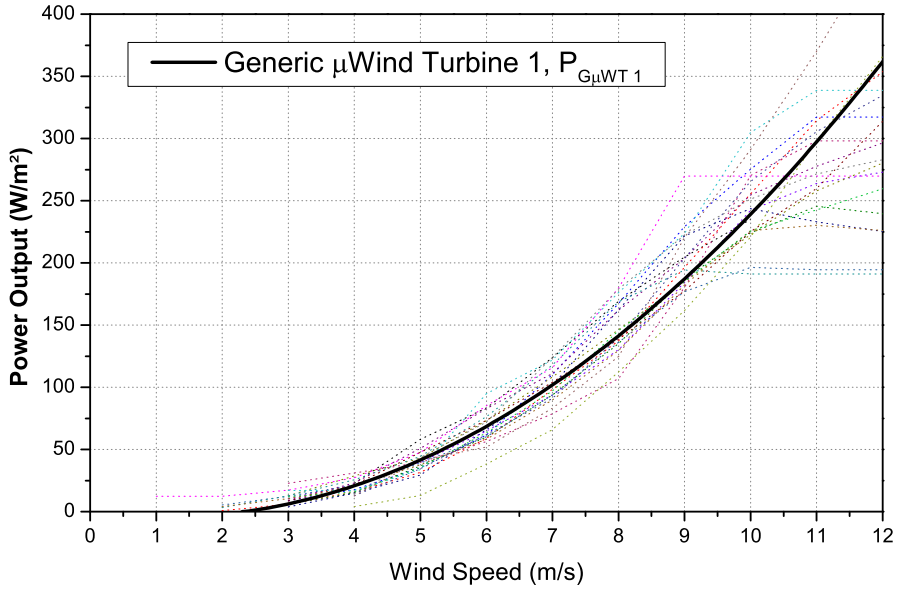

Figure 5.2: *Comparison of generic wind turbine 1 power curve with the corresponding wind turbine power curves.*

with all the turbines it represents in Figure 5.3:

$$P_{G_{\mu WT2}} = -11.5\nu + 4.26\nu^2 - 0.12\nu^3 \left[\frac{W}{m^2}\right], \qquad for\ \nu \geq 3^{m}/_{s} \tag{5.2}$$

Generic wind turbine 3 is analytically represented by (5.3), and plotted together with all the turbines it represents in Figure 5.4:

$$P_{G_{\mu WT3}} = -13.1\nu + 4.34\nu^2 - 0.16\nu^3 \left[\frac{W}{m^2}\right], \qquad for\ \nu \geq 3.5^{m}/_{s} \tag{5.3}$$

Generic wind turbine 4 is analytically represented by (5.4), and plotted together with all the turbines it represents in Figure 5.5:

$$P_{G_{\mu WT4}} = -6.2\nu + 2.86\nu^2 - 0.11\nu^3 - 9 \left[\frac{W}{m^2}\right], \qquad for\ \nu \geq 3.6^{m}/_{s} \tag{5.4}$$

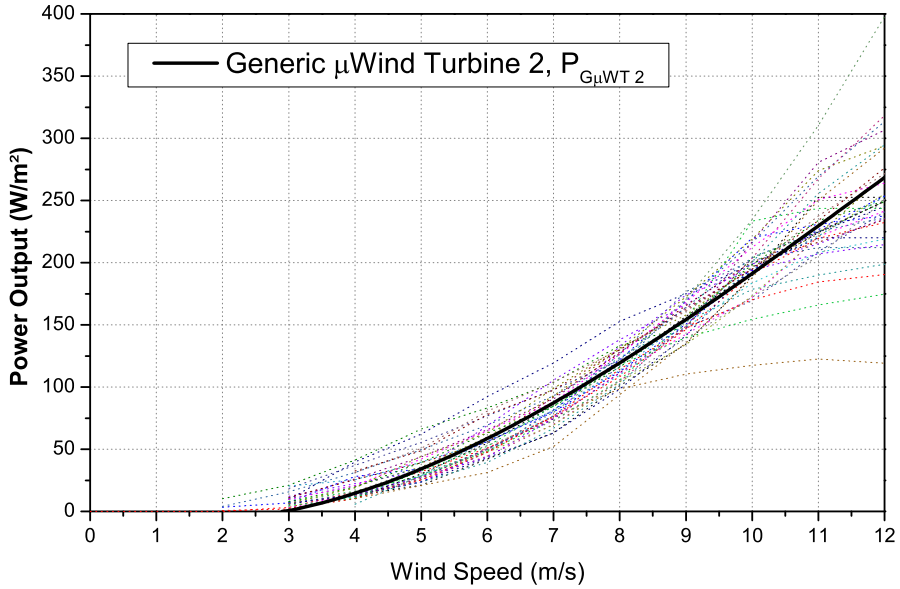

Figure 5.3: *Comparison of generic wind turbine 2 power curve with the corresponding wind turbine power curves.*

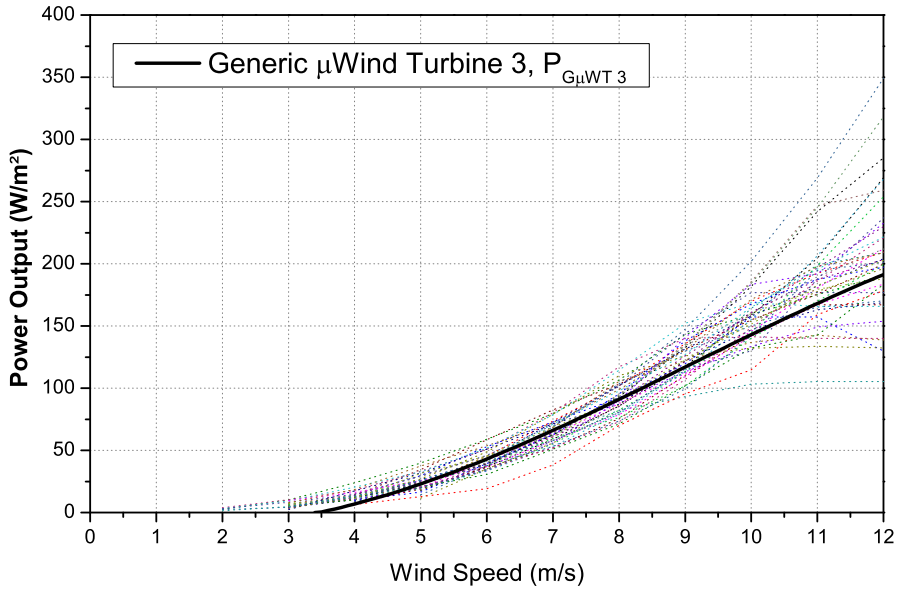

Figure 5.4: *Comparison of generic wind turbine 3 power curve with the corresponding wind turbine power curves.*

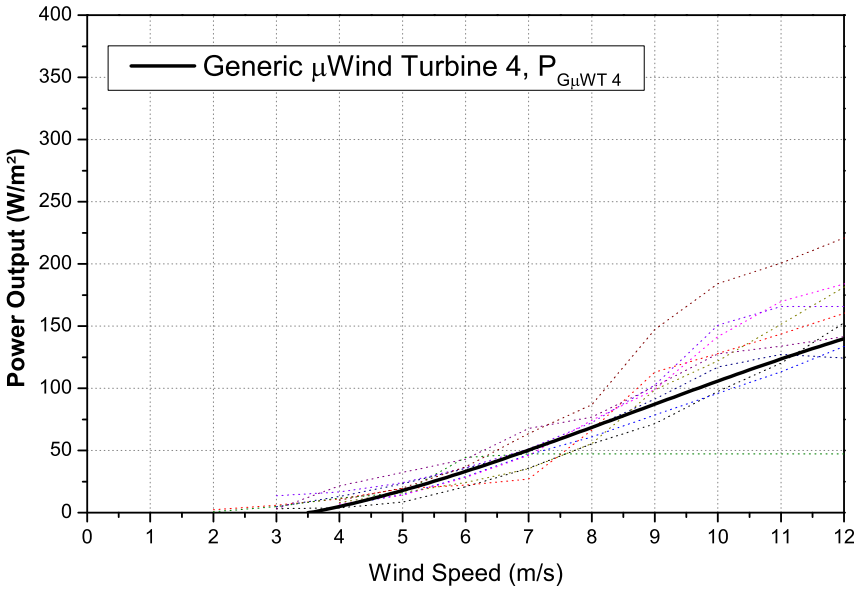

Figure 5.5: *Comparison of generic wind turbine 4 power curve with the corresponding wind turbine power curves.*

These four generic wind turbine models can be used to replace the typical power curves group of turbines with the same C_p range, which simplifies the analysis similar to that presented in [12]. However, the methodology can be further simplified in order to be used for power systems studies. These generic proposals can be identified as very efficient (generic 1), efficient (generic 2), low-efficient (generic 3) and very low-efficient (generic 4). This classification makes it easier to identify turbines and their performance, i.e. Savonious wind turbines are known to be between low-efficient and very low-efficient [30] and based on wind database belong to the category of generic 4. In this way, all the turbines found in the market could be identified by their performance and aggregated without the actual power curve, but with a mathematical expression that helps process the wind speed data in a time-series form and fed into the power flow simulation.

From the wind turbine database the "percentage of contribution" of each generic wind turbine model has been estimated as a representative of the aggregate wind turbine microgeneration. The percentage of contribution is: 18% for generic wind turbine 1, 32% for generic wind turbine 2, 32% for generic wind turbine 3 and 18% for generic wind turbine 4. This participation is an example of how the generics can be used, as it was assumed with this example that the database reflects the possible installation of a large number of micro and small-scale wind turbines in urban area. The percentage can be modified as the market develops or better turbines

(e.g. more generic 1 and generic 2 turbine representatives) are introduced to formulate a more adequate aggregate micro wind turbine model. With this mix, the equation used for an "aggregate generic" is defined as:

$$P_{G_{Aggregate}} = -10.3\nu + 3.83\nu^2 - 0.11\nu^3 \left[\frac{W}{m^2}\right], \qquad for\ \nu \geq 3^{m}/_{s} \tag{5.5}$$

The formulation of the generic wind turbine models allows to use their power curves for the calculation of annual power outputs based on input wind speed probability distributions. However, as previously mentioned the generic wind turbine models are also identified by C_p. This coefficient is the electrical power output from the turbine that basically represents the capacity of the turbine to absorb the energy from the wind and deliver it as electricity to the network. The maximum C_p that can be achieved is determined by the Betz limit of 59.3%, as previously explained in Chapter 2. Figure 5.6 shows the four generic wind turbine models' C_p values compared to the aggregate generic C_p value. Figure 5.6 is obtained under the assumption that

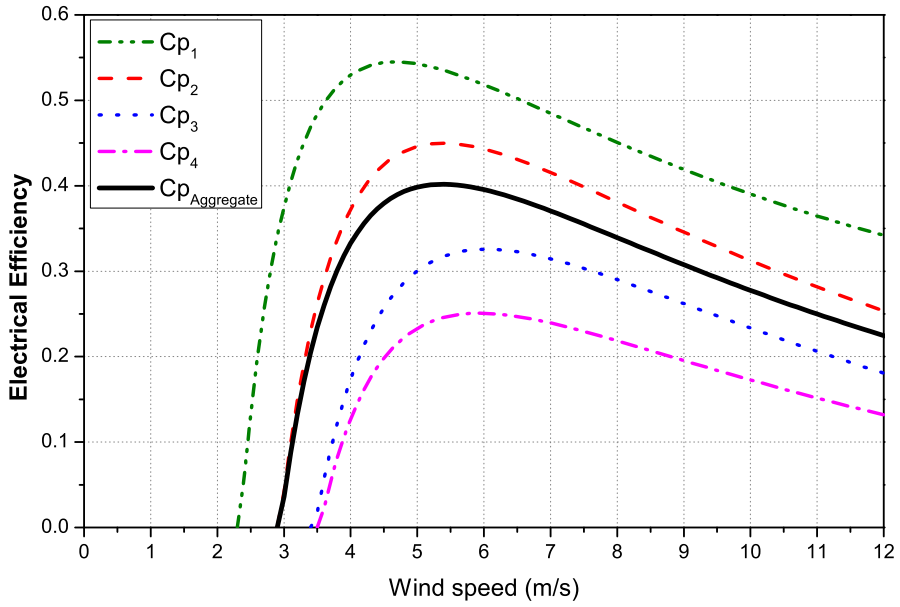

Figure 5.6: *Power coefficient of proposed generic wind turbine models.*

all turbine manufacturers are in compliance of the BS 61400-12-1 [28]. From Figure 5.1 can be appreciated that for some speeds the turbines are above the Betz limit. Causing a higher than possible efficiency. If a quick calculation is made of the maximum possible electrical efficiency is performed, Betz limit dictates a maximum aerodynamic efficiency of 59.7%, a typical PMSG efficiency is of about 85% and the inverter having an efficiency of 91%. The maximum value

should be roughly around 47%. Generic 1 would be performing better than possible, this can be possibly corrected as soon as the manufacturers update their specifications.

5.3 Micro and Small-scale Photovoltaic Energy Market

Similarly to the wind turbine database, the PV database is created taking into account the majority of PV modules available in the world market. This database will be used as the wind turbine database to identify the generic models of the PV technologies considered. The parameters considered and gathered for this database are the peak power (P_{max}), maximum power point voltage and current (V_{mpp}, I_{mpp}), the open circuit voltage (V_{oc}), the short circuit current (I_{sc}), voltage and current temperature coefficients (K_v, K_i), area of the panel in square metres and number of cells in a panel. All these parameters are typically obtained using the Standard Testing Conditions (STC). Typically the manufacturers report the V-I curves of the panel at different solar irradiance inputs. However, these curves are not collected for the database since the model reported in the previous chapter can reproduce these curves using the provided parameters. The PV database consists of 247 different PV panels. From this database the participation percentage for each PV technology was found to be as follows:

- Monocrystalline silicon 98 modules (39.7%),
- Polycrystalline silicon 106 modules (42.9%),
- Thin-film technology 43 modules (17.4%).

However, inside the thin-film technology 20 panels were HIT (Heterojunction Intrinsic Thin layer) technology. This technology as previously mentioned has a higher efficiency than any other technology. Therefore, it will be considered as the fourth technology, making 9.3% for Thin-film and 8.1% for HIT Thin-film modules. The database includes panels with peak power from $40W$ to $295W$ and eleven manufacturers of PV modules.

5.4 The Generic Photovoltaic Models

Using the V-I characteristics from the PV database described in the previous section, generic PV models are built for the considered four technologies, basically repeating the same approach

for the microwind systems. However, in this case the PV technologies have already been identified and it was easier to find the trends for each generic PV model. Photovoltaic systems do not have a "power curve" as wind turbines, due to the different nature of the technology. Bearing this in mind, all the PV panels found for each specific technology are then processed to obtain the efficiency curves. These efficiency curves have been obtained under the assumption of both Maximum Power Point (MPP) achieved and Standard Testing Conditions (STC). Figure 5.7 to Figure 5.11 show the generic PV models compared to the whole range of actual PV panels in the database.

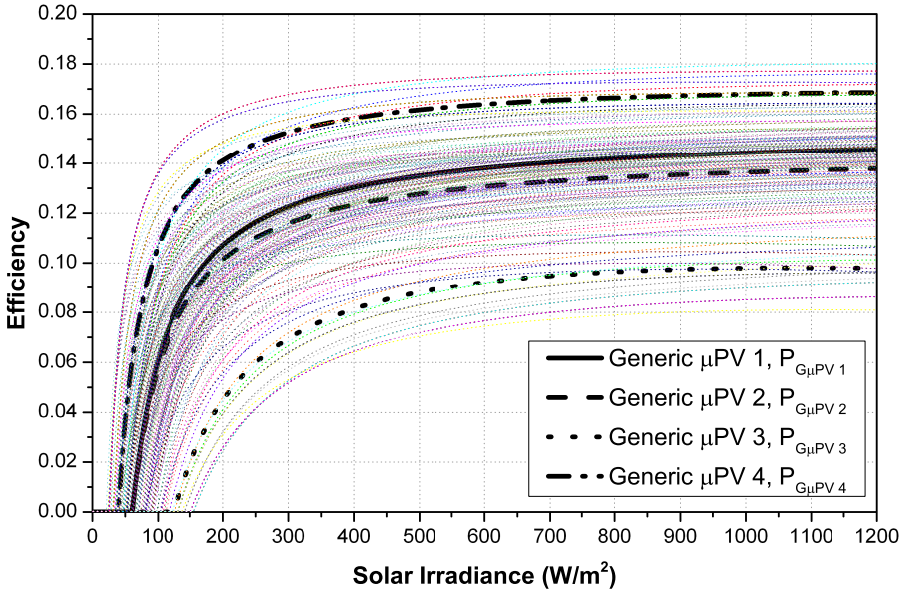

Figure 5.7: *Comparison of four generic and a number of actual PV panel efficiency curves.*

Apart from the identified generic PV model for each technology available in the market, it is important to obtain an analytical model that correctly describes the efficiency. The model obtained from this analysis is an exponential model describing the overall efficiency. Generic PV 1, corresponding to monocrystalline technologies is described by (5.6). generic PV 2, corresponding to polycrystalline technologies is described by (5.7), generic PV 3, corresponding to thin-film technologies is described by (5.8) and generic PV 4, corresponding to HIT Thin-film technologies is described by (5.9).

$$\eta_{PV_{G1}} = 0.144\left(1 - e^{-0.008(S_{irr}-60)}\right), \qquad for\ S_{irr} \geq 60^{W}/_{m^2} \tag{5.6}$$

$$\eta_{PV_{G2}} = 0.136\left(1 - e^{-0.008(S_{irr}-60)}\right), \qquad for\ S_{irr} \geq 60^{W}/_{m^2} \tag{5.7}$$

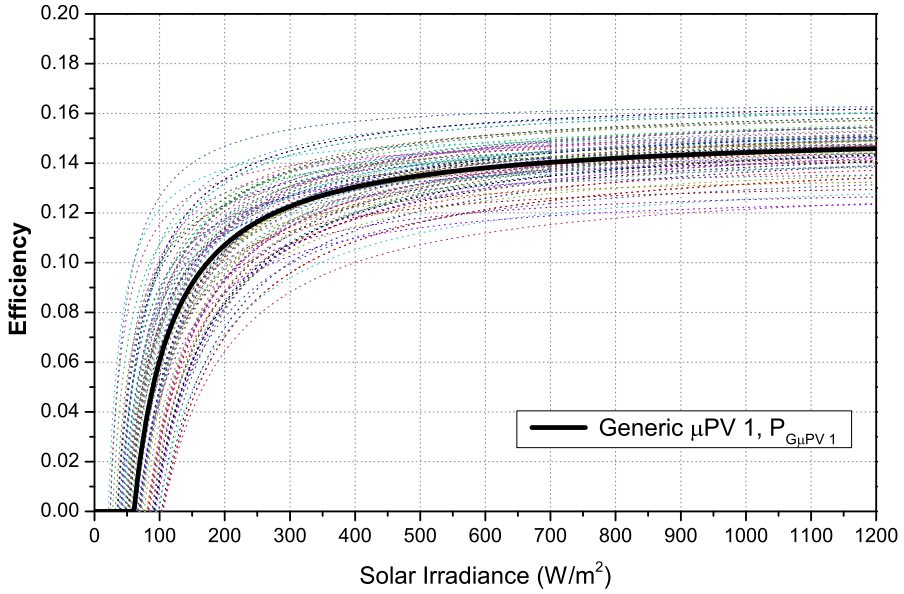

Figure 5.8: *Comparison of generic PV 1 efficiency with the corresponding PV panel efficiencies.*

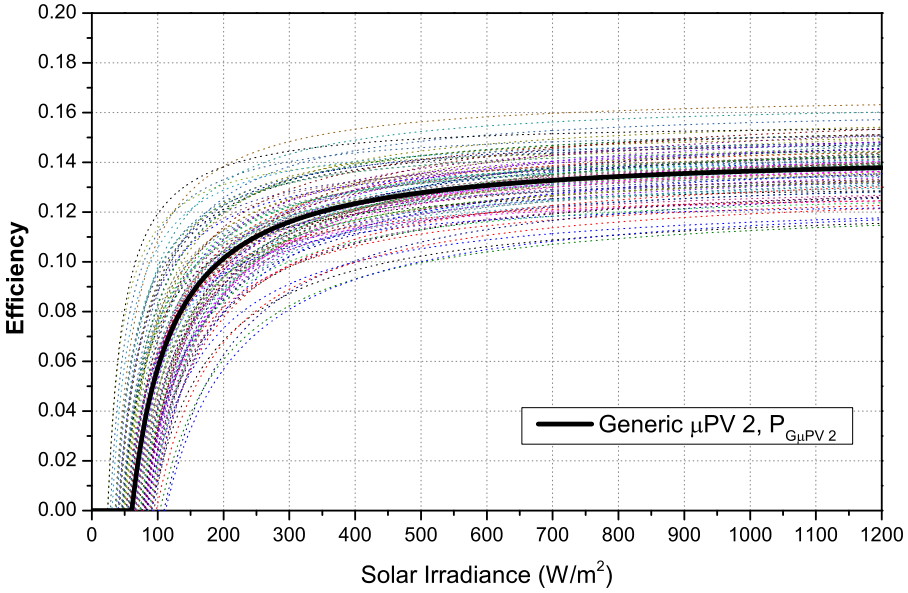

Figure 5.9: *Comparison of generic PV 2 efficiency with the corresponding PV panel efficiencies.*

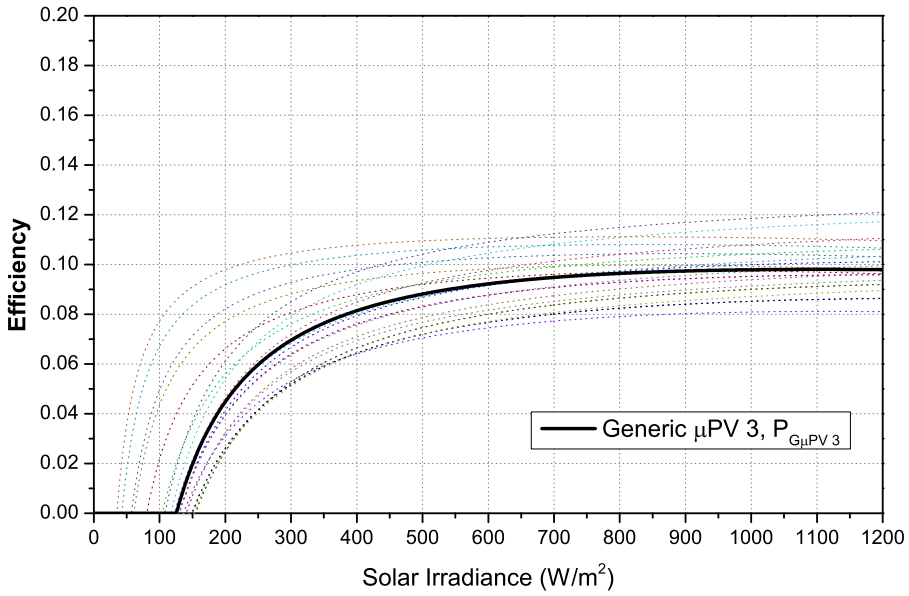

Figure 5.10: *Comparison of generic PV 3 efficiency with the corresponding PV panel efficiencies.*

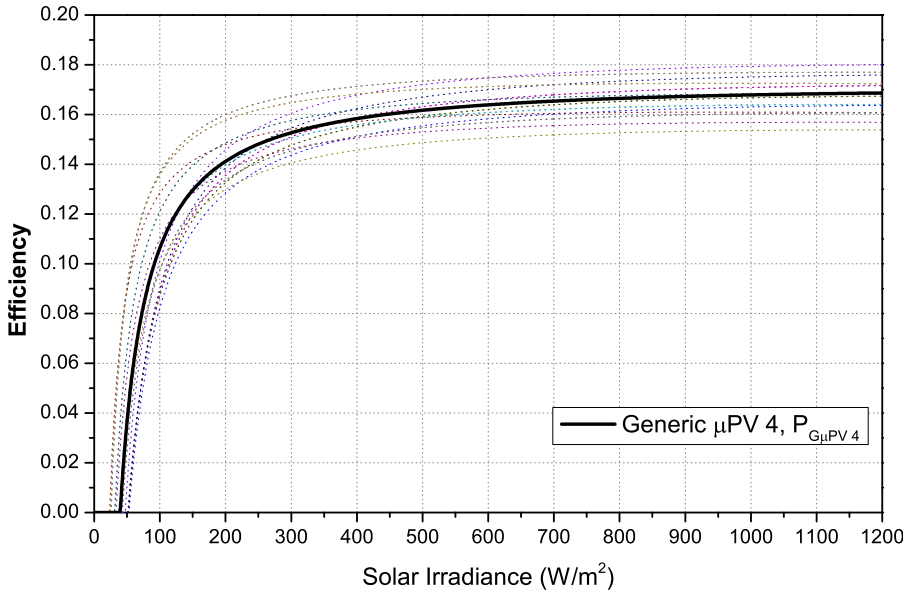

Figure 5.11: *Comparison of generic PV 4 efficiency with the corresponding PV panel efficiencies.*

$$\eta_{PV_{G3}} = 0.098\left(1 - e^{-0.008(S_{irr}-125)}\right), \qquad for\ S_{irr} \geq 125^{W}/_{m^2} \tag{5.8}$$

$$\eta_{PV_{G4}} = 0.168\left(1 - e^{-0.008(S_{irr}-40)}\right), \qquad for\ S_{irr} \geq 40^{W}/_{m^2} \tag{5.9}$$

where, S_{irr} is the input solar irradiance of the PV panel.
These analytical formulations of the generic PV models can be used to identify the power outputs of any PV system currently available in the market in W/m^2, as the efficiency is directly related to the amount of energy a panel can absorb form the sunlight.

5.5 Electronic Interface

As discussed, PV panels and wind turbines need an interface to be connected to the grid, in order to adjust and control their outputs. This interface is required because the output cannot be directly and fully regulated due to variations of sunlight or wind speed. A wind turbine is a mechanical device that transforms wind speed into kinetic rotating mechanical energy that is converted to electrical energy. For this process to be accomplished a generator and a power converter have to be considered in the analysis. From the wind database, the generators commonly used for micro and small-scale wind applications were found to be brushless PMSG. The PMSG produces variable frequency and amplitude waveforms that are then rectified and controlled at constant value by a boost chopper control ensuring that the DC voltage at the inverter input is constant. This additional part of the system is not needed for modelling wind turbines as the power curves are reported as electrical output including the inverter [28]. The inverter adjusts the power from DC to AC form to supply the load or in most cases the electrical grid. This element in the generation side of the system have to be simplified so PV panels can be connected, adding losses to the system. However, inverter systems are non-linear, therefore a simplification is attempted while still trying to preserve the variable behaviour of the interface at different power inputs.

5.5.1 Inverter Simplification

After the DC boost chopper control the power is then inverted to the appropriate frequency and amplitude by the inverter which can be a single or a three phase system. Data from five different inverter manufacturers for microgeneration systems are collected, Figure 5.12 shows the three main inverter sizes and compares their efficiencies. The efficiencies have been identified by

rated power: low power denotes systems with less than $1.5kW$ rated power, medium power range between $1.5kW$ and $10kW$ and finally high power corresponds to inverters above $10kW$. As expected the higher the power the higher the efficiency. From Figure 5.12 the exponential

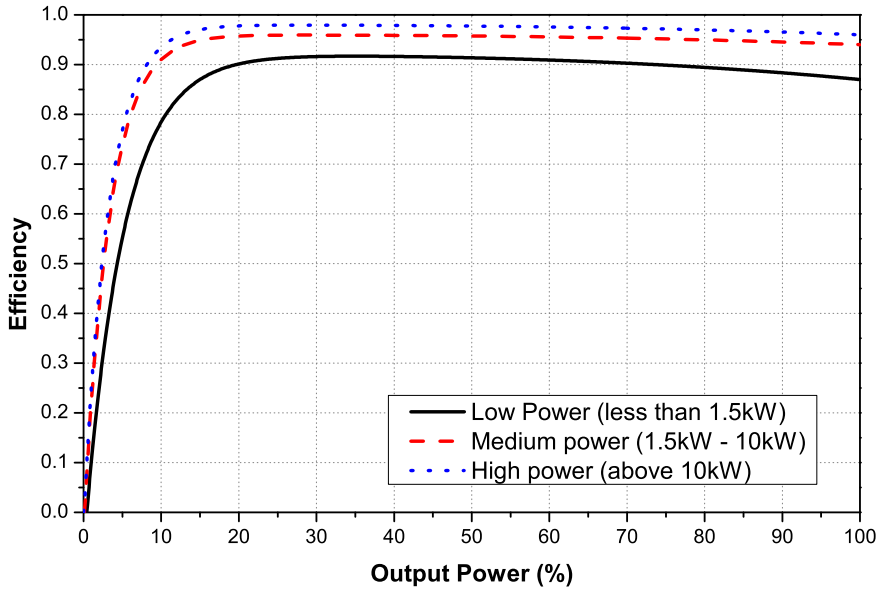

Figure 5.12: *Identified inverter efficiencies for different output powers.*

characteristic of the inverter efficiency can be modelled and formulated. These equations are presented as follows:

$$\eta_{LowPower} = 0.92 - e^{-0.2P_{out}} + 3 \times 10^{-10} P_{out}^2 - 5 \times 10^{-8} P_{out}^3 \tag{5.10}$$

$$\eta_{MediumPower} = 0.96 - e^{-0.2P_{out}} + 3 \times 10^{-10} P_{out}^2 - 2 \times 10^{-8} P_{out}^3 \tag{5.11}$$

$$\eta_{HighPower} = 0.98 - e^{-0.2P_{out}} + 3 \times 10^{-10} P_{out}^2 - 5 \times 10^{-8} P_{out}^3 \tag{5.12}$$

where, P_{out} is the actual inverter's power output. The equations are formulated using the actual output expressed as the percentage of rated power for ease of comparison, in order to have a common scale between them and to be included alongside the other systems involved in the generation. This methodology intends to aggregate for steady-state analysis the impact of micro and small-scale energy systems connected to the urban distribution network (uDN). Typically PV panels in urban area will lack space for big installations. Considering that each PV panel such as a monocrystalline technology will provide a peak power output of $290W$ for an area of around $1.5m^2$, to achieve a peak power of $1.5kW$ would require at least five panels, requiring an exposed area of $7.5m^2$. With this information the low power inverter is the one

to be used as the electrical interface between the microgeneration and the network, since the most typical case scenario is to be analysed for steady-state and it is appropriate to assume the lowest inverter efficiency for the systems. The purpose of this analysis is to aggregate the microgeneration systems into a simple family of curves that consider the electronic efficiencies and the microgeneration technologies. As all the systems have been identified and modelled, the equation (5.10) is then simplified to a single exponential term for low-power inverters, for easier representation and analysis (the simplification causes less than 1% difference in the results). The final representation of the inverter efficiency is:

$$\eta_{inv}|_{\%P_{rated}} = 0.92\left(1 - e^{(-0.2P_{out})}\right) \tag{5.13}$$

5.6 Aggregate Generic PV Models

Similarly to the analysis carried out for wind turbines, the PV generics are modified by adding the inverter efficiency (this was more straightforward since the models are already exponential). Figure 5.13 shows the corresponding five curves, including the "aggregate generic PV model" all considering the inverter efficiency. These curves now have different expressions but, as

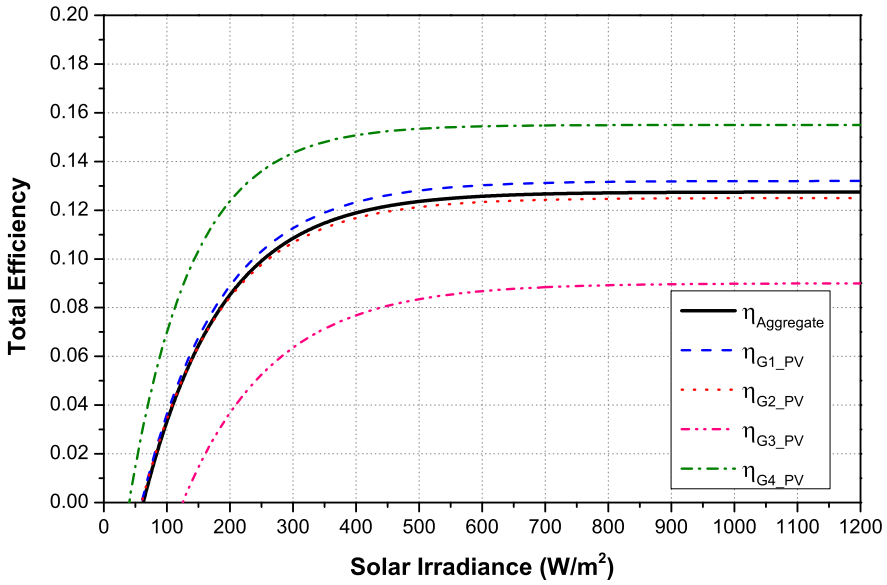

Figure 5.13: *Total efficiency of all proposed generic PV models.*

previously mentioned the simplification is straightforward since both PV and inverter models are exponential. The time constants are not affected because the dynamics of the inverter are

faster than that of the PV panel, therefore the final equations that describe the efficiency of the Generic PV panels are:

$$\eta_{PV_{1T}} = 0.132\left(1 - e^{-0.008(S_{irr}-60)}\right), \qquad for\ S_{irr} \geq 60^{W}/_{m^2} \tag{5.14}$$

$$\eta_{PV_{2T}} = 0.125\left(1 - e^{-0.008(S_{irr}-60)}\right), \qquad for\ S_{irr} \geq 60^{W}/_{m^2} \tag{5.15}$$

$$\eta_{PV_{3T}} = 0.155\left(1 - e^{-0.008(S_{irr}-125)}\right), \qquad for\ S_{irr} \geq 125^{W}/_{m^2} \tag{5.16}$$

$$\eta_{PV_{4T}} = 0.9\left(1 - e^{-0.008(S_{irr}-40)}\right), \qquad for\ S_{irr} \geq 40^{W}/_{m^2} \tag{5.17}$$

The percentage of contribution for each PV technology in the total aggregate was reported in Section 5.3. Using these figures the final "aggregate generic PV model" is then described as:

$$\eta_{PV_{AT}} = 0.127\left(1 - e^{-0.008(S_{irr}-60)}\right), \qquad for\ S_{irr} \geq 60^{W}/_{m^2} \tag{5.18}$$

Micro and small-scale generation systems are commonly connected to the UK low-voltage networks. The analysis presented simplifies the problem of aggregating wind turbine micro-generation systems by using only one equation that depending on the input wind speed can give the corresponding power output. Using this methodology, power output analysis was carried out and reported by Collin et al. [17]. However, equation (5.5) has to be per unitised in order to calculate power outputs that could be used for network analysis. It has to be noted that even though the methodology intends to simplify microwind and PV technologies in the same way, the PV representation is already in per-unit. The PV generic has to be used alongside with the solar irradiance as an input, the solar irradiance is given in $^{W}/_{m^2}$ then multiplied by the per-unit efficiency and would give the output as $^{W_e}/_{m^2}$. Whereas for microwind the input is given in $^{m}/_{s}$ and the output then would be given in $^{W_e}/_{m^2}$ by the generic models previously presented.

In this thesis the analysis is processed from the renewable energy resources available in Edinburgh to the final power curve/efficiency curve including all losses in the system in order to quantify the maximum possible power output delivered to the network coming from micro and small-scale energy systems, using the profiles identified in Section 2.6.2. This aggregation methodology is used next when aggregate models are connected to a distribution network model, alongside with component-based models of the load later in the next chapter of this thesis.

5.7 Economic and Cost-benefit Analysis of Wind Microgeneration

This section presents a detailed economic and cost-benefit analysis of micro and small-scale wind turbine installations in urban areas. Both actual wind turbines and generic wind turbine models introduced in the previous section are used to illustrate the results of the analysis. The presented economic analysis includes: capital costs, power and energy outputs, Feed-in tariffs, loan interest rates and operation and maintenance (O&M) costs. The capital costs of micro and small-scale wind turbines are obtained from the market survey performed previously for the purpose of this thesis, with the following typical minimum/maximum capital costs of micro wind turbines: $£4,128/kW$ - $£5,310/kW$ for turbines rated $1.5kW$ or less, between $£2,917/kW$ - $£3,114/kW$ for turbines rated $1.5kW$ - $15kW$ and between $£2,453/kW$ - $£2,525/kW$ for turbines rated $15kW$ - $100kW$. The interest rates on loans available for wind turbine developers currently offered by a number of investment companies and banks for different sizes of wind turbine projects, are in this chapter assumed to be: 15% for loans up to $£4,999$, 9% for loans $£5,000$ - $£7,499$, 8% for loans $£7,500$ - $£14,999$ and 7% for loans greater than $£15,000$. The annual O&M costs are assumed to be 2% of the total capital cost and currently available UK Feed-in Tariffs (valid for the next 20 $years$ for $\leq$ $50kW$ installations) for generated and/or exported electricity, based on the year in which the wind turbine developer signs the contract, are shown in Table 5.1. It should be noted that currently in the UK

wind turbine Rated Power	Year1: 4/01/2010 to 3/31/2011	Year 2: 4/01/2011 to 3/31/2012	Year 3: 4/01/2012 to 3/31/2013	Tariff Lifetime ($years$)
$\leq 1.5kW$	34.5	34.5	32.6	20
$1.5kW - 15kW$	26.7	26.7	25.5	20
$15kW - 100kW$	24.1	24.1	23	20

Table 5.1: *UK tariffs (pence per kWh) for micro and small-scale wind turbine [88].*

there are no grant schemes available to subsidise capital costs of micro and small-scale wind turbine systems (previous grants are no longer available due to a high demand of wind turbine developers and introduced government cut-backs [92]). The only incentive available to the wind turbine developers and a sole criterion of economic merits of the wind turbine projects, are Feed-in tariffs (see Table 5.1). Under this scheme, wind turbine developers who generate their own electricity from wind turbine systems will receive a minimum payment for all the electricity produced by the system.

5.7.1 Calculated Annual Energy Outputs

The results presented in this chapter assume that annual input wind energy resources could be represented using a general Weibull distribution, for which mean wind speeds vary in the range from $1^{m}/_{s}$ - $8^{m}/_{s}$, while shape factor k varies from 1.2 to 2.2. Based on this assumptions, annual energy outputs of wind turbines are calculated by multiplying the probability values of average wind speeds from the corresponding Weibull distributions by 8760 (i.e. 100% availability of the wind turbine systems is assumed) and then applying these values on normalised power curves of selected actual and generic wind turbines. It is also assumed that power curves give electrical power output of wind turbines (this is discussed further in this chapter). Tables 5.2 to 5.5 present detailed results for the calculated annual energy outputs per metre squared of swept area for four generic wind turbines ($G1$, $G2$, $G3$ and $G4$) for Weibull distributions with different mean wind speeds and shape factors. Tables 5.6 to 5.8 give results calculated for three actual wind turbines (WT1, WT2 and WT3), details of which are provided in Section 3.3.

Wind Speed ($^{m}/_{s}$)	Annual Generation of $G_1(^{kWh}/_{m^2})$ at values of k					
	1.2	1.4	1.6	1.8	2	2.2
1	5.6	2.8	1.33	0.6	0.26	0.1
2	75.37	56.71	44.36	35.75	29.45	24.7
3	227.8	193.94	166.7	146.6	131.7	120.34
4	416.93	393.7	362.24	332.28	307.55	288.1
5	591.2	605.1	596.25	574	548.04	522.85
6	727.15	785.16	817.11	827.04	820.94	805.3
7	822.44	917.1	990.1	1041.5	1073	1087.7
8	883.4	1002.45	1105	1193.1	1263.2	1316.7
Turbine Rating	Minimum Mean Wind Speed (m/s) for a payback period of					
	15 years		10 years		5 years	
$\leq 1.5kW$	$> 6.3(k = 2)$		$> 6.75(k = 2.2)$		$> 9.2(k = 2.2)$	
$1.5kW$ - $15kW$	$> 4.75(k = 1.2)$		$> 5.4(k = 1.6)$		$> 7.4(k = 2)$	
$1.5kW$ - $100kW$	$> 4.5(k = 1.2)$		$> 5.2(k = 1.4)$		$> 7(k = 1.8)$	

Table 5.2: *Calculated annual energy outputs in $^{kWh}/_{m^2}$ and minimum wind speeds for required payback periods for generic wind turbine 1.*

5.7.2 Calculated Pay-back Periods

Based on the assumed capital, operation and maintenance costs, also taking into account applied loan interest rates and currently available Feed-in tariffs (only for generated electricity without exporting), this section presents the results for the calculated minimum payback periods for four

Wind Speed ($^m/_s$)	Annual Generation of $G_2(^{kWh}/_{m^2})$ at values of k					
	1.2	1.4	1.6	1.8	2	2.2
1	2.99	1.11	0.37	0.1	0.02	0
2	56.76	40.57	29.6	21.9	16.4	12.4
3	179.6	152.5	129.8	112.2	98.55	87.8
4	329.2	313	289.6	266.6	246.8	230.7
5	464.65	478.5	474.9	460.8	442.85	425
6	569	616.9	645.3	657	656.4	648.2
7	641.13	716.7	776.14	819.4	847.7	863.3
8	686.7	780.3	862.2	931.75	988.6	1033
Turbine Rating	Minimum Mean Wind Speed (m/s) for a payback period of					
	15 years		10 years		5 years	
$\leq$ 1.5kW	$> 6(k = 1.8)$		$> 6.48(k = 2.2)$		$> 8.52(k = 2.2)$	
1.5kW - 15kW	$> 4.56(k = 1.2)$		$> 5.2(k = 1.6)$		$> 7(k = 2)$	
1.5kW - 100kW	$> 4.4(k = 1.2)$		$> 5(k = 1.4)$		$> 6.7(k = 2)$	

Table 5.3: *Calculated annual energy outputs in $^{kWh}/_{m^2}$ and minimum wind speeds for required payback periods for generic wind turbine 2.*

Wind Speed ($^m/_s$)	Annual Generation of $G_3(^{kWh}/_{m^2})$ at values of k					
	1.2	1.4	1.6	1.8	2	2.2
1	1.38	0.4	0.1	0.01	0	0
2	37.3	25	16.7	11.13	7.4	4.9
3	126.5	105.65	87.7	73.5	62.32	53.4
4	235.9	223.83	206.24	188.5	172.8	160
5	334.6	345.15	343	333.14	320.2	307
6	410.2	445.7	467.35	477.1	478	473.2
7	462.3	517.8	561.9	594.7	616.8	630
8	495.1	563.4	623.4	675	717.5	751.3
Turbine Rating	Minimum Mean Wind Speed (m/s) for a payback period of					
	15 years		10 years		5 years	
$\leq$ 1.5kW	$> 5.88(k = 1.8)$		$> 6.34(k = 2)$		$> 8.19(k = 2.2)$	
1.5kW - 15kW	$> 4.48(k = 1.2)$		$> 5.12(k = 1.4)$		$> 6.8(k = 2)$	
1.5kW - 100kW	$> 4.3(k = 1.2)$		$> 4.9(k = 1.4)$		$> 6.5(k = 2)$	

Table 5.4: *Calculated annual energy outputs in $^{kWh}/_{m^2}$ and minimum wind speeds for required payback periods for generic wind turbine 3.*

Wind Speed ($^m/_s$)	Annual Generation of $G_4(^{kWh}/_{m^2})$ at values of k					
	1.2	1.4	1.6	1.8	2	2.2
1	1.82	0.66	0.21	0.06	0.01	0
2	34.8	25.1	18.33	13.5	10	7.5
3	107.1	92.5	79.7	69.45	61.3	54.7
4	191.9	185	173.5	161.7	151.1	142.2
5	266.8	277.1	277.7	272.4	264.4	256.1
6	323.3	352.2	370.6	380	382.4	380.6
7	361.7	405.23	440.1	466.3	485	496
8	385.4	438.1	484.5	524.3	557.3	583.6
Turbine Rating	Minimum Mean Wind Speed (m/s) for a payback period of					
	15 years		10 years		5 years	
$\leq$ 1.5kW	$> 5.6(k = 1.8)$		$> 6.1(k = 2)$		$> 7.8(k = 2.2)$	
1.5kW - 15kW	$> 4.25(k = 1.2)$		$> 4.9(k = 1.4)$		$> 6.5(k = 2)$	
1.5kW - 100kW	$> 4.1(k = 1.2)$		$> 4.7(k = 1.4)$		$> 6.2(k = 2)$	

Table 5.5: *Calculated annual energy outputs in $^{kWh}/_{m^2}$ and minimum wind speeds for required payback periods for generic wind turbine 4.*

Wind Speed ($^m/_s$)	Actual Annual Generation of $WT1(kWh)$ at values of k					
	1.2	1.4	1.6	1.8	2	2.2
1	41	33.75	28	23.3	19.2	15.5
2	197.2	178.2	166.34	158.8	154	150.6
3	434.7	401.5	374.44	355	341.2	331.1
4	701	685.4	656	625.44	600	580
5	936.3	970.3	972	954.2	928.1	901.4
6	1115.1	1205.8	1260.3	1284.5	1286.3	1274
7	1237.45	1374.24	1480.5	1557.2	1607.3	1635
8	1313.15	1480	1633	1744.7	1842.64	1918.7
	Minimum Mean Wind Speed (m/s) for a payback period of					
	15 years		10 years		5 years	
	$> 5.6(k = 1.8)$		$> 6.1(k = 1.8)$		$> 7.94(k = 2.2)$	

Table 5.6: *Calculated annual energy outputs in $^{kWh}/_{m^2}$ and minimum wind speeds for required payback periods for actual WT1.*

Wind Speed (m/s)	Actual Annual Generation of $WT2(kWh)$ at values of k					
	1.2	1.4	1.6	1.8	2	2.2
1	3	0.8	0.18	0.03	0	0
2	113	65.2	39.1	24.3	15.6	10.2
3	477.2	359	267.44	203.5	159.15	127.7
4	995.5 892.3	768	651.7	556	481.1	
5	1499.8	1503	1441	1342	1230	1122.6
6	1906.5	2042.5	2104.65	2104.55	2058.4	1983.5
7	2200.6	2450.35	2639.3	2768.3	2842.3	2869.4
8	2396.2	2724.6	3010.1	3250.14	3444.1	3593.34
	Minimum Mean Wind Speed (m/s) for a payback period of					
	15 years		10 years		5 years	
	$> 6.65(k = 2)$		$> 7.4(k = 2.2)$		-	

Table 5.7: *Calculated annual energy outputs in $^{kWh}/_{m^2}$ and minimum wind speeds for required payback periods for actual WT2.*

Wind Speed (m/s)	Actual Annual Generation of $WT3(kWh)$ at values of k					
	1.2	1.4	1.6	1.8	2	2.2
1	14	5.8	2.44	1	0.36	0.1
2	301.3	196.7	135.35	97.5	72.8	56.1
3	1120	879.4	692.75	562.7	471.3	404.3
4	2230	2040.5	1793.5	1559.2	1370	1225.4
5	3271.75	3327.1	3231.6	3041	2814	2595.4
6	4081.4	4423.24	4608.34	4650.35	4577.5	4427.4
7	4643	5214.4	5668.7	6000	6206.85	6300
8	4997	5714.6	6358	6918	7388.5	7765
	Minimum Mean Wind Speed (m/s) for a payback period of					
	15 years		10 years		5 years	
	$> 5.5(k = 1.6)$		$> 6.11(k = 1.8)$		$> 7.8(k = 22))$	

Table 5.8: *Calculated annual energy outputs in $^{kWh}/_{m^2}$ and minimum wind speeds for required payback periods for actual WT3.*

generic wind turbines (G1-G4). These assume a Weibull average wind speed distributions with mean annual wind speed of $6^{m}/_{s}$ (typically assumed for the UK) and different shape factors. It can be seen from Figure 5.14 to Figure 5.17 that the minimum pay-back periods will generally decrease as the wind turbine rating increases (lower cost per kW installed and lower interest rates for larger development) and as the shape factor of Weibull distributions for average annual wind speeds increases (higher wind energy contents). A slight increase in the payback periods for high values of shape factors is due to the nature of the Weibull distribution: at low mean wind speeds, the highest proportion of the total annual generation occurs at low values of shape factor, while at high mean wind speeds, the highest annual generation occurs at high shape factors. Also, in Figure 5.14 to Figure 5.17, the mean wind speed is $6^{m}/_{s}$, therefore the highest annual generation is occurring when the shape factor is about 1.8. In Figure 5.17, no results are shown for wind turbine G4 for $k \leq 1.3$, as the corresponding payback periods are longer than 15 years.

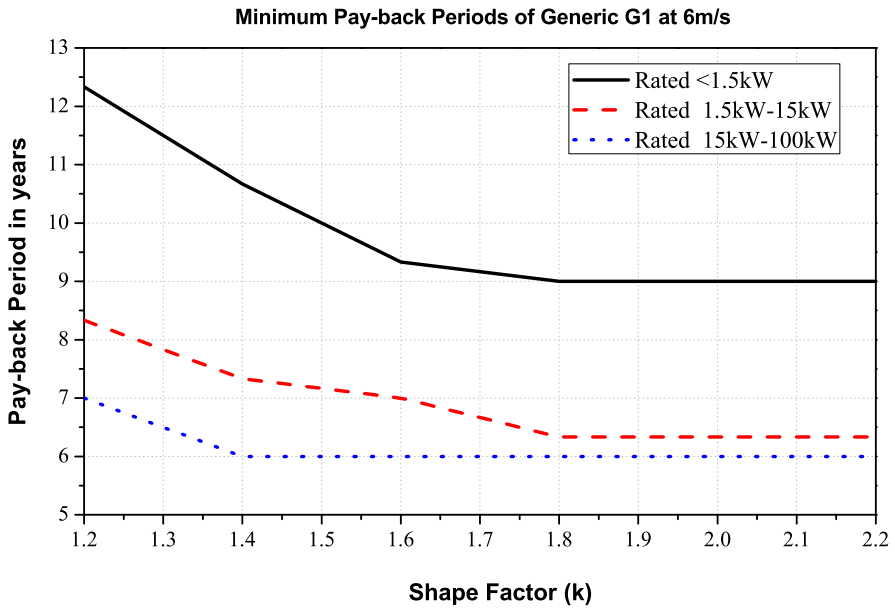

Figure 5.14: *Calculated minimum payback periods for Weibull distributions with mean wind speeds* $6\ ^{m}/_{s}$ *and different shape factors for generic wind turbine 1.*

5.7.3 Minimum Mean Wind Speed for Required Payback Periods

To ensure the turbine will pay for itself during its lifetime, the site has to have sufficient/minimum wind energy resources (i.e. mean wind speed). Using the "reverse calculation" of payback pe-

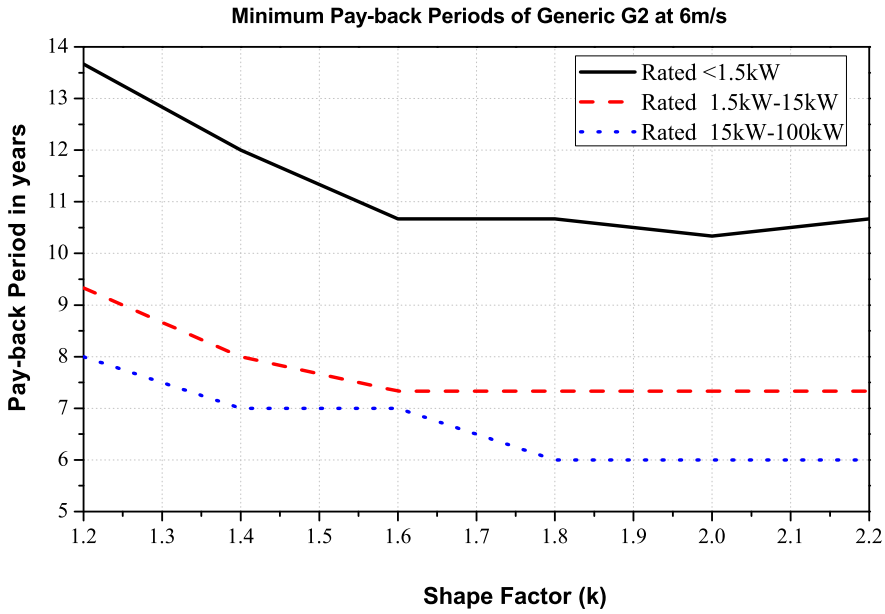

Figure 5.15: *Calculated minimum payback periods for Weibull distributions with mean wind speeds* $6\ ^{m}/_{s}$ *and different shape factors for generic wind turbine 2.*

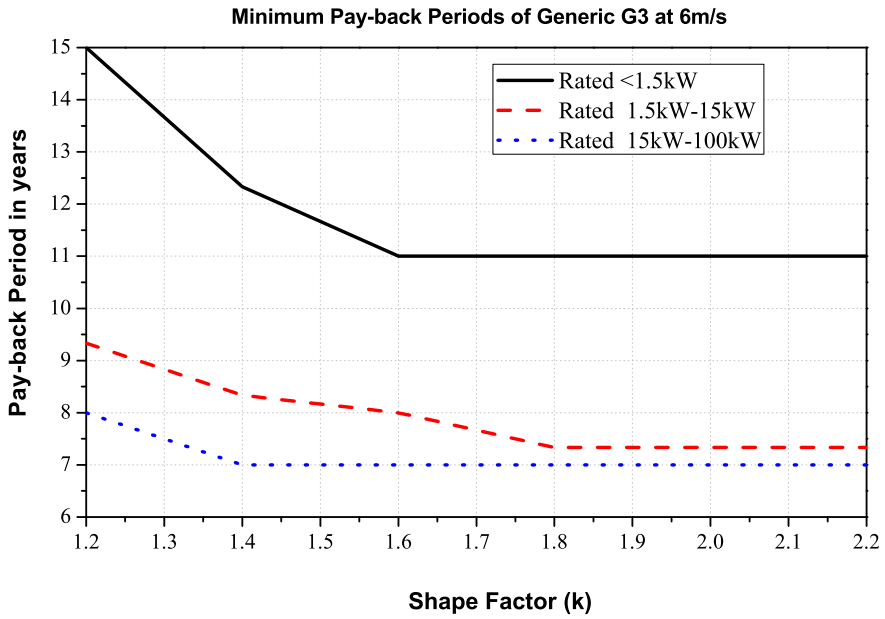

Figure 5.16: *Calculated minimum payback periods for Weibull distributions with mean wind speeds* $6\ ^{m}/_{s}$ *and different shape factors for generic wind turbine 3.*

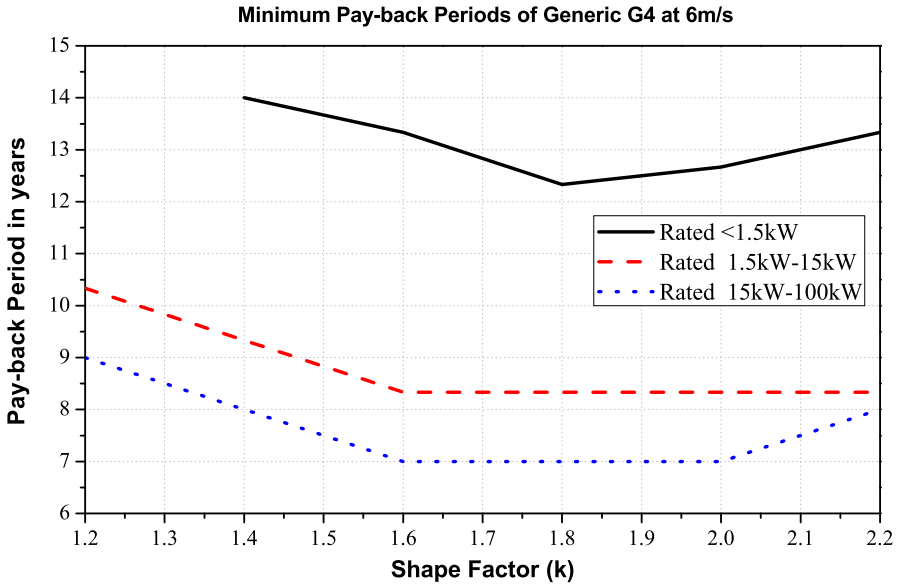

Figure 5.17: *Calculated minimum payback periods for Weibull distributions with mean wind speeds* $6\ ^{m}/_{s}$ *and different shape factors for generic wind turbine 4.*

riods from the previous section, the results for minimum mean wind speeds required to achieve a pre-defined pay-back period (5, 10 or 15 $years$) are calculated and illustrated from Table 5.2 to Table 5.8, together with the detailed results for calculated annual energy outputs for three actual wind turbines ($WT1$, $WT2$ and $WT3$) and four generic wind turbines ($G1$, $G2$, $G3$ and $G4$). The most common type of urban wind turbine systems (with rated power $\leq 1.5kW$) would require higher than $5.5^{m}/_{s}$ mean wind speed to achieve a pay-back period of 15 $years$. Mean wind speeds greater than this in urban environments may not be available, as the analysis in Chapter 2 has shown and therefore, householders and wind turbine developers should be careful in selecting suitable micro and small-scale wind turbines, as the payback period may otherwise exceed their lifetimes.

5.8 Economic and Cost-benefit Analysis of PV Microgeneration

This section presents a detailed economic and cost-benefit analysis of micro-PV installations in urban areas. For this analysis the generic PV models are used to illustrate the results of the analysis. AS before, the presented economic analysis include: capital costs, power and energy outputs, Feed-in Tariffs, loan interest rates and operation and maintenance (O&M) costs.The capital costs of PV systems are obtained from the PV market survey, with the following typi-

cal minimum/maximum capital costs: $£193/panel$ - $£507/panel$ for monocrystalline panels, between $£183/panel$ - $£497/panel$ for polycrystalline panels, $£90.85/panel$ - $£183/panel$ for thin-film panels and between $£623/panel$ - $£1,043/panel$ for HIT thin-film panels.The interest rates on loans available for PV panels currently offered by a number of investment companies and banks for different sizes of PV installations, are the same as for wind energy systems earlier in this chapter: 15% for loans up to $£4,999$, 9% for loans $£5,000$ - $£7,499$, 8% for loans $£7,500$ - $£14,999$ and 7% for loans greater than $£15,000$. The annual O&M costs are assumed to be 1% of the total capital cost and currently available UK Feed-in Tariffs (valid for the next 20 $years$ for $\leq 50kW$ installations) for generated and/or exported electricity, based on the year in which the PV developer signs the contract, are given in Table 5.9. As

PV installation Rated Power	Previous FIT level (p/kWh)	New FIT level (p/kWh)	Tariff Lifetime ($years$)
$\leq 4kW$ (Retrofit)	45.4	21	25
$\leq 4kW$ (New build)	39.6	21	25
$4kW - 10kW$	39.6	16.8	25
$10kW - 50kW$	34.5	15.2	25

Table 5.9: *UK tariffs (pence per kWh) for PV installations [88].*

micro and small-scale wind energy, micro-PV installations lack of incentives to increase the level of penetration in low-voltage networks, the only incentive available to the PV developers is the Feed-in Tariffs from Table 5.9. Under this scheme, PV developers who generate their own electricity from PV systems will receive a minimum payment for all electricity produced by the system, plus an extra payment for any electricity exported to the grid.

5.8.1 Calculated Annual Energy Outputs

To facilitate the calculation of power delivered to the grid, a change in units is required. This change is performed by multiplying the average annual solar irradiance in W/m^2 by a factor of $24h/day$. Therefore, the unit of input solar irradiance is: $Wh/(m^2 \cdot day)$. This solar irradiance will be used to calculate the energy output for a year by multiplying it with the generic PV model average efficiency and 365 days of the year. Moreover, according to the European Commission PVGIS the yearly average solar irradiance for Edinburgh city is $2.8 kWh/(m^2 \cdot day)$. A value of $117 W/m^2$, similar to the south of Spain is found to have an average solar irradiance of $5.5 kWh/(m^2 \cdot day)$ corresponding to $230 W/m^2$, therefore the analysis considers a reasonable range

of solar irradiance to calculate the energy outputs. This analysis for wind energy systems considered probabilistic distributions and the power curves of the systems. For PV energy systems this approach is not required, as previously shown the solar irradiance consists of a single value that then can be multiplied by the average efficiency of the PV system.

The results presented in this chapter assume that average annual input solar irradiance could go above the highest value of solar irradiance found in mainland Europe (i.e. South of Spain), covering the range from $100^{W}/_{m^2}$ to $300^{W}/_{m^2}$ since the monthly average of solar irradiance for the summer months reaches that value in Europe [9]. Based on this assumption, annual energy outputs of PV systems are calculated by multiplying the average efficiency of the generic PV models with the average solar irradiance. However for this calculation the solar irradiance has to be represented in different units to utilise the calculation. Table 5.10 present detailed results for calculated annual energy outputs per metre squared of exposed area for four generic PV systems ($G1$, $G2$, $G3$ and $G4$) for the range of solar irradiance increasing by $50^{W}/_{m^2}$ steps.

Solar Irradiance $(^{W}/_{m^2})$	Annual Generation of Generic PV systems$(^{kWh}/_{m^2})$			
	G_1	G_2	G_3	G_4
100	52.6	52.6	8.8	96.4
150	123.5	114.3	38.1	173.5
200	185.7	175.2	8.8	96.4
250	256.2	241	135.8	328.5
300	323.2	302.2	186.6	404.7

Table 5.10: *Calculated annual energy outputs for Generic PV systems.*

5.8.2 Calculated Pay-back Periods

Based on the assumed capital, operation and maintenance costs, as well as applied loan interest rates and currently available Feed-in tariffs this section presents the results for the calculated minimum payback periods for four identified PV systems (monocrystalline, polycrystalline, thin-film, HIT thin-film), for a range of different input average solar irradiance values, giving the pay-back periods for lower and higher capital costs found for the technologies. It can be seen from Figure 5.18 to Figure 5.20 that the minimum pay-back periods corresponds to lower capital costs. For higher capital costs only thin-film PV installations have a pay-back period below 25 years. The lower capital costs present an interesting case: with an increase in the demand of these panels, installation costs will decrease and a lower and more realistic pay-back period can be achieved.

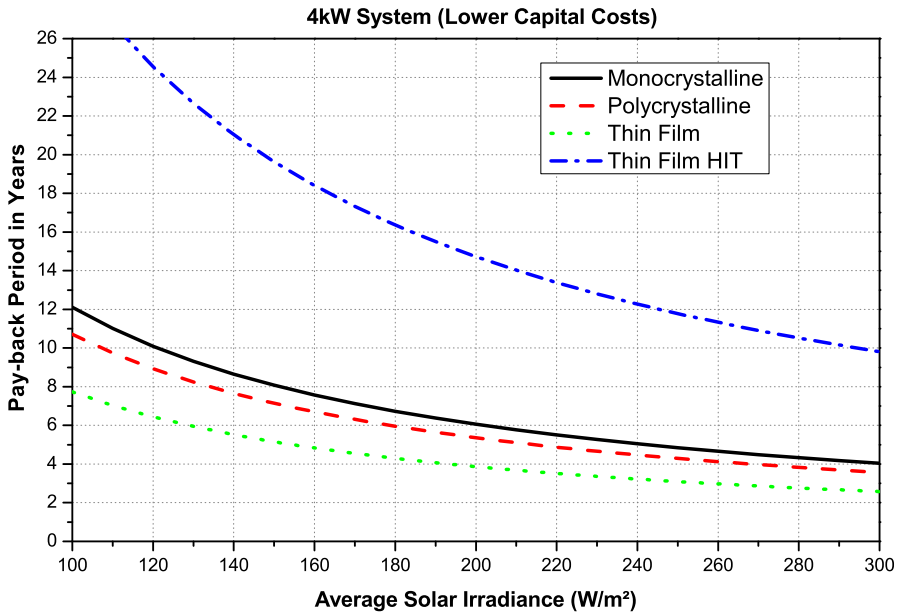

(a)

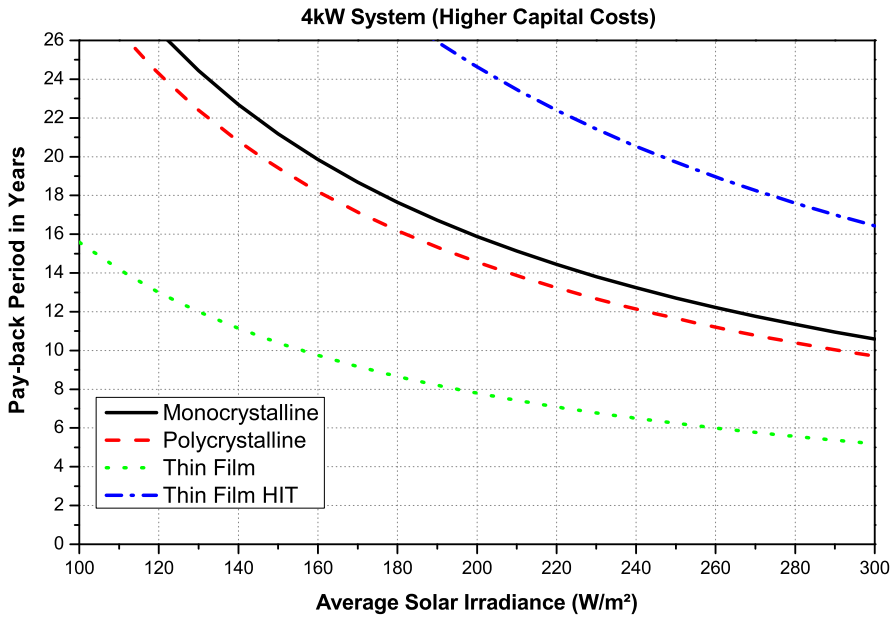

(b)

Figure 5.18: *Calculated minimum payback periods for different average annual solar irradiance values and average efficiencies for a 4kW PV system.*

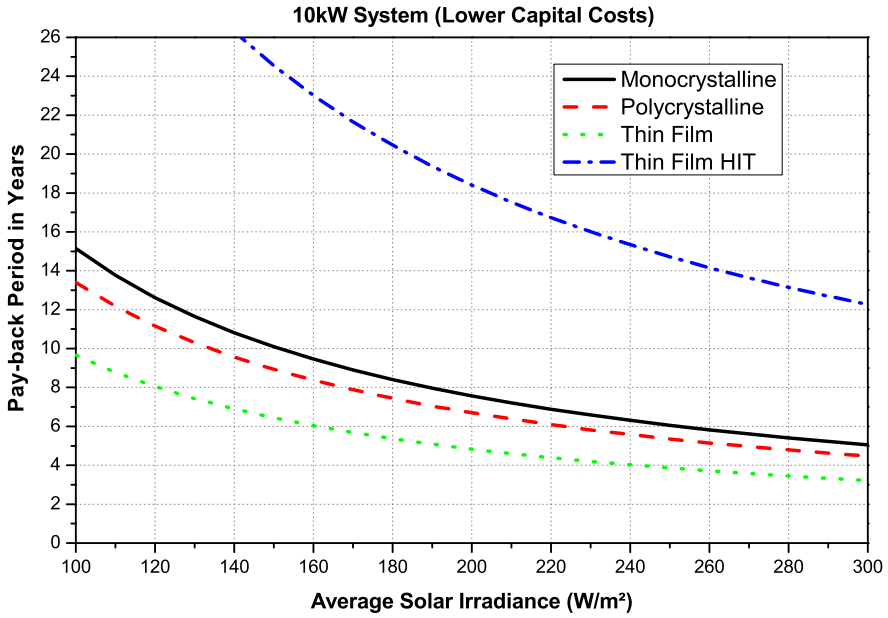

(a)

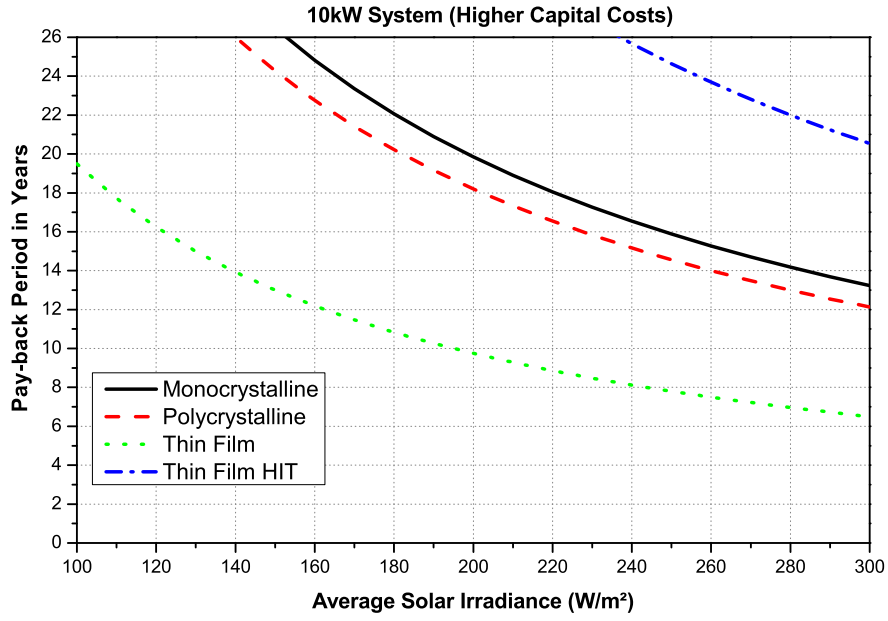

(b)

Figure 5.19: *Calculated minimum payback periods for different average annual solar irradiance values and average efficiencies for a 10kW PV system.*

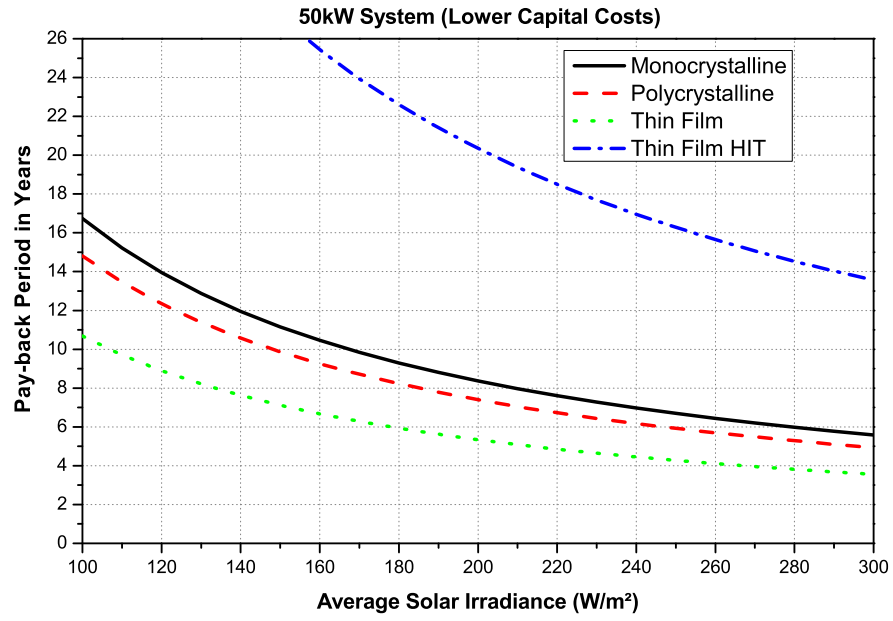

(a)

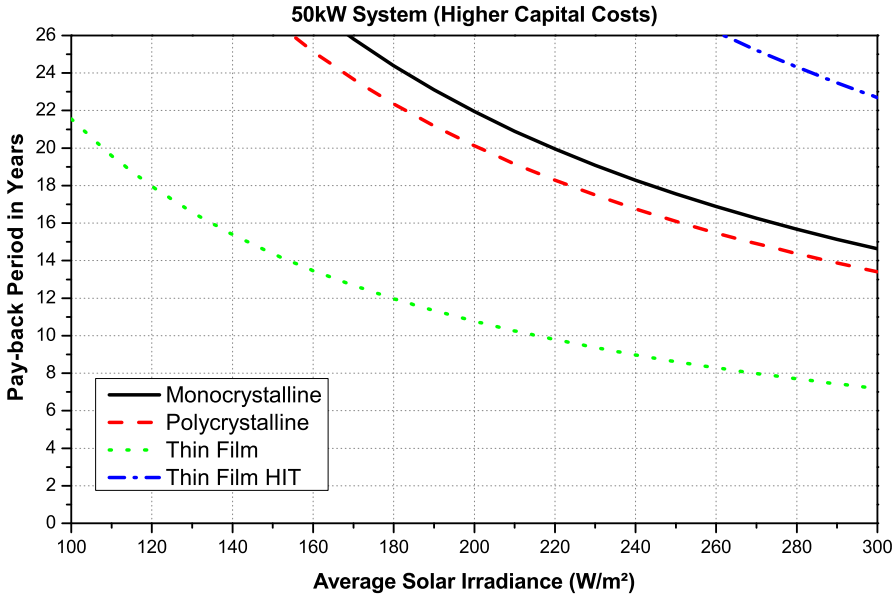

(b)

Figure 5.20: *Calculated minimum payback periods for different average annual solar irradiance values and average efficiencies for a 50kW PV system.*

5.9 Conclusions

In order to address some difficulties and uncertainties related to the analysis of micro and small-scale renewable-based generation systems in urban areas, this chapter discussed and compared the generalisation methodology used for both wind and PV technologies. This generalisation allows one equation to represent many different manufacturers and characteristics. The steady-state performance assessment is based on the use of low-resolution input data (i.e. measured, estimated or Weibull distribution represented hourly average wind speeds and 5-minute resolution measurements for solar irradiance) and the use of only some basic information of considered technologies (i.e. wind turbine manufacturer's power curve and PV panel specifications). For the initial selection of optimal systems in target applications, the chapter proposed four generic PV models and four generic wind turbine models. Although practically all considered systems differ in both rated power and swept/exposed areas, the presented analysis demonstrates that four proposed generic PV and wind microgeneration models can be used for the accurate representation of the majority of PV and wind energy systems currently available on the market. The four generic models can be further used for the development of an accurate aggregate model of a large number of micro and small-scale energy systems (e.g. in a metropolitan urban area), which is initially discussed in [12] and is a subject of discussion in the next chapter.

The proposed methodology also allows for a simple addition of the new "generic models", with appropriate characteristics to represent a range of new systems. This chapter presented the methodology followed to aggregate PV and wind energy systems. This methodology then can be used in particular (e.g. in the UK) by assuming the percentage of contribution from the database and building a single "aggregate generic". Using this generic and the time-series profiles proposed for Edinburgh city in Chapter 2, it is possible to represent micro and small-scale generation connected in Edinburgh distribution network and aggregate these system as one combined aggregate microgeneration model.

Chapter 6
All Technologies Aggregation and Analysis of the Impact on the Network

6.1 Introduction

Correct modelling of renewable-based generation technologies implemented in urban areas is not a simple task, as it requires a detailed representation of highly dispersed and uncontrolled generation systems, which are small in size, but high in numbers and usually experience large variations in available renewable energy inputs. This chapter presents the use of the aggregate models of urban micro and small-scale generation systems developed in Chapter 5, which are connected to a low-voltage network together with an aggregate system load model and a detailed model of a typical UK urban distribution network. This chapter uses the developed models to analyse the impact of urban microgeneration connected to the network, based on the time-series profiles described in Chapter 2, presenting the results for steady-state network performance (power flows and voltage profiles). The presented analysis is of particular importance for the analysis of the future power supply systems, which will have significantly higher penetration levels of renewable-based distributed generation technologies, resulting in a much wider range of interactions between microgeneration systems, loads and transmission/distribution networks. This chapter presents the results of this work in collaboration with Load modelling and network modelling projects in the Institute for Energy Systems at the University of Edinburgh.

6.2 Microgeneration Aggregation Methodology for the Analysis of Distribution Network Performance

Figure 6.1 shows the connection of microgeneration to the low-voltage network in parallel with the load, based on the approach presented in [12]. The proposed aggregation methodology, which aims to derive an aggregate model of all low-voltage microgeneration and loads at $11kV$ busbar, has been presented in [12]- [19]. Three sets of input data are required:

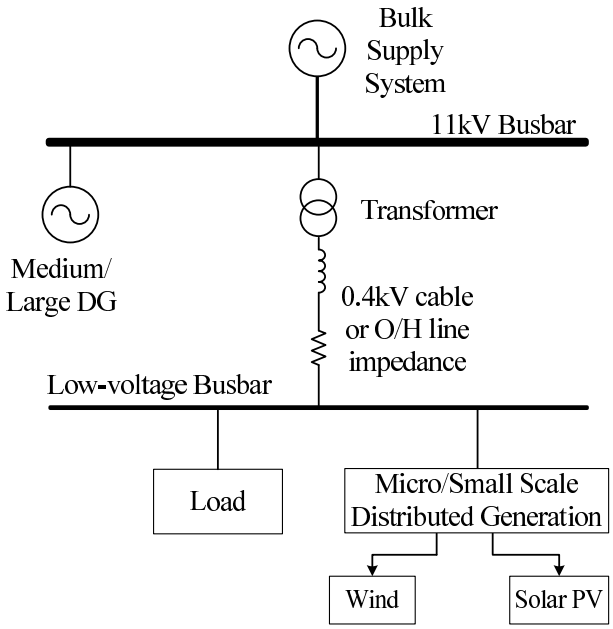

Figure 6.1: *Microgeneration and load connected in parallel to the network.*

(a) Measured or estimated load curves and statistical information on the load structure,

(b) Accurate models of the main load/microgeneration categories, including estimated input energy resources of microgeneration technologies,

(c) Network configuration and network component parameters/models.

The aggregation methodology can be broken down into six steps, which are illustrated using the example of the UK residential load sector. The "flow chart" for the proposed aggregation methodology is shown in Figure 6.2.

6.2.1 Load Modelling

The term "aggregate load model" denotes an analytical/mathematical, equivalent-circuit or physical component based representation of a group of loads connected to a single system bus. The main purpose of a load model is to correctly represent the changes in active and reactive power demands of the modelled load as a function of variations of certain supply system parameters. This information is required for the analysis of the network loading/operating conditions and assessment of the network performance in power system studies. The most frequently used load models are simple analytical/mathematical formulations describing the relationship between the active and reactive power demands of the load as a function of the load

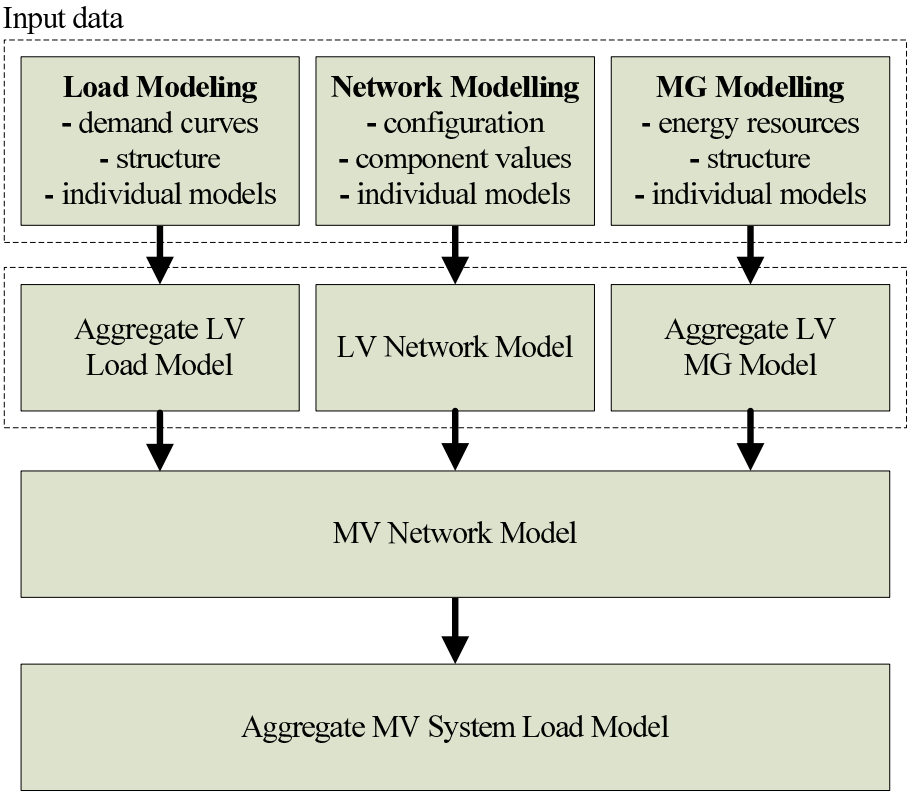

Figure 6.2: *Aggregation methodology at distribution voltage level.*

supply voltage. If these models are used for steady-state power flow analysis, they do not consider frequency variations, which are small during the steady-state operating conditions. The two following general forms are traditionally the most common: the exponential load model, shown in (6.1) - (6.2) and the polynomial load model, (6.3) - (6.4). It should be noted that although it is possible to include a frequency dependency in the load model, this is usually not done during the steady state analysis of power supply systems, as the corresponding frequency variations are very small.

$$P = P_0 \left(\frac{V}{V_0} \right)^{np} \tag{6.1}$$

$$Q_1 = P_{1,0} \left(\frac{V}{V_o} \right)^{nq} \tag{6.2}$$

$$P = P_0 \left[Z_P \left(\frac{V}{V_o} \right)^2 + I_P \left(\frac{V}{V_0} \right) + P_P \right] \tag{6.3}$$

$$Q_1 = Q_{1,0} \left[Z_Q \left(\frac{V}{V_o} \right)^2 + I_Q \left(\frac{V}{V_0} \right) + P_Q \right] \tag{6.4}$$

where, P, Q_1 - actual active and (fundamental) reactive powers; V - actual supply voltage; V_0 - nominal supply voltage; P_0, $Q_{1,0}$ -nominal/rated active and (fundamental) reactive powers;

np, nq - exponential model coefficients; Z_P, I_P, P_P, Z_Q, I_Q, P_Q - polynomial/ZIP model coefficients.

The exponential load model uses two coefficients (i.e. exponents), np and nq, to define the relationship between the active and reactive power demands and the supply system voltage. When the coefficients equal 0, the load behaves as a constant power load; when the coefficients equal 1, the load behaves as a constant current load; and when the coefficients equal 2, the load behaves as a constant impedance load. The exponents may also take an arbitrary value, to more accurately represent power demand characteristics of the modelled load. The polynomial load model represents the load as the sum of constant impedance (Z), constant current (I) and constant power (P) types of loads (they should add up to $1pu$, or 100% of the total load) and is often abbreviated as the "ZIP" model. Generally, polynomial/ZIP models are able to provide better representation of characteristics of modelled load, particularly in case of non-linear load, when fundamental components of power demands are of the most interest. Typical load curves of the UK urban residential load sector are shown in Figure 6.3 (Note: Reactive power characteristic is shown as a percentage of the reactive power demand occurring during the maximum active power demand). It is not the scope of this research to go into details on how these profiles were obtained, they are suitable for urban microgeneration since they are profiles from residential customers. More information on how they were built and used can be found in: [16], [17], [18], [19].

Figure 6.4 shows the average loading condition profile decomposed into load types. The actual residential load mix will vary depending on the location of the load, as well as on the time of the day, day of the week and season of the year. The load profile used in this thesis to represent aggregate low-voltage residential customers in the UK for average (i.e. Spring/Autumn) loading conditions is shown in Figure 6.4. This profile is obtained using a UK government report on residential load [93]. The number of customers is defined from Figure 6.5 where a number of 9120 individual households is modelled with a peak demand of $2.27kW$ per customer. All electrical devices and equipment found in the urban load sector are divided in following types of loads: consumer electronics and information and communication technology (ICT) equipment; cooking load; "wet" load; "cold" load; direct and storage domestic hot water (DHW) load; direct, storage and top-up space heating load; and lighting load. The maximum UK residential loading conditions (100% peak load) occur during the Winter. This load profile is then converted into a usable load model using the methodology outlined in [16], where aggregate load is represented using general load categories. Models of load categories are combined us-

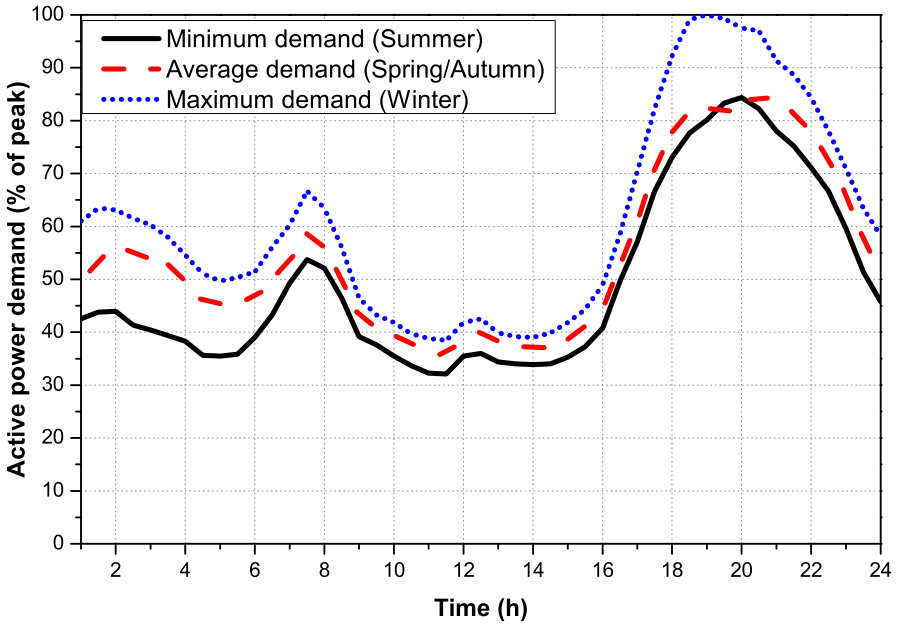

(a)

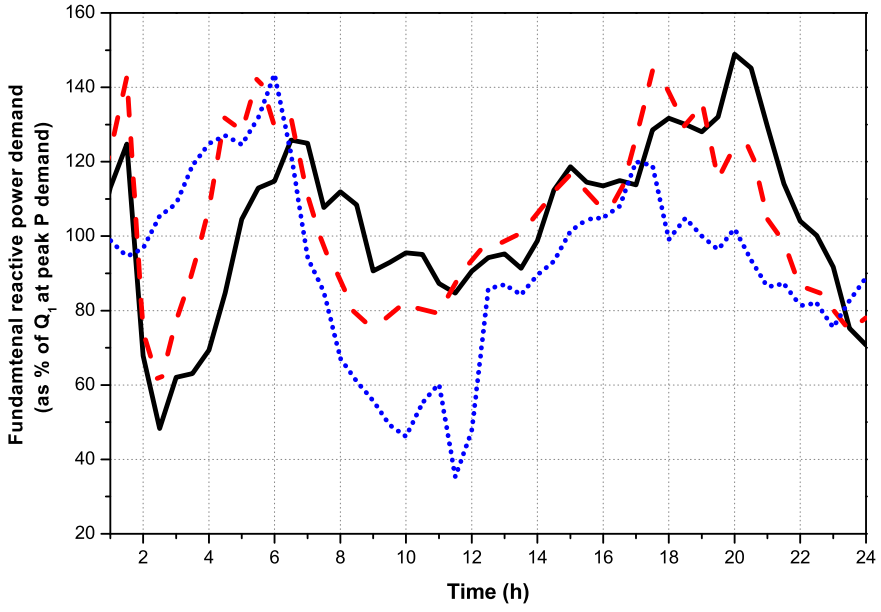

(b)

Figure 6.3: *Load profiles for different demands (three characteristic system operating conditions): a) active power, b) fundamental reactive power.*

ing their percentage contributions for each $30min$ period during the day to create the aggregate low-voltage load model.

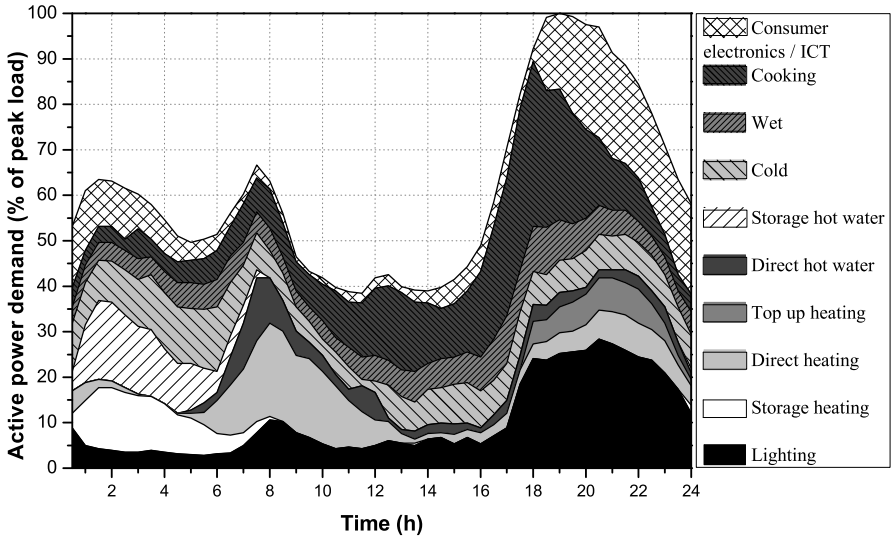

Figure 6.4: *Decomposition of load curve/profile into load types for the UK urban residential sector and average loading conditions [94].*

6.2.1.1 Load Sectors

The term "load sector" denotes an aggregation or collection of loads from different load categories representing a typical structure and composition of electrical devices and equipment found in a specific end-use application, where similar activities and tasks are performed (e.g. residential or commercial load sector). This usually results in inherent similarities in the characteristics and patterns of active and reactive power demands of end-users from the same load sector, allowing use of same or similar load models for the representation of their aggregate demands. The UK residential load sector can be divided into the four following sub-sectors: highly-urban, urban, suburban and rural. These categories were described and used in [16] and [17]. The description of every load sub-sector is as follows:

A. *Highly-urban residential load sub-sector*

This sub-sector is represented by flat-type dwellings, usually found in large cities (e.g. "metropolitan areas"), in multi- storey and high-rise buildings. It is characterised by highly

concentrated power demand (both per m^2 and km^2) and high levels of penetration of modern power electronic loads. Three- phase motors will be used for elevators, pumps and central air- conditioning systems, which are usually not present in other residential sub-sectors. The number of rooms per dwelling is lower than in other sub-sectors, and there will be additional interior lighting load for illumination of communal areas. Dedicated public/street lighting is also greater than in other sub-sectors, due to the presence of parking spaces and higher required lighting levels in metropolitan areas.

B. *Urban residential load sub-sector*

This sub-sector consists of house-type dwellings, ranging from one to few-storey buildings, located in city urban areas. It is characterised by medium to high concentration of power (per m^2 and km^2) and medium to large penetration of modern power electronic loads. As the average number of residents and rooms per household is greater than in highly urban sub- sector, higher power demands per household may occur. The public/street lighting in this sector is slightly reduced in comparison with the highly urban sub-sector.

C. *Suburban residential load sub-sector*

This sub-sector is similar to the urban sub-sector, generally representing individual house dwellings located in city suburban areas and towns in close proximity to big cities. The load mix is similar to the urban sub-sector and the contribution from public/street lighting is similar, or smaller. It is further characterised by medium power density (per m^2 and km^2) and medium penetration of modern power electronic loads.

D. *Rural residential load sub-sector*

House-type dwellings in this sub-sector are one to few-storey buildings, located in more remote areas. Concentration of power (per m^2 and km^2) is low, and penetration of modern loads is smaller. Some (smaller) three-phase motors are used for agricultural works, and there is no public/street lighting.

For the purpose of this thesis, the urban load sub-sector model is used for the connection of microgeneration models to the network.

6.2.2 Distribution Network Model

Before presenting the low-voltage (LV) generic network model used in this thesis to analyse the effect of microgeneration on system performance, the most important technical characteristics

of public secondary distribution grids must be described in detail. These networks typically operate at a nominal voltage of $400V$, after the primary distribution voltage is stepped down by means of $11/0.4kV$ distribution transformers. Generally, these networks are connected radially, with a number of low-voltage trunk feeders starting from the low-voltage busbars of the infeeding substation, as shown in Figure 6.5. These main trunk feeders may supply one or more lateral spurs and service connections (3-phase or single-phase), which finally supply the customer'. In terms of symmetry, the connection of multiple single-phase customers to the three-phase network makes low-voltage networks inherently unbalanced.

Low-voltage distribution conductors can be in the form of underground cables or overhead conductors depending on location and load density to be supplied, Table 6.1 provides conductor cross-sections typically used in the UK for different low-voltage distribution main feeders and spurs, as well as for each residential load sub-sector defined. As specified in Table 6.1, low-voltage underground lines are mainly used in highly-urban and urban areas, while in sub-urban and rural areas of overhead lines are used. These were traditionally constructed by aluminium (Al) or copper (Cu) bare conductors [95]. However ease of installation and environmental issues have led to the extensive use of bundled insulated overhead conductors in recent years. Table D.2 in Appendix D provides detailed information about typical configurations and parameters of low-voltage lines used for electricity distribution in the UK. This table allocates an identification letter to each of the different low-voltage lines in order to facilitate the construction and classification of distribution feeders in the low-voltage network models presented in the subsequent sections. Another important component of low-voltage distribution networks is

Highly Urban/Urban Underground network	
Interconnector	**Cross-sections (mm^2)**
Main trunk Feeder	$4 \times 300(Al)$; $4 \times 185(Al)$; $4 \times 120(Al)$
Lateral spurs	$4 \times 185(Al)$; $4 \times 120(Al)$; $4 \times 95(Al)$
Service connection	$4 \times 120(Al)$; $4 \times 95(Al)$; $4 \times 70(Al)$; $4 \times 35(Al)$; $2 \times 35(Cu)$
Suburban/Rural Aerial network	
Interconnector	**Cross-sections (mm^2)**
Main trunk Feeder	$4 \times 120(Al)$; $4 \times 95(Al)$; $4 \times 70(Al)$
Lateral spurs	$4 \times 95(Al)$; $4 \times 70(Al)$; $4 \times 50(Al)$
Service connection	$4 \times 70(Al)$; $4 \times 50(Al)$; $4 \times 35(Al)$; $2 \times 35(Cu)$; $2 \times 25(Cu)$

Table 6.1: *Typical UK low-voltage line cross-sections for urban residential load sector [68], [96], [97], [98], [95].*

the MV/LV substation, which typically comprises a single transformer with a rating of a few hundred kVA up to $1MVA$, [69]. Table D.1 in Appendix D provides full documentation of

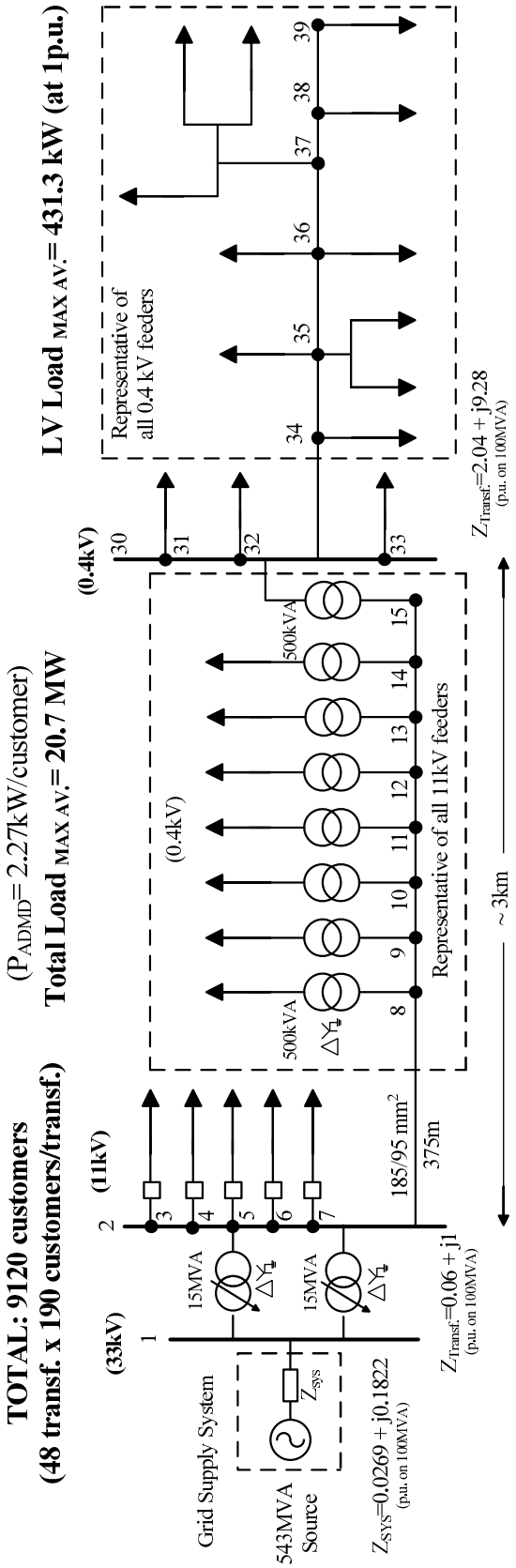

Figure 6.5: *Modelled MV/LV distribution network configuration.*

typical $11/0.4kV$ transformers operating in the UK ([99], [100], [69], [101]), together with a direct correlation to the load sub-sector where each of them is typically used. The transformer primary is usually connected in delta in order to isolate the earth fault on the secondary side from primary side, while the secondary is normally connected in star with neutral earthed. This connection enables the supply of single-phase loads operating at $230V_{nominal}$ (loads connected between phase and neutral). The low-voltage network model provided in Figure 6.5 corresponds to the urban residential sub-sector (high loading), which also presents a radial underground arrangement. The typical $11/0.4kV$ transformer used in the UK for this type of networks has a power rating of $500kVA$ (Table D.1), supplying a total of 190 single-phase customers with a peak average (after load diversity) demand of $2.27kW$ per costumer. In this model, the total average load is measured at $\sim 431kW$ during maximum and $\sim 71kW$ during minimum loading conditions, corresponding to the 190 single-phase customers. The urban low-voltage network is on average $1,588m$ long, with the following underground cables in use: $300mm^2$ ($122m$), $185mm^2$ ($41m$), $120mm^2$ ($62m$), $95mm^2$ ($315m$) and $70mm^2$ ($1,048m$). Detailed data are provided in Table D.2 in Appendix D.

6.3 Estimation of PV and Wind Microgeneration Power Outputs

Wind and solar resources identified in Chapter 2 are used as an input to the generic models described in Chapter 5. The analysis of the resources for Edinburgh city uses the time-series profiles as a representative of the available wind and solar resources. Chapter 5 described how developed generic models for both technologies (i.e. PV and wind), can be generalised into a single equation, which using the time-series profiles as input provides timer-series power outputs. The installed capacity for wind and solar is set for the network topology in Figure 6.5. There are 9120 (190 customers per transformer) customers connected to the network with a peak average demand of $2.27kW$ per customer. Three scenarios or penetration levels are calculated: 10%, 25% and 50% to assess the load demand reduction.

6.3.1 Per-Unit Power Output of Aggregate Wind Microgeneration Systems

Using the temporal assessment from Chapter 2, Figure 6.6 to Figure 6.9 show the capacity factor for wind microgeneration power output for the 4 different sub-sectors based on inputs from Figure 2.36 to Figure 2.39, which are used with the load profiles. Focused in the urban

profiles (ED2) in accordance with the urban network model.

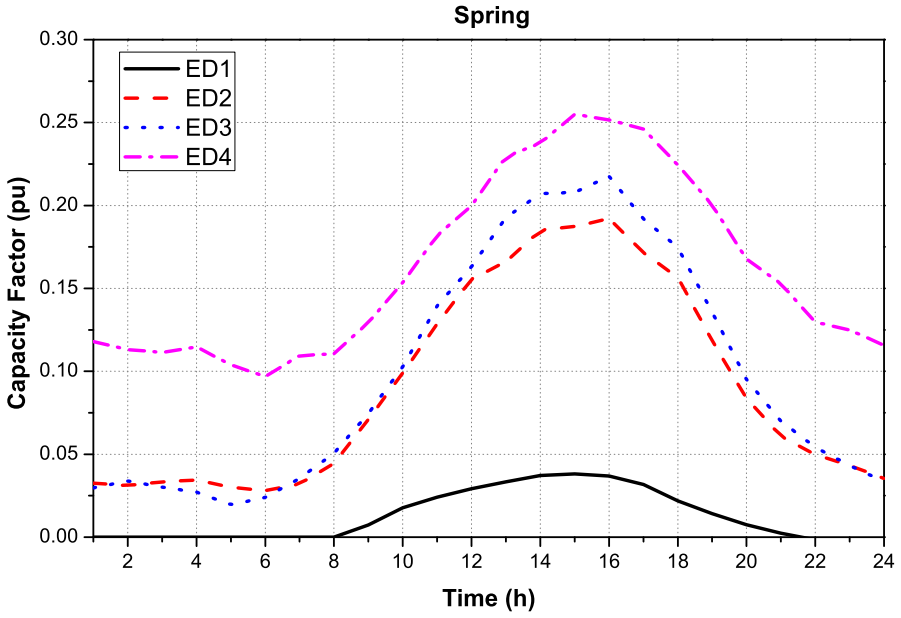

Figure 6.6: *Capacity factor of aggregated wind microgeneration of 4 defined sub-sectors for Spring.*

6.3.2 Per-Unit Power Outputof Aggregate PV Microgeneration Systems

Figure 6.10 show the assessed average PV microgeneration power outputs in pu based on inputs from Figure 2.49 to Figure 2.52,which are used with the load profiles.

6.4 Reduction in Load Demands by Aggregate Microgeneration

From the previously shown/calculated UK load profiles shown in Figure 6.3 it can be appreciated that the load demand changes depending on the time of the year, where Spring/Autumn are found to be in the middle of the maximum and maximum demand, Winter corresponding the maximum demand and Summer to the minimum demand. Using the outputs from the microgeneration technologies from the previous section, the reduction of the load demand can be calculated as shown in Figure 6.11, where the maximum Winter demand is reduced by wind microgeneration outputs. The installed capacity of wind microgeneration capacity is 10%, 25% and 50% of the peak demand at maximum loading conditions for every considered case. The total output of installed power of microgeneration is determined by the rated power of the

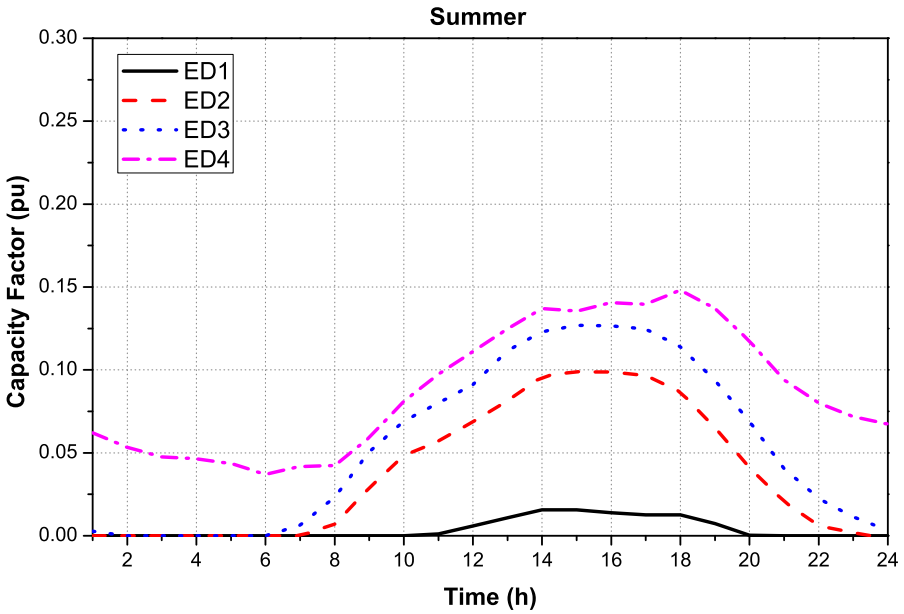

Figure 6.7: *Capacity factor of aggregated wind microgeneration of 4 defined sub-sectors for Summer.*

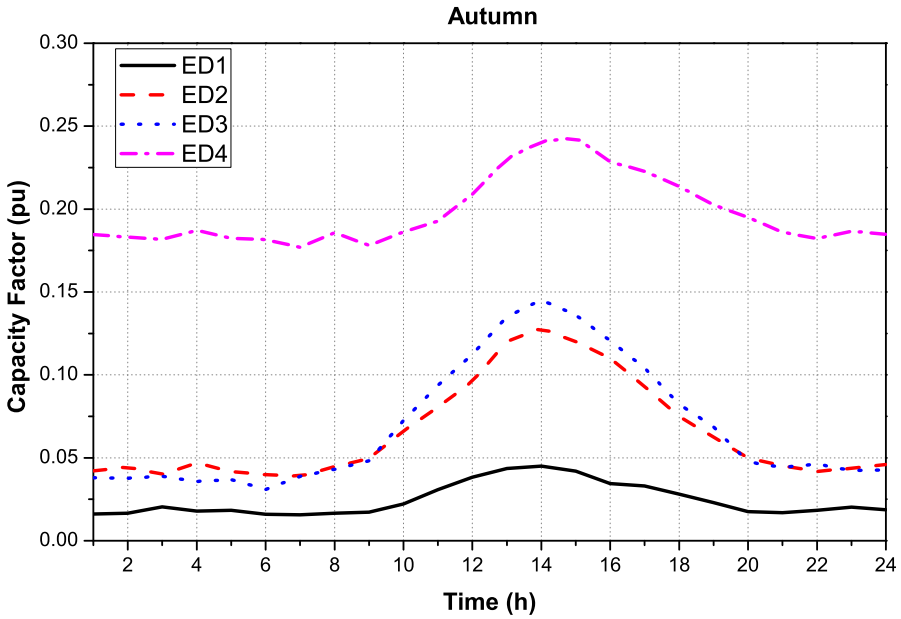

Figure 6.8: *Capacity factor of aggregated wind microgeneration of 4 defined sub-sectors for Autumn.*

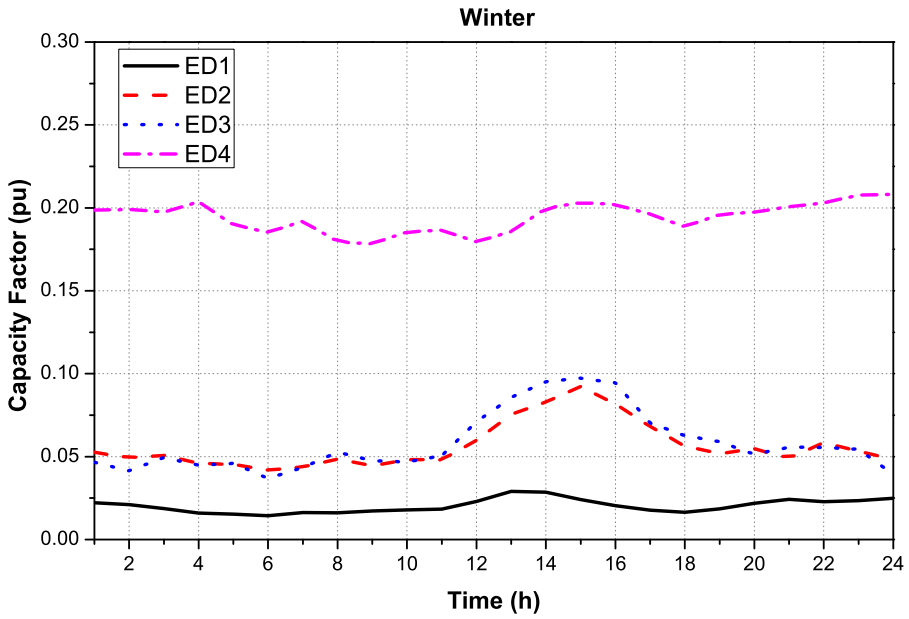

Figure 6.9: *Capacity factor of aggregated wind microgeneration of 4 defined sub-sectors for Winter.*

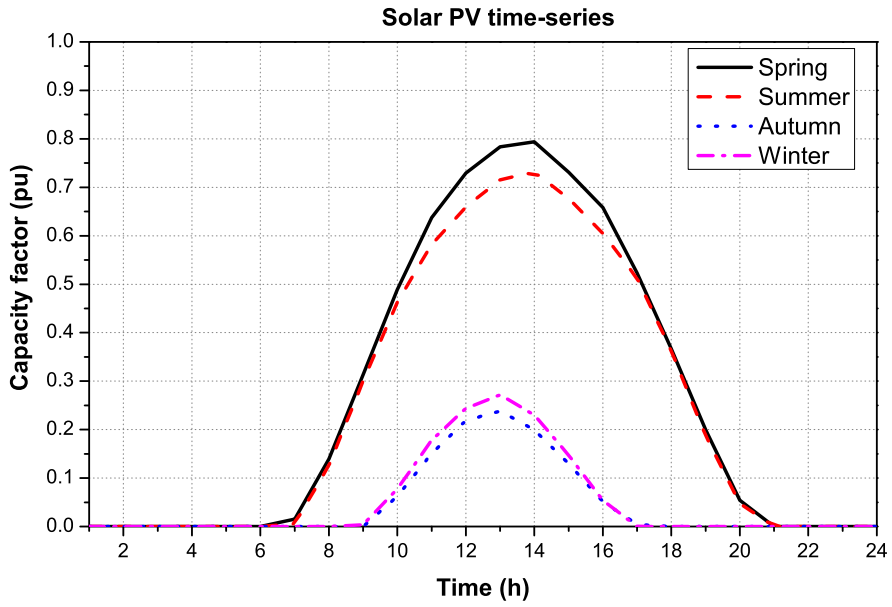

Figure 6.10: *Estimated average power outputs of aggregated PV microgeneration in pu for each season.*

generator as $1pu$. These penetration level are considered to be realistic values as the Microgeneration Strategy suggests that up to 40% of the UK's electricity demand could be met through microgeneration by 2050 and decreasing the carbon emission per household up to 15% per annum [1].

6.4.1 Demand Reduction: Wind-based Microgeneration

Figure 6.11 and Figure 6.12 show that at any hour of the day for maximum Winter loading conditions there is a reduction throughout the day in the load demand with all penetration levels. The 50% penetration level shows that at some point of the day it might be a reduction of around 95% of the load demand. This scenario even though is unrealistic at the moment provides details on how the micro and small-scale could have a large contribution to the energy demand. Minimum Summer loading conditions are more interesting due to the pronounced diurnal variation of the wind profile, even though during the night there is no wind contribution, the extreme case of 50% penetration, shows that at the maximum diurnal peak of the day (between 13:00hrs - 16:00hrs) this penetration would start exporting power energy to the grid. These reverse power flows will have an impact mostly in protection systems, these impacts however, are not in the scope of this thesis but it would be useful to consider the phenomenon in more detail. Generally, the reduction in maximum Winter energy demand is greater due to the increased wind speeds but the greater impact on the network is present at minimum Summer loading condition due to a possible reverse power flow for the high penetration case. The probability of occurrence of wind speeds can be expressed using the Weibull distribution. Based on the Weibull distribution analysis found in Chapter 2 in Figure 2.20 (for maximum Winter loading conditions at the specified location of urban residential load), the probabilities of wind speeds higher than $12^m/_s$ (resulting in maximum wind turbine power output) and lower than $3^m/_s$ (resulting in zero wind turbine power output) are approximately 2.35% and 16%, respectively. For the minimum Summer loading condition, the probability of maximum and zero wind turbine outputs for the same $12^m/_s$ and $3^m/_s$ input wind speeds are less than 1% and around 21%, respectively. These results confirm, that even though the winter has a higher capacity factor due to higher wind speeds, the offset of energy is higher in the Summer thanks to the combination of higher probability of higher wind speeds (pronounced diurnal variation) and the lower power demand during the Summer months. Also, from Figure 6.12 shows a roughly a 10 hour period of zero output from wind generation, which according to the Weibull distribution for the site is far less than it actually is, showing the limitations (explained in Chapter 2) of the diurnal variation profiles.

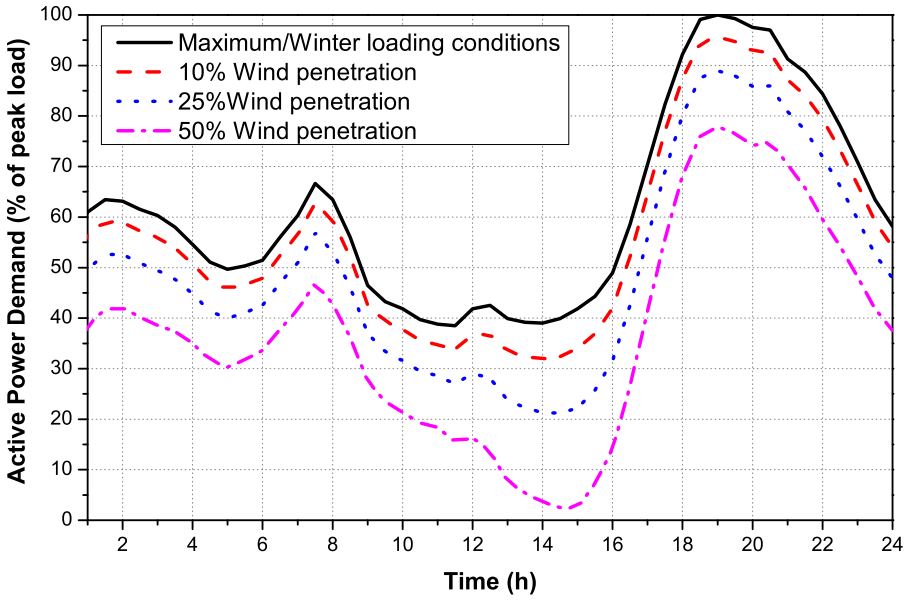

Figure 6.11: *Reduction of the maximum/Winter load demand due to wind microgeneration.*

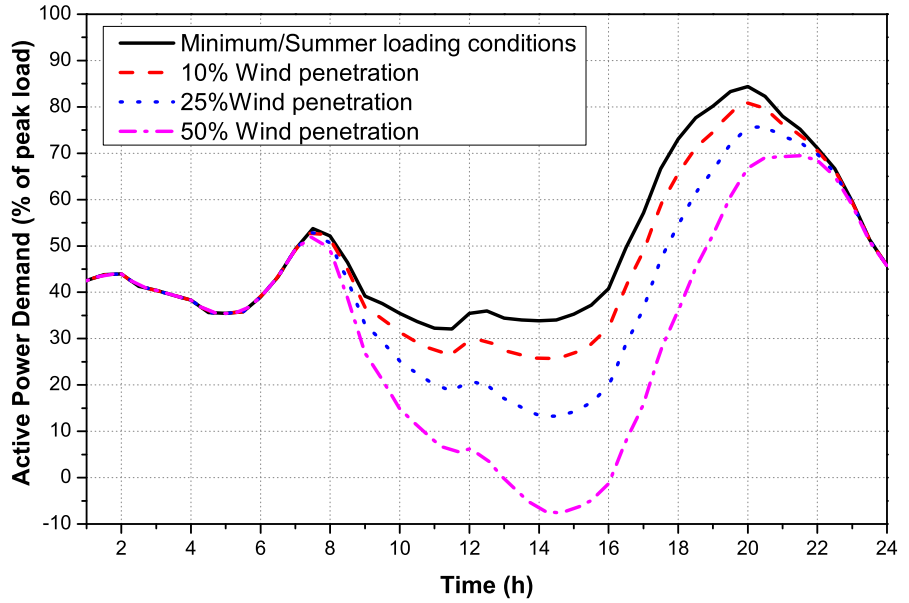

Figure 6.12: *Reduction of the minimum/Summer load demand due to wind microgeneration.*

6.4.2 Demand Reduction: PV Microgeneration

While wind microgeneration may produce power output during the whole day, solar irradiance is only available during daylight hours. This period of time also exhibits seasonal variation. Figure 6.13 and Figure 6.14 show that at any hour of the day for both maximum Winter and minimum Summer loading conditions the potential maximum contribution of small-scale PV can be significant (up to 15% of the current demand may be offset by small-scale PV with a penetration of 10% of the peak load during the minimum Summer loading conditions). The reduction for minimum load demand is higher throughout the day because for the Summer period, the days are longer and with longer solar irradiance levels than for the Winter. Therefore, the load reduction expected from PV will be greater during the summer. Similar as the wind during minimum loading conditions, there is a potential for exporting power to the grid.

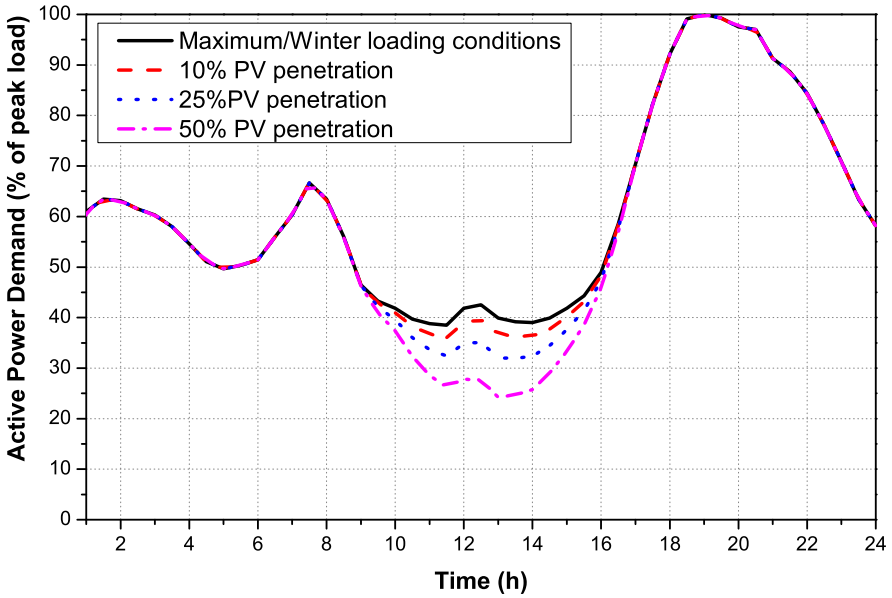

Figure 6.13: *Reduction of the maximum/Winter load demand due to PV microgeneration.*

6.4.3 Demand Reduction: Combined Wind and PV Microgeneration

The effect of the combined PV and wind microgeneration is also presented in this section. These results assume equal contribution/installed capacity of micro and small-scale wind and PV generation systems (i.e. 50% Wind + 50% PV), adding up to the 10%, 25% and 50% penetration levels as before. Figure 6.15 and Figure 6.16 show the results when both technologies

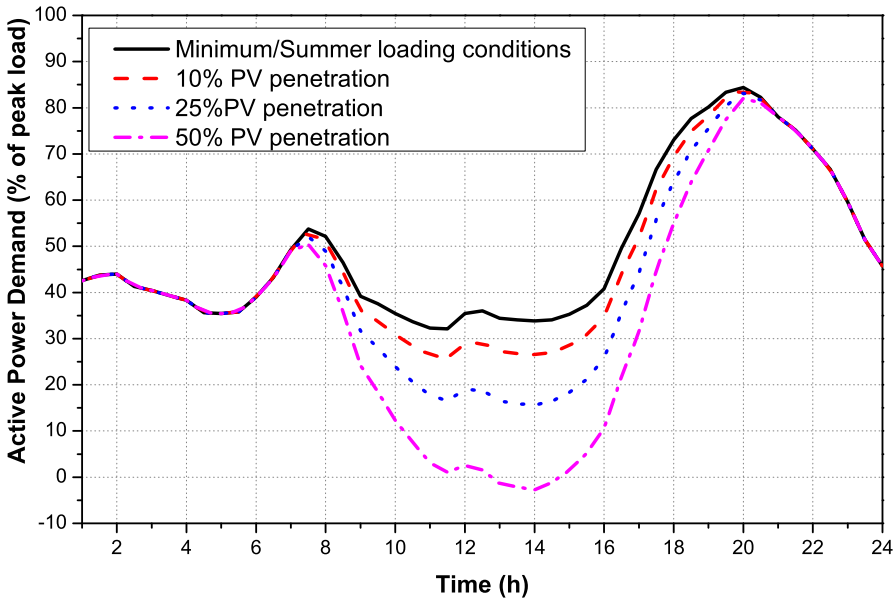

Figure 6.14: *Reduction of the minimum/Summer load demand due to PV microgeneration.*

contribute to the reduction of the load demand.

The maximum/Winter load profile presents a consistent reduction throughout the 24 hour period. There is a considerable reduction up to 70% for the 50% penetration scenario. However for the minimum/Summer loading conditions as similarly presented in previous sections, the reduction is higher due to a lower load demand and higher contribution of the solar PV power output. The 50% penetration scenario exhibits a negative demand, which as described earlier would cause reverse power flows.

6.5 Impact of Microgeneration in Future Load Profile Scenarios

The previous section presented the use of the profile power outputs obtained using the diurnal variation assessment profiles from Chapter 2 and the generic models from Chapter 5. However, from the point of view of power systems, it is useful to obtain a range where microgeneration could operate in future scenarios. The load reduction presented earlier is useful to quantify the real power output using actual load profiles and the performance of wind and solar using measurements of many years. This section now presents a range where microgeneration can operate alongside with future load profiles. The results of this section were published in [18] and [19] with the purpose of giving a future view of the distribution networks.

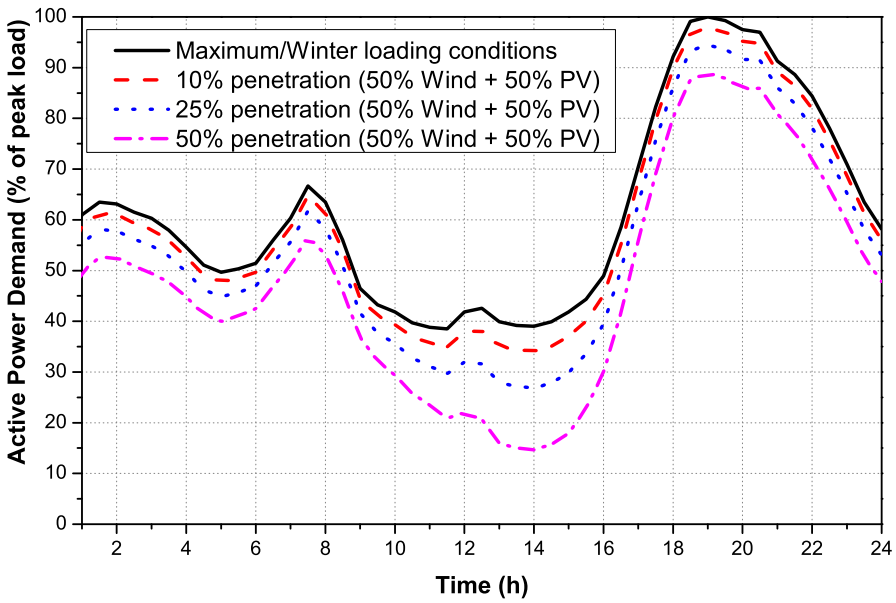

Figure 6.15: *Reduction of the maximum/Winter load demand due to combined wind and PV microgeneration: 50% contribution of each technology.*

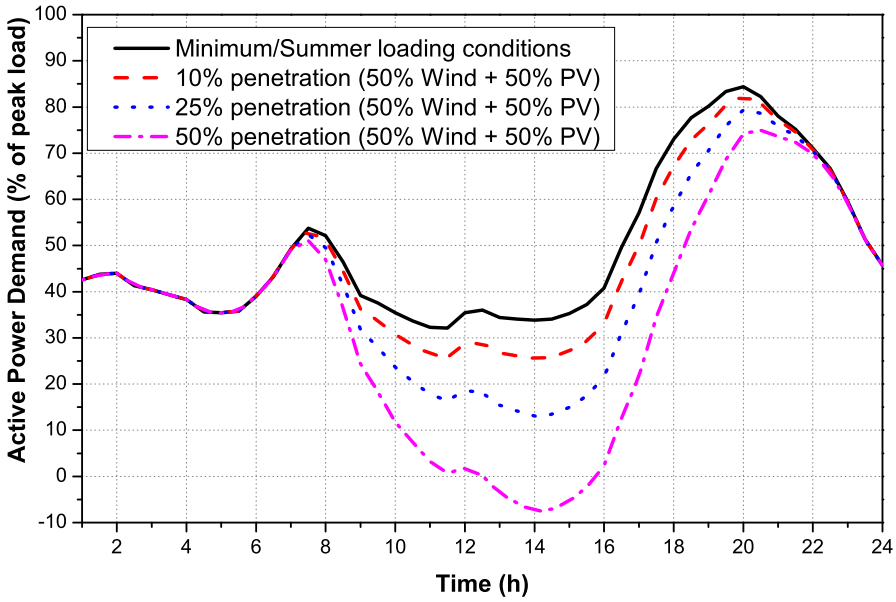

Figure 6.16: *Reduction of the minimum/Summer load demand due to combined wind and PV microgeneration: 50% contribution of each technology.*

6.5.1 Microgeneration Profiles

In order to give a range for the impact of microgeneration, the range assessment profiles from Chapter 2 are used. It was discussed before the usefulness of having a maximum value to delimit the power/energy production of microgeneration. Using profiles shown in Figure 2.32 to Figure 2.35 for wind and Figure 2.49 to Figure 2.52 for solar irradiance and the use of the generic models from Chapter 5 a new set of profiles is obtained and used in this section. Figure 6.17 to Figure 6.24 show the capacity factor profiles for microgeneration technologies.

This section assumes combined use of PV and wind microgeneration. Using the profiles

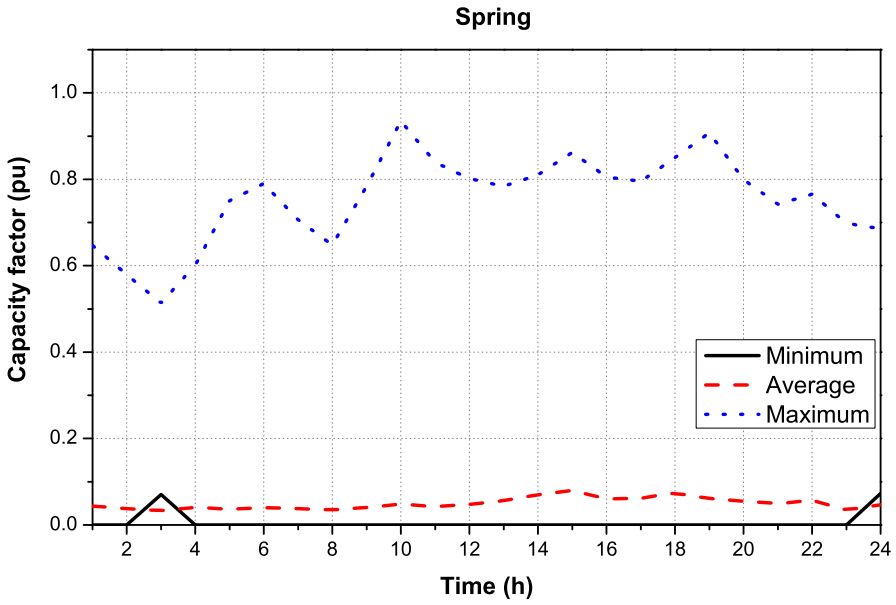

Figure 6.17: *Estimated minimum, maximum and average power outputs of aggregated wind microgeneration in pu for Spring.*

presented before and a combined 50% PV and 50% wind installed capacity, Figure 6.25 to Figure 6.28 show the new profiles.

6.5.2 Load Profile

Collin et al. [18] presented two residential load mix scenarios. The "present" scenario was based on the current (2008) residential load mix [93], which is shown in Figure 6.4, while the "near future" scenario was based on a wholesale substitution of general incandescent lamps (GILs) with compact fluorescent lamps (CFLs) influencing a reduction factor of 4 in the active power demand for lighting [102]. As the current penetration of microgeneration technologies is

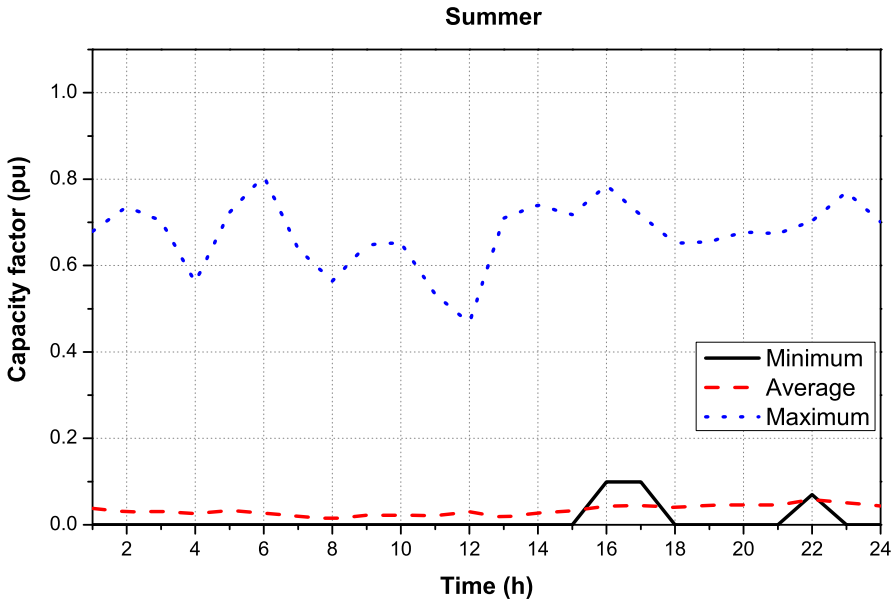

Figure 6.18: *Estimated minimum, maximum and average power outputs of aggregated wind microgeneration in pu for Summer.*

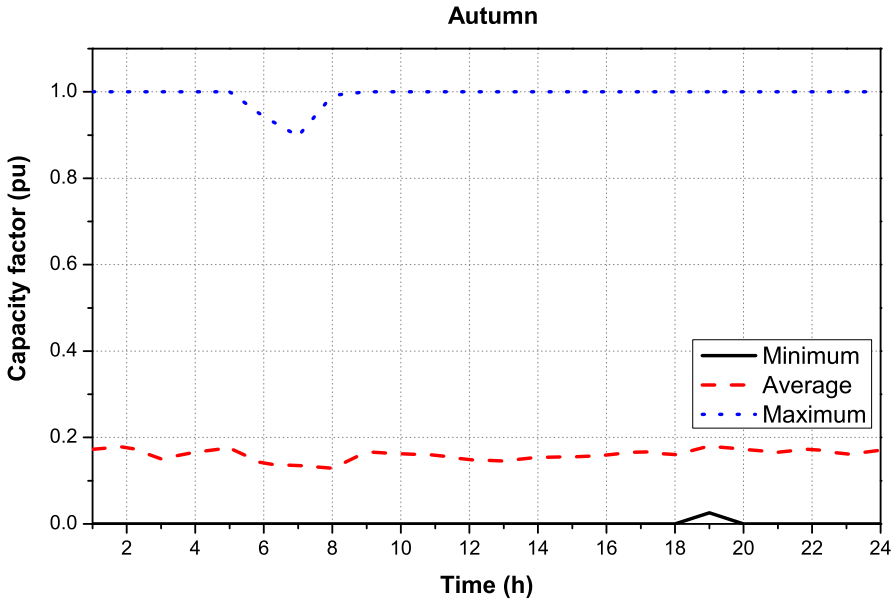

Figure 6.19: *Estimated minimum, maximum and average power outputs of aggregated wind microgeneration in pu for Autumn.*

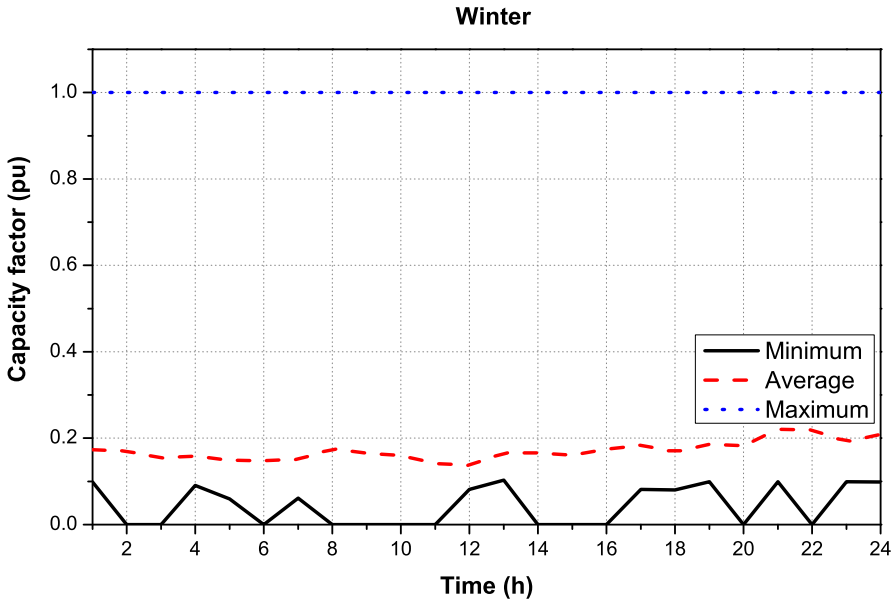

Figure 6.20: *Estimated minimum, maximum and average power outputs of aggregated wind microgeneration in pu for Winter.*

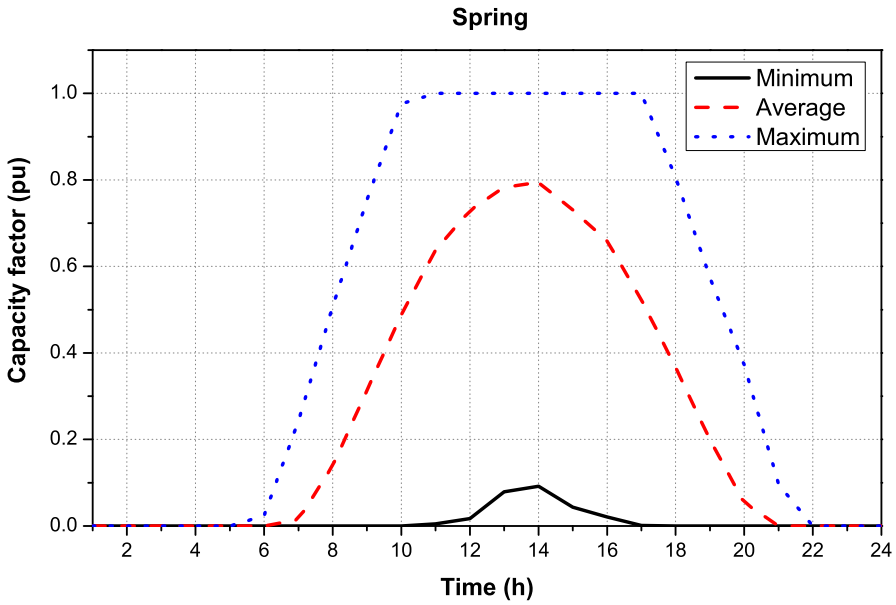

Figure 6.21: *Estimated minimum, maximum and average power outputs of aggregated PV microgeneration in pu for Spring.*

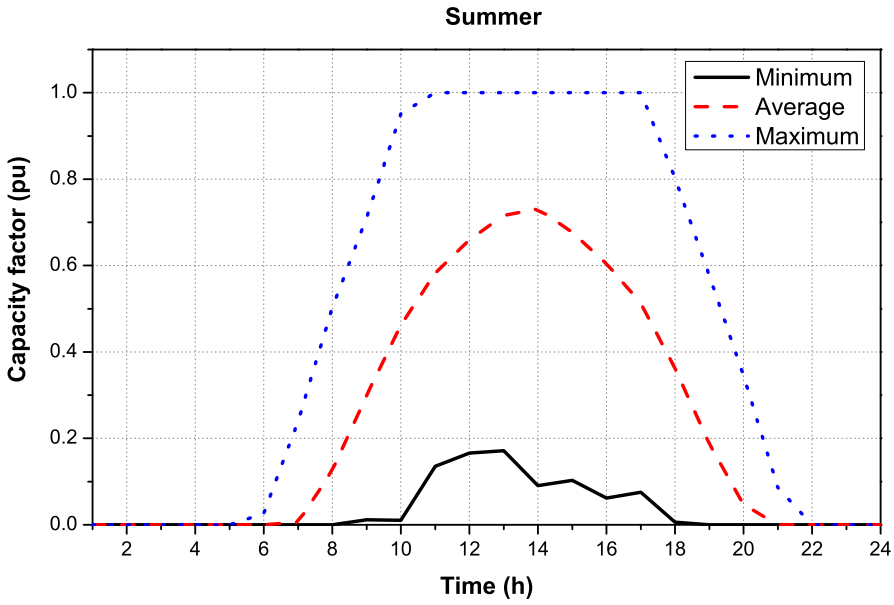

Figure 6.22: *Estimated minimum, maximum and average power outputs of aggregated PV microgeneration in pu for Summer.*

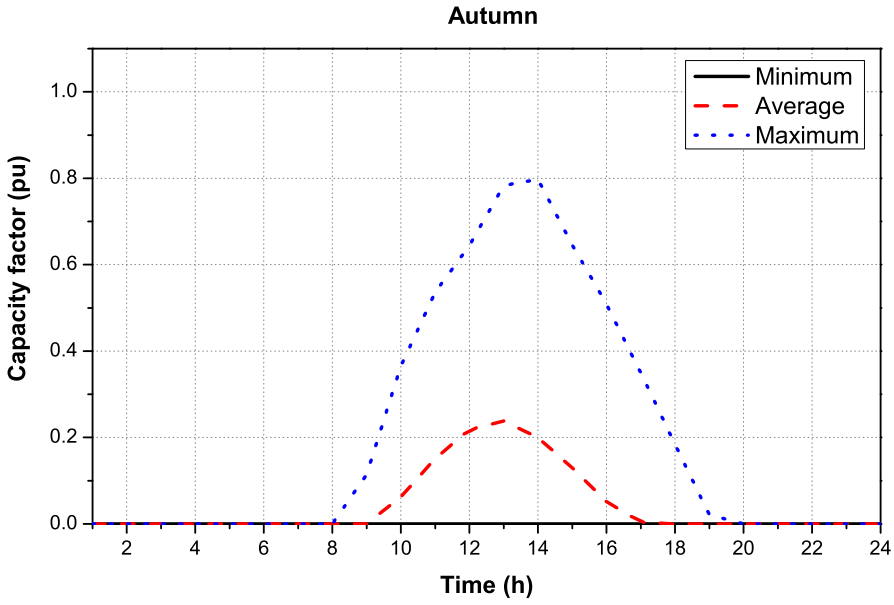

Figure 6.23: *Estimated minimum, maximum and average power outputs of aggregated PV microgeneration in pu for Autumn.*

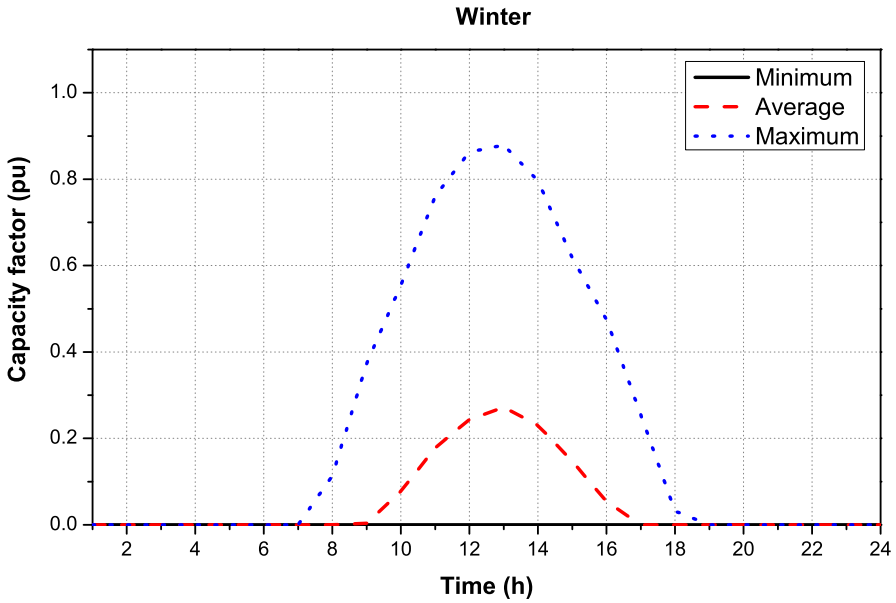

Figure 6.24: *Estimated minimum, maximum and average power outputs of aggregated PV microgeneration in pu for Winter.*

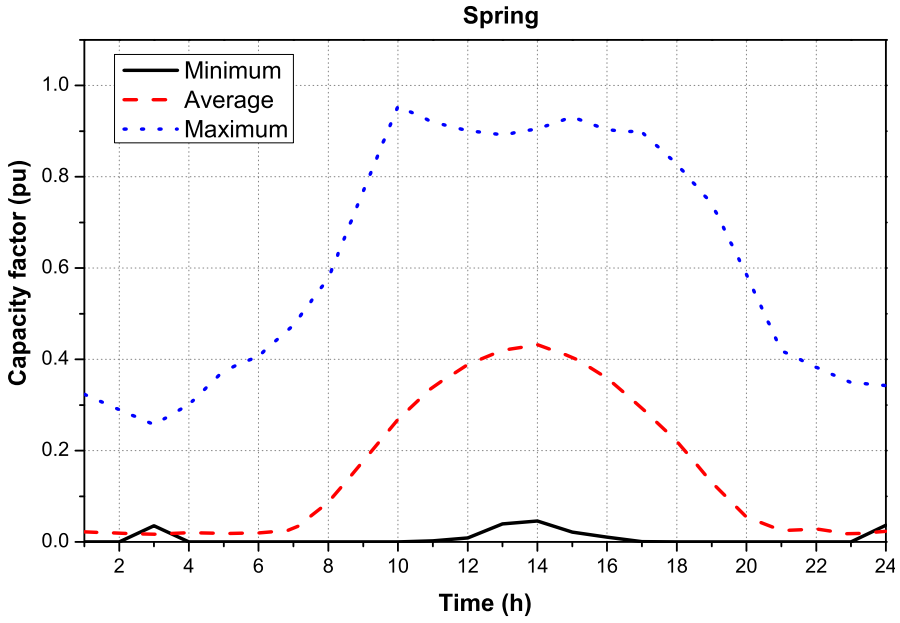

Figure 6.25: *Combined wind and PV microgeneration power outputs in pu for Spring.*

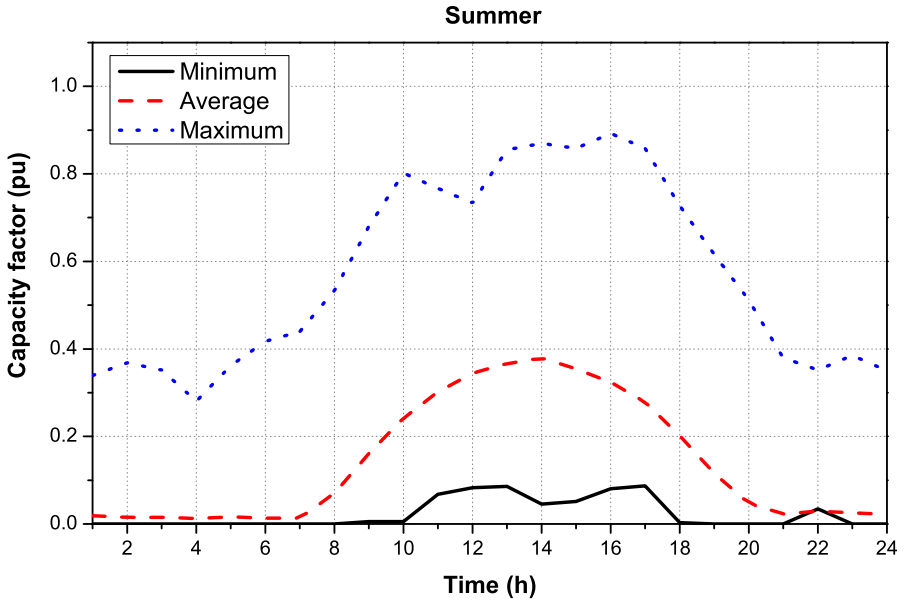

Figure 6.26: *Combined wind and PV microgeneration power outputs in pu for Summer.*

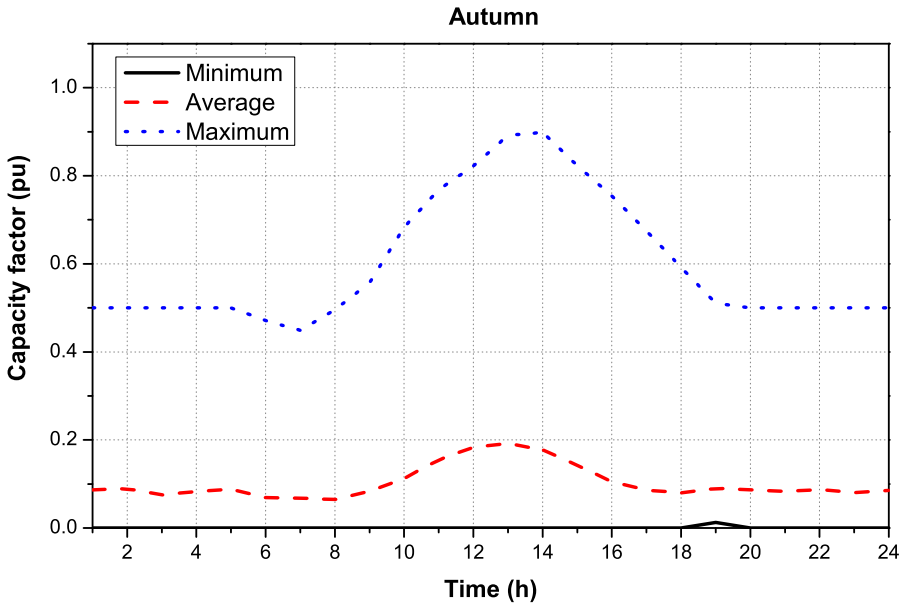

Figure 6.27: *Combined wind and PV microgeneration power outputs in pu for Autumn.*

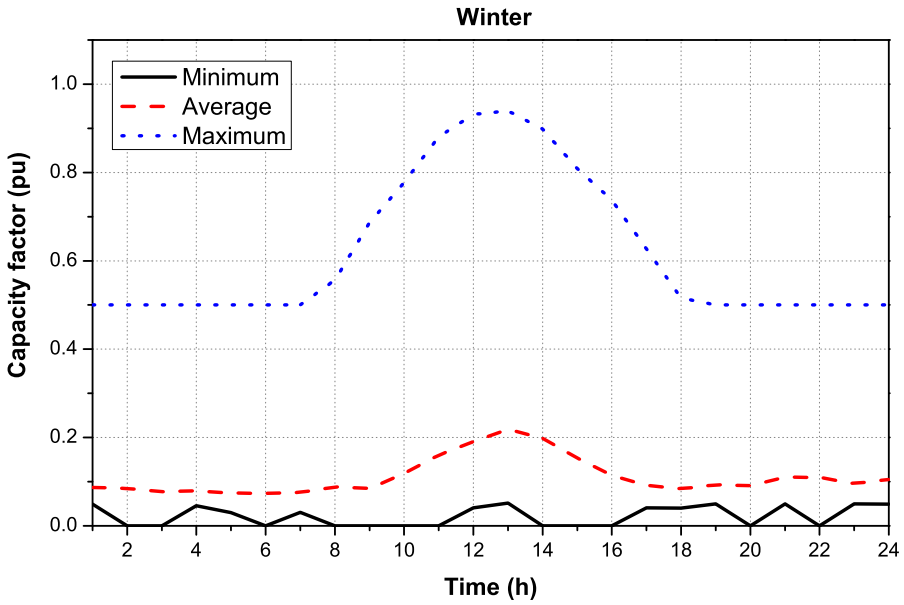

Figure 6.28: *Combined wind and PV microgeneration power outputs in pu for Winter.*

quite low, the "near future" scenario is used as the base case for analysing the effects of microgeneration (assuming that the penetration levels of microgeneration will increase significantly in the future). This allows for a more realistic assessment of system performance.

6.5.3 Impact on Power Flows

Only one scenario is presented in this section, a penetration level of 10% of the peak residential demand is assumed. Although microgeneration can be operated with energy storage systems to increase its benefits, this is not expected to be widely implemented. Therefore PV and wind microgeneration is connected in the scenario where the microgeneration is not controlled. A comparison of the changes in the active power flows after introducing microgeneration is shown in Figure 6.29. Figure 6.29 presents a similar analysis as that in Figure 6.11 to Figure 6.14 but with a different load profile, including the combined PV/wind in the analysis. The obvious advantage of connecting microgeneration is the reduction in active power demand. The microgeneration systems are connected to the grid via an inverter interface, allowing control of both generated active and reactive powers, it is assumed that the microgeneration systems are operating with unity power factor [7] (this is also stipulated in Engineering Recommendation G83/1 [57]). The addition of microgeneration of 10% penetration level would reduce peak active and reactive power demands by 1% and 2%, when they produce average power output. If

microgeneration produces maximum outputs, the reduction will reach values of about 6% and 8%, respectively. During the evening peak period (18:00-22:00) aggregate active and reactive power demands at the $33kV$ bus in Figure 6.5 are reduced by 1% and 1.5% in the average case and 7.7% and 11.6% in the maximum case.

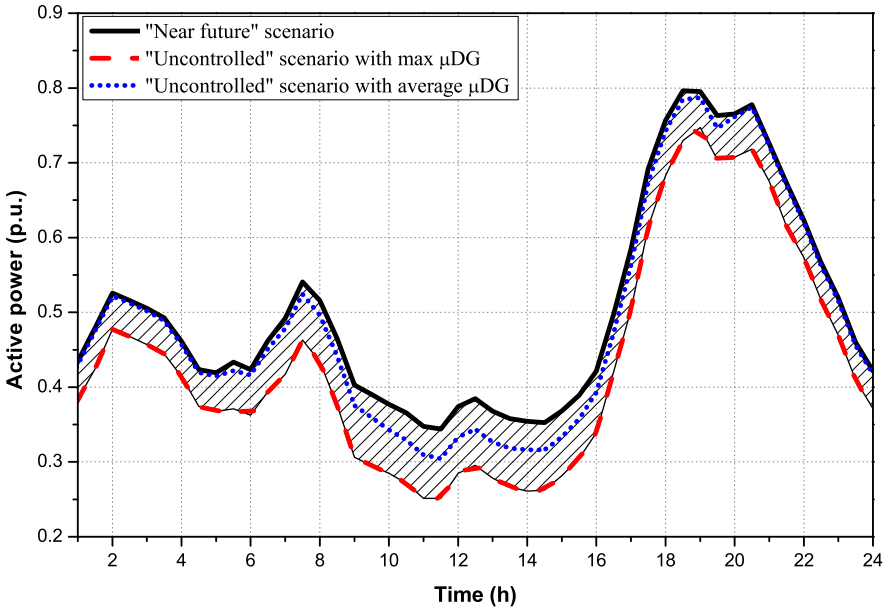

Figure 6.29: *Changes in active power flows in near future scenario with combined contribution of PV-wind microgeneration.*

6.5.4 Impact on Voltage Profiles

The results in Figure 6.30 show two different buses, as can be appreciated in Figure 6.5 bus 30 is the point of connection of the 500kVA transformer and bus 39 is the last point of connection in the network, showing the lowest voltage value in the network as this is the last customer served by the network. As expected and reported by Thomson [7], the connection of micro-generation operating with unity power factor will raise the voltage and actually improve the voltage regulation of the low-voltage network for most of the time. This voltage rise is often a problem when connecting large distributed generation units, as voltage may increase outside the allowed range during the minimum loading conditions. However, the voltage increase for the considered level of penetration of microgeneration (10%) is relatively small and it is well within the acceptable range for the analysed network.

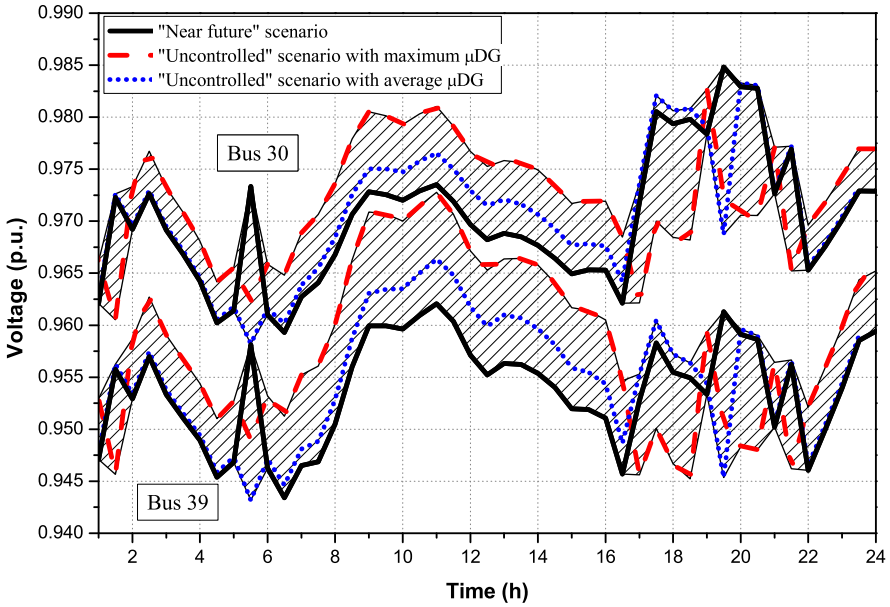

Figure 6.30: *Voltage profiles for the near future scenario.*

6.5.5 Impact on Harmonic Distortion

The power flow was based on a aggregate inverter model with the typical specification based on usual manufacturers [55], [56]. However, this analysis is limited because of the validity of the models and it is a steady-state analysis, as previously mentioned this section explores ranges and analyses a future scenario. The aggregation of many micro and small-scale inverters is far from simple and further work should be done in the area with models validated. Nevertheless, this section presents the impact of the inverter-based wind and PV connected to the distribution system using the single time-series model developed in Chapter 3 and Chapter 4. It is important to note that these are not definitive results and much more research needs to be done, but this section intends to just demonstrate how developed aggregate microgeneration models can be used in power system studies.

When connected to an ideally sinusoidal supply grid voltage, the inverter interface of micro-generation aims to produce a sinusoidal voltage waveform. There will be some high-frequency components (typically greater than 20 kHz) due to the switching nature of inverter operation, but the overall voltage total harmonic distortion (THD) will be very low ($\leq 0.5\%$). However, when the inverter is connected to a low-voltage supply with a distorted voltage, the THD value of the inverter output voltage will significantly increase. The detailed full model developed in Chapter 3 was connected to a distorted supply voltage waveform with a THD of about 2.4%,

which was measured at an Edinburgh urban location. In this case, the inverter aims to produce voltage waveforms with increased low-frequency harmonics at the same frequencies as the network voltage (notably 3^{rd}, 5^{th} and 7^{th}, see Figure 6.32), with additional emission of high frequency harmonics. This will result in an increase of the voltage THD value in inverter's output voltage to 4.93% (Figure 6.32). This value is just below the allowed low-voltage

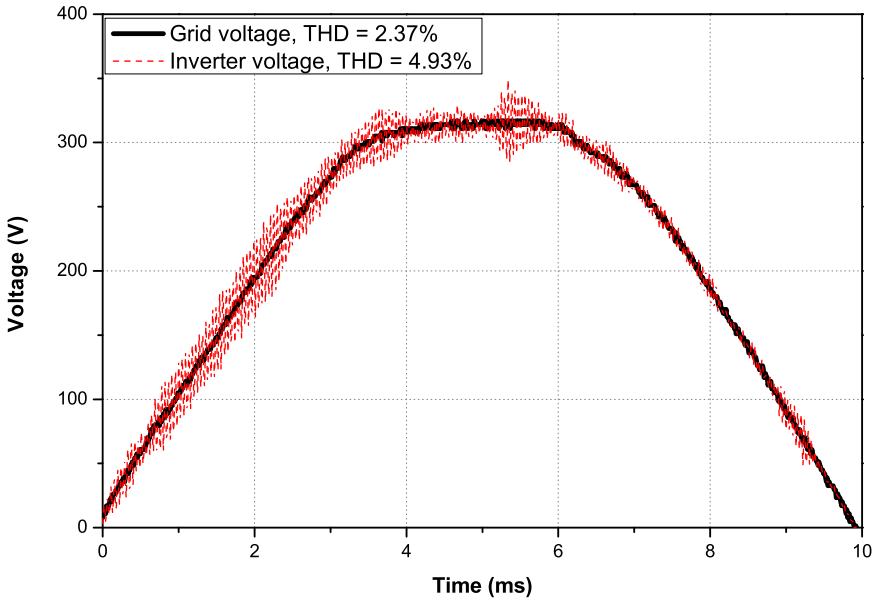

Figure 6.31: *Influence of distorted grid voltage on the inverter output voltage waveform and THD.*

network limit for voltage THD of 5% (stipulated in [103]). When a large number of microgeneration units are connected to the same low-voltage network, the combined effect of microgeneration and load harmonics will increase THD values, which may propagate through the system. Figure 6.33 shows that both the emission and propagation of harmonics will increase at a higher-voltage bus when microgeneration technologies are connected to the low-voltage network. Slight variations in the current THD levels are observed between the maximum and average microgeneration power output cases. This occurs during the periods of low microgeneration output, as the inverter and associated filter operating below their rated power produce higher level of harmonics.

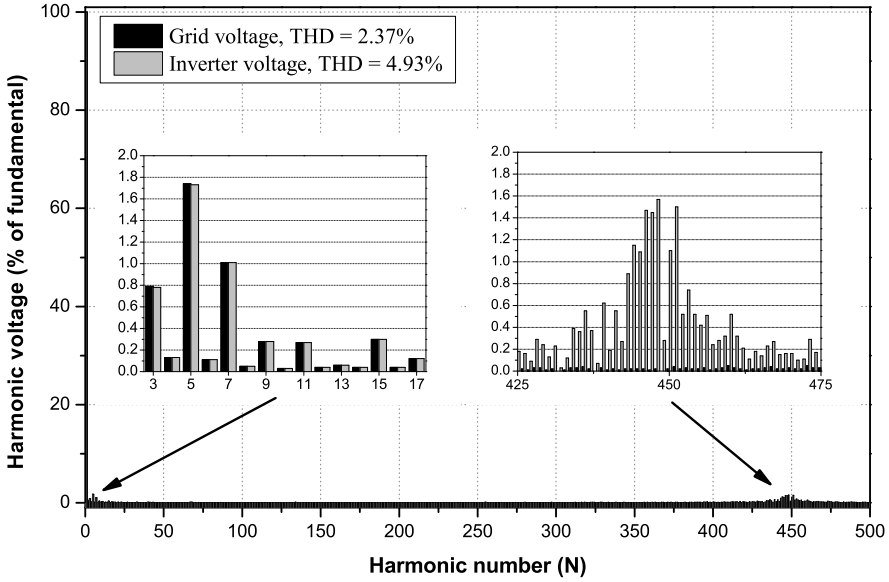

Figure 6.32: *Harmonic spectrum after fast Fourier transform applied to the inverter voltage output when connected to the network.*

6.6 Conclusions

This chapter presented the applications of the aggregate PV and wind microgeneration models developed in this thesis combined with detailed models of the distribution network and the load, developed independently at the University of Edinburgh. The analysis of the impact of a relatively low penetration of microgeneration technologies to the low-voltage network and their impact on the power flow. A special case was presented including a future scenario of load profile with voltage profiles and THD analysis. The reduction of the active power demand was expected, which then leads to an improvement in the voltage profile and reduction in the transmission system losses. The purpose of this chapter is to combine all the results obtained from the previous ones and show how the methodology for microgeneration aggregation can be used alongside with load models and distribution network models. For this purpose, the wind and PV profiles built and called time-series profiles are used as inputs to the generic models, to produce a spatial and temporal vector of power outputs produced by these microgeneration technologies. The aggregated PV-wind models can be scaled as required for different scenarios during the power system studies, as demonstrated in this chapter. The aggregation is based on Figure 6.2 where the load aggregation and microgeneration aggregation was part of the same aggregation methodology.

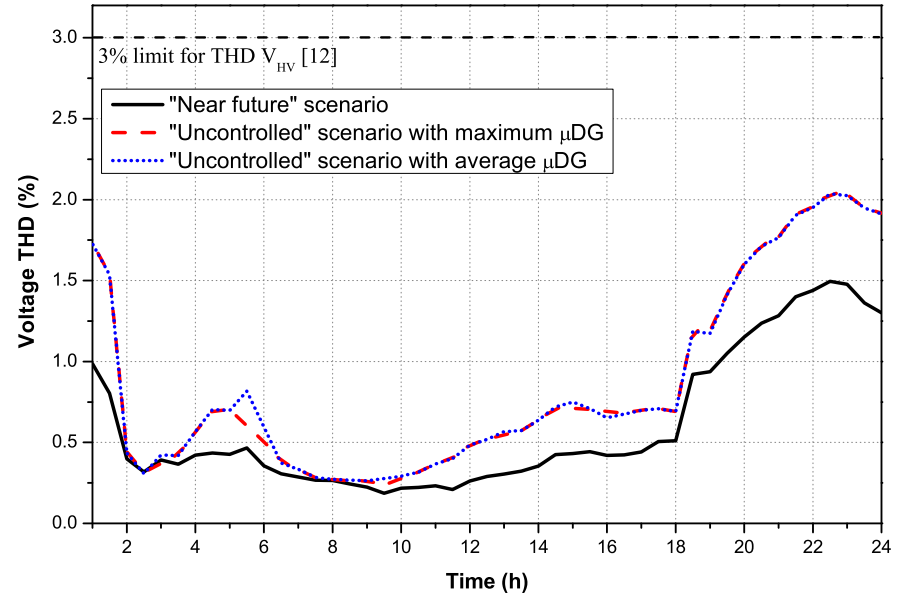

(a)

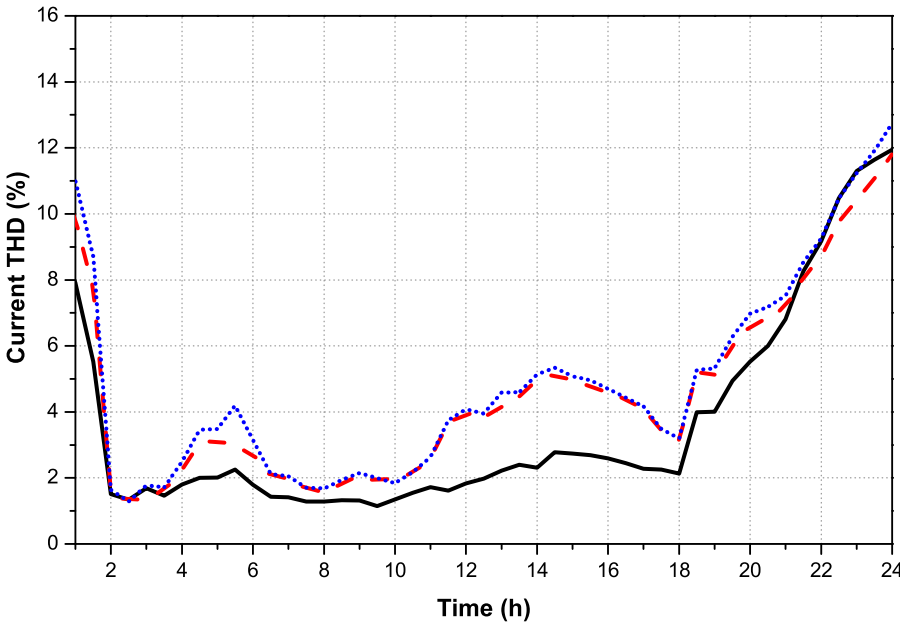

(b)

Figure 6.33: *THD at 33kV bus: a) voltage; b) current.*

Chapter 7
Conclusions and Further Work

This thesis has presented an "input to output" or "whole system" modelling of micro and small-scale wind turbines and photovoltaic systems. One of the main aims of this thesis was to estimate solar and wind resources in urban area, focusing generally on the UK, but with particular attention given to Edinburgh city, assuming that good/acceptable sites are available and uniformly distributed for the specified penetration levels across the city. The modelling of these systems was presented with a methodology for the aggregation of a large number of micro and small-scale devices connected to the distribution network. This is illustrated through a number of considered different cases and scenarios, where some interesting results for the interaction of simple and detailed PV-wind models and detailed distribution network models are obtained.

7.1 Resource Assessment

The use of the NOABL database to identify the mean wind speed for any urban site at different heights will overestimate the actual energy resources available in the UK urban areas. The importance of a correct resource assessment in urban areas was discussed in Chapter 2. There was an overestimation coming from the assumed reference wind speed of $6^{m}/_{s}$ average wind speed in urban areas, where the actual mean wind speed was found to be less than that at different altitudes in Edinburgh city which was discussed in detail. Also, the importance of the correct representation of wind energy resources using the Weibull distribution, as was reported in other site-related studies, such as the Warwick Wind Trials, demonstrated that installation of wind turbines in urban areas should be carefully considered in order not to result in underperforming systems. Similar analysis was carried out for solar irradiance, where the difference in the nature of this resource led to the conclusion that solar simulators (e.g. PVGIS) cannot be used instead of measurements and unlike wind speed, the recording of solar irradiance is not as sensitive to locational/spatial changes on a city like Edinburgh. The measurements obtained from the University of Edinburgh were compared to the adjusted European Commission simulator and proved to be different and inadequate for Edinburgh. This is important, because

even though information on installed PV systems is available, site-specific measurements of solar irradiance are not typically done or widely available for most of the sites, even as raw data for analysis. It is generally concluded that an understanding of the renewable resources in urban areas is crucial for the installation of microgeneration systems, in order to correctly acknowledge the potential of a site from the cost-benefit point of view.

7.2 Modelling of PV/Wind Single-units

The PV and wind microgeneration technologies analysed in this thesis are both inverter-based. This was an advantage from the modelling point of view, since the parameters of the control can be easily changed to model either technology. These models provided interesting results as to what the output and performance would be in typical PV-wind installations. The calculated efficiency of these systems, particularly, microwind generation systems, were lower than the one reported by most manufacturers of wind turbines. The calculated outputs from the models included the losses of the systems, the power quality and actual output, including the quasi-dynamics of the models, from one value to another. The models showed how changing the energy input would affect the power generation output and the quality of the energy delivered to the grid.

The wind model was based on the availability of aerodynamic power curves, which helps build a component by component modelling of the system. Figure 3.6 showed the stages of the modelled system. The aerodynamic power curve was useful for these three cases to compute the C_p and use the mechanical input to the PMSG and the inverter stages.

Similarly, the PV model was based on the same inverter and the measurement from Belgium lab. These measurements, even though with a presence of shadowing of the solar irradiance measurement for the first half of the day, could be used for the second half to validate the models.

7.3 Microgeneration Aggregation Methodology

Chapter 5 presented the aggregation methodology required to correctly represent large numbers of micro and small-scale generation systems connected to the grid. This methodology is based on the analysis of data available from a market survey of the power curves/efficiency curves for the PV/wind systems currently available in the market. This thesis used the market survey and

information of the actual manufacturers to create a generic model to represent a considerable number ($> 95\%$) of currently available PV and wind microgeneration systems. This methodology is novel as it presents a general approach for analysing and quantifying the impact of large numbers of unknown size/efficiency systems on MV/LV networks. Using the same aggregation methodology, all the components were aggregated and identified using simple mathematical representations in order to aggregate them correctly. Inverters were also aggregated and represented by simple exponential efficiency relations, based on manufacturers specifications. The purpose of this simplification was to account for all the losses in the system, from the input energy resource to the grid interface, i.e. to present a realistic output of these systems.

7.4 Network Connection

Chapter 6 presented the impact of the aggregate PV and wind microgeneration connected with component-based load models to a detailed model of the distribution network. Even though this is undergoing work at the University of Edinburgh, some interesting results were produced and published. The penetration level assumed for the analysis of microgeneration was 10% (based on the UK government's potential forecast), 25% and 50% representing a moderate/low to high penetration of these systems in urban area. The considered scenarios were based on future electricity networks and could be implemented with the so called "smart grids" functionalities and customer control on the demand side. The reduction of the load demands was different for different penetration levels for Edinburgh city. These results show some of the potential of microgeneration for reducing load demand. Furthermore, the presented analysis demonstrated an improvement in voltage profile when microgeneration is connected, as well as an increase on the harmonics present in the network. This is an interesting result presenting a challenge for inverter-based technologies connected to the network, to reduce harmonic emissions and increase efficiency of future microgeneration technologies. The models used were based on the validated models from Chapter 3 and Chapter 4, which are valid for single devices not as an aggregate, requiring further work to be developed to build accurate models for the aggregation of microgeneration in the network. The main limitation was to validate an aggregate model of many systems connected to the network when this is not yet an actual scenario but a future one. An important use of the aggregate wind generic model was presented by Hayes et al. in [20]. This is part of undergoing work at the University of Edinburgh, which used the developed regional distributed generation aggregate generic and presented wind microgeneration models

for all-scale modelling of wind generation at transmission network level, demonstrating that the models developed in this thesis can be used for at least theoretical analysis of higher voltage levels.

7.5 Research Limitations

This research used the generic models to model, represent and analyse the impact of micro and small-scale generation systems connected to distribution networks. Nevertheless, some limitations are found in the resource assessment and the methodology/modelling faced some challenges and particular problems when network performance is modelled. These limitations have to be considered when using these models.

(1) The resource assessment was focused on the UK urban areas, with an hourly resolution for measured wind speeds at most sites. Different characteristics for Weibull distributions were found and a linear trend can be identified in Figure 7.1. Figure 7.1 shows the linear fits for

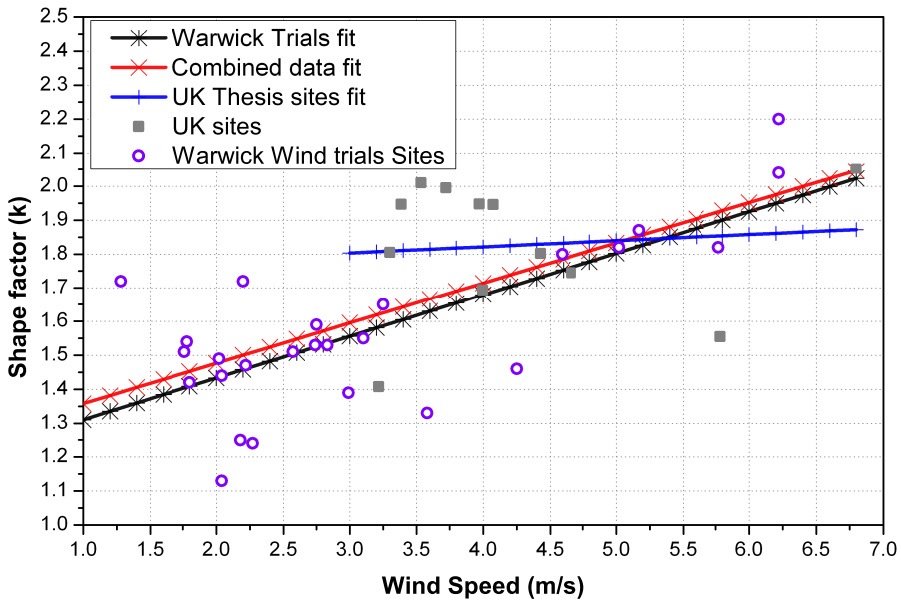

Figure 7.1: *Identified linear relationship between mean wind speed and shape factor k.*

three cases: only the data from Warwick Wind trials report, the UK sites found for this thesis and provided by the Met Office and the combination of both. It can be appreciated that for the case of the UK sites from the Met Office the linear relationship is limited by the number of sites considered. The other two relationships are very similar, but when the Met

Office sites were included it was shifted slightly up. These relationships show the trend between the mean wind speed and the shape factor.

The effect of turbulence was neglected in this research as explained in Chapter 2. This effect may decrease or increase (depending on the turbine/turbulence characteristics) the power output of wind turbines. Even though turbulence is one of the main issues of micro and small-scale wind generation in urban area, it was found in literature that it is difficult for this phenomenon to be simplified and generalised and therefore, it was not quantified by the results presented in Chapter 2.

Similarly, for solar irradiance the European Commission simulator (PVGIS) was found not to be suitable for the analysis in the case of Edinburgh. Shadowing effects were also not considered for the Edinburgh, as it was also difficult to model or to generalise this phenomenon. Nevertheless, the impact should be analysed further to understand how much input solar energy would be lost by this effect in practical applications.

(2) The modelling of single-units for PV and wind energy systems was successfully validated for the purposes of this thesis. Nevertheless, a simple control was implemented during the modelling, not considering novel efficient/robust controls for microgeneration. These controls and their effect on the microgeneration output could have an impact on the power output, increasing the efficiency and improving the overall performance of the system.

The developed steady-state models are simplified in order to efficiently model commonly found systems connected to the network and to understand their behaviour, ignoring the possible benefits of using more detailed components and control models. The outputs of the developed detailed model relies on the resolution of the input energy data. In order to generate more detailed responses and how the model would react in fast changing dynamic conditions, this would require availability of high-resolution data (for wind analysis the highest resolution available was 1-second measurement for a limited dataset and the solar high resolution data was not found for Edinburgh). However, for steady state analysis, as presented in Chapter 3, the high resolution measurements are not needed. The further data would be needed for a more detailed analysis in harmonic performance of microgeneration models.

(3) The aggregation of micro and small-scale PV and wind energy systems was based on the market survey. The main disadvantage of this approach is the fast moving market of microgeneration. The models (analytical power curve representations) of these systems will certainly vary with time and therefore the models have to be constantly updated to increase

their accuracy and keep up with the changes in the market. However, the general methodology could be easily implemented for any expected new technologies occurring in the future.

The other limitation is the capability of the models to correctly represent many systems connected to the network and the network itself. The technology mix, which determines the aggregate efficiency and output, requires a more detailed installation data to correctly represent the systems connected to the network. This data is not publicly available and is also constantly changing, which, as before, will need the constant update of the models.

(4) The connection to the grid considered a number of scenarios defined in Chapter 6. This approach is limited by the actual requirements for connection and actual operation conditions of microgeneration. These scenarios are not possible to validate by measurement, since no measurements are available for widespread microgeneration. The assumptions and results in this thesis were based on the potential of microgeneration, but the distribution network operators are not currently aware of how many systems are clustered in some sites. This information will certainly appear with the introduction of smart metering systems. Then again, the developed general methodology can be used with appropriate adjustments and modifications.

7.6 Further Work

Some aspects of the presented modelling methodology and some particularities of each modelled technology could be improved, in order to get a more accurate/detailed result or a higher resolution and dynamic responses from the modelled systems. From the resource assessment point of view, the results were quite straightforward and it seems that not much space for further improvements was left, besides including a turbulence/shadowing effects in the analysis. However, the approach selected in this research was to aggregate microgeneration into one generic model and analyse its steady-state performance when connected to the distribution network. This approach could be modified and some aspects of the presented analysis could be improved as follows:

(1) This thesis presented a generic representation of PV and wind microgeneration systems in an attempt to effectively represent different manufacturers, efficiencies and sizes of these two most widely used microgeneration technologies. This generic representation has a

wider potential to represent new and different technologies and further work could give the generic representation for micro-CHP systems, fuel-cells or other technologies that are or could be used as microgeneration systems in distribution networks. Also, further work could help to improve the actual representation of the PV/Wind generic models with simpler mathematical expressions or more detailed analysis of dynamic interactions with the grid.

(2) Chapter 3 and Chapter 4 discussed in the conclusions sections some of the modelling issues with the DC current component output. Even though it is small, it does not comply with the limits established in the G83/1. This model could be improved to eliminate this constraint and improve performance, including possibly the development of new control schemes for increasing the efficiency of the systems, with new features and new filtering designs with inverters incorporating better and more robust topologies. This is also important for further work, since other technologies that could be connected to the grid, such as fuel-cells, will also require inverters. Accordingly, this model could be the starting point for modelling other inverter-based technologies.

(3) Even though this thesis presents two chapters on PV modelling, it was found that some particularities of the actual PV systems could not be fully studied, modelled and understood. Furthermore, this technology is rapidly changing, with the introduction of cheaper and more efficient systems. Solar photovoltaics should be analysed further, with more accurate measurements to understand grid-system interactions and how other types of installation topologies could be utilised (e.g. energy storage). This will help to understand and improve the performance of these system in providing a more constant output, giving a more reliable network support, similar to "conventional generation" technologies.

References

[1] UK Department for Business Enterprise and Regulatory Reform, "Our Energy Challenge: Power from the People, Microgeneration Strategy", March 2006.

[2] UK Department for Business Enterprise and Regulatory Reform, "Microgeneration strategy progress report", June 2011.

[3] UK Department of Business and Regulatory Reform, "Low carbon buildings program", April 2006.

[4] N.J. Stannard and J.R. Bumby, "Energy yield and cost analysis of small scale wind turbines", in *Universities Power Engineering Conference, 2006. UPEC '06. Proceedings of the 41st International*, Sept. 2006, vol. 1, pp. 108 –112.

[5] N. Stannard, J.R. Bumby, P. Taylor, and L.M. Cipcigan, "AC and DC aggregation effects of small-scale wind generators", *Renewable Power Generation, IET*, vol. 1, no. 2, pp. 123 –130, June 2007.

[6] N. Stannard and J.R. Bumby, "Performance aspects of mains connected small-scale wind turbines", *Generation, Transmission Distribution, IET*, vol. 1, no. 2, pp. 348 –356, March 2007.

[7] M. Thomson and D.G. Infield, "Impact of widespread photovoltaics generation on distribution systems", *Renewable Power Generation, IET*, vol. 1, no. 1, pp. 33 –40, March 2007.

[8] The School of Geosciences, "The University of Edinburgh weather station", [Online] Available: http://www.ed.ac.uk/schools-departments/geosciences/weather-station/weather-station-data, 2011.

[9] European Commission: Joint Research Center, "PVGIS: Solar irradiation data", [Online] Available: http://re.jrc.ec.europa.eu/pvgis/, 2011.

[10] J.L. Acosta and S.Z. Djokic, "Assessment of renewable wind resources in UK urban areas", in *MELECON 2010 - 2010 15th IEEE Mediterranean Electrotechnical Conference*, April 2010, pp. 1439 –1444.

[11] J. L. Acosta, K. Combe, S. Z. Djokic, and I. Hernando-Gil, "Performance assessment of micro and small-scale wind turbines in urban areas", *IEEE Systems Journal*, vol. 6, no. 1, pp. 152–163, 2011.

[12] J. L. Acosta, A. J. Collin, B. Hayes, and S. Z. Djokic, "Micro and small-scale wind generation in urban distribution networks", in *Power Generation, Transmission, Distribution and Energy Conversion (MedPower 2010), 7th Mediterranean Conference and Exhibition on*, November 2010, pp. 1 –9.

[13] J. Matevosyan, S. Martinez-Villanueva, S. Z. Djokic, J.L. Acosta, S. Mat-Zali, F.O. Resende, and J.V. Milanovic, "Aggregated Models of Wind-based Generation and Active Distribution Network Cells for Power System Studies – Literature Overview", in *PowerTech, 2011 IEEE Trondheim*, June 2011.

[14] A. J. Collin, J. L. Acosta, B. P. Hayes, and S. Z. Djokic, "Component-based aggregate load models for combined power flow and harmonic analysis", in *Power Generation, Transmission, Distribution and Energy Conversion (MedPower 2010), 7th Mediterranean Conference and Exhibition on*, Nov. 2010, pp. 1 –10.

[15] B. P. Hayes, A. J. Collin, J. L. Acosta, and S. Z. Djokic, "Assessment of the influence of distributed generation and demand side management on transmission system performance", in *Power Generation, Transmission, Distribution and Energy Conversion (MedPower 2010), 7th Mediterranean Conference and Exhibition on*, Nov. 2010, pp. 1 –10.

[16] A.J. Collin, I. Hernando-Gil, J.L. Acosta, and S.Z. Djokic, "An 11 kV steady state residential aggregate load model. Part 1: Aggregation methodology", in *PowerTech, 2011 IEEE Trondheim*, June 2011, pp. 1 –8.

[17] A.J. Collin, J.L. Acosta, I. Hernando-Gil, and S.Z. Djokic, "An 11 kV steady state residential aggregate load model. Part 2: Microgeneration and demand-side management", in *PowerTech, 2011 IEEE Trondheim*, June 2011, pp. 1 –8.

[18] A. J. Collin, I. Hernando-Gil, J. L. Acosta, Irinel-Sorin Ilie, and S. Z. Djokic, "Realising the potential of smart grids in LV networks. Part 1: Demand-side management", in *Innovative Smart Grid Technologies (ISGT Europe), 2011 2nd IEEE PES International Conference and Exhibition on*, Dec. 2011, pp. 1 –7.

[19] A. J. Collin, I. Hernando-Gil, J. L. Acosta, Irinel-Sorin Ilie, and S. Z. Djokic, "Realising the potential of smart grids in LV networks. Part 2: Microgeneration", in *Innovative Smart Grid Technologies (ISGT Europe), 2011 2nd IEEE PES International Conference and Exhibition on*, Dec. 2011, pp. 1 –8.

[20] B P. Hayes, A. J. Collin, I. Hernando-Gil, J. L. Acosta, S. Hawkins, G. Harrison, and S. Z. Djokic, "All-scalle Modelling of Wind Generation and Responsive Demand in Power System Studies", in *IEEE Power Engineering Society General Meeting*, July 2012, pp. 1 –8.

[21] F.S. Burch and F. Ravenscroft, "Computer modelling of the UK wind energy resource: Overview report", Tech. Rep., UK Dept. for Business Enterprise and Regulatory Reform, 1992.

[22] I. Troen and E. Lundtang Petersen, "European wind atlas", Tech. Rep., 1989.

[23] UK Dept. for Business Enterprise and Regulatory Reform, "The UK Wind Resource", UK, 2001.

[24] Department of Energy and Climate Change [Online], "Wind speed database", http://www.decc.gov.uk, 2009.

[25] Department of Energy and Climate Change, "Microgeneration Installation Standard MIS 300", Tech. Rep., DECC, 2008.

[26] Encraft, "Warwick wind trial: Final report", Tech. Rep. UK, Encraft, 2009.

[27] British Wind Energy Association, "Small wind turbine performance and safety standard", Tech. Rep., BWEA Standard, 2008.

[28] British Standard 61400-12-1, *Power Performance Measurements of Electricity Producing Wind Turbines*, 2006.

[29] M.J. Stevens and P.T. Smulders, "The estimation of the parameters of the Weibull wind speed Distribution for wind energy utilization purposes", Tech. Rep., Wind Eng. 3 (2), 1979.

[30] E. Hau, *Wind turbines: Fundamentals technologies, application and economics*, Springer, New York, 2nd english edition, 2006.

[31] UK Meteorogical Office British Atmospheric Data Centre, "MIDAS Land Surface Stations Data (1853-current", [Online] Available: http://badc.nerc.ac.uk/data/ukmo-midas, 2011.

[32] Quiet Revolution, "Power curve", England, UK.

[33] Aircon, "Aircon 10 datasheet", UK.

[34] Ampair, "Ampair 600 datasheet", Warfield, Berkshire, UK, 2010.

[35] MCS Working group 3: Micro and Small Wind Systems, *Product Certification Scheme Requirements: Micro and Small Wind Turbines*, Department of Energy and Climate Change, issue 1.5 edition, 2009.

[36] William David Lubitz, "Impact of ambient turbulence on performance of a small wind turbine", *Renewable Energy*, , no. 0, pp. –, 2012.

[37] Y. Zhou and A. Kareem, "Definition of wind profiles in ASCE 7", Tech. Rep. 128:1082-6, Journal of Structural Engineering, August 2002.

[38] B. Ziter, "Alternative methods of estimating hub-height wind speed for small wind turbine performance evaluation", Master's thesis, School of Engineering, University of Guelph, Ontario, Canada, May 2010.

[39] M. Seitzler, "The electrical and mechanical performance evaluation of a roof-mounted, one-kilowatt wind turbine", Tech. Rep. Report CWEC-2009-003, California Wind Energy Collaborative, University of California, Davis CA, USA, 2009.

[40] J. Smith, "Effects of turbulence intensity on the performance of smallwind turbines.", in *Small wind conference*, Stevens Point, WI, USA, June 2010.

[41] J. Van Dam, M. Meadors, H. Link, and P. Migliore, "Power performance test report for the southwest wind power AIR-X wind turbine", Tech. Rep. TP-500-34756, National Renewable Energy Laboratory, September 2003.

[42] Sara Louise Walker, "Building mounted wind turbines and their suitability for the urban scale—a review of methods of estimating urban wind resource", *Energy and Buildings*, vol. 43, no. 8, pp. 1852 – 1862, 2011.

[43] "Technology roadmap: Solar photovoltaic technology", OECD/IEA, International Energy Agency, 2010.

[44] Achim Woyte, Johan Nijs, and Ronnie Belmans, "Partial shadowing of photovoltaic arrays with different system configurations: literature review and field test results", *Solar Energy*, vol. 74, no. 3, pp. 217 – 233, 2003.

[45] Ahmed E. Ghitas and M. Sabry, "A study of the effect of shadowing location and area on the si solar cell electrical parameters", *Vacuum*, vol. 81, no. 4, pp. 475 – 478, 2006.

[46] Energy Saving Trust, "Location, location, location: Domestic small-scale wind field trial report", Tech. Rep., Department of Trade and Industry, UK, July 2009.

[47] C.G. Anderson, "North Harris Community Wind Farm: Wind Measurements at Monan Site", Final report, North Harris Trading Company, Perth, Australia, 2007.

[48] Solener, "Aerogenerador Vélter D", 2007.

[49] Renewable Devices, "Swift turbine performance", Edinburgh, Scotland, UK, 2010.

[50] Ltd. Carbon Concepts, "Wind turbine brochure", Chesterfield, UK, 2010.

[51] N. Stannard, *Generator for, and modelling of, small-scale wind turbines*, PhD thesis, School of Engineering, University of Durham, Durham, UK, 2008.

[52] SMA, "SMA Solar Technology News".

[53] Y. Xia, K.H. Ahmed, and B.W. Williams, "A new maximum power point tracking technique for permanent magnet synchronous generator based wind energy conversion system", *Power Electronics, IEEE Transactions on*, vol. 26, no. 12, pp. 3609 –3620, dec. 2011.

[54] K. Martens, B. Meersman, J. De Kooning, B. Renders, T. Vandoorn, and L. Vandevelde, "Influence of bus voltage variations on two maximum power point control loops", in *Harmonics and Quality of Power (ICHQP), 2010 14th International Conference on*, Sept. 2010, pp. 1 –6.

[55] SMA Technology, "Windy boy 1100 l. installation guide", Niestetal, Germany, 2010.

[56] SMA Technology, "Windy boy 2500/3000 inverter for wind energy power plants", Niestetal, Germany, 2010.

[57] Energy Networks Association, London, UK, *Engineering Recommendation G83/1: Recommendations for the Connection of Small-Scale Embedded Generators (Up to 16A per phase) in Parallel with Public Low-Voltage Distribution Networks*, September 2003.

[58] Energy Networks Association, London, UK, *Engineering Recommendation G59/1: Recommendations for the Connection of Embedded Generation Plant to the Public Electricity Suppliers' Distribution System*, 1991.

[59] British Standard (EN/IEC) 61000-3-2, *Electromagnetic Compatibility (EMC)—Part 3-2: Limits—Limits for Harmonic Current Emissions (Equipment Input Current < 16 A per Phase)*, 2006.

[60] International Electrotechnical Commission (IEC), *Electromagnetic Compatibility (EMC)—Part 3-15: Limits—Assessment of Low Frequency Electromagnetic Immunity and Emission Requirements for Dispersed Generation Systems in LV Network, Committee Draft,*, IEC, Geneva, Switzerland, 2008.

[61] J.M. Carrasco, L.G. Franquelo, J.T. Bialasiewicz, E. Galvan, R.C.P. Guisado, Ma.A.M. Prats, J.I. Leon, and N. Moreno-Alfonso, "Power-electronic systems for the grid integration of renewable energy sources: A survey", *Industrial Electronics, IEEE Transactions on*, vol. 53, no. 4, pp. 1002 –1016, June 2006.

[62] H. Akagi, "Active harmonic filters", *Proceedings of the IEEE*, vol. 93, no. 12, pp. 2128 –2141, Dec. 2005.

[63] M. El-Habrouk, M.K. Darwish, and P. Mehta, "Active power filters: A review", *IEE Proceedings Electric Power Applications*, vol. 147, no. 5, pp. 403 –413, Sep 2000.

[64] Yun Wei Li, "Control and Resonance Damping of Voltage-Source and Current-Source Converters With LC Filters", *Industrial Electronics, IEEE Transactions on*, vol. 56, no. 5, pp. 1511 –1521, May 2009.

[65] C. Hanju and T.-K. Vu, "Comparative analysis of low-pass output filter for single-phase grid-connected photovoltaic inverter", in *Applied Power Electronics Conference and Exposition (APEC), 2010 Twenty-Fifth Annual IEEE*, Feb. 2010, pp. 1659 –1665.

[66] S. Ando, A. Ueda, and A. Torii, "Characteristics of three-phase boost type rectifier with lc filter in ac side", in *Power Conversion Conference, 2002. PCC Osaka 2002. Proceedings of the*, 2002, vol. 3, pp. 1211 –1216 vol.3.

[67] A.A. Rockhill, M. Liserre, R. Teodorescu, and P. Rodriguez, "Grid-filter design for a multimegawatt medium-voltage voltage-source inverter", *Industrial Electronics, IEEE Transactions on*, vol. 58, no. 4, pp. 1205 –1217, April 2011.

[68] E. Lakervi and E.J. Holmes, *Electricity Distribution Network Design*, IEE Power Engineering Series 21, 2nd edition, 2003.

[69] "Information to assist third parties in the design and installation of secondary substations for adoption or use by SSE Power Distribution", Tech. Rep., SSE Power Distribution, November 2007.

[70] American National Standard, *IEEE Recommended Practices and Re- quirements for Harmonic Control in Electrical Power Systems*, IEEE Standard 519, USA, 1992.

[71] Ofgem, *Distribution Code: Modification to the Distribution Code to Implement a Change to Engineering Recommendation G59/2 Relating to the Limits of Direct Current Injection*, Office of Gas and Electricity Markets, London, UK, April 2011.

[72] D.G. Infield, P. Onions, A.D. Simmons, and G.A. Smith, "Power quality from multiple grid-connected single-phase inverters", *Power Delivery, IEEE Transactions on*, vol. 19, no. 4, pp. 1983 – 1989, Oct. 2004.

[73] RenewableUK, "Small Wind Systems UK Market Report", April 2010.

[74] WINEUR, "Report on resource assessment", Bristol, UK, February 2007.

[75] Lemcko Energy and Power Quality Lab, "Elektrotechnical expertise centre of Howest", 2011.

[76] A. Goetzberger, *Photovoltaic solar energy generation*, Springer, May 2005.

[77] M.G. Villalva, J.R. Gazoli, and E.R. Filho, "Comprehensive approach to modeling and simulation of photovoltaic arrays", *Power Electronics, IEEE Transactions on*, vol. 24, no. 5, pp. 1198 –1208, May 2009.

[78] British Standard (EN/IEC) 60904-3:2008, *Photovoltaic devices. Measurement principles for terrestrial photovoltaic (PV) solar devices with reference spectral irradiance data*, 2008.

[79] Suntech power, "Mono-crystalline solar panel STP1755-24/AC", 2008.

[80] Yingli Solar, "YL185 P/1310x990 Series", 2008.

[81] Sharp, "NA series Microamorphous silicon thin-film photovoltaic modules", 2009.

[82] Sanyo Component Europe GmbH Solar division, "HIP-230HDE1 HIT photovoltaic module", 2009.

[83] C. Carrero, J. Amador, and S. Arnaltes, "A single procedure for helping pv designers to select silicon pv modules and evaluate the loss resistances", *Renewable Energy*, vol. 32, no. 15, pp. 2579 – 2589, 2007.

[84] W. De Soto, S.A. Klein, and W.A. Beckman, "Improvement and validation of a model for photovoltaic array performance", *Solar Energy*, vol. 80, no. 1, pp. 78 – 88, 2006.

[85] S.K. Firth, *Raising efficiency in photovoltaic systems: High resolution monitoring performance analysis*, PhD thesis, The Insitute of Energy and sustainable Development, 2006.

[86] G. Notton, V. Lazarov, and L. Stoyanov, "Optimal sizing of a grid-connected pv system for various pv module technologies and inclinations, inverter efficiency characteristics and locations", *Renewable Energy*, vol. 35, no. 2, pp. 541 – 554, 2010.

[87] M. Munzinger, F. Crick, E.J. Dayan, N. Pearsall, and C. Martin, "Domestic photovoltaic field trials: Final technical report", Tech. Rep., Depatment of Trade and Industry, 2006.

[88] Department of Energy and Climate Change, "Feed-in Tariffs Government's Response to the Summer 2009 Consultation", Tech. Rep., UK, February 2010.

[89] BWEA, "Small wind systems", Market report, British Wind Energy Association, UK, 2010.

[90] AWEA, "Small Wind turbine Global Market Study", Tech. Rep., American Wind Energy Association, USA, 2008.

[91] Vestas wind systems A/S, "V164 7mw", 8940 Randers SV, Denmark.

[92] Energy Saving Trust, "Home renewables grants", [Online] Available: http://www.energysavingtrust.org.uk/scotland/Scotland-Welcome-page/ At-Home/Grants-and-offers/Energy-Saving-Scotland-home-renewables- grants.

[93] Hunter Danskin, "Final Report: The impact of changing energy use patterns in buildings on peak electricity demand in the UK", Tech. Rep., Department of Energy and Climate Change, December 2008.

[94] Building Research Establishment, "The impact of changing energy use patterns in buildings on peak electricity demand in the UK", Tech. Rep., 2008.

[95] S. Papathanassiou, N. Hatziargyriou, and K. Strunz, "A benchmark low voltage microgrid network", in *CIGRE Symp. Power Systems with Disp. Gen*, Athens, Greece, April 2005.

[96] Hemant Joshi, *Residential, commercial and industrial electrical systems: Network and Installation*, vol. 2, Tata McGraw-Hill, 2008.

[97] P. Trichakis, P.C. Taylor, P.F. Lyons, and R. Hair, "Predicting the technical impacts of high levels of small-scale embedded generators on low-voltage networks", *IET Renewable Power Generation*, vol. 2, no. 4, pp. 249–262, 2008.

[98] S. Ingram, S. Probert, and K. Jackson, "The impact of small scale embedded generation on the operating parameters of distribution networks", Tech. Rep., Department of Trade and Industry, London, UK, June 2003.

[99] "Long Term Development Statement for the Electricity Distribution System of South Wales and South West", Tech. Rep., Western Power Distribution plc, April 2010.

[100] "Long Term Development Statement, Central Networks West", Tech. Rep., E-ON Central Networks plc, 2009.

[101] F. Garnacho Vecino, "Transformers. course on medium voltage level electric material (in Spanish)", Tech. Rep., Fund for the development of industrial innovation. Ministry of Science and Technology, Spain, 1999.

[102] S.Z. Djokic, A. J. Collin, and C.E. Cresswell, "The Future of Residential Lighting: Shift from Incandescent to CFL to LED light sources", in *Annual conference*. Illuminating Engineering Society of North America, November 2009.

[103] Energy Networks Association, London, UK, *Planning Levels for Harmonic Voltage Distortion and the Connection of Non-Linear Equipment to Transmission and Distribution Systems in the United Kingdom*, February 2001.

[104] "Long term development statement", Tech. Rep., Electricity North West plc, 2010.

[105] "Long Term Development Statement for Scottish Hydro Electric Power Distribution plc's Electricity Distribution System", Tech. Rep., Scottish and Southern Energy Power Distribution, 2009.

[106] "Specification for overhead line work used during the installation of new connections", Tech. Rep., Scottish and Southern Energy Power Distribution, October 2001.

[107] "Specification for electricity service and distribution cables for use during the installation of new connections", Tech. Rep., Scottish and Southern Energy Power Distribution, July 2010.

[108] SP Distribution plc, "Technical specification for power cables up to and including 33kV and associated auxiliary cables", Tech. Rep., SP Transmission and Manweb Networks, February 2005.

[109] DRAKA Product Range, "Cable specifications", Tech. Rep., DRAKA UK Limited, http://www.drakauk.com, 2010.

[110] NKT Cables Product Catalogue, "Cable specifications", Tech. Rep., NKT Cables, http://www.nktcables.cz.

[111] J.L. Sanz Serrano and J.C. Toledano Gasca, *Techniques and processes in MV/LV electrical installations (in Spanish)*, 6th edition, 2007.

Appendix A
Matlab Codes

Code used for UK Urban Areas.

```
res=0:0.5:15;
res2=0:0.5:15;
rho=1.225;

%hourly data of edinburgh university weather station average values
edi=dlmread('2008Edihourlydata.dat',',');
edihist=hist(edi(:,5),res);
vedi=size(edi);
edihhist=edihist./(vedi(1,1)*.5);
sumedi=res.*edihhist;
meanedi=(sum(sumedi))/(sum(edihhist));
%fitting 1 weibull distribution
[pedi pedici]=wblfit(edi(:,5));
aedi=pedi(1,1)
bedi=pedi(1,2)
weiedi=((res2./aedi).^(bedi-1)).*(exp(-((res2./aedi).^bedi))).*(bedi/aedi);
weiedih=weiedi.*(vedi(1,1)*.5);
meanediw=(aedi)*gamma(1+(1/bedi))

 % hourly Sheffield uni weather station
sheffield=dlmread('Sheffield2000.dat',',');
sheffield=sheffield.*0.51444;
shefhist=hist(sheffield,res);
vshef=size(sheffield);
shefhhist=shefhist./(vshef(1,1)*.5);
sumshef=res.*shefhist;
meanshef=(sum(sumshef))/(sum(shefhist))
%fitting 1 weibull distribution
[pshef pshefci]=wblfit(sheffield);
as=pshef(1,1);
bs=pshef(1,2);
weishef=((res./as).^(bs-1)).*(exp(-((res./as).^bs))).*(bs/as);
weishefh=weishef.*(vshef(1,1)*.5);
meanshefw=(as)*gamma(1+(1/bs));

 % Manchester city hourly data metoffice
manchester=dlmread('Manchester2008.dat',',');
manchester=manchester.*0.51444;
manhist=hist(manchester,res);
vman=size(manchester);
manhhist=manhist./(vman(1,1)*.5);
```

```
summanh=res.*manhhist;
meanman=(sum(summanh))/(sum(manhhist))
%fitting 1 weibull distribution
[pman pmanci]=wblfit(manchester);
aman=pman(1,1);
bman=pman(1,2);
weiman=((res./aman).^(bman-1)).*(exp(-((res./aman).^bman))).*(bman/aman);
weimanh=weiman.*(vman(1,1)*.5);
meanmanw=(aman)*gamma(1+(1/bman));

 % London city centre hourly data
london=dlmread('London2007.dat',',');
london=london.*0.51444;
lonhist=hist(london,res);
vlon=size(london);
lonhhist=lonhist./(vlon(1,1)*.5);
sumlon=res.*lonhhist;
meanlon=(sum(sumlon))/(sum(lonhhist))
%fitting 1 weibull distribution
[plon plonci]=wblfit(london);
alon=plon(1,1);
blon=plon(1,2);
weilon=((res./alon).^(blon-1)).*(exp(-((res./alon).^blon))).*(blon/alon);
weilonh=weilon.*(vlon(1,1)*.5);
meanlonw=(alon)*gamma(1+(1/blon));

%Other 2 london sites for the K versus mean speed
london2=dlmread('London2007.dat',',');
london2=london2.*0.51444;
[plon2 plonci]=wblfit(london2);
alon2=plon2(1,1);
blon2=plon2(1,2);
meanlon2w=(alon2)*gamma(1+(1/blon2));
london3=dlmread('London20072.dat',',');
london3=london3.*0.51444;
[plon3 plonci]=wblfit(london3);
alon3=plon3(1,1);
blon3=plon3(1,2);
meanlon3w=(alon2)*gamma(1+(1/blon3));


 % Glasgow hourly data
glasgow=dlmread('Glasgow2000.dat',',');
glasgow=glasgow.*0.51444;
glahist=hist(glasgow,res);
vgla=size(glasgow);
glahhist=glahist./(vgla(1,1)*.5);
sumgla=res.*glahhist;
meangla=(sum(sumgla))/(sum(glahhist))
fitting 1 weibull distribution
[pgla pglaci]=wblfit(glasgow);
agla=pgla(1,1);
bgla=pgla(1,2);
```

```
weigla=((res./agla).^(bgla-1)).*(exp(-((res./agla).^bgla))).*(bgla/agla);
weiglah=weigla.*(vgla(1,1)*.5);
meanglaw=(agla)*gamma(1+(1/bgla));

%Aberdeeen hourly data
aberdeen=dlmread('aberdeen2008.dat',',');
aberdeen=aberdeen.*0.51444;
abehist=hist(aberdeen,res);
vabe=size(aberdeen);
abehhist=abehist./(vabe(1,1)*.5);
sumabe=res.*abehhist;
meanabe=(sum(sumabe))/(sum(abehhist))
fitting 1 weibull distribution
[pabe pabeci]=wblfit(aberdeen);
aabe=pabe(1,1);
babe=pabe(1,2);
weiabe=((res./aabe).^(babe-1)).*(exp(-((res./aabe).^babe))).*(babe/aabe);
weiabeh=weiabe.*(vabe(1,1)*.5);
meanabew=(aabe)*gamma(1+(1/babe));

 % New Castle hourly data
newcastle=dlmread('Newcastle2000.dat',',');
newcastle=newcastle.*0.51444;
nchist=hist(newcastle,res);
vnc=size(newcastle);
nchhist=nchist./(vnc(1,1)*.5);
sumnc=res.*nchhist;
meannc=(sum(sumnc))/(sum(nchhist))
%fitting 1 weibull distribution
[pnc pncci]=wblfit(newcastle);
anc=pnc(1,1);
bnc=pnc(1,2);
weinc=((res./anc).^(bnc-1)).*(exp(-((res./anc).^bnc))).*(bnc/anc);
weinch=weinc.*(vnc(1,1)*.5);
meanncw=(anc)*gamma(1+(1/bnc));
```

Code used for Edinburgh Data.

```
res=0:0.5:15;
res2=0:0.5:25;
res3=0:0.1:25;
 hourly data of edinburgh university weather station avergae values
ediuh=dlmread('2008Edihourlydata.dat',',');
ediuhist=hist(ediuh(:,5),0:0.5:25);
vediu=size(ediuh);
ediuhhist=ediuhist./(vediu(1,1)*.5);
sumunih=res2.*ediuhhist;
meaneduh=(sum(sumunih))/(sum(ediuhhist));
%fitting 1 weibull distribution
[pediuh pediunicih]=wblfit(ediuh(:,5));
aeh=pediuh(1,1);
beh=pediuh(1,2);
```

```
weiediuh=((res./aeh).^(beh-1)).*(exp(-((res./aeh).^beh))).*(beh/aeh);
weiediuhh=weiediuh.*(vediu(1,1)*.5);
meaneduhw=(aeh)*gamma(1+(1/beh));
weiediuhc=((res3./aeh).^(beh-1)).*(exp(-((res3./aeh).^beh))).*(beh/aeh);

% hourly data of Leith port 2008
leith=dlmread('Leith1999.dat',',');
leith=leith*0.51444;
leithhist=hist(leith,res);
vleith=size(leith);
leithhhist=leithhist./(vleith(1,1)*.5);
sumleith=res.*leithhhist;
meanleith=(sum(sumleith))/(sum(leithhhist));
%fitting 1 weibull distribution
[pleith pleithci]=wblfit(leith);
al=pleith(1,1);
bl=pleith(1,2);
weileith=((res./al).^(bl-1)).*(exp(-((res./al).^bl))).*(bl/al);
weileithh=weileith.*(vleith(1,1)*.5);
meanleithw=(al)*gamma(1+(1/bl));

% hourly data of edinburgh university weather station maximum values
ediuhmaxhist=hist(ediuh(:,7),0:0.5:25);
ediuhmaxhist=ediuhmaxhist./(vediu(1,1)*.5);
ediuhhmaxhist=ediuhmaxhist*(vediu(1,1));
sumunihmax=res2.*ediuhmaxhist;
meaneduhmax=(sum(sumunihmax))/(sum(ediuhmaxhist));
%fitting 1 weibull distribution
[pediuhmax pediunicihmax]=wblfit(ediuh(:,7));
aehm=pediuhmax(1,1);
behm=pediuhmax(1,2);
weiehmx=((res./aehm).^(behm-1)).*(exp(-((res./aehm).^behm))).*(behm/aehm);
weiediuhhmax=weiehmx*(vediu(1,1));
meaneduhwmax=(aehm)*gamma(1+(1/behm));


%minute by miute data from edinburgh university weather station average
ediunimm=dlmread('Edinburghuni2008n2.dat',',');
ediummhist=hist(ediunimm(:,4),0:0.5:25);
vediumm=size(ediunimm(:,4));
ediummhist=ediummhist./(vediumm(1,1)*.5);
ediumhist=ediummhist.*(vediumm(1,1)/60*.5);
sumunimm=res2.*ediummhist;
meanedumm=(sum(sumunimm))/(sum(ediummhist));
%fitting a weibull distribution
[pediunimm pediunimmci]=wblfit(ediunimm(:,4));
aem=pediunimm(1,1);
bem=pediunimm(1,2);
weiediumm=((res./aem).^(bem-1)).*(exp(-((res./aem).^bem))).*(bem/aem);
weiediumh=weiediumm.*(vediumm(1,1)/60*.5);
meanedumw=(aem)*gamma(1+(1/bem));
weiediummc=((res3./aem).^(bem-1)).*(exp(-((res3./aem).^bem))).*(bem/aem);
%maximum values
```

```
ediummaxhist=hist(ediunimm(:,6),0:0.5:25);
ediummaxhist=ediummaxhist./(vediumm(1,1)*.5);
ediummaxhhist=ediummaxhist.*(vediumm(1,1)/60*.5);
sumunimmax=res2.*ediummaxhist;
meanedummax=(sum(sumunimmax))/(sum(ediummaxhist));
%fitting a weibull distribution
[pediunimmax pediunimmaxci]=wblfit(ediunimm(:,6));
aemm=pediunimmax(1,1);
bemm=pediunimmax(1,2);
weiemmx=((res./aemm).^(bemm-1)).*(exp(-((res./aemm).^bemm))).*(bemm/aemm);
weiemmxh=weiemmx.*(vediumm(1,1)/60*.5);
meanedummaxw=(aemm)*gamma(1+(1/bemm));

 %blackford hill data
 In knots the speed, 1 knot=0.51444m/s
edibl=dlmread('Ediblackford2008.dat',',');
edibl=edibl.*.514444;
ediblhist=hist(edibl,res);
vedib=size(edibl);
ediblhist=ediblhist./(vedib(1,1)*.5);
sumedibl=res.*ediblhist;
meanedibl=(sum(sumedibl))/(sum(ediblhist));
%fitting 1 weibull distribution
[pedibl pediblici]=wblfit(edibl);
aeb=pedibl(1,1);
beb=pedibl(1,2);
weiedibl=((res./aeb).^(beb-1)).*(exp(-((res./aeb).^beb))).*(beb/aeb);
weiediblh=weiedibl.*(vedib(1,1)*.5);
meanediblw=(aeb)*gamma(1+(1/beb));

 %Edinburgh Airport hourly data
ediairport=dlmread('Edinburghairport19992.dat',',');
ediairport=ediairport.*0.51444;
ediahist=hist(ediairport,res);
vedia=size(ediairport);
ediahist=ediahist./(vedia(1,1)*0.5);
sumedia=res.*ediahist;
meanedia=(sum(sumedia))/(sum(ediahist));
 %fitting 1 weibull distribution
[pedia pedia]=wblfit(ediairport);
aea=pedia(1,1);
bea=pedia(1,2);
weiedia=((res./aea).^(bea-1)).*(exp(-((res./aea).^bea))).*(bea/aea);
weiediah=weiedia.*(vediu(1,1)*.5);
meanediaw=(aea)*gamma(1+(1/bea));
```

Appendix B
Simulink Models

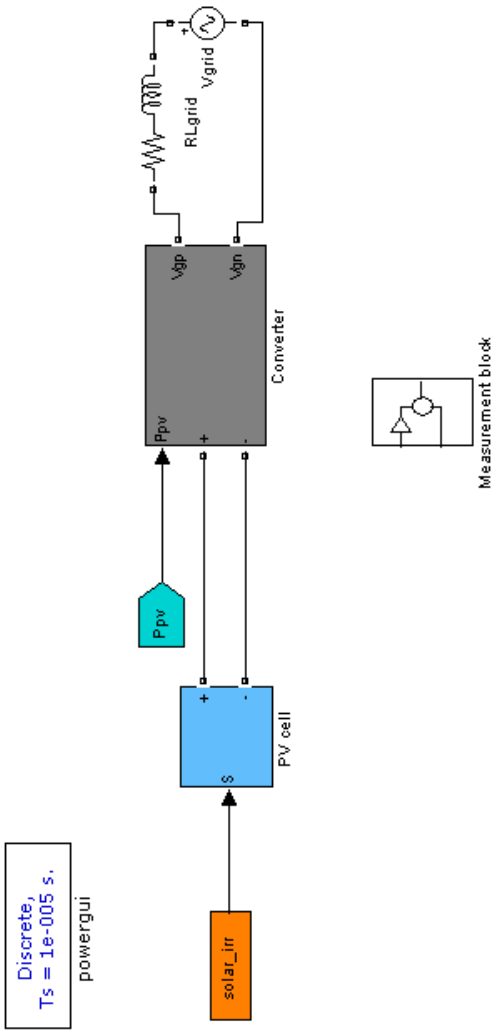

Figure B.1: *Simulink PV model.*

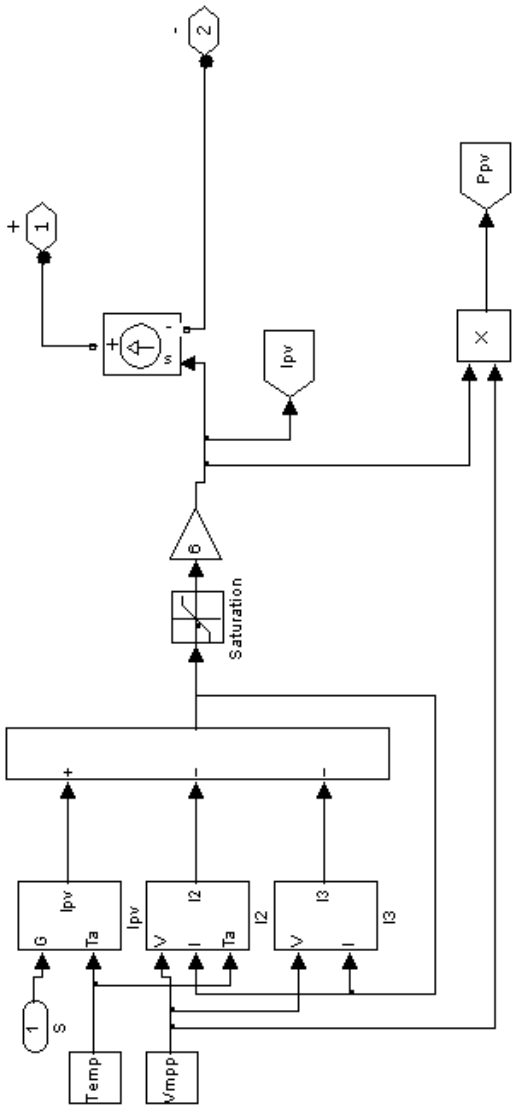

Figure B.2: *Simulink PV cell model.*

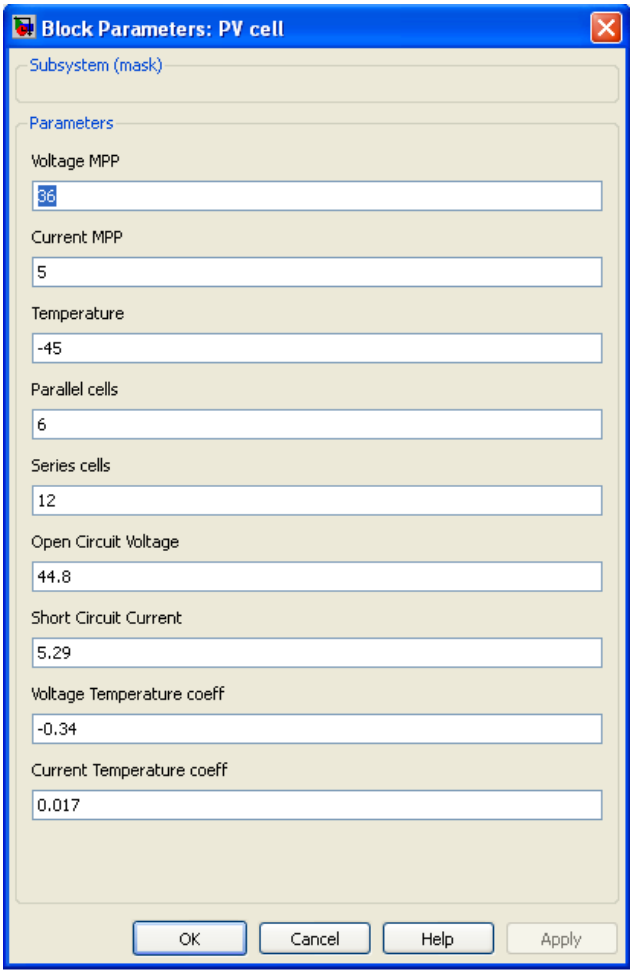

Figure B.3: *Simulink PV cell input window.*

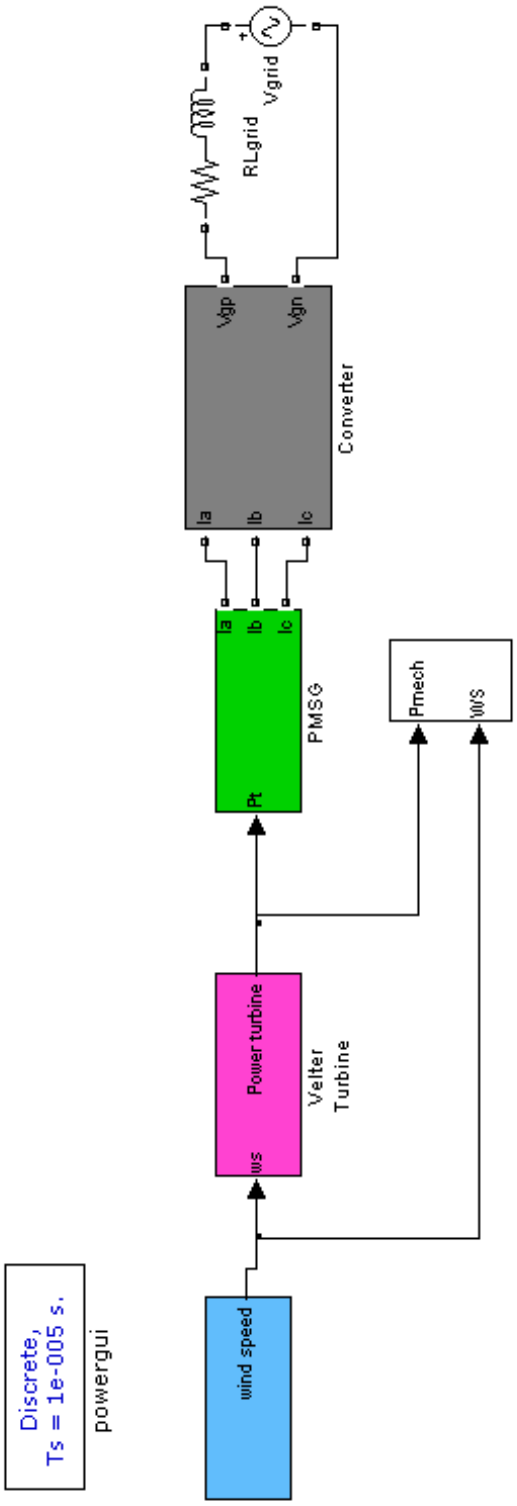

Figure B.4: *Simulink wind turbine model.*

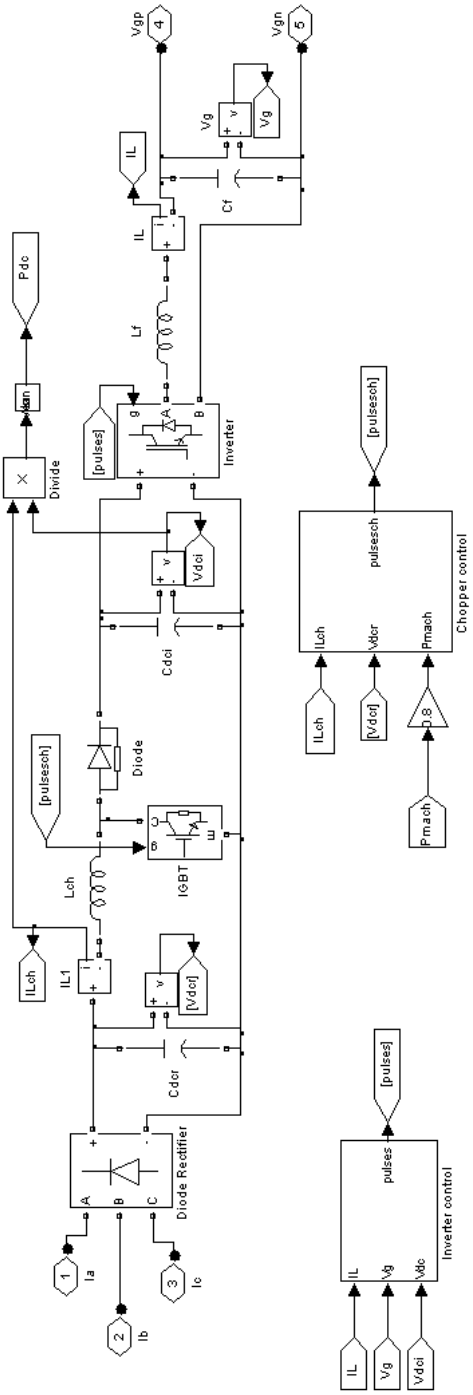

Figure B.5: *Simulink inverter model.*

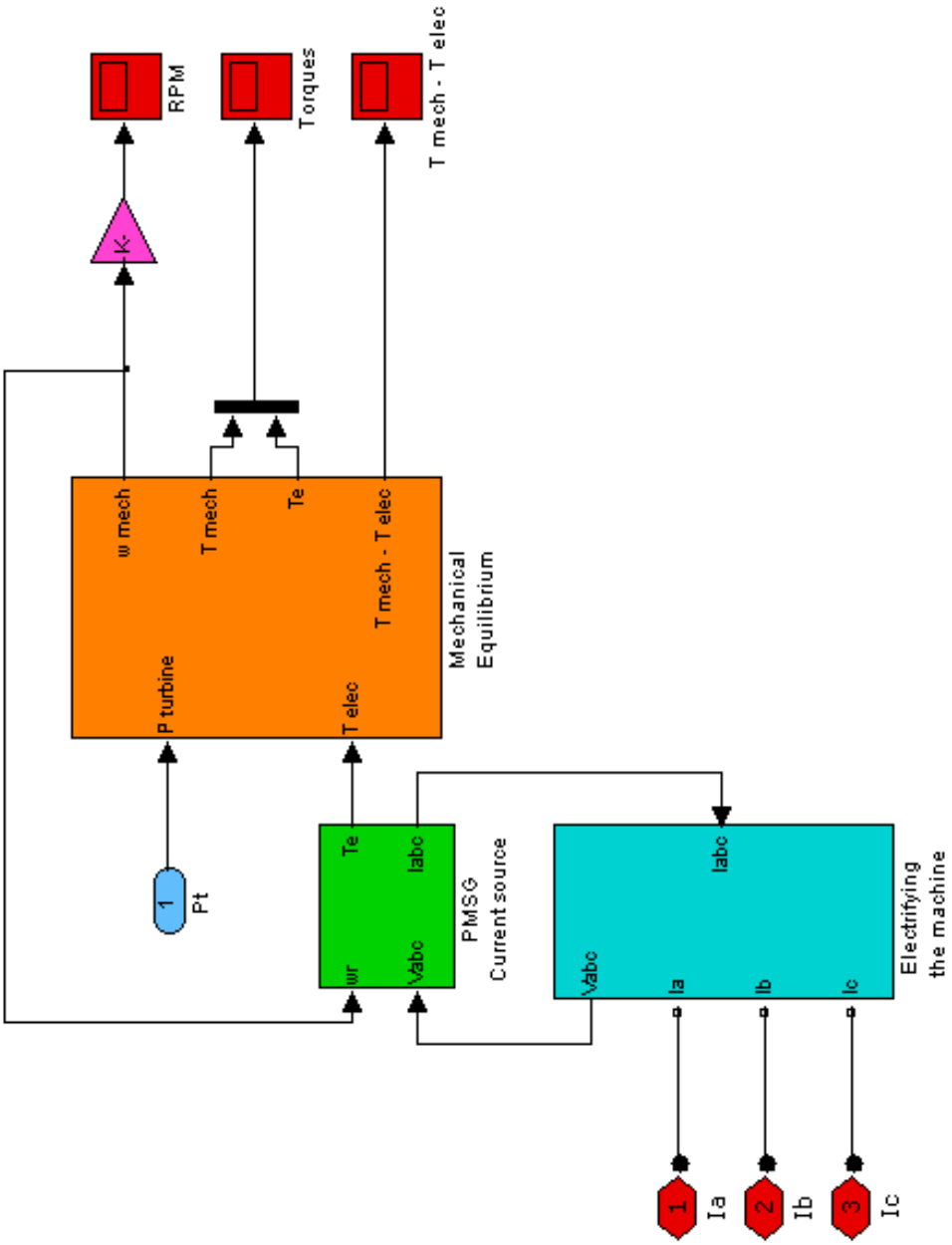

Figure B.6: *Permanent Magnet Synchronous Generator components.*

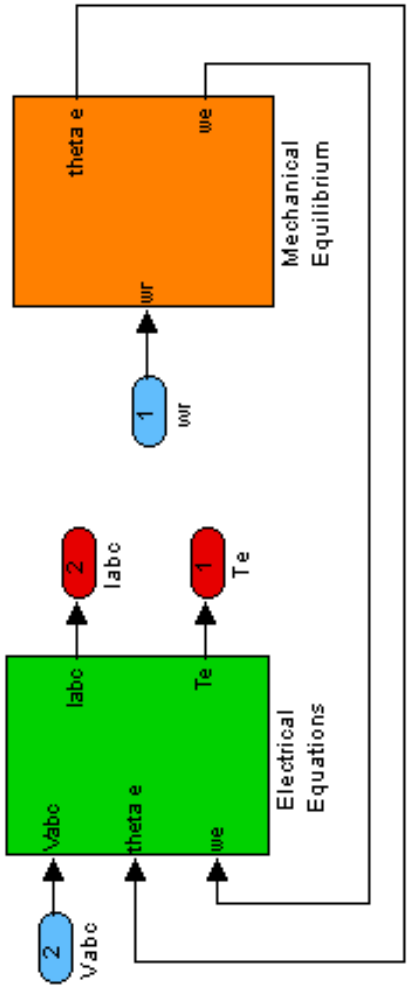

Figure B.7: *PMSG electro-mechanical modelling.*

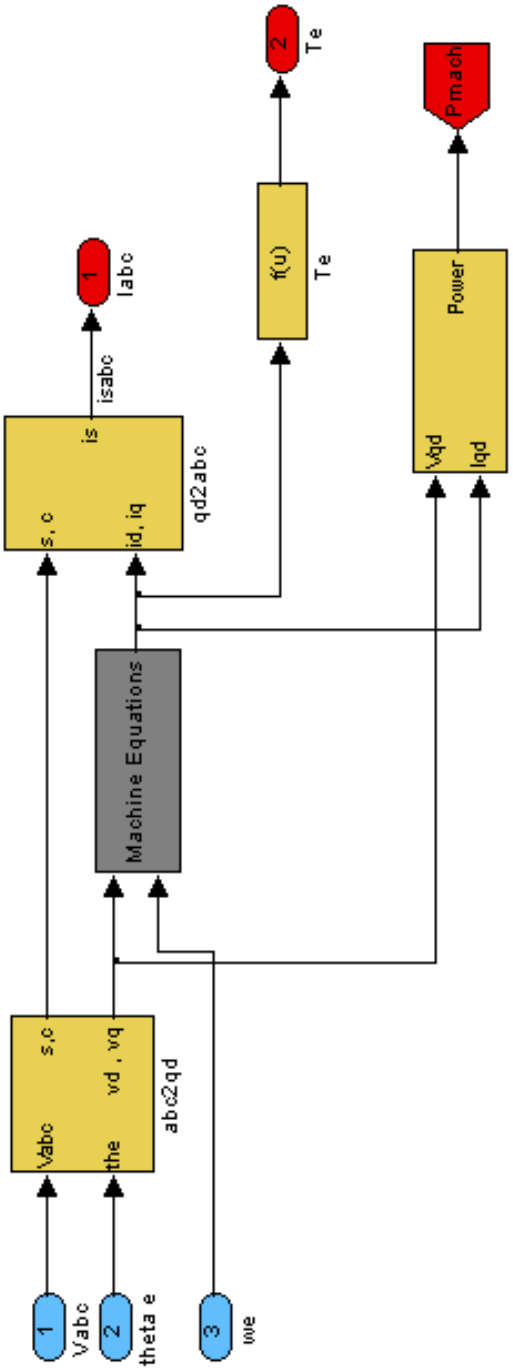

Figure B.8: *PMSG electrical d/q reference frame modelling.*

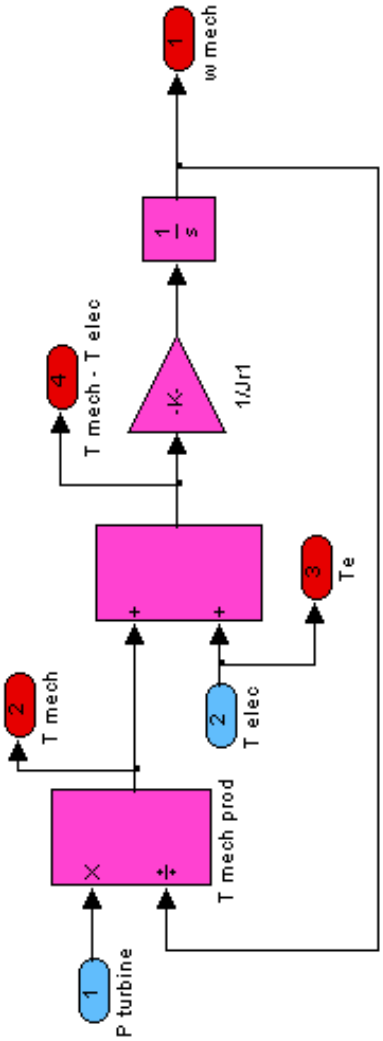

Figure B.9: *PMSG mechanical equilibrium modelling.*

Appendix C
PV Measured Efficiencies

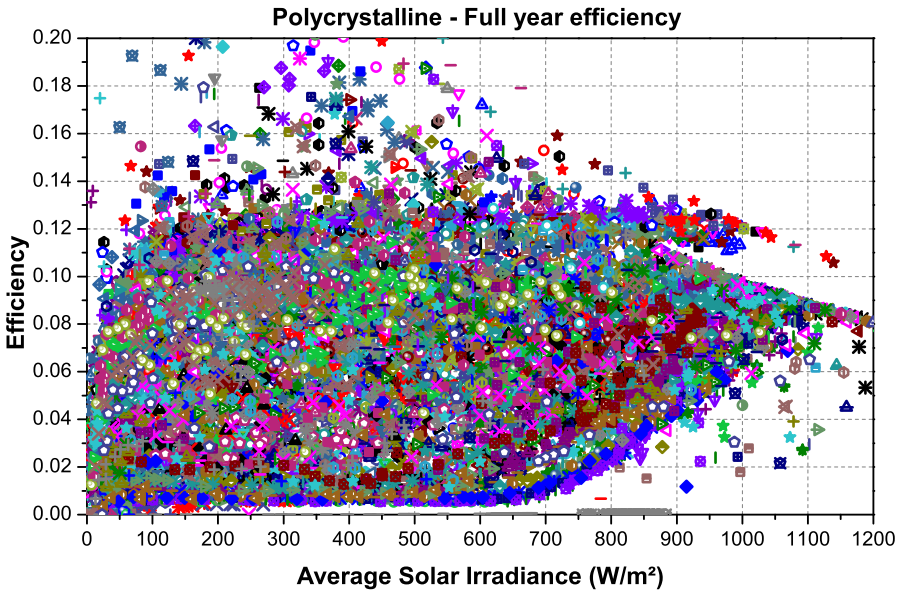

Figure C.1: *Efficiency identified in the Belgian data for polycrystalline PV technology for the full year.*

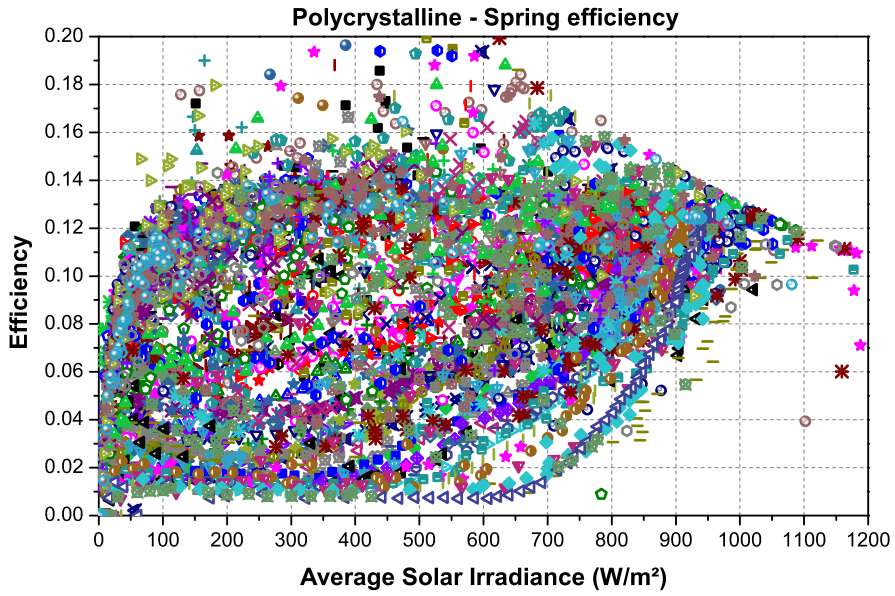

Figure C.2: *Efficiency identified in the Belgian data for polycrystalline PV technology during the Spring.*

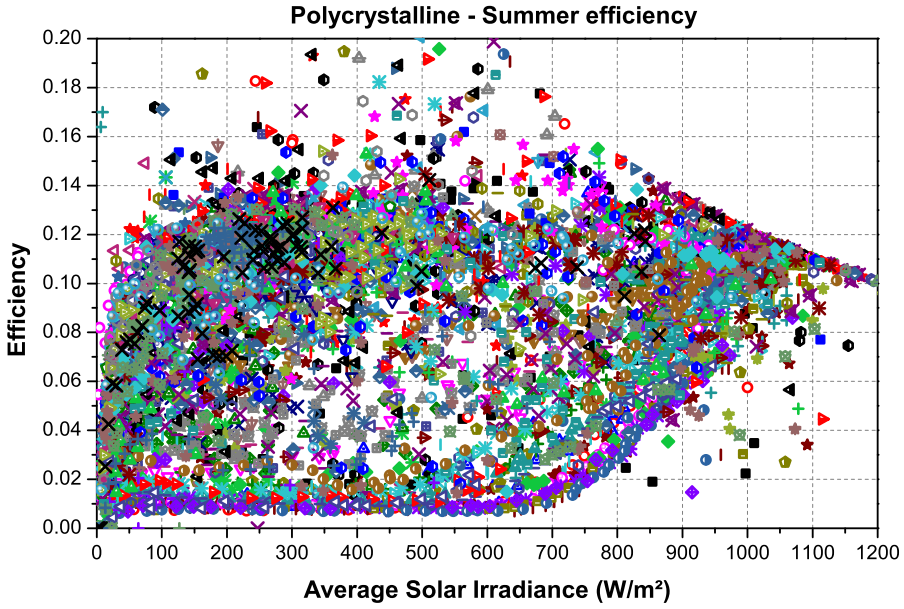

Figure C.3: *Efficiency identified in the Belgian data for polycrystalline PV technology during the Summer.*

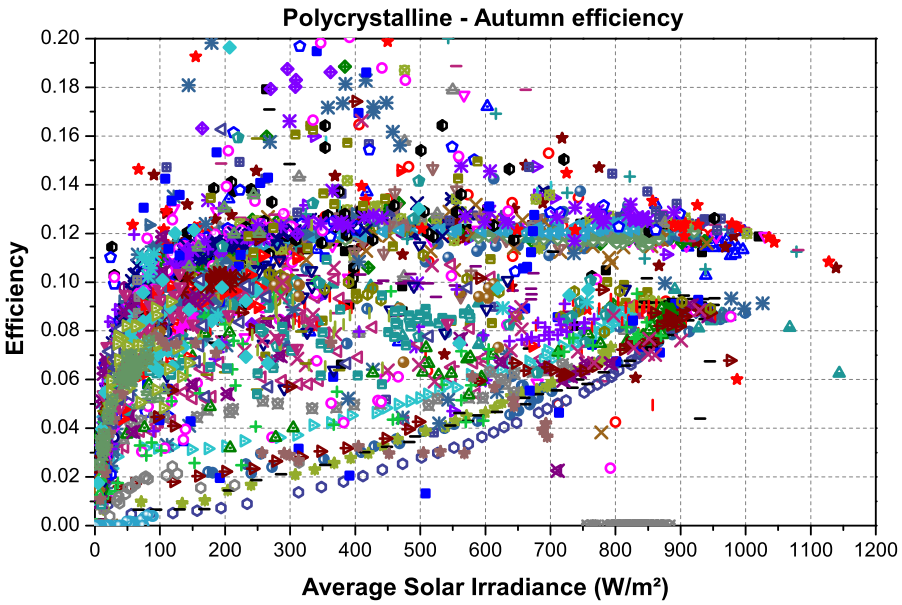

Figure C.4: *Efficiency identified in the Belgian data for polycrystalline PV technology during the Autumn.*

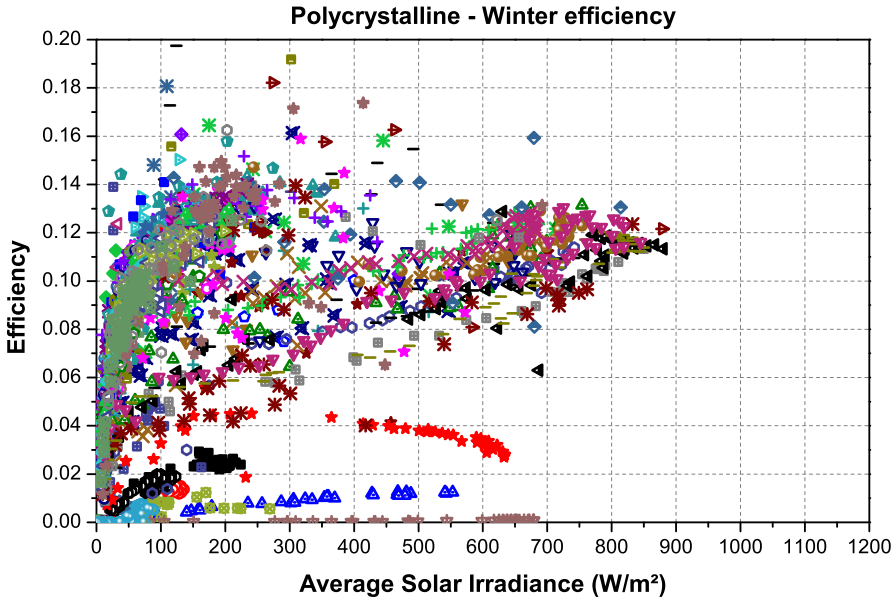

Figure C.5: *Efficiency identified in the Belgian data for polycrystalline PV technology during the Winter.*

Appendix D
Network Parameters

Operating Voltage (kV)	Subsector	Transformer Rating (kVA)	Tapping Range	Basic Impulse Level (kV)	Load Losses at $75°C$ (W)	No-load Losses (W)	Impedance (%)	Model Parameters (Impedance on 2^{ary} side)	
								R_{LV}	X_{LV}
								(pu)	
11/0.4	Highly Urban	1500	±5% in 2.5% taps	75	15810	1400	5	0.01054	0.048876
		1000			11000	1350	4.75	0.011	0.0462
		800			7410	1000	4.75	0.00926	0.0458
	Urban Suburban	500			5100	680	4.75	0.0102	0.0464
		315			3420	580		0.01085	0.04625
		200			2900	540		0.015	0.045
	Rural	100			1750	320	4.5	0.0175	0.04145
		50			1100	190		0.02186	0.0393

Table D.1: *Parameters of typical* $11/0.4kV$ *secondary distribution transformers [99], [100], [69], [101].*

Low-voltage Line Type		Cross Sectional Area (CSA)	Positive sequence Z		Neutral Z	Zero-sequence Z		Maximum sustained current
Id.	**Configuration**		R_{ph}	X_{ph}	$R_{neutral}$	R_0	X_0	$I_{Z_{ph}}$
		mm^2	Ω/km					Amps
A	Underground Line (Cable) $0.6/1kV$ $4\times$(CSA) Al/Cu (earth)	300	0.1	0.073	0.168	0.593	0.042	465
B		185	0.164	0.074	0.168	0.656	0.05	355
C		120	0.253	0.071	0.253	1.012	0.046	280
D		95	0.320	0.075	0.320	1.280	0.051	245
E		70	0.443	0.076	0.443	1.772	0.052	205
F		35	0.87	0.085	0.87	3.481	0.058	156
G	Overhead line Aerial Bundled $4\times$(CSA) Al Service Connection $0.6/1kV4\times$(CSA) Al/Cu(earth) Public Lighting $0.6/1kV4\times$(CSA) Al/Cu(earth)	120	0.284	0.083	-	1.136	0.417	261
H		95	0.32	0.085	-	-	-	228
I		70	0.497	0.086	0.63	2.387	0.447	195
J		50	0.397	0.279	-	-	-	168
K		35	0.574	0.294	-	-	-	148
L		35	0.851	0.041	0.9	3.404	0.03	120
M		25	1.191	0.043	1.26	4.766	0.03	100
N		25	1.18	0.043	0.9	4.72	0.03	100

Table D.2: *Typical configurations and parameters of low-voltage lines in the UK [104], [99], [100], [105], [106], [107], [108], [109], [110], [68], [96], [111].*